



**VYSOKÉ UČENÍ TECHNICKÉ V BRNĚ**

BRNO UNIVERSITY OF TECHNOLOGY

**FAKULTA STROJNÍHO INŽENÝRSTVÍ**

FACULTY OF MECHANICAL ENGINEERING

**ENERGETICKÝ ÚSTAV**

ENERGY INSTITUTE

**DIGITÁLNÍ DVOJČE PLYNULÉHO ODLÉVÁNÍ OCELI  
A JEHO OPTIMALIZACE**

DIGITAL TWIN OF CONTINUOUS STEEL CASTING AND ITS OPTIMIZATION

**HABILITAČNÍ PRÁCE**

HABILITATION THESIS

**AUTOR PRÁCE**

AUTHOR

**Ing. TOMÁŠ MAUDER, Ph.D.**

BRNO 2022



## Abstrakt

Digitální dvojče jako matematicko-numerický model ZPO (zařízení pro plynulé odlévání oceli), jeho tvorba i optimalizace je moderní klíčový nástroj k dosažení požadované kvality odlévané oceli a produktivity výroby. Simuluje vlastní výrobní proces na ZPO a zohledňuje aspekty produkce oceli včetně její kvality a včetně ekologických dopadů na životní prostředí. Práce dokládá význam digitálního modelu reálného procesu plynulého lití a metod numerické matematiky při jeho tvorbě. Optimalizace reálného provozu ZPO se provede optimalizací parametrů jejího digitálního dvojčete. Výsledkem je nejen ukázka implementace předloženého algoritmu a souhrn aplikačních možností navrhovaného přístupu ale především verifikovaný plnohodnotný digitální obraz skutečného lícího stroje a důkaz jeho možnosti prediktivně reagovat na dynamické změny lícího procesu a dosáhnout maximální produkce při dodržení výsledné kvality oceli i zvyšujících se ekologických požadavků.

## Abstract

The digital twin as a mathematical-numerical model of CC (continuous steel casting) process and its optimization is a modern tool to achieve the required steel quality and high productivity of casting. Described digital twin simulates production process at CC and considers main aspects of steel production, including its quality and environmental impact. This work demonstrates the importance of a digital model of a real process and methods of numerical mathematics used on its creation. The optimization of real CC operation is performed by optimizing the digital twin parameters. The results conclude verified full digital image of a real CC process, demonstration of the model implementations, application possibilities and its ability to predictively change dynamic casting process parameters to achieve maximum production and high steel quality products with respect to increasing environmental requirements.

## Klíčová slova

Digitální dvojče, optimalizace procesu, výroba oceli, ekologická stopa.

## Keywords

Digital twin, process optimization, steel production, ecological footprint.

## Citace

MAUDER, Tomáš. *Digitální dvojče plynulého odlévání oceli a jeho optimalizace*. Brno, 2022. Habilitační práce. Vysoké učení technické v Brně, Fakulta strojního inženýrství.

## Prohlášení

Prohlašuji, že jsem tuto habilitační práci vypracoval samostatně a uvedl jsem všechny literární prameny, publikace a další zdroje, ze kterých jsem čerpal.

.....  
Tomáš Mauder  
7. listopadu 2022

## Poděkování

Děkuji rodině, přátelům a kolegům, kteří mi poskytli morální, profesní a odbornou podporu. Jmenovitě chci poděkovat prof. Ing. Josefu Štětinovi, Ph.D., který mě dlouhodobě podporoval od počátku doktorského studia a věnoval mi nespočet konzultací ohledně problematiky zpracování oceli a teplotních modelů. Dále chci poděkovat prof. Ing. Františku Kavičkoví, CSc., který byl zakladatelem výzkumu v problematice ocelářství na katedře Termomechaniky. Děkuji RNDr. Pavlu Popelovi, Ph.D., který mě seznámil se světem optimalizace a využití matematického programování v inženýrských úlohách. Můj dík patří rovněž všem dalším kolegům, kteří se mnou na tomto výzkumu spolupracovali, poskytovali mi množství nových podmětů a procházeli se mnou nespočet slepých uliček, zejména tak děkuji doc. Ing. Lubomíru Klimešovi, Ph.D. Z mladších kolegů pak Ing. Michalovi Březinovi a dalším.

# Obsah

<b>1 Úvod</b>	<b>3</b>
1.1 Vývoj průmyslu . . . . .	3
1.2 Ekologická perspektiva . . . . .	4
1.3 Hutnický průmysl . . . . .	6
1.4 Digitální dvojče a jeho význam . . . . .	8
<b>2 Digitalizace zařízení pro plynulé odlévání</b>	<b>10</b>
2.1 Proces výroby oceli . . . . .	10
2.2 Kvalita oceli a faktory, které ji ovlivňují . . . . .	11
2.3 Digitální dvojče ZPO . . . . .	13
2.4 Nelinearity digitálního dvojčete ZPO . . . . .	18
2.5 Validace digitálního dvojčete ZPO . . . . .	20
<b>3 Využití digitálního dvojčete a jeho optimalizace</b>	<b>23</b>
3.1 Optimization of Quality of Continuously Cast Steel Slabs by Using Firefly Algorithm . . . . .	26
3.2 Optimal Control Algorithm for Continuous Casting Process by Using Fuzzy Logic . . . . .	27
3.3 Assessment of Basic Approaches to Numerical Modeling of Phase Change Problems—Accuracy, Efficiency, and Parallel Decomposition . . . . .	29
3.4 High Quality Steel Casting by Using Advanced Mathematical Methods . . .	30
3.5 Comparison of optimization-regulation algorithms for secondary cooling in continuous steel casting . . . . .	31
3.6 Dry cooling as a way toward minimisation of water consumption in the steel industry: A case study for continuous steel casting . . . . .	32
3.7 Reduction of CO <sub>2</sub> Emissions in Steelmaking by Means of Utilization of Steel Plant Waste Heat to Stabilize Seasonal Cooling Water Temperature . . . .	34
3.8 Celé texty článků . . . . .	35
<b>4 Závěr</b>	<b>115</b>
<b>Literatura</b>	<b>118</b>



# Kapitola 1

## Úvod

### 1.1 Vývoj průmyslu

Průmyslovou revoluci lze popsat jako postupnou změnu v hospodářství a průmyslu, kdy díky pokroku ve vědě a technice dojde k zásadní změně v zemědělství, výrobě, těžbě, dopravě a dalších hospodářských sektorech. Zejména se tato změna týká ulehčení náročné práce lidí, snížení nákladů a maximalizaci možných zisků [33].

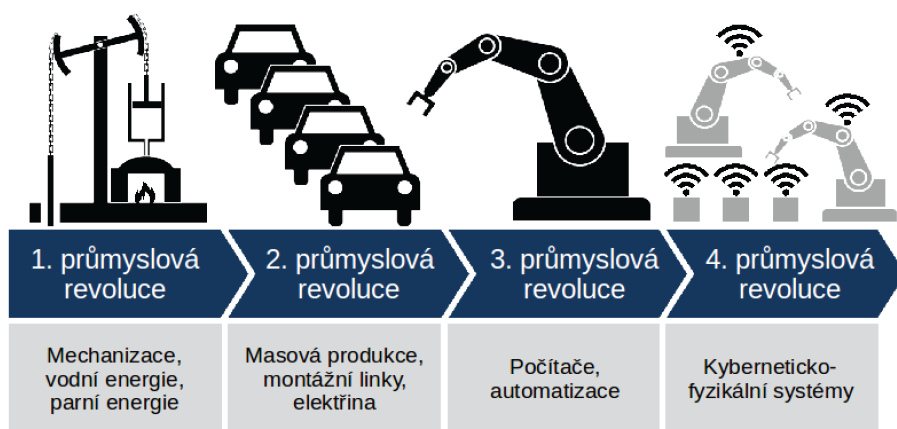
První průmyslová revoluce probíhala v 18. a 19. století, po zdokonalení parního stroje Jamesem Watterem. Začaly se využívat dosud nevyužívané zdroje energie, jako je uhlí, které pro parní stroj zajistilo výrobu páry. Do této doby v hospodářství dominovalo zemědělství, které bylo postupně nahrazováno výrobním průmyslem. Dosud využívaná manufakturní výroba začala být nahrazována strojovou velkovýrobou. Na kvalitu výrobních strojů byly kladeny čím dál tím vyšší požadavky, a tak se neustále rozvíjel i nový obor strojírenství. Protože na výrobu součástek strojů byl využíván kov, pokrok v technice se musel projevit i v hutní výrobě. Vznikly vysoké pece, ve kterých se dosahovalo mnohem vyšších teplot a tavba železné rudy tak byla kvalitnější. Rovněž muselo nutně dojít k velkým změnám v dopravě, kdy koně a povozy již nestačily na dopravu výrobních surovin, což vedlo k vynálezu parní lokomotivy a parní lodi [22].

Druhou průmyslovou revolucí nazýváme období následující po první průmyslové revoluci na konci 19. a na počátku 20. století. Je označována za revoluci technickovědeckou a je zejména spojována s objevem elektrické energie. Mezi zásadní vynálezy lze uvést telefon Alexandera Grahama Bella, žárovku Thomase Alva Edisona, dynamit Alfreda Nobela a díky spalovacímu motoru mohl Henry Ford dát impuls k rozmachu automobilové výroby. Začaly se využívat ve výrobě nové materiály, což přineslo nové výrobní procesy a masovou výrobu zavedením montážních výrobních linek. Druhou průmyslovou revolucí byl ovlivněn rovněž ocelářský průmysl, který musel na novou poptávku reagovat rozmanitější a kvalitnější produkcí oceli [22].

Počátek třetí průmyslové revoluce bývá označován rok 1969, kdy vznikl první paměťový programovatelný logický počítač (zkratka PLC) [54]. Toto období se nese v duchu aplikace informační technologie, elektroniky a automatizace výroby. Od té doby lidstvo pokročilo o další kus kupředu k automatizaci celých výrobních procesů. Jako příklad lze uvést roboty vykonávající naprogramované sekvence operací bez potřeby zásahu člověka. Mezi zásadní objevy patří vznik internetu, bez kterého se dnes již neobejde žádná domácnost [22]. Automatizace a elektronika prostoupila výrobní ocelářské podniky a vedla k výraznému zvýšení produktivity výroby. Tento trend však dostatečně nezachytila produkce oceli ve východním

bloku, kde nedocházelo k obměně investic, což vedlo k zastaralosti strojů a ztrátě konkurenceschopnosti.

V současné době jsme svědky čtvrté průmyslové revoluce označované Průmysl 4.0 (angl. Industry 4.0) spojené s digitalizací a pokročilou automatizací/optimalizací výroby a změnami na pracovním trhu [56]. Koncept Průmyslu 4.0, představeného na veletrhu v Hannoveru v roce 2013, je založen na vytvoření „Chytrých továren“ využívající kyberneticko-fyzikální systémy a jejich komunikaci přes tzv. IoT – Internet of Things, což označuje síť pro decentralizované řízení. V praxi to pak znamená, že zařízení ve výrobním procesu se mohou sama rozhodovat na základě dat, které mají ze senzorů, kamer a cloudového úložiště. Dnešní výrobní proces je spojen s novými metodami strojového učení, autokonfigurace a autodiagnostiky, se kterou může komunikovat vzdálená obsluha přes internet. Dále se budou využívat cloudová úložiště, 3D tisk a chytrá datová centra. Průmyslu 4.0 přinese zánik některých pracovních míst, ale nová zase vzniknou, proto je nutné změnit i systém vzdělávání [11]. Grafické znázornění průmyslových revolucí je zobrazeno na obrázku 1.1.



Obrázek 1.1: Grafické znázornění průmyslových revolucí [8]

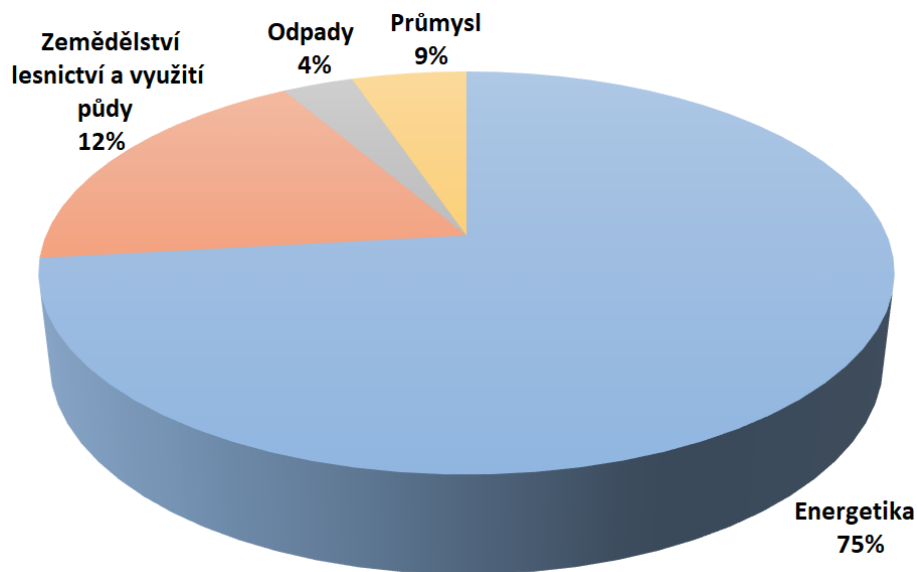
## 1.2 Ekologická perspektiva

Mohutný rozvoj průmyslu však sebou přinesl i řadu pro naši planetu negativních důsledků. Právě průmyslová výroba, na které je současná civilizace v podstatě závislá, je jedním z hlavních znečišťovatelů životního prostředí [11]. Průmysl na jedné straně zabezpečuje ekonomický rozvoj a růst životní úrovně člověka, na straně druhé znehodnocuje kvalitu životního prostředí jak pro sebe, tak pro ostatní organismy, které připravuje o čistý vzduch, vodu a půdu [18]. Na životní prostředí se nebraly žádné ohledy, jeho katastrofální stav byl zlehčován nebo dokonce před veřejností utajován. Koncem 80. let minulého století ale již nebylo pochyb, že se jedná o vážný problém. Po roce 1990 dochází k rozsáhlé transformaci průmyslu, kterou doprovází snižování jeho zátěže na životní prostředí a první environmentální politika. Rovněž se začalo hovořit u účinku tzv. skleníkových plynů, který byl plně vyčíslen v roce 1896 švédským vědcem Svantem Arrheniusem, který provedl první kvantitativní odhad globálního oteplování Termín „skleníkový efekt“ byl poprvé použit švédským meteorologem Nilsem Gustafem Ekholmem v 1901 [17].

Skleníkové plyny vyskytující se v atmosféře země přispívají ke skleníkovému efektu, což je proces, při kterém tyto plyny v atmosféře způsobují ohřívání planety tím, že pohl-



cují dopadající sluneční záření a zároveň brání jeho zpětnému odrazu do vesmíru. Zatím co přirozený skleníkový efekt je rozhodující pro zachování života na Zemi, antropogenní skleníkový efekt způsobený lidskou činností zvyšuje koncentrace zejména oxidu uhličitého (CO<sub>2</sub>) v atmosféře na takovou úroveň, že dochází k postupnému ohřívání planety [27]. Ve 20. století došlo ke zvýšení průměrné teploty o 0,6 °C. V případě, že by došlo ke zvýšení teploty o 2 °C, lze očekávat vážné následky v podobě podstatných změn klimatu. Důsledkem potom může být tání ledovců, zvýšení hladiny oceánů spojené se záplavami, některá místa na planetě by mohli být v budoucnu neobyvatelná v důsledku rozšiřování pouští a bude docházet k vymírání živočišných druhů v oceánech i na souši.



Obrázek 1.2: Globální produkce emisí skleníkových plynů v roce 2020 podle sektoru [52]

V roce 1997 byl přijat Kjótský protokol k Rámcové úmluvě OSN o změně klimatu [27]. Země úmluvy se v protokolu zavázaly do konce prvního kontrolního období (2008 - 2012) snížit emise skleníkových plynů nejméně o 5,2 % ve srovnání s předindustriálním stavem v roce 1990. V prosinci 2012 byl schválen dodatek, kterým bylo potvrzeno pokračování Kjótského protokolu a jeho druhé kontrolní období, které bylo stanoveno na osm let (2013 - 2020). EU a jejích 28 členských států se zavázalo snížit do roku 2020 emise skleníkových plynů o 20 % v porovnání s rokem 1990. Kjótský protokol vstoupil v platnost v roce 2005, více než 7 let po svém vzniku, díky dlouhodobým problémům s jeho ratifikací, kterou muselo podepsat minimálně 55 států. Dokument má od počátku řadu kritiků. Jedni mu vyčítají, že je vzhledem k vynaloženým nákladům neefektivní, jiní jej zase kritizují jako málo ambiciózní. Svého cíle protokol nedosáhl. EU se daří Kjótský protokol plnit, ale podle programu OSN pro životní prostředí z roku 2012 se koncentrace skleníkových plynů od roku 2000 naopak zvýšila asi o 20 % [27].

V návaznosti na Kjótský protokol byla podepsána Pařížská klimatická dohoda [53], která vstoupila v platnost v listopadu 2016. Jejím zásadním cílem je udržení oteplování oproti předindustriálnímu období pod 2 °C. Od roku 2020 pak Kjótský protokol nahrazuje. Signatáři dohody se zavázali, že proto dále výrazně omezí ve svých zemích emise, především oxidu uhličitého. EU se zavázala ke společnému cíli snížit do roku 2030 emise skleníkových plynů o nejméně 40 % ve srovnání s rokem 1990. Evropský parlament si dokonce představuje ještě

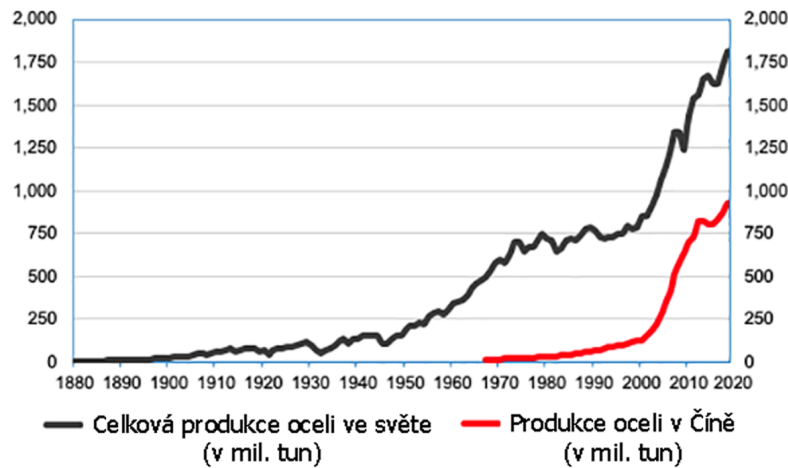
dosáhnout ambicioznější cíl a to redukovat emise do roku 2030 o 60 %. Ekologická představa EU pak spočívá v dosažení uhlíkové neutrality do roku 2050. V roce 2017 od dohody odstoupili USA, což znamená, že bude zapotřebí ještě hodně úsilí a dlouhého politického vyjednávání, aby se efektivně splnily stanovené cíle. Další ránou pro ekologické plány by mohl být válečný konflikt na Ukrajině a budoucí ekologické směřování Ruské federace.

Navrhovaných způsobů na dosažení uhlíkové neutrality do roku 2050 je několik. Mezi ty hlavní patří masivní využívání obnovitelných zdrojů energie, zvýšení energetické účinnosti, obchodování s emisními povolenkami, mechanismus uhlíkového vyrovnání na hranicích (zabránění přesouvání neekologických výrobních procesů do zemí, které mají méně přísné pravidla pro emise skleníkových plynů), elektrifikace automobilové dopravy, konzumace laboratorně pěstěného masa a zalesňování kontinentů [53]. Důležitým ukazatelem je rozložení produkce emisí podle jednotlivých sektorů, obrázek 1.2. Z něj je vidět, že průmyslový sektor je jedním z největších znečišťovatelů životního prostředí. Metody Průmyslu 4.0 by pak synergicky měli přispět k takové optimalizaci výrobních procesů, která bude mít mimo ekonomických zisků i pozitivní vliv na životní prostředí [51].

### 1.3 Hutnický průmysl

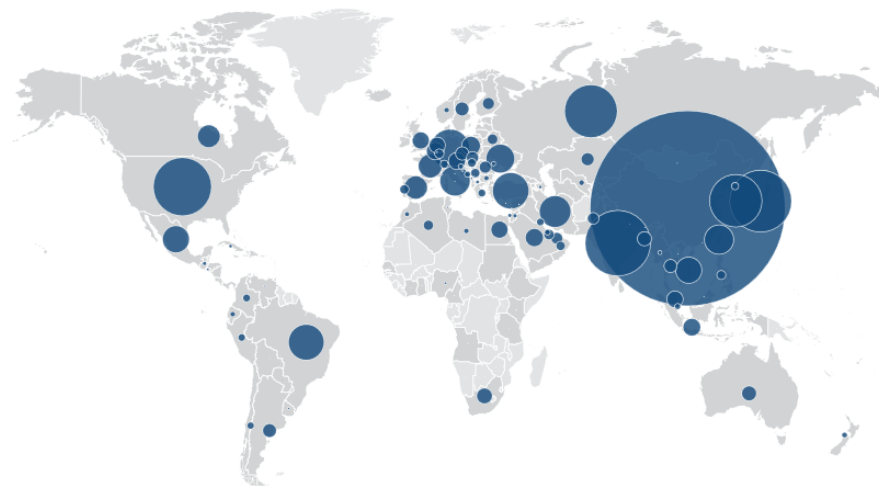
Historie zpracování kovů započala již v době kamenné, kdy lidé nacházeli kov v přírodě, v jeho ryzí formě. Postupně se zdokonalovali v jeho opracování, až byli schopni zpracovat měď, nebo vyrobit bronz a další slitiny barevných kovů. Znamky první výroby železa se datují kolem 3 000 let před naším letopočtem. Kolem roku 1 250 před naším letopočtem pak se výroba železa rozšířila masivněji. Hutnictví pak mělo přímý vliv na pokrok v různých odvětvích hospodářství [7]. Železo se přitom vyrábělo redukcí oxidických rud získaných především díky povrchové těžbě. Jeho výroba byla náročným procesem díky vysokému bodu tání železa (1535 °C) [6]. První vysoké pece, které umožňovaly zpracovávat železo v tekuté formě, jsou na našem území datovány v 16. století. V roce 1855 si Henry Bessemer nechal patentovat své metalurgické zařízení a s ním i proces výroby oceli jako slitiny železa s uhlíkem a dalšími kovovými a nekovovými prvky [4]. Výroba oceli dnes nepředstavuje pouze proces zkujňování, ale složitý pochod výroby železných slitin o předepsaném chemickém složení, případně předepsaných vlastností, kterých se dosahuje řízeným procesem tuhnutí a dalšího metalurgického zpracování. Na počátku 20. století se začala při výrobě oceli uplatňovat i elektrická energie v elektrických obloukových a v indukčních pecích. Hutnictví nadále procházelo dalšími modifikacemi, jako jsou nové vyzdívky konvertoru, oxidaci, proces legování, technologie plynulého odlévání nahrazující neekonomické lití ingotů do kokil a proces teplého a studeného válcování. Dnes existuje více než 2 000 různých druhů ocelí s přesně definovaným složením a mechanickými vlastnostmi, jako je pevnost, tvrdost, chemická odolnost, které jsou široce používány v průmyslu, stavebnictví a v dalších odvětvích [4].

Ocel dnes patří mezi základní materiály, ovlivňující každý aspekt lidského života. Spotřeba oceli na jednoho obyvatele je důležitým indexem společenského rozvoje [74]. Světová produkce oceli od roku 1900 do roku 2020 je zachycena v grafu 1.3. Z grafu je patrný neustálý rostoucí trend, způsobený stále větší poptávkou po této surovině. Na druhou stranu je ocelářský průmysl energeticky náročným procesem a jedním z největších výrobců skleníkových plynů, v roce 2020 produkoval 3 miliony tun CO<sub>2</sub> a tvořil přes 7 % celosvětové produkce CO<sub>2</sub> [58]. Je tedy zřejmé, že tyto dva ukazatele jdou proti sobě a je nutné hledat možnosti, jak výrobu této suroviny co nejvíce ekologizovat.



Obrázek 1.3: Světový vývoj produkce oceli [73]

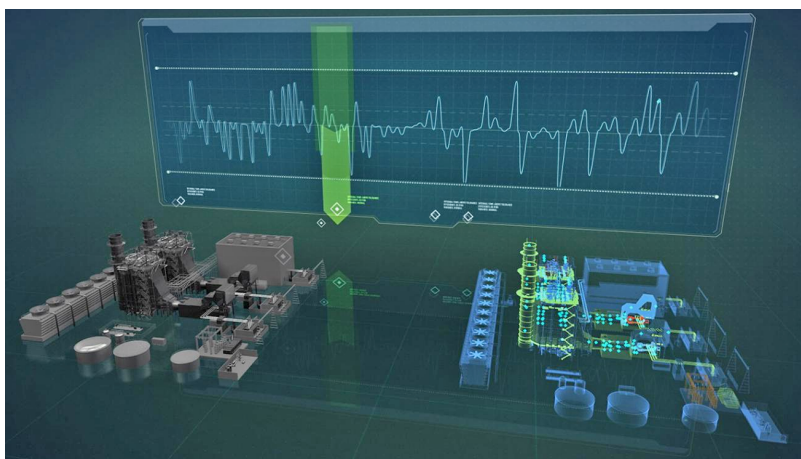
Výroba oceli je zejména orientovaná do zemí, jako je Čína (53,3% v roce 2020) a Indie (obrázek 1.4) [73], kde zatím nejsou striktní emisní limity v porovnání se západními zeměmi. Přesto, že je Čína největším emitentem skleníkových plynů na světě (cca. 29,7%), předsevzala si za cíl dosáhnout uhlíkové neutrality do roku 2060. Ke splnění tohoto cíle však budou muset proběhnout velké transformace zejména v energetice a těžkém průmyslu, který je v Číně soustředěn. Jednou z transformací hutní výroby by mělo být zapojení metod Průmyslu 4.0, čímž by došlo jak ke snížení emisí skleníkových plynů, tak ke snížení výrobních nákladů, což je jediná možnost pro oceláře jak si udržet svoji konkurenceschopnost na trhu, zvláště v dnešní době, kdy dramaticky zdražují základní vstupní suroviny a tlačí tak cenu oceli radikálně nahoru (v roce 2021 o 20-30%).



Obrázek 1.4: Koncentrace světové produkce oceli [73]

## 1.4 Digitální dvojče a jeho význam

Vývoj výpočetní techniky umožňuje tvorbu stále dokonalejších digitálních replik reálných výrobních zařízení tzv. digitálních dvojčat [39]. Taková virtuální replika pak funguje jako systém pro podporu lidského rozhodování a pomáhá např. odhalit různé výrobní chyby, nalézt úzká místa procesu, optimálně reagovat na nestandardní/poruchové výrobní situace, a to nejen při provozu, ale dokonce v předstihu, než se dané zařízení do provozu uvede. Digitální dvojče může rovněž sloužit k trénování operačního personálu, nebo být využito pro optimalizaci výrobního procesu ve smyslu zvýšení produktivity výroby, plánování údržby či zkrácení doby zprovoznění nových výrobních linek. Soubor těchto digitálních dvojčat pak můžeme nazvat virtuální továrnou [39].



Obrázek 1.5: Grafické znázornění digitálního a reálného dvojčete [39]

Digitální transformaci podstupují všechny obory, přičemž průmyslová výroba a logistika se v přijímání nových technologií zařazují na přední příčky, a to především z důvodu maximalizace produktivity, kvality a variability produktů a služeb, stejně jako přidané hodnoty, kterou podniky dokážou generovat. Mezi technologie, jež nabývají stále většího významu v éře kyberprůmyslu a inteligentní logistiky, se zařazuje i technologie digitálního dvojčete, který umožňuje neustále na dálku monitorovat stav skutečného objektu, jakož i simulovat různé situace s přesnými a reálnými daty. Podle studie mezinárodní analytické společnosti Gartner [20] již 75 % podniků využívá inteligentní řešení a implementuje technologii digitálního dvojčete nebo to plánuje udělat v rámci jednoho roku. Digitální dvojče se tak dostává do základního inventáře průmyslu a podniků digitálního věku spolu s internetem věcí (IoT) [13], velkými daty (Big Data) [10] a strojovou inteligencí (Machine Intelligence) [50]. Přestože pojem digitálního dvojčete se dostal do širšího povědomí až v roce 2002, kdy ho Michael Grieves definoval v souvislosti s řízením životního cyklu výrobku, jeho koncept předcházet éru Průmyslu 4.0 [21], jeho kořeny sahají do sedmdesátých let, kdy NASA pracovala na projektu Apollo. Nicméně nasazení přesných virtuálních kopií, které by dokázaly zpracovávat informace v reálném čase a navíc proces optimalizovat, bránil výpočetní výkon. Dnes se nacházíme v situaci, kdy se dá do značné míry tvrdit, že zajistit potřebný výpočetní výkon již není problém a tudíž mohou vznikat propojené digitální uzly simulující celou výrobní továrnu (Smart Factory). Využití digitálního dvojčete se označuje za paradigmatický posun, neboť konvenční metody již nedokážou vyhovět náročným požadavkům projektů nové generace. A totéž se vztahuje i na výrobní a logistické procesy, tradiční technologie

a metody, které jsou již nedostatečné pro zabezpečení udržitelného růstu a nemohou tak vyhovovat novým požadavkům, od optimalizace nákladů až po spotřebitelskou kustomizaci v masové výrobě.

V současnosti je pojem digitální dvojče chápán především jako virtuální reprezentace fyzických objektů, výrobních a přepravních zařízení, ale také procesů, systémů, pracovníků nebo celého prostředí. Digitální dvojče tak již není pouze virtuální model reálného protějšku, ale dynamický nositel dat a stavových informací získaných prostřednictvím množství senzorů a snímačů propojených internetem věcí [39]. Digitální dvojče v této podobě tedy slouží k monitorování fyzických objektů a procesů v reálném prostoru a čase, jelikož tato technologie umožňuje vytvářet velmi detailní digitální obraz se skutečnými daty (viz obrázek 1.5). V komplexních simulačních modelech dvojče zrychluje a ulehčuje rozhodovací procesy, usnadňuje přímou identifikaci možných následků a zvažovaných změn, jakož i klíčových vzorců chování v jednotlivých procesech. Tato forma implementace přináší hlubší poznatky chování jednotlivých složek v procesech, ale i schopnost odhalovat slabá místa provozu, která je nutné stabilizovat a optimalizovat, aby došlo k udržitelnému nárůstu výkonnosti procesů a k posílení robustnosti prostředí [61]. Nově vznikla i aktivní forma digitálního dvojčete, která disponuje řídicí funkcionalitou a dokáže provádět zadaný úkol bez přímé lidské obsluhy v podobě umělé inteligence [39].

Technologie digitálního dvojčete navíc má všestranný potenciál nejen pro dynamické a autonomní řízení výrobních podniků a inteligentní průmysl, ale její funkčnost dnes již proniká do oblasti zdravotní péče, projektování, maloobchodu, údržby a v neposlední řadě i do digitální transformace měst (Smart City) [2]. Ústřední postavení digitálního dvojčete vyplývá i z jeho organického provázání s ostatními technologiemi, jako jsou internet věcí a služeb, umělá inteligence, strojové učení nebo rozšířená analytika a zpracování velkých dat.

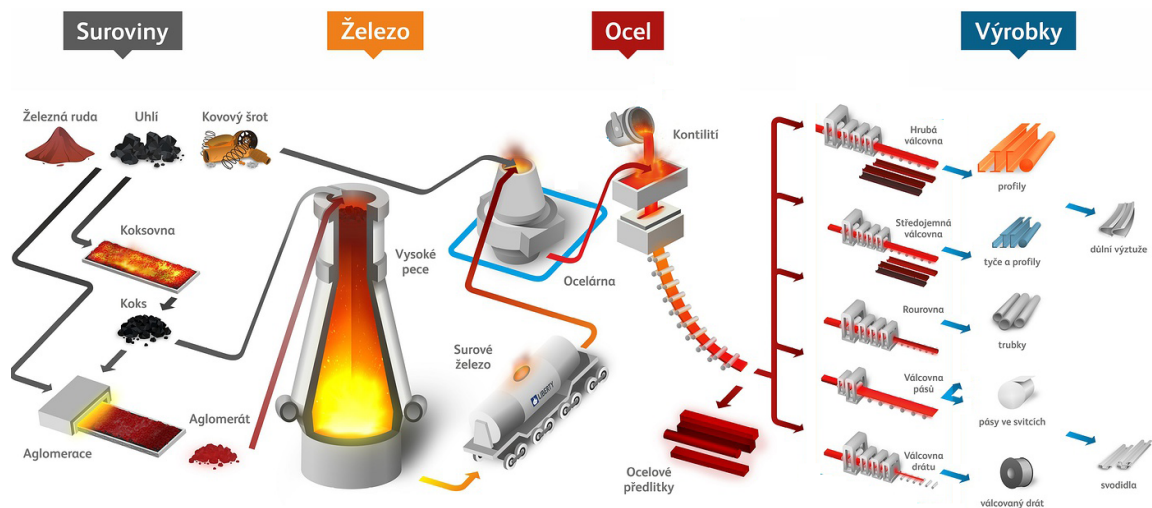
V kontextu předchozích kapitol lze konstatovat, že digitální dvojče je jedna z metod Průmyslu 4.0, která by měla přispět k transformaci a optimalizaci hutních procesů, tak aby tyto provozy byly ekonomičtější, ekologičtější a energeticky efektivnější. Toto je pak nosné téma habilitační práce, tedy vytvoření digitálního obrazu reálného hutního provozu, který je verifikován a nad kterým je vytvořen optimalizační modul na hledání parametrů pro zvýšení ekonomičnosti a ekologičnosti procesu. Práce je vystavěna na přiložených autorových článcích uvedených v kapitole 3 a seznamu literatury [9], [37], [41] - [45].

## Kapitola 2

# Digitalizace zařízení pro plynulé odlévání

### 2.1 Proces výroby oceli

Na začátku výroby oceli je surové železo, které se vyrábí ve vysoké peci z železné rudy za pomoci koksu, vápence a dalších přísad [4], [6]. Ocel se vyrábí zkujňováním surového železa s přísadou ocelového šrotu anebo pouze z ocelového šrotu v obloukových pecích. V první fázi se snižuje obsah uhlíku a odstraňují se nežádoucí prvky pomocí oxidace. Druhá fáze se nazývá rafinace, kdy se z oceli odstraňuje přebytečný kyslík pomocí feroslitin manganu a křemíku nebo pomocí hliníku. Nakonec se ocel odsiřuje. Tekutá ocel je pak v pánvích (s kapacitou 50 - 250 tun) převážena do zařízení na plynulé odlévání (ZPO) [6]. Zde se lije do tzv. mezipánve, s regulovanou výpustí. Z mezipánve je ocel přiváděna do vodou chlazené měděné formy tzv. krystalizátoru. Hlavní funkce mezipánve spočívá v udržení konstantní hladiny oceli v krystalizátoru a zajištění nepřerušovaného lití po dobu výměny pánve. Má rovněž zásadní vliv na kvalitu a čistotu oceli. Krystalizátor tvoří primární zónu chlazení ZPO, kde vzniká pevná skořepina schopna udržet tekuté jádro při vstupu do sekundární chladicí zóny. Mezi stěny krystalizátoru a tekutou ocel je přiváděn licí prášek [67], který zabraňuje oxidaci oceli a jejímu přichytávání na stěny krystalizátoru. Tomu rovněž zabraňuje jeho oscilace. Tvar krystalizátoru pak určuje tvar a velikost ocelového polotovaru. Sekundární zóna ZPO je tvořena soustavou chladících trysek a vodících válců. Vzhledem k požadavkům na vysokou produktivitu výroby, která je přímo úměrná licí rychlosti, musí sekundární chlazení dokončit tuhnutí tekutého jádra před místem řezání. Ocel dále pokračuje do terciální chladicí zóny, kde probíhá její chlazení formou přirozené konvekce a radiace. Na konci terciální zóny je pálicí zařízení, které dělí proud oceli podle typu ZPO a podle odlévaného profilu obdélníkového/čtvercové/válcového na jednotlivé bramy/sochory/válce [4], [6]. Ocelový polotovar za pálicím strojem nazýváme společným názvem předlitek. Podle druhu těchto ocelových produktů může následovat teplá válcovna, studená válcovna, proces žíhání, proces kalení, proces tažení a povrchové úpravy jako je např. zinkování. Schéma výroby oceli je na obrázku 2.1.



Obrázek 2.1: Schéma výroby oceli [65]

## 2.2 Kvalita oceli a faktory, které ji ovlivňují

Z pohledu kvality oceli je na ZPO rozhodující ta jeho část, ve které dochází ke změně skupenství kapalného (taveniny) na pevné [67]. Předlitek jak je nazýván ocelový polotovár určený k dalšímu zpracování prochází při průchodu ZPO velkými teplotními a mechanickými změnami. Nadměrné chlazení v zóně sekundárního chlazení může snížit povrchové teploty a umožnit zvýšení licí rychlosti, avšak může rovněž způsobit velké teplotní napětí na povrchu předlitku a tím inicializovat vznik trhlin [4]. Odvod tepla stěnami krystalizátoru, jeho oscilace a použití různých licích prášků má také významný vliv na kvalitu předlitku [6]. ZPO je rovněž z pohledu řízení nejsložitějším zařízením ve výrobním řetězci produkce oceli, přičemž podíl plynule lité oceli ve světě přesahuje 97 % [57]. Z pohledu kvality ocelového produktu vychází nejlépe gravitační (vertikální) lití, nejčastěji se však kvůli rozměrům ZPO používá radiální ZPO [6], ve kterém se předlitek v určité části ZPO zakřivuje a následně zase rovná, což může způsobovat z pohledu mechanického napětí vznik dalších trhlin a prasklin.

V procesu výroby oceli jsou z pohledu ekonomických i ekologických zásadní dva ukazatele a to kvalita finálního výrobku a produktivita výroby. Tyto dva ukazatele však jdou do jisté míry proti sobě. Z pohledu produktivity výroby oceli je právě licí rychlost ZPO hlavním určujícím faktorem, který udává rychlost ve všech předchozích i navazujících operacích [14]. Dá se říci, že z pohledu průchodu oceli celým výrobním řetězcem je ZPO úzkým místem. Z ekologického hlediska zvýšení produktivity zpracování oceli může vést ke snížení emisí skleníkových plynů. Z pohledu procesu tuhnutí oceli však má licí rychlost zásadní vliv (tedy ovlivňuje výslednou kvalitu oceli) a její navyšování bez dalších informací o kvalitě a rovněž bezpečnosti procesu není možné.

Z pohledu kvality výsledného ocelového produktu-předlitku je právě optimální nastavení ZPO zcela zásadní. Kvalita je zákazníky posuzována dle vlastností v pevném stavu, a to vlastností mechanických (pevnost, tažnost, mez kluzu, atd.), fyzikálních (hustota, pružnost, součinitel tepelné vodivosti, atd.), chemických (korozivzdornost, odolnost v sirovodíkovém prostředí, atd.) či technologických (svařitelnost, prokalitelnost, atd.). Dosažení požadované kvality je však pro výrobce složité, protože musí tyto vlastnosti predikovat na základě mě-

řených technologických veličin a materiálu v litém stavu [67]. Kvalitu ocelového polotovaru určuje především charakter její makrostruktury a výskyt jejích vad. Požadovaná čistota materiálu potom znamená absenci nebo minimalizaci nekovových vměstků v materiálu [15]. Dalším parametrem ovlivňujícím koncovou kvalitu předlitku je chemické složení oceli. To však lze ještě ovlivnit přidáváním příměsí v mezipánvi před zalitím krystalizátoru [6], při průchodu proudy strojem již nikoli. Při lití oceli na ZPO vystupuje celá řada technologií, které finální kvalitu ovlivňují. Mezi tyto technologie patří:

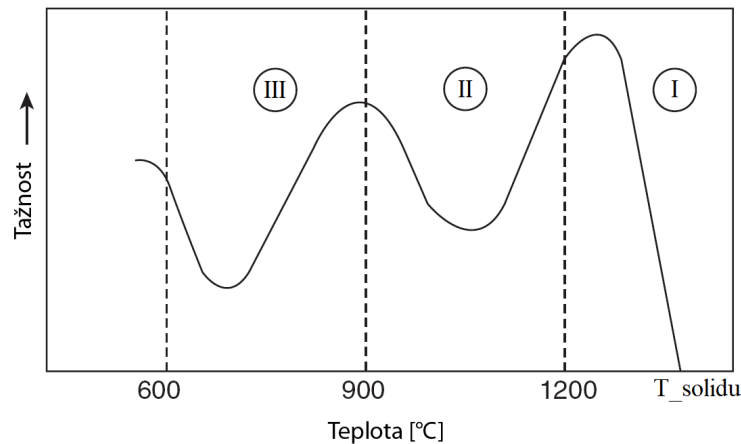
- zpracování oceli v mezipánvi (mezipánvová metalurgie),
- elektromagnetické míchání oceli (především u sochorů),
- elektromagnetická brzda,
- protiprůvalové systémy,
- technologie oscilací krystalizátoru,
- automatizace řízení,
- aplikace teplotních modelů,
- systémy predikce kvality předlitku.

V dnešní době jsou tyto technologie řízeny počítačově a jsou doplněny algoritmy pro podporu lidského rozhodování [57]. Např. protiprůvalové systémy mohou být opatřeny neuronovými algoritmy, které mají za úkol rozpoznat hrozbu průvalu s vysokou pravděpodobností.

Ukazatelem nedodržení kvality oceli je tvorba trhlin, jejich tvar a jejich počet [19]. Tvorba trhlin souvisí s tzv. tažností, která charakterizuje plastické vlastnosti materiálu a představuje trvalou relativní deformaci [68]. Lze jí definovat jako schopnost oceli po překročení meze kluzu se prodlužovat, aniž by docházelo k výraznému nárůstu napětí [62]. Tažnost oceli za vyšších teplot je obvykle měřena tahovou zkouškou provedenou na ohříváním vzorku, mnohdy vyrobeném přímo z plynule odlitého předlitku, která se provádí v inertní atmosféře až do lomu. Obecně jsou pozorovány tři identifikovatelné oblasti teplot (obrázek 2.2), ve kterých má ocel sníženou tažnost a je proto náchylná k tvorbě trhlin:

- První se nachází pod teplotou solidu v intervalu 40 - 70 °C. S výjimkou příčných povrchových trhlin se téměř všechny trhliny v předlitcích tvoří v této vysokoteplotní zóně nízké tažnosti. Poznatek, že se při plynulém odlévání oceli téměř všechny podélné trhliny tvoří ve známém teplotním intervalu, je velmi důležitý. Ze znalosti rozložení teplot v předlitku plyne, že všechny povrchové podélné trhliny se tvoří především v krystalizátoru, kdežto podpovrchové trhliny se tvoří pod krystalizátorem, kde je tloušťka ztuhlé skořepiny silnější [19].
- Druhá zóna nízké tažnosti se objevuje v rozsahu teplot 800 - 1200 °C. Tato ztráta tažnosti významně závisí na poměrném obsahu manganu a síry a na teplotní historii oceli. Nepotvrdilo se však, že by tato nízká tažnost, která je výsledkem precipitace sulfidů na hranicích zrn, významně přispívala k tvorbě trhlin při plynulém odlévání oceli [15].
- Třetí zóna nízké tažnosti se nalézá v teplotním rozsahu 700 - 900 °C a je důležitým faktorem při tvorbě příčných trhlin. Tažnost v tomto teplotním rozsahu je snižována rostoucím obsahem hliníku, dusíku, niobu a vanadu. Ztráta tažnosti je v tomto případě spojena s vylučováním nitridů a karbonitridů na hranicích zrn [15].





Obrázek 2.2: Oblasti snížené tažnosti oceli [68]

Ocel, u níž by bylo možno očekávat, že bude za vysokých teplot tažná, je ve skutečnosti značně náchylná k tvorbě trhlin. Má-li být zabráněno tvorbě trhlin, je potřeba pečlivě sledovat teplotní průběhy během lití oceli a nastavit podle toho parametry ZPO [25]. Přestože je plynulé lití je proces dynamický, právě teplotní stabilita procesu je pro výslednou kvalitu oceli zásadní. Tato skutečnost je autorem zpracována v kapitole 3.4 [43], kde je statisticky sledován vliv teplotních průběhů na povrchu předlitku a vznik souvisejících vad. Pro jejich minimalizaci pak digitální dvojče spolu s optimalizačním algoritmem navrhuje nové nastavení intenzity chlazení, tak aby byla i pro rozdílné rychlosti lití zachována požadovaná teplotní stabilita.

### 2.3 Digitální dvojče ZPO

Jak vyplývá z výše uvedeného textu, je pro dosažení kvalitního ocelového produktu a zároveň dosažení co nejvyšší produktivity výroby nutné mít optimálně nastaveny všechny parametry lití na ZPO. Hledat tyto parametry na základě měření povrchových teplot a materiálových analýz odlitých polotovárů není při množství odlévaných ocelových značek reálné. To je důvod, proč se celá řada autorů snaží vytvořit co nejvěrnější digitální kopii reálného lícího provozu, na které je možné zkoušet různé lící scénáře a vypracovávat různé parametrické studie [1], [5], [23], [24], [28], [40], [55], [71]. Rovněž je od těchto virtuálních dvojčat požadováno, aby byly schopny v reálném čase zaznamenávat parametry lití, zejména informace o teplotním poli [69]. Aby však bylo možné mít digitální dvojče ZPO, které je schopné pracovat v reálném čase, resp. rychleji, je nutné si uvědomit, že proces plynulého lití je ovlivněn celou řadou níže uvedených parametrů:

- kompletní turbulentní přechodový tok v krystalizátoru,
- termodynamické reakce mezi lícím práškem a tuhoucím předlitkem,
- přenos tepla mezi tekutým a pevným práškem na povrchu krystalizátoru,
- dynamický pohyb tekuté oceli uvnitř krystalizátoru na rozhraní mushy zóny a tekuté fáze, včetně vlivu gravitace, oscilací a rychlosti odlévání,
- přenos tepla v přehřáté tavenině s ohledem na turbulentní proudění,

- přechodové (směsné) složení oceli při změně jakosti oceli,
- tepelná a mechanická interakce v oblasti hladiny oceli mezi tuhnoucím, pevným licím práškem a tekutou ocelí,
- přenos tepla z povrchu ztuhlé skořepiny do prostoru mezi skořepinou a pracovní plochou krystalizátoru (včetně vrstev licího prášku a vzduchové mezery),
- přenos licího prášku během jeho svislého pohybu mezerou mezi skořepinou a krystalizátorem,
- kontakt ztuhlé vrstvy s formovacími a podpůrnými válci,
- výskyt krystalů uvnitř taveniny,
- proces mikrosegregace a makrosegregace,
- výskyt smršťování v důsledku teplotního smrštění oceli a inicializace vnitřního napětí,
- výskyt napětí a deformace v ztuhlé skořepině v důsledku vnějších vlivů, jako je tření uvnitř krystalizátoru, vyboulení mezi vodícími válci, válcování, teplotní napětí a deformace,
- výskyt trhlin v důsledku vnitřního napětí,
- tok oceli v důsledku elektromagnetického míchání a vliv míchání na teplotní pole a primární strukturu,
- výskyt napětí a napětí v důsledku uvolnění (odlehčení vnější síly),
- tepelné záření,
- vodní a vodovzdušné chlazení.

S ohledem na složitost procesu lití včetně výše uvedených faktorů není možné, ani při dnešních výpočetních výkonech, vyvinout matematický model, který by zahrnoval všechny vlivy a byl schopen výpočtu v reálném čase. Jednotlivé faktory lze seskupit podle tří hlavních vlivů: přenosu tepla a hmoty, mechanických jevů a strukturních jevů. Primární a rozhodující je vliv přenosu tepla a hmoty, protože je to právě teplotní pole, které vede k mechanickým a strukturálním změnám [4]. Předkládané digitální dvojčte představuje komplexní matematicko-numerický model ZPO, který je schopen výpočtů přesahující reálný čas, je dlouhodobě validovaný na několika reálných provozech, je opatřen uživatelským rozhraním a jeho součástí je optimalizační algoritmus pro nalezení optimálních licích parametrů, viz kapitola 3.2 [42].

Matematicky lze model přenosu tepla se změnou fáze a přenosu hmoty ve směru lití popsat Fourierovou-Kirghoffovou rovnicí [4], [32]

$$\frac{\partial (h\rho(T))}{\partial \tau} + v_{cast} \frac{\partial (h\rho(T))}{\partial z} = \nabla \cdot [\lambda_{eff}(T) \nabla T], \quad (2.1)$$

kde  $\nabla \equiv \left( \frac{\partial}{\partial x}, \frac{\partial}{\partial y}, \frac{\partial}{\partial z} \right)$  je nabla operátor,  $h$  [J/kg] je měrná entalpie,  $\rho$  [kg/m<sup>3</sup>] je hustota,  $\tau$  [s] je čas,  $v_{cast}$  [m/s] je licí rychlost,  $z$  [m] je souřadnice ve směru lití,  $\lambda_{eff}$  [W/mK] je efektivní tepelná vodivost zahrnující složku konvekce a  $T$  [°C (K)] je teplota. Výsledkem

řešení rovnice je teplota jako funkce času a polohy, tedy  $T(x, y, z, \tau)$ . Vztah mezi entalpií a teplotou je potom vyjádřen vztahem [49]

$$h = \int_0^T \left( c(\zeta) - L \frac{\partial f_s}{\partial \zeta} \right) d\zeta, \quad (2.2)$$

kde  $L$  [J/kg] je latentní teplo skupenské nebo strukturální přeměny a  $f_s$  [0-1] je tzv. podíl tuhé fáze, kde pro  $f_s = 0$  je element ve stavu tekutém (kapalném), pro  $f_s = 1$  je ve stavu tuhém a při  $0 < f_s < 1$  se element nachází v tzv. mushy zóně (směs tuhé a tekuté fáze).

Modelování konvekce tekuté taveniny je komplexní úlohou, které je často řešeno pomocí CFD metod [67]. S tímto přístupem by však nebyl možný výpočet v reálném čase a proto se složka konvekce taveniny zahrnuje v hodnotě teplotní vodivosti. Existuje několik postupů jak určit hodnotu efektivní vodivosti. Např. podle vzdálenosti od hladiny oceli v krystalizátoru lze psát podle [79]

$$\lambda_{eff} = \begin{cases} \lambda & \text{pro } T \leq T_S \\ 4\lambda + \frac{3\lambda(T-T_L)}{T_{casting}-T_L} & \text{pro } T \geq T_L \wedge 0 \leq z \leq 1 \text{ m} \\ \lambda + \frac{3\lambda(T-T_S)}{T_L-T_S} & \text{pro } T_L \geq T \geq T_S \wedge 0 \leq z \leq 1 \text{ m} \\ \lambda + \frac{\lambda(T-T_L)}{T_{casting}-T_L} & \text{pro } T \geq T_L \wedge 1 \leq z \leq 3 \text{ m} \\ \lambda & \text{pro } z \geq 3 \text{ m.} \end{cases} \quad (2.3)$$

Vždy je potřeba podle geometrie ZPO volit tyto koeficienty (zejména vzdálenosti od hladiny krystalizátoru) a nalézt je v rámci validace modelu.

Řešení rovnic (2.1) - (2.3) je závislé na fyzikálních podmínkách na okrajích média a na podmínkách, při kterých se médium nachází v počátečním čase výpočtu. Počáteční podmínka se dá charakterizovat vztahem [32]

$$T(x, y, z, \tau = 0) = T_p(x, y, z), \quad (2.4)$$

který popisuje rozložení teploty napříč výpočetní doménou. V případě simulace stacionárního stavu lze často zadat konstantní teplotu v celé doméně na hodnotě která je rovna lici teplotě  $T_p(x, y, z) = T_{casting}$ . V případě simulace dynamických změn je nutné zadávat počáteční podmínku z již předem vypočteného teplotního stavu.

Okrajové podmínky pro výpočet teplotního pole předlitku jsou popsány rovnicemi podle jednotlivých chladících zón [43]

$$\begin{aligned} T(x, y, z) |_{z=0} &= T_{casting} && \text{hladina oceli (na začátku ZPO)} \\ -\lambda \frac{\partial T}{\partial n} &= 0 && \text{rovina symetrie a v místě konce ZPO} \\ -\lambda \frac{\partial T}{\partial n} &= \dot{q}_{mold} = \frac{\dot{m}_w c_w (T_{in} - T_{out})}{S_{mold}} && \text{v krystalizátoru} \\ -\lambda \frac{\partial T}{\partial n} &= \dot{q}_{roll} = \frac{\pi (l_{roll}/2) d_{roll} htc_{roll} (T_{roll} - T_{amb}) + \sigma \varepsilon (T_{roll}^4 - T_{amb}^4)}{S_{roll}} && \text{pod válcem} \\ -\lambda \frac{\partial T}{\partial n} &= htc (T - T_w) + \sigma \varepsilon (T^4 - T_w^4) && \text{v místě ostříku chlací tryskou} \\ -\lambda \frac{\partial T}{\partial n} &= 0,84 (T - T_{amb})^{4/3} + \sigma \varepsilon (T^4 - T_w^4) && \text{v terciární zóně} \end{aligned} \quad (2.5)$$

kde  $\dot{q}_{mold}$  [W/m<sup>2</sup>] a  $\dot{q}_{roll}$  [W/m<sup>2</sup>] je měrný tepelný tok do krystalizátoru resp. do vodícího válce,  $S_{mold}$  [m<sup>2</sup>] je plocha krystalizátoru,  $S_{roll}$  [m<sup>2</sup>] je plocha válce,  $l_{roll}$  [m] a  $d_{roll}$  [m] je délka a průměr válce,  $\dot{m}_w$  [kg/s] a  $c_w$  [W/kgK] je hmotnostní tok chladicí vody v krystalizátoru a měrná tepelná kapacita chladicí vody,  $htc$  [W/m<sup>2</sup>K] je součinitel přestupu tepla pod chladicí tryskou,  $htc_{roll}$  [W/m<sup>2</sup>K] je součinitel přestupu tepla z vodícího válce do okolí,  $\sigma$  [W/m<sup>2</sup>K<sup>4</sup>] je Stefanova–Boltzmannova konstanta,  $\varepsilon$  [-] je emisivita povrchu a teploty  $T_{in}$ ,  $T_{out}$ ,  $T_{roll}$ ,  $T_{amb}$ ,  $T_w$  [°C (K)] jsou teploty vstupní a výstupní vody do krystalizátoru, teplota na povrchu válce, teplota okolí a teplota chladicí vody vycházející z chladicí trysky v sekundární chladicí zóně, viz kapitola 3.2 [42].

Rovnice (2.1) - (2.5) nejsou analyticky řešitelné, proto je třeba použít numerického řešení [32]. Existuje několik numerických schémat, které jsou ze své podstaty buď explicitní nebo implicitní, či kombinace obou. Protože jde o problém nelineární (více o nelinearitě systému v kapitole 2.4), není možné použití prosté implicitní numerického schéma, které by nebylo doplněno o vnitřní iterace. Využívá se tak semiimplicitních numerických schémat. Autorova literatura uvedená v kapitole 3.3 [41] se věnuje porovnání několika numerických schémat, pro řešení úloh s fázovou změnou z hlediska robustnosti, přesnosti a paralelizovatelnosti. Z výsledků je zřejmé, že dnešní masivní paralelizovatelnost, tedy možnost výpočtů na grafických kartách GPU, jednoznačně upřednostňuje explicitní numerická schémata, která jsou pro tento druh paralelizace vhodná. Explicitní diskreditací rovnice (2.1) dostaneme [12], [47]

$$h_{i,j,k}^{n+1} \rho_{i,j,k}^{n+1} = h_{i,j,k}^n \rho_{i,j,k}^n + \Delta\tau \left[ \dot{Q}_x + \dot{Q}_y + \dot{Q}_z \right] - \Delta\tau v_{cast} \frac{h_{i,j,k+1}^n \rho_{i,j,k+1}^n - h_{i,j,k}^n \rho_{i,j,k}^n}{\Delta z_{k-1}}, \quad (2.6)$$

kde  $\dot{Q}_x$ ,  $\dot{Q}_y$ ,  $\dot{Q}_z$  jsou tepelné toky, které lze rozepsat

$$\dot{Q}_\psi = 2 \frac{\left( \frac{0,5}{\lambda_{\xi+1}^n} + \frac{0,5}{\lambda_\xi^n} \right)^{-1} \frac{T_{\xi+1}^n - T_\xi^n}{\Delta\psi_\xi} - \left( \frac{0,5}{\lambda_{\xi-1}^n} + \frac{0,5}{\lambda_\xi^n} \right)^{-1} \frac{T_\xi^n - T_{\xi-1}^n}{\Delta\psi_{\xi-1}}}{\Delta\psi_\xi + \Delta\psi_{\xi-1}}, \quad \begin{aligned} \psi &\in \{x, y, z\}, \\ \xi &\in \{i, j, k\}. \end{aligned} \quad (2.7)$$

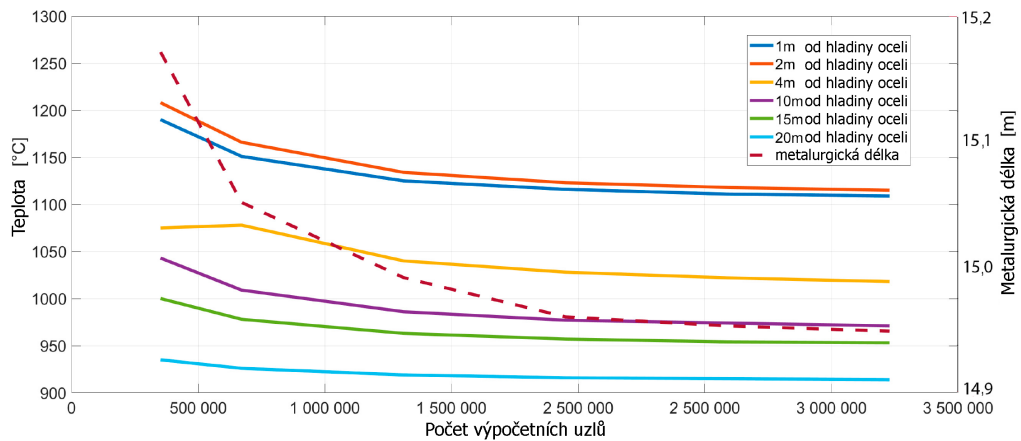
Index  $n$  značí aktuální časový krok, index  $n + 1$  krok následující. Délka časového kroku je potom  $\Delta\tau$ . V kartézských souřadnicích  $x, y, z$  indexy  $i, k, j$  označují obecný uzel výpočetní sítě.

Podmínka stability omezující délku časového kroku v závislosti na délce kroku prostorového je dána vztahem [12], [47]

$$\Delta\tau \leq \frac{1}{\left( \frac{2\lambda(T)}{\rho(T)c(T)} \right) + \left( \sum \psi \frac{1}{\psi^2} \right) + \frac{v_{cast}}{\Delta z}}, \quad \psi \in \{x, y, z\}. \quad (2.8)$$

Z důvodu rychlosti a přesnosti výpočtu není rozložení výpočetní sítě ekvidistantní ve všech směrech. Lokální zjemnění je nastaveno na povrchu předlitku, kde dochází k velkým teplotním gradientům. Ve směru lití je síť také zjemněna zejména v oblastech, kde dochází ke kontaktu povrchu s chladicí tryskou, viz kapitola 3.2 [42]. Test nezávislosti sítě pro výpočet teplot na bramovém ZPO ukazuje, že numerický model by měl mít nejméně 2 500 000 výpočetních uzlů, jak znázorňuje obrázek 2.3. Lze na něm vidět, jak se mění povrchové teploty se změnou sítě a jak se mění hodnota metalurgické délky (tj. vzdálenosti místa posledního ztuhnutí taveniny v předlitku od hladiny taveniny v krystalizátoru). Používání jednoduchých modelů s hrubou výpočetní sítí by vedlo k velice nepřesným výsledkům.

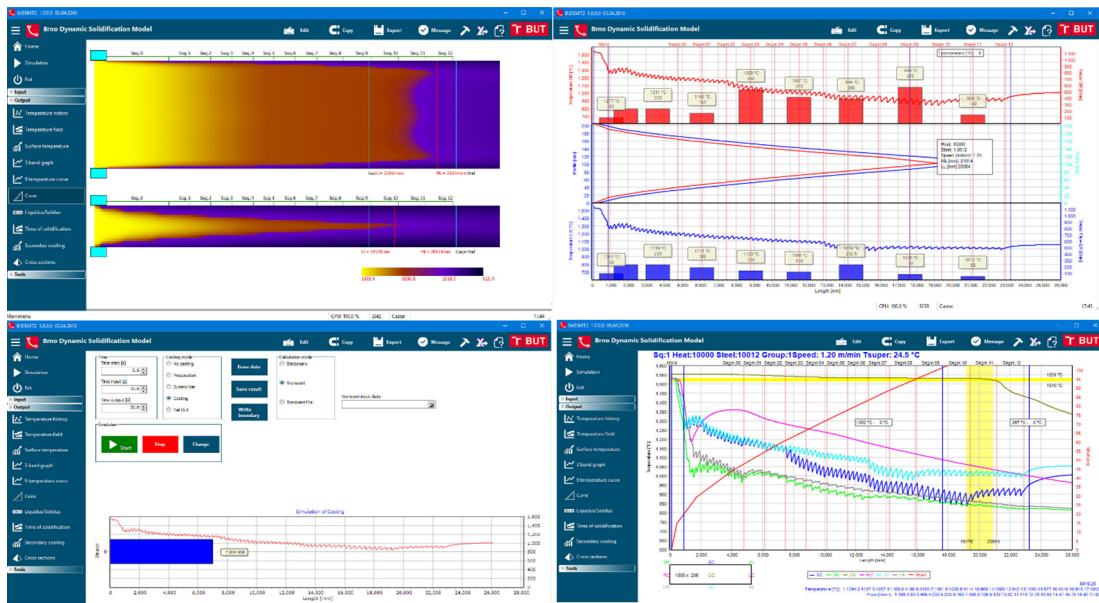
Výpočetní jádro předkládaného digitálního dvojčete umožňuje výpočty jak na jednom tak na více výpočetních jádrech. Cyklus přes prostorovou doménu (rovnice (2.6)) je rozdělen



Obrázek 2.3: Stabilita numerické sítě [42]

na jednotlivé jádra a po výpočtu opět složen do výsledné matice. Hlavní výhodou je možnost výpočtu jak na CPU tak na GPU, což dokládá autorova publikace v kapitole 3.4 [43]. S využitím GPU je pak možný výpočet několika modelů paralelně i v čase kratším než je reálný čas. To pak umožňuje využít výpočty predikce budoucích stavů a pomocí optimálního řízení nalézt nejlepší lící scénář.

Digitálním dvojčtem ZPO je tedy pokročilý 3D nestacionární numerický model tuhnutí, predikující rozložení teplotního pole podél předlitku a pozici tekutého jádra. Ukázka uživatelského rozhraní je na obrázku 2.4. Uživatelské prostředí je tvořeno tak, aby jej bylo možné ovládat z tabletu a mobilního zařízení. Toto prostředí komunikuje přes internet s výpočetní stanicí, na které probíhá numerický výpočet a sběr dat. Uživatel tak vidí aktuální informace o tavbě, chemickém složení odlévané oceli, průběhu teplot, intenzitě chlazení, lící rychlosti a dalších parametrech ZPO, zcela podle konceptu Průmyslu 4.0.



Obrázek 2.4: Uživatelské rozhraní digitálního dvojčete ZPO

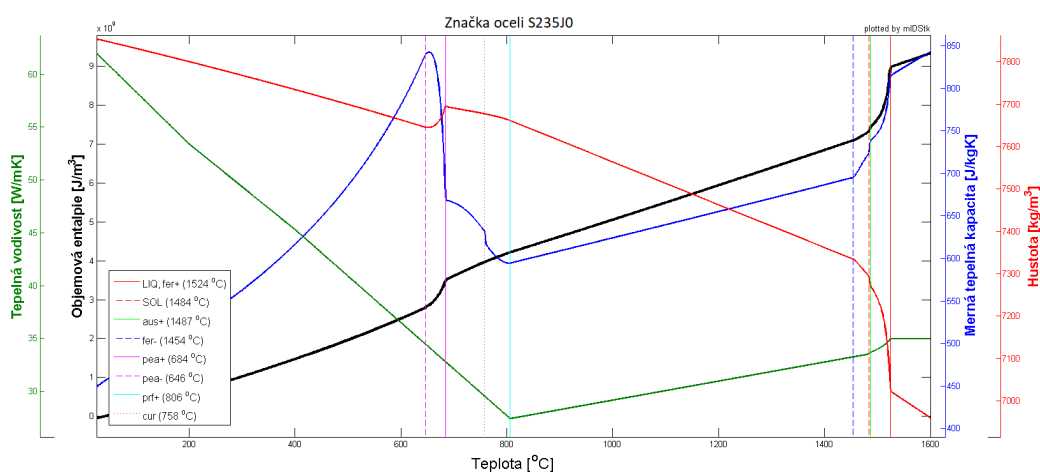
## 2.4 Nonlinearity digitálního dvojčete ZPO

V matematickém modelu, což je základ digitálního dvojčete ZPO, popsaného rovnicemi (2.1)-(2.5) se objevují tři druhy nelinearit:

- nelinearita ve vztahu mezi teplotou a entalpií při uvolňování latentního tepla fázové nebo strukturální změny,
- nelinearity termofyzikálních vlastností oceli (teplotní závislost hustoty, měrné tepelné kapacity a tepelné vodivosti),
- nelinearita okrajových podmínek (zejména závislost součinitele přestupu tepla pod chladicí tryskou na povrchové teplotě).

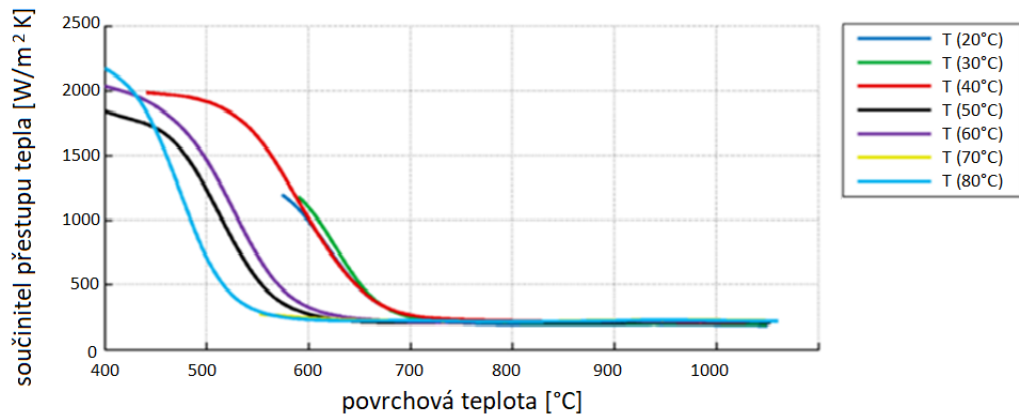
První dva typy nelinearit, tedy teplotní závislost termofyzikálních vlastností a objemové entalpie je demonstrována na obrázku 2.5 pro vybranou typicky odlévanou značku oceli S235J0. Pro další vybrané druhy ocelí jsou tyto nelineární závislosti graficky uvedeny v autorových článcích v kapitole 3. Výpočet termofyzikálních vlastností byl proveden solidifikačním softwarem IDS [46]. Zde je zřejmá silná nelinearita na teplotě, přes kterou proces chlazení probíhá. Při modelování procesu lití oceli je důležitý teplotní interval mezi 600 - 1550 °C.

Nelinearita v okrajové podmínce může být vyjádřena jako závislost součinitele přestupu tepla na povrchové teplotě. Pro různé teploty chladicí vody je potom ukázána na obrázku 2.6 a detailněji popsána v autorově článku, kapitola 3.7 [45]. I zde je zřejmá nelinearita, která je připisována tzv. Leidefrostovému jevu [60].



Obrázek 2.5: Ukázka teplotní závislosti termofyzikálních vlastností oceli

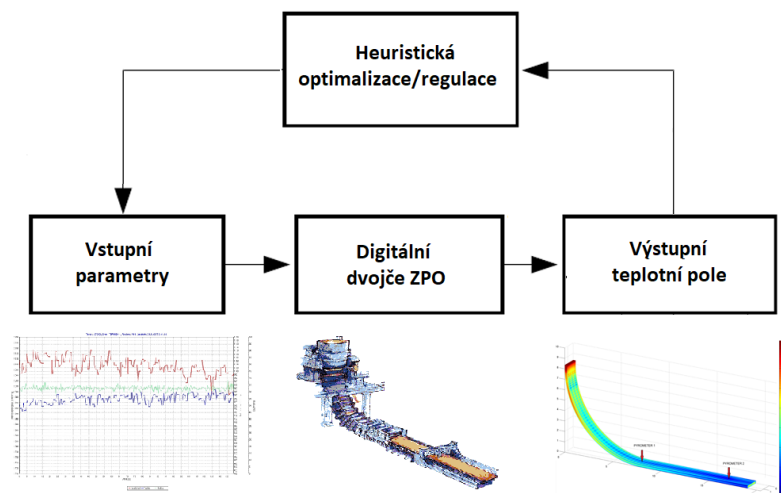
Z pohledu optimalizace pro nelineární systémy, na rozdíl od systémů lineárních, neexistuje metoda, která je schopna zajistit nalezení globálního optima [3]. Navíc řešení nelineárního optimalizačního problému je obecně podle definice výpočetní náročnosti NP-problém [3]. Je-li to v praxi možné, používají se metody na zlinearizování dané úlohy. Vzhledem k silným nelinearitám, které jsou pro proces ZPO typické, však nejsme schopni provést linearizaci systému bez značné výsledné chyby. Optimalizační výpočetní čas tak není úměrný velikosti systému, v tomto případě velikosti diskretizační sítě, která by v případě brambového lití měla mít podle obrázku 2.3 alespoň  $N = 2,5$  milionů výpočetních uzlů. Z pohledu optimalizace je pak počet rovnic úměrný počtu uzlů  $N$  ještě vynásobený počtem časových kroků



Obrázek 2.6: Ukázka závislosti součinitele přestupu tepla na povrchové teplotě a teplotě chladicí vody [26]

potřebných na dosažení stacionárního stavu. Počet časových kroků závisí na podmínce stability (2.8) a na volbě podmínky počáteční. Pro výpočty prezentované na obrázku 2.3 bylo k dosažení výsledku v průměru provedeno cca.  $\tau = 2000$  časových kroků. Optimalizační problém by potom musel řešit  $N \cdot \tau = 3$  miliardy nelineárních rovnic. Přímá optimalizace pomocí metod matematického programování možná je, ale její časová náročnost by překračovala její smysluplné použití [3].

Jedinou možností je potom oddělení numerického modelu od modelu optimalizačního. Numerický model potom bude pro model optimalizační vystupovat jako tzv. černá skříňka (black-box) [76], viz obrázek 2.7. Detailní popis tohoto přístupu je pak zpracován v autorově publikaci 3.2 [42].



Obrázek 2.7: Schéma regulace digitálního dvojčete pomocí optimalizace [42]

Tento koncept řešení lze nalézt v několika literárních zdrojích [29], [30], [34], [35], [38], [64], [66], [72], [75], [80]. V nich je však často využito pouze zjednodušených 1D a 2D numerických modelů, jednoduchých okrajových podmínek, zanedbání linearit, a tedy není zcela jasná možnost využití na reálném provozu, kde je nutné mít co nejlepší výsledek. Současně

jsou tyto práce navzájem neporovnatelné a je nutné testovat různé optimalizační přístupy na jednom numerickém modelu, nejlépe komplexním a validovaném 3D modelu. Toto porovnání popisuje autorova publikace v kapitole 3.5 [9], kde je demonstrována aplikace několika druhů optimalizačních přístupů na jednom konkrétním modelu ZPO. Z výsledků je jasně vidět, že některé optimalizační algoritmy dosahují v této problematice výrazně lepších výsledků, než ostatní.

## 2.5 Validace digitálního dvojčete ZPO

Pro nasazení digitálního dvojčete ZPO v provozu a pro jeho následnou optimalizaci je nezbytné ověřit jeho výsledky s reálným provozem [4]. Proces plynulého lití je natolik komplexním problémem, že lze numerické modely ověřovat laboratorně, pouze v omezeném rozsahu. Laboratorně lze ověřit např. termofyzikální vlastnosti pro konkrétní ocel v závislosti na teplotě [63]. Některé typy okrajových podmínek lze rovněž ověřit laboratorně, např. součinitel přestupu tepla pod chladicí tryskou [59]. Obecně je však nezbytné digitální dvojčete ZPO validovat přímo na reálném provozu. To má však několik omezení. Vždy je možné pouze měřit hodnoty v místech, ve kterých to ZPO svou konstrukcí vůbec umožňuje. Navíc v případě tvrdého chlazení dochází k velké přeměně chladicí vody v páru a v některých místech ZPO může pyrometrické měření vykazovat zcela zkreslené výsledky. Kvůli vysokým teplotám je nutné volit speciální měřicí techniku. Ze stejného důvodu se kontinuálně měří přímo na trati relativně malé množství veličin.

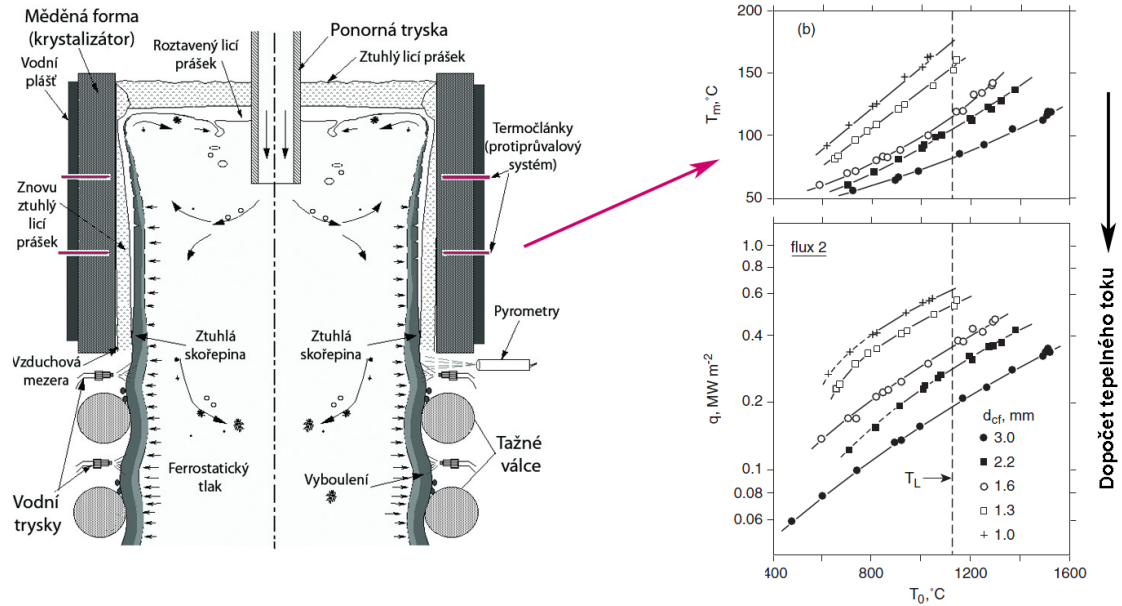
Pro validaci solidifikačního modelu se nejčastěji využívají na ZPO tři druhy měření, které nejsou invazivní [6]:

- měření pomocí termočlánků umístěných ve stěně krystalizátoru,
- termovizní a pyrometrické měření povrchu předlitku,
- radioskopická metoda.

Naopak mezi metody invazivní patří např. řízený průval, při kterém se hledá poloha metalurgické délky [6]. Pro výrobce oceli je však použití experimentálních invazivních metod obecně nepřijatelné. Spíše se pak používají informace a data z havarijních situací, kdy např. k průvalu již došlo.

Měření pomocí termočlánků umístěných ve stěně krystalizátoru má tu výhodu, že toto měření probíhá kontinuálně, ale pouze v primární zóně chlazení. Hlavním účelem používání těchto termočlánků je tzv. protiprůvalový systém, který zabraňuje možným havarijním scénářům při provozu. Naměřené teploty mají pouze informativní charakter, protože mezi teplotou měřenou termočlánkem a teplotou na povrchu předlitku je několik tepelných odporů v podobě licích prášků, vzduchové mezery a měděné stěny krystalizátoru [4]. Na druhou stranu, síť termočlánků zachycuje přibližné rozložení povrchových teplot, ze kterého lze optimalizačně dopočítat tepelný tok, ten dosadit do simulace a porovnat vypočítané teploty s měřením, obrázek 2.8. Ukázka měřených dat z několika termočlánků instalovaných ve stěně krystalizátoru je na obrázku 2.9-vlevo. Zde je vidět, že je nutné před výpočtem tepelného toku data nejdříve filtrovat, např. filtry ARMA [48].

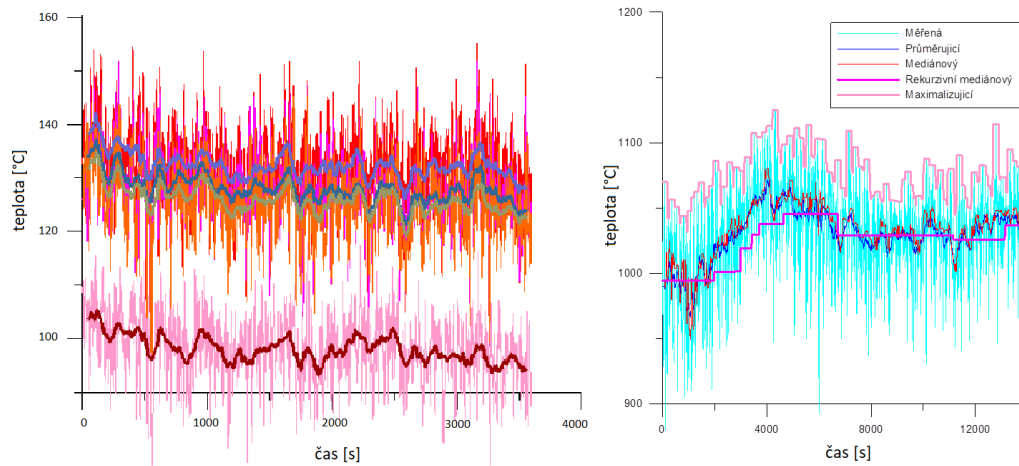




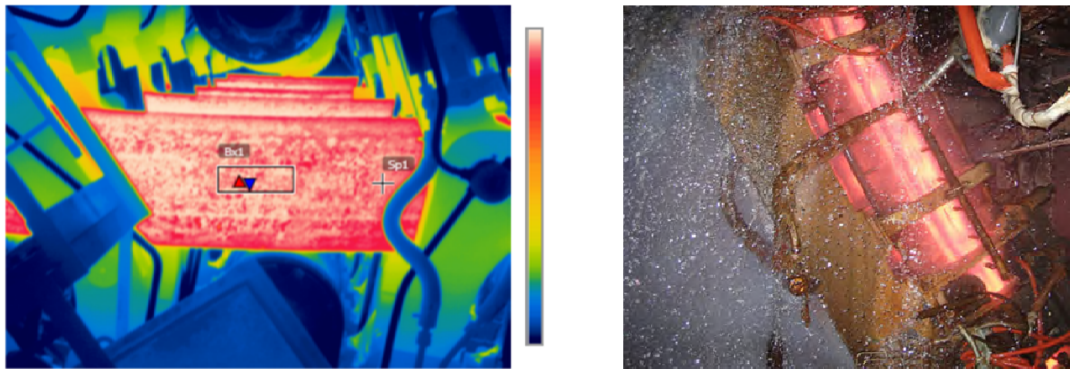
Obrázek 2.8: Schéma krystalizátoru se zapojením termočlánků, měření teplot a vypočítaný tepelný tok [4]

Termovizní a pyrometrické měření povrchových teplot je nejčastěji používaná metoda na ověření digitálního dvojčete ZPO, obrázek 2.10. Reálné lící provozy mají poměrně často permanentně instalovány na několika místech lící trati pyrometry nebo teplotní skenery, které dávají dlouhodobou informaci o povrchových teplotách [69]. Lze tak dlouhodobě sledovat teplotní chování oceli s rozdílným chemickým složením, popř. vyhodnocovat opotřebení lícího stroje. Toto dlouhodobé měření povrchových teplot pak lze s výhodou využít na validaci a zpřesňování parametrů digitálního dvojčete ZPO, což je i případ předkládaného digitálního dvojčete. Autorova publikace 3.2 [42] obsahuje porovnání počítaných povrchových teplotních průběhů spolu s naměřenými pyrometrickými daty, kde dochází k dobré shodě mezi simulací a reálným provozem. Je však nutné zmínit, že se zde ověřuje a porovnává pouze povrchová teplota. O teplotním rozložení uvnitř předlitku získaného pomocí simulace validované pouze na základě povrchových teplot nelze s jistotou rozhodnout, jak je simulace vzdálena od reálného stavu. To znamená, že např. řízení odlévání na ZPO pomocí hodnoty metalurgické délky získané pouze simulací bez dodatečné validace může způsobit snížení výsledné kvality oceli, nebo dokonce havarijní situaci na lící dráze, tzv. průval. Odstranění následků takovéto poruchy lícího stroje je značně nákladné a zdlouhavé. Ukázka dat z pyrometrického měření je zobrazena na obrázku 2.9-vpravo. Vznik okujů způsobuje měnící se emisivitu povrchu, proto je nutné stejně jako v případě dat z protiprůvalového systému použít vhodnou filtraci měřených dat [48].

Poslední zmiňovanou metodou je validace modelu pomocí radioskopické metody [6]. Tento způsob validace modelu probíhá pomocí radioizotopových částic, které jsou dávkovány přímo do taveniny. Radioaktivní prvky se rovnoměrně rozloží v tavenině a lze je pomocí speciálních metod sledovat. Tato metoda je technicky i ekonomicky ze všech neinvazivních metod nejnáročnější, avšak jako jediná slouží k určení metalurgické délky. Z důvodu přítomnosti radioaktivních izotopů přímo na ZPO se však tato metoda používá pouze ve výjimečných případech a jenom pro výzkumné účely [36].



Obrázek 2.9: Vlevo data termočlánků ve stěně krystalizátoru, vpravo data z pyrometrického měření povrchu předlitku včetně filtrace [69]



Obrázek 2.10: Vlevo: Ukázka termovizního měření, Vpravo: umístění pyrometru na licí trati [69]

Validace předkládaného digitálního dvojčete ZPO probíhala dlouhodobě v rámci rozsáhlé spolupráce v několika ocelárnách včetně zahraničních: Evraz Vítkovice Steel, a.s., Třinecké železárny, a.s., Železiarne Podbrezová, a.s., U. S. Steel Košice, s.r.o. a Pohang Iron and Steel Company (POSCO). Díky této úzké spolupráci s reálnými provozy bylo možno dlouhodobě validovat a zpřesňovat digitální dvojčete pro různé geometrie ZPO, různé okrajové podmínky a licí parametry, pro nespočet ocelí s různým chemickým složením, což dokládají například autorovy publikace v kapitole 3.2 a 3.4 [42] [43]. Validace zejména probíhaly pomocí nainstalovaných pyrometrů v různých místech ZPO, pomocí hodnot z termočlánků protiprůvalového systému a pomocí teplotních skenerů a termovizí. Rovněž bylo provedeno radioizotopové měření na bramovém lití o průřezu 250 x 1 500 mm. Radioizotopovým zdrojem byl radionuklid Fe 59, 20 MBq. Na měření metalurgické délky byly provedeny celkem čtyři pokusy. Experiment s radioizotopy potvrdil přesnost simulace a ukázal, že model tuhnutí je schopen předpovědět nejen polohu metalurgické délky, ale i tvar tuhnoucího kužele [36]. Validace metalurgické délky vypočtené pomocí digitálního dvojčete byla zásadní, protože metalurgická délka je limitem pro optimalizaci rychlosti lití, tzn. produktivity provozu.

## Kapitola 3

# Využití digitálního dvojčete a jeho optimalizace

Tato kapitola dokládá tvorbu, potenciál a možnosti využití digitálního dvojčete ZPO. Je sestavena ze sedmi průřezových článků publikovaných v níže uvedených recenzovaných časopisech, které mají impakt faktor podle WOS:



MAUDER, T.; ŠANDERA, Č.; ŠTĚTINA, J.; ŠEDA, M. Optimization of Quality of Continuously Cast Steel Slabs by Using Firefly Algorithm. *Materiali in tehnologije*, 2011, vol. 45, no. 4, p. 347-350.

Podíl autora této práce na článku 45 %.

**ISSN: 1580-2949. IF 2011:0,804 (Q3).**



MAUDER, T.; ŠANDERA, Č.; ŠTĚTINA, J. Optimal Control Algorithm for Continuous Casting Process by Using Fuzzy Logic. *STEEL RESEARCH INTERNATIONAL*, 2015, vol. 86, no. 7, p. 785-798.

Podíl autora této práce na článku 70 %.

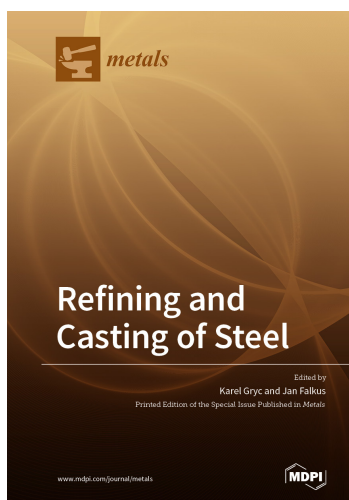
**ISSN: 1611-3683. IF 2015:1,021 (Q2).**



MAUDER, T.; CHARVÁT, P.; ŠTĚTINA, J.; KLIMEŠ, L. Assessment of Basic Approaches to Numerical Modeling of Phase Change Problems—Accuracy, Efficiency, and Parallel Decomposition. JOURNAL OF HEAT TRANSFER-TRANSACTIONS OF THE ASME, 2017, vol. 139, no. 8, p. 1-5.

Podíl autora této práce na článku 40 %.

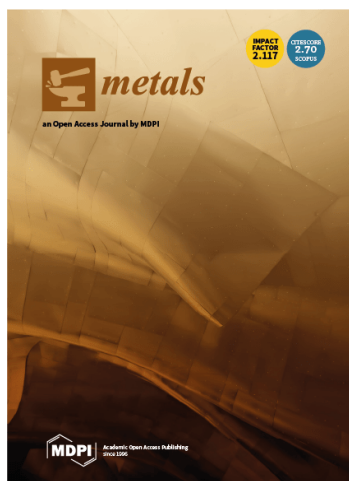
ISSN: 0022-1481. IF 2017:1,602 (2x Q3).



MAUDER, T.; ŠTĚTINA, J. High Quality Steel Casting by Using Advanced Mathematical Methods. Metals, 2018, vol. 8, no. 12, p. 1-13.

Podíl autora této práce na článku 70 %.

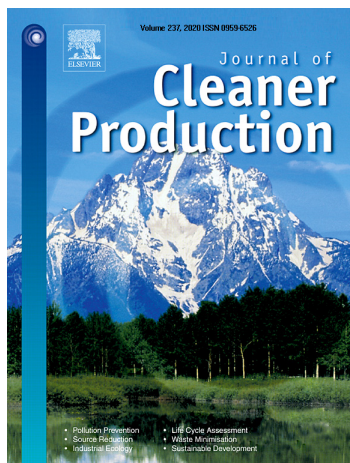
ISSN: 2075-4701. IF 2018:2,259 (Q1/Q3).



BŘEZINA, M.; MAUDER, T.; KLIMEŠ, L.; ŠTĚTINA, J. Comparison of optimization-regulation algorithms for secondary cooling in continuous steel casting. Metals, 2021, vol. 11, no. 2, p. 1-19.

Podíl autora této práce na článku 20 %.

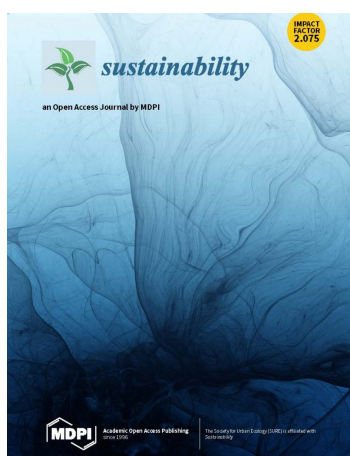
ISSN: 2075-4701. IF 2021:2,695 (Q2/Q3).



KLIMEŠ, L.; BŘEZINA, M.; MAUDER, T.; CHARVÁT, P.; KLEMEŠ, J.; ŠTĚTINA, J. Dry cooling as a way toward minimisation of water consumption in the steel industry: A case study for continuous steel casting. *Journal of Cleaner Production*, 2020, vol. 275, no. 1, p. 123109-1 (123109-12 p.).

Podíl autora této práce na článku 15 %.

**ISSN: 0959-6526. IF 2020:9,297 (3x Q1).**



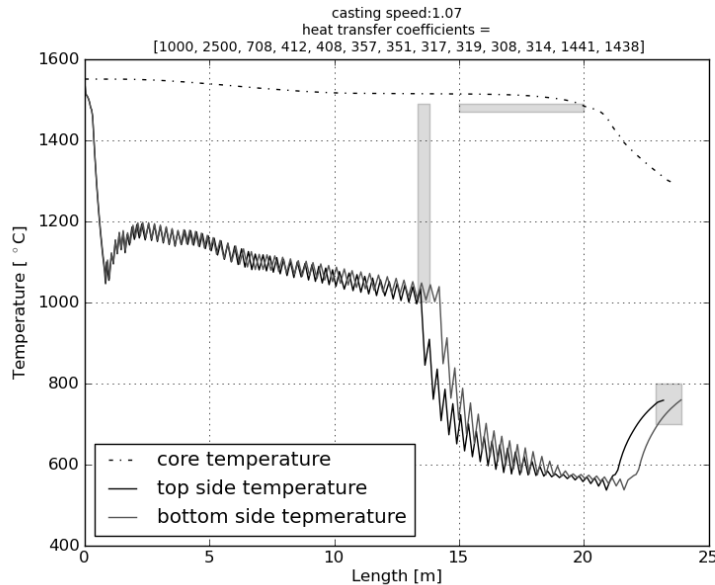
MAUDER, T.; BŘEZINA, M. Reduction of CO<sub>2</sub> Emissions in Steelmaking by Means of Utilization of Steel Plant Waste Heat to Stabilize Seasonal Cooling Water Temperature. *Sustainability*, 2021, vol. 13, no. 11, p. 1-12.

Podíl autora této práce na článku 70 %.

**ISSN: 2071-1050. IF 2021:3,889 (Q2/Q3).**

### 3.1 Optimization of Quality of Continuously Cast Steel Slabs by Using Firefly Algorithm

Tento článek popisuje možnost využití metaheuristického optimalizačního algoritmu inspirovaného přírodními ději v problematice hledání optimálního nastavení ZPO. Autor zvolil nový algoritmus založený na chování hejna světlušek (tzv. Firefly algorithm) [77]. Optimalizační algoritmus je propojen s digitálním dvojčtem ZPO ve smyslu black-box přístupu [76]. Firefly algoritmus byl v problematice optimalizace parametrů ZPO použit vůbec poprvé, z tohoto pohledu jde tedy o unikátní článek.



Obrázek 3.1: 2D teplotní pole předlitku a omezení pro teploty a metalurgickou délku [44]

Algoritmus náhodně vygeneroval  $N$  vektorů vstupních parametrů (13 intenzit chlazení pro 13 chladících okruhů a hodnotu licí rychlosti) a digitální dvojče ZPO pro tyto vstupní parametry napočítalo  $N$  řešení (teplotní pole). Dále se stanovila hodnota účelové funkce, pro všechny řešení, jako rozdíl teplot spočítaných digitálním dvojčtem ZPO a teplot požadovaných (optimálních). Rovněž se sledovala hodnota metalurgické délky, která byla z bezpečnostních důvodů omezena. Řešení potom představovalo světlušku a hodnota účelové funkce její intenzitu záření. Světlušky s vyšší intenzitou záření potom k přitahují světlušky ostatní. Podle toho jsou upraveny parametry světlušek pro další výpočet digitálního dvojčete ZPO. Nové řešení pro iteraci  $n + 1$  je potom vždy dáno předpisem [77]

$$\mathbf{x}_i^{n+1} = \mathbf{x}_i^n + \beta_0 e^{-\gamma r_{ij}^2} (\mathbf{x}_j^n - \mathbf{x}_i^n) + \alpha \boldsymbol{\epsilon}_i. \quad (3.1)$$

Mezi jakýmkoliv dvěma světluškami  $\mathbf{x}_i$  a  $\mathbf{x}_j$  majícími souřadnice v kartézském souřadném systému lze stanovit vzdálenost mezi nimi jako  $r_{ij} = \|\mathbf{x}_i - \mathbf{x}_j\| = \sqrt{\sum_{k=1}^n (x_{i,k} - x_{j,k})^2}$ . První člen pravé strany rovnice (3.1) vyjadřuje původní polohu světlušky  $i$ . Druhý člen vyjadřuje přitažlivost ke světlušce  $j$ . Třetí člen obsahuje náhodný parametr  $\alpha$ . Symbol  $\boldsymbol{\epsilon}_i$  označuje vektor náhodných čísel daný normálním rozdělením nebo rovnoměrným rozdělením pravděpodobnosti. Pro většinu aplikací můžeme dosadit  $\beta_0 = 1$  a  $\alpha \in [0, 1]$ . V případě  $\beta_0 = 0$  jde o tzv. náhodnou procházku. Parametr  $\gamma$  mění přitažlivost světlušek a jeho

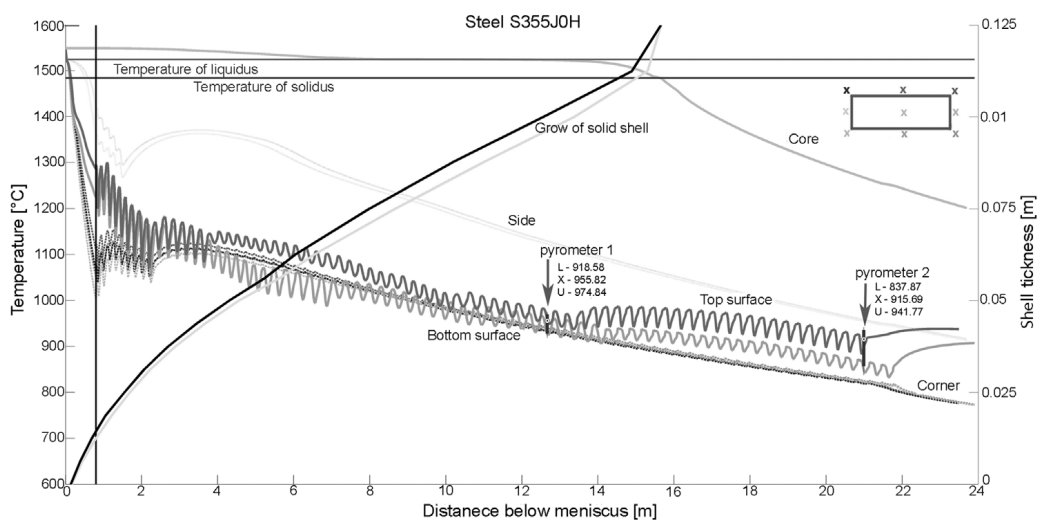
hodnota je kritická z pohledu rychlosti konvergence řešení a tedy ovlivňuje celé chování algoritmu. Teoreticky může tato hodnota ležet v intervalu  $\gamma \in \langle 0, \infty \rangle$ , v praxi se však většinou nastavuje mezi hodnotami 0,1 až 10.

Pro testování optimalizačního algoritmu bylo speciálně vytvořeno 2D digitální dvojčete ZPO. K otestování stability a univerzálnosti optimalizačního algoritmu bylo zvoleno několik druhů ocelí s různým chemickým složením a několik druhů omezení na povrchové teploty a na hodnotu metalurgické délky. Hlavním cílem algoritmu bylo nalezení maximální možné rychlosti při zachování omezujících teplotních podmínek. Bylo dosaženo nejenom optimálního výsledku, ale navíc byl tento výsledek dosažen i s relativně malým počtem světlušek a malým počtem iterací. Lze tedy konstatovat, že pro tento typ úloh Firefly algoritmus konverguje k optimu rychle i při menším počtu světlušek, tzn. s menšími výpočetními nároky. Výsledek lze vidět na obrázku 3.1.

Firefly optimalizační algoritmus se tak ukázal být na tento problém vhodnou volbou. Nicméně jeho další nasazení na 3D digitální dvojčete ZPO již vyžadovalo kvůli komplexnosti (nelinearitě) v okrajových podmínkách mnohem více opakovaných optimalizačních iterací a větší počet použitých světlušek. Tím extrémně narůstal výpočetní čas a bylo nutné hledat jiný druh řešení.

## 3.2 Optimal Control Algorithm for Continuous Casting Process by Using Fuzzy Logic

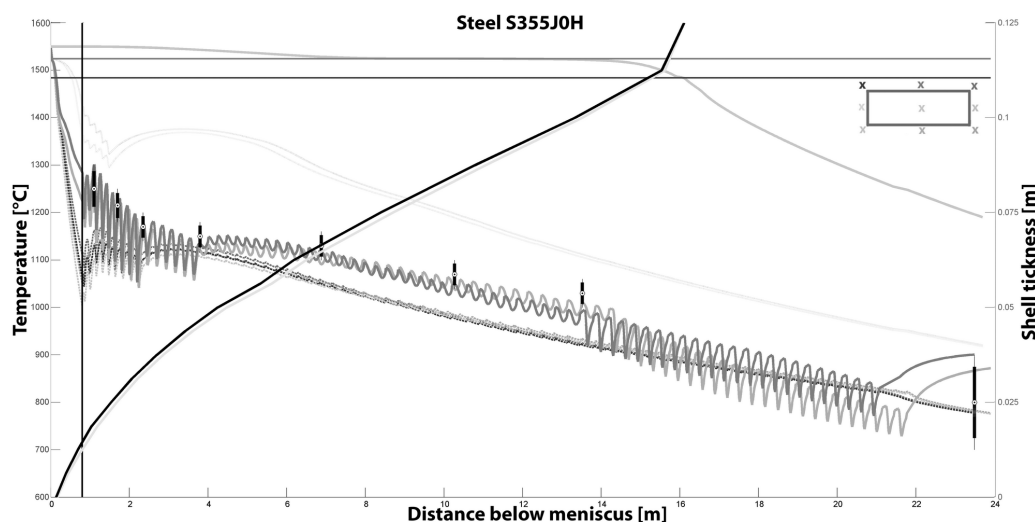
Tento článek v úvodu popisuje současný stav poznání v oblasti digitalizace procesu plynulého lití a navazujících optimalizačních technik. Článek je rozdělen do dvou hlavních sekcí. První část představuje původní matematický popis problému, včetně numerické diskretizace (byla zvolena Alternující Explicitní metoda ADE s testem nezávislosti sítě) a detailního popisu okrajových podmínek (druhy použitých trysek a jejich umístění). Tedy tvorbu digitálního dvojčete ZPO podle reálného lícího stroje firmy EVRAZ VÍTKOVICE STEEL, a.s. V první části článku je rovněž ukázána verifikace digitálního dvojčete pomocí dvou pyrometrů snímajících teploty na horním povrchu předlitku, viz obrázek 3.2.



Obrázek 3.2: Ukázka verifikace virtuálního dvojčete pomocí pyrometrů [42]

Další část se věnuje optimalizačnímu modelu, který již nekomunikuje s digitálním dvojčtem ZPO ve smyslu přístupu black-box, ale obsahuje vyšší logiku poznání procesu lití. Tato logika vychází z jednoduchého lidského uvažování a to: JESTLIŽE je teplota na povrchu příliš vysoká PAK přidej v tomto a předcházejících místech ZPO intenzitu chlazení, JESTLIŽE je teplota na povrchu příliš nízká PAK uber v tomto a předcházejících místech ZPO intenzitu chlazení, JESTLIŽE je teplota na povrchu v optimálním teplotním intervalu PAK nic nevykonávej. Autor navrhl a sestavil původní optimalizačně-regulační algoritmus založený na fuzzy logice [78], která je schopna simulovat lidské uvažování a tím nalézt optimální řešení v rychlejším čase, než je schopen algoritmus založený na black-box přístupu. Vstupem pro fuzzy regulátor je optimální rozložení povrchových teplot, které by mělo být voleno s ohledem na druh oceli tak, aby byla dosažena požadovaná výsledná kvalita oceli. Dalším vstupem do fuzzy regulátoru je hodnota metalurgické délky, která nesmí být překročena z důvodu bezpečnosti. Fuzzy regulace pak hledá optimální nastavení licí rychlosti za účelem zvýšení produktivity výroby. Jde tedy o kombinaci optimalizace zvyšující kvalitu odlitých výrobků a zároveň zvyšující produktivitu procesu.

Optimalizace byla provedena na 3D komplexním digitálním dvojčeti ZPO a bylo nalezeno nové rozložení teplotního pole, které je zobrazeno na obrázku 3.3. V tomto případě byla téměř dosažena maximální povolená hodnota metalurgické délky, což indikuje maximální možnou produktivitu lití. Rovněž je vidět, že všechny požadované limity hodnot povrchové teploty byly ve všech kontrolních bodech (kontrolní bod je vždy umístěn za každý chladicí okruh) splněny (povrchové teploty prochází krabicovými grafy).



Obrázek 3.3: Teplotní rozložení po optimalizaci [42]

Důležitou otázkou pro operátora reálného licího stroje je nastavení optimálního chlazení pro různé hodnoty licí rychlosti, která se v průběhu dynamického procesu mění a je třeba na tuto změnu reagovat. Rovněž pro různé velikosti odlévaného předlitku je třeba nalézt nové hodnoty chlazení. Na závěr článku je pak ukázka optimálních chladících křivek (získaných pomocí kombinace fuzzy regulace a digitálního dvojčete ZPO) v provozním intervalu licích rychlostí pro různé velikosti předlitku. Tyto hodnoty jsou získány pro stacionární stavy. V případě dynamických změn dochází k dopravnímu zpoždění systému a je nutné s těmito hodnotami pracovat obezřetně [42].



Přístup kombinace fuzzy regulace spolu s digitálním dvojčetem se ukázal jako velmi užitečný a byl dále rozvíjen pro různé geometrie ZPO a zejména pro optimální řízení při dynamických změnách parametrů lití.

### 3.3 Assessment of Basic Approaches to Numerical Modeling of Phase Change Problems—Accuracy, Efficiency, and Parallel Decomposition

Digitalizace procesu plynulého lití oceli na ZPO pomocí modelu digitálního dvojčete založeného na numerické matematice je spojena s otázkou přesnosti, efektivnosti a robustnosti. Numerické modelování procesu plynulého lití je v podstatě problémem přenosu tepla se změnou fáze (nelineární problém, viz kapitola 2.4). Je nutné dobře zvolit jak numerickou metodu, tak metodu na modelování změny fáze. Tento článek porovnává čtyři metody numerické diskretizace se třemi metodami modelování změny fáze, navíc pro čtyři různé hustoty výpočetní sítě. V porovnání je nabídnuta i varianta výpočtu dekomponované sítě na více procesorech nebo při použití grafické výpočetní karty GPU. Jako nejvíce přesnou metodou pro 1 D případ (porovnávaný s analytickou metodou) se ukázala numerická alternující implicitní metoda ADI s modelováním změny fáze pomocí tzv. metody teplotního zotavení (tzv. Temperature recovery) [16]. Ve 3D již byla nejuspěšnější entalpická metoda [70] s využitím jednoduchého explicitního schématu (tzv. simple explicit) SE popř. alternující explicitní schéma ADE [47]. S využitím paralelizace výpočtu byla nejuspěšnější metoda SE počítaná na grafické kartě GPU [41]. Výsledky výpočtů jsou uvedeny na obrázku 3.4.

Numerical scheme	Efficiency—computation time (s)		
	Enthalpy method	Effective heat capacity	Temperature recovery
Very-coarse-mesh			
SE	1.93	<b>1.10</b>	8.66
ADE	1.81	6.51	2.82
SI	9.55	14.05	11.40
ADI	7.47	15.36	9.16
Coarse-mesh			
SE 1CPU/12CPU	<b>11.54/135.28</b>	21.35	71.98
ADE	27.02	80.87	79.10
SI	83.38	309.74	333.35
ADI 1CPU/12CPU	41.80/58.61	176.85	271.61
SE GPU	18.67	—	—
Fine-mesh			
SE 1CPU/12CPU	887.14/1 122.13	1051.11	1926.70
ADE	2359.07	3461.83	4331.50
SI	3251.27	7929.16	9517.30
ADI 1CPU/12CPU	714.73/824.32	6109.06	7809.40
SE GPU	<b>97.72</b>	—	—
Very-fine-mesh			
SE 1CPU/12CPU	54 362.19/35 124.51	—	—
ADI 1CPU/12CPU	36 210.45/32 416.32	—	—
SE GPU	<b>972.49</b>	—	—

Obrázek 3.4: Výpočetní čas pro různé druhy výpočtových schémat a metod modelování fázové změny [41]

Hůře paralelizovatelné implicitní metody počítané i na několika procesorech (pro jemné výpočetní sítě) byly sice přesnější, ale v rychlosti oproti kombinaci SE na GPU nebyly schopné konkurence [41]. Cílem virtuálního dvojčete ZPO je vytvořit velmi přesnou kopii reálného lití, tzn. numerický model s velmi jemnou výpočetní sítí, která bude schopna provádět výpočty v reálném čase nebo dokonce přepočítávat stavy budoucí. Kombinace explicitních numerických metod s entalpickou metodou na modelování změny fáze s jejím GPU ekvivalentem se tak stala hlavním směrem tvorby digitálního dvojčete ZPO.

### 3.4 High Quality Steel Casting by Using Advanced Mathematical Methods

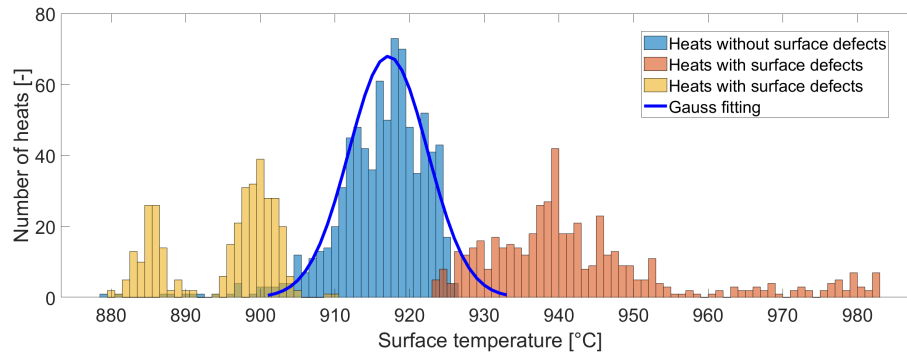
Autor rozšiřuje obsah článku 3.1 [44] ve smyslu rozšíření výpočetního jádra digitálního dvojčete ZPO a to zejména o masivní paralelizaci počítanou na grafické procesorové jednotce GPU. Pro ověření předpokladu využitelnosti GPU podle článku 3.3 [41] výpočet probíhal pro tři rozdílné hustoty numerické sítě (10 000, 100 000 a 1 000 000 výpočetních uzlů) a dvě numerické metody SE a ADI počítané na jednom či více procesorech. Výsledek přináší obrázek 3.5. Smysl této paralelizace výpočtu je zejména v dosažení takové rychlosti výpočtu, která bude předstihovat i pro jemné numerické sítě čas reálný. Digitální dvojče ZPO, které dokáže provádět výpočty rychleji, než je čas reálný dokáže předpočítávat budoucí teplotní rozložení a na základě budoucího výsledku učinit změnu v licích parametrech okamžitě. Mluvíme tak o prediktivním řízení procesu.

Numerical Scheme	Computational Time (s)		
	Coarse mesh	Fine-mesh	Very-fine mesh
SE—1 CPU	11.54	887.14	54,362.12
SE—12 CPU	135.28	1122.13	35,124.54
ADI—1 CPU	41.81	714.73	36,210.41
ADI—12 CPU	58.61	824.32	32,416.32
SE—GPU	18.67	97.72	972.49

Obrázek 3.5: Výpočetní čas pro různé hustoty vypočtení sítě a pro dvě numerická schémata schémat [43]

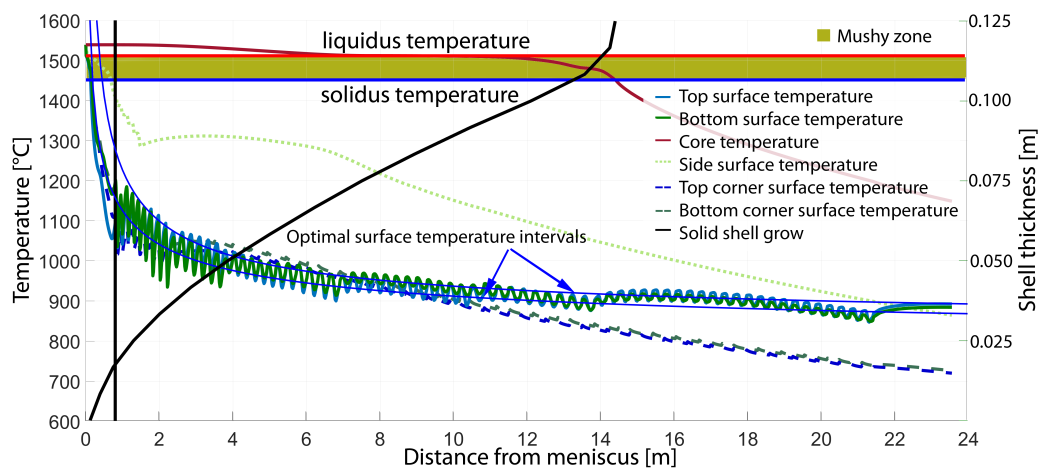
Unikátnost článku je rovněž v hledání možné odpovědi na otázku, jak je vhodné nastavit povrchové teplotní limity pro konkrétní značku oceli tak, aby byla dosažena požadovaná kvalita předlitku (minimalizace vnitřních a povrchových trhlin). Z pohledu složitosti procesu lití oceli, kdy dochází při změně fáze k tvorbě tuhoucích krystalů, segregací, tepelného zpracování je téměř nemožné na základě licích parametrů předpovídat finální kvalitu ztuhlého ocelového polotovaru. V tomto článku je ukázán statistický přístup, kdy je pomocí statistického vyhodnocení reálných provozních dat pro jednu značku odlévané oceli S355 sledováno, jestliže došlo k tvorbě povrchových trhlin či nikoliv (celkově bylo statisticky zpracováno přes 2000 taveb). Obrázek 3.6 ukazuje statistické vyhodnocení povrchových teplot, měřených v místě rovnání předlitku, názorně rozdělených podle vzniku vady. Tavby kde nebyl vznik vady pozorován jsou proloženy hustotou pravděpodobnosti normálního rozdělení, se střední hodnotou 916,03 °C a rozptylem 6,89 °C.

Statistická data sloužila jako základ pro nastavení optimálních povrchových teplot, podle kterých musel fuzzy regulátor regulovat intenzitu chlazení pro libovolnou licí rychlost.



Obrázek 3.6: Třídění sledovaných taveb podle vzniku vady a teploty v místě rovnání [43]

Výsledné teplotní pole je pak zobrazeno na obrázku 3.7. Zde je vidět, že podmínka udržení povrchových teplot je splněna.



Obrázek 3.7: Výsledek optimalizace chlazení ZPO s teplotními limity [43]

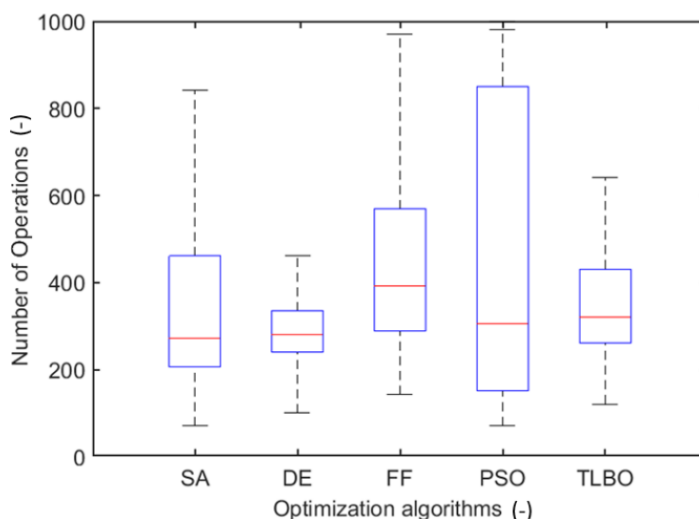
Článek uzavírá ukázkou využití fuzzy regulace a digitálního dvojčete ZPO pro optimalizaci dynamických změn licích parametrů. Konkrétně jde o simulaci poklesu licí rychlosti z 1,5 na 1,2 m/min na přibližně 8 minut (která může odpovídat např. rychlé výměně mezipánve). Na tuto změnu musí reagovat operátor změnou intenzity chlazení v sekundární chladicí zóně. Fuzzy regulátor prokázal, že s jeho použitím dochází k minimálním povrchovým teplotním výkyvům a tedy kvalita odlévaného oceli by měla zůstat zachována [43].

### 3.5 Comparison of optimization-regulation algorithms for secondary cooling in continuous steel casting

Tento článek ukazuje další možnosti využití optimalizačních algoritmů pro digitální dvojčete ZPO a rozšiřuje článek 3.1 [44]. Pro účely testování optimalizačních algoritmů byl speciálně vytvořen nový 2,5D model (tzv. slice model) [9], a to zejména pro jeho rychlé vyhodnocení bez nutnosti paralelizace. Autoři využívají různé optimalizační techniky v problematice plynulého lití, ale z důvodu rozdílnosti jejich digitálních dvojčat ZPO jsou však rozdílné přístupy neporovnatelné. Unikátnost tohoto článku je v porovnání různých optimalizačních

algoritmů na jednom digitálním dvojčeti ZPO a popřípadě tak nalézt vhodnou alternativu k fuzzy regulaci při hledání optimálních licích parametrů ZPO. Z každého typu optimalizačních technik byly zvoleny jeden až dva algoritmy. Z evolučních algoritmů byla zvolena metoda diferenciální evoluce, z fyzikálně orientovaných algoritmů metoda simulovaného žíhání, z hejnových algoritmů potom světluščí algoritmus a optimalizace hejnem částic a závěrem algoritmus z kategorie algoritmů založených na lidském usuzování teaching-learning optimalizace [77].

Důležitým faktorem je rychlost konvergence těchto algoritmů k optimálnímu řešení a pak samozřejmě výpočetní čas. Porovnání algoritmů z hlediska průměrného počtu výpočetních iterací (volání dvojčete ZPO) je na obrázku 3.8, ze kterého je vidět, že nejúspěšnější je metoda diferenciální evoluce. Dobře dopadla i metoda teaching-learning, která má tu výhodu, že nepotřebuje nastavovat žádné vnitřní parametry optimalizačního algoritmu [77]. Každá z těchto metod však potřebovala značné množství opakovaného volání digitálního dvojčete ZPO, nedosáhla tak na výsledky obdržené pomocí přístupu fuzzy regulace, která je tak dále hlavním optimalizačním algoritmem předkládaného digitálního dvojčete ZPO.

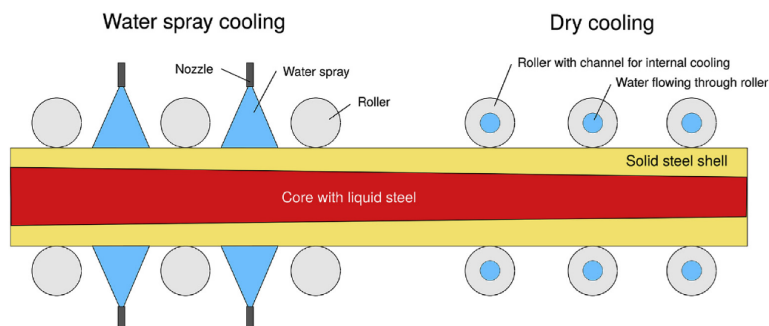


Obrázek 3.8: Porovnání optimalizačních přístupů [9]

### 3.6 Dry cooling as a way toward minimisation of water consumption in the steel industry: A case study for continuous steel casting

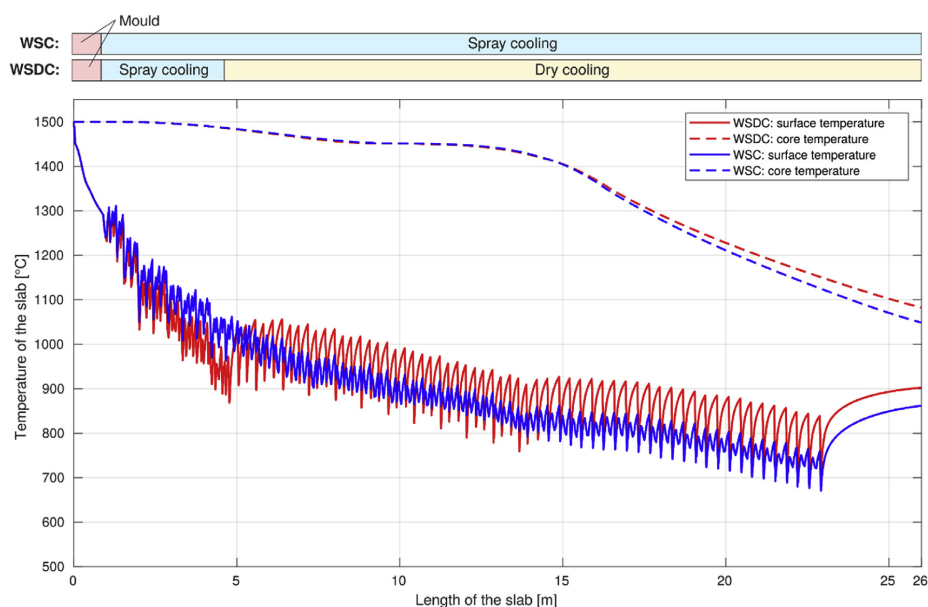
Předkládané články 3.1 - 3.5 [9], [41], [42], [43], [44] se zaměřují na tvorbu digitálního dvojčete ZPO a na možnosti jeho optimalizace z pohledu kvality a produktivity procesu. Originalita tohoto článku však spočívá v dalším možném využití digitálního dvojčete ZPO a to na tzv. prototypování rekonstrukcí samotného zařízení. Cílem článku bylo navrhnout chladicí systém pro sekundární chladicí sekci pomocí tzv. suchého chlazení, kdy jsou v sekundární chladicí zóně některé soustavy chladicích trysek nahrazeny vnitřně chlazenými válci (jde o chladicí okruhy, které jsou umístěné 5 m a dále od hladiny oceli v krystalizátoru). Rozdíl mezi vodním/vodo-vzdušným chlazením a suchým chlazením je zobrazen na obrázku 3.9.

Hlavní význam takové náhrady je pak v úspoře vody, která je využita v uzavřené chladicí smyčce a nedochází k jejímu odpaření a ztrátě při chlazení. Jde tedy o tzv. ekologickou optimalizaci, tedy optimalizaci, jejímž cílem je úspora vodních zásob a snížení uhlíkové stopy.



Obrázek 3.9: Schematicky znázorněné klasické a suché chlazení [37]

Hlavním kritériem bylo mít v obou režimech chlazení střední teplotní průběhy na povrchu a ve středu předlitku identické, tak aby v případě chlazení vodními válci nedošlo ke zhoršení kvality odlévané oceli. Výsledek teplotního výpočtu jsou graficky na obrázku 3.10 (WSC - chlazení pomocí trysek, WSDC - chlazení v kombinaci trysek a suchého chlazení). Z obrázku lze pozorovat, že povrchové teploty prvních chladících sekcí jsou obdobné, protože jsou v obou případech použity chladící trysky. Ve vzdálenost 5 m od hladiny oceli se výsledky mírně rozcházejí. Povrchová teplota při použití suchého chlazení na první pohled více osciluje, její střední hodnota má však stejný průběh jako v případě chlazení pomocí trysek. Tento výsledek byl dosažen opět pomocí fuzzy regulace.



Obrázek 3.10: Teplotní průběhy pro klasické a suché chlazení [37]

Výsledky článku pak shrnuje tabulka 3.11, ze které je zřejmá značná úspora spotřeby chladicí vody při dosažení ekvivalentního chlazení předlitku. Tím článek zároveň prokázal

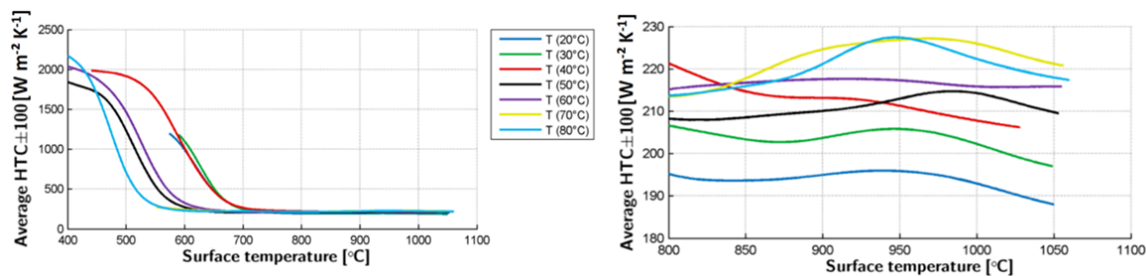
	Water flow rate for cooling [L/min]		
	Total	Closed-loop	Once-through
WSC scenario	9166	6000/65%	3166/35%
WSDC scenario	34,417	32,784/95%	1633/5%
WSDC-to-WSC ratio	3.75	5.46	0.52

Obrázek 3.11: Porovnání spotřeby vody při klasickém a suchém chlazení při opětovném využití vody [37]

další možnost využití digitálního dvojčete ZPO ve smyslu ekologické optimalizace, což je jeho hlavním originálním přínosem. Využití suchého chlazení při odlévání oceli je stále více zastoupeno, i když zatím spíše využíváno při odlévání tzv. tenkých bram, proto využití digitálního dvojčete ZPO má stále větší potenciál.

### 3.7 Reduction of CO<sub>2</sub> Emissions in Steelmaking by Means of Utilization of Steel Plant Waste Heat to Stabilize Seasonal Cooling Water Temperature

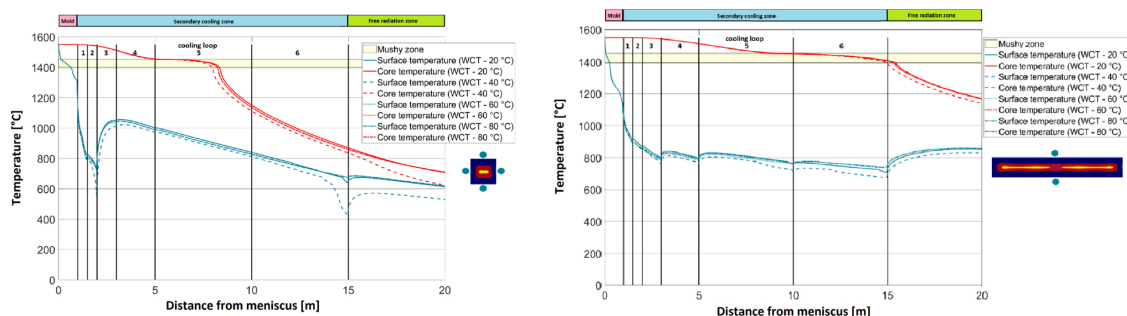
Tento článek se rovněž věnuje využití digitálního dvojčete ZPO pro ekologickou optimalizaci procesu plynulého lití a snížení CO<sub>2</sub> emisí. V případech, kdy by nebylo možné použít suché chlazení, jak popisoval článek 3.4 [37] je nezbytné se zabývat podrobněji procesem vodního chlazení a sledovat parametry, které toto chlazení ovlivňují. Z mnoha výzkumných prací je znám vliv Leidenfrostova efektu na intenzitu chlazení [60]. Tzv. Leidenfrostova teplota silně závisí na povrchové teplotě chlazeného objektu. Některé výzkumy však ukazují, že na její hodnotu může mít vliv i teplota chladicího média [26]. V Laboratoři přenosu tepla a proudění FSI VUT v Brně, byly experimentálně změřené průměrné součinitele přestupu tepla v závislosti na teplotě povrchu chlazeného objektu a teplotě chladicího média, viz obrázek 3.12. Podle výsledků experimentu má teplota chladicí vody přímý vliv na průměrný součinitel přestupu tepla pod tryskou a to jak v nízkoteplotní oblasti 3.12-vlevo tak ve vysokoteplotní oblasti 3.12-vpravo.



Obrázek 3.12: Výsledek výpočtu teplotního pole pro různé teploty chladicí vody [45]

Výsledky experimentu byly vloženy jako okrajové podmínky do digitálního dvojčete ZPO. Následné simulace byly provedeny pro sochorové i bramové ZPO, přičemž jejich výsledky jsou na obrázku 3.13. Zejména z rozložení teplot na povrchu sochoru je patrné, že teplota vody má na teplotní rozložení předlitku přímý vliv (zejména pro případ sochorového lití, kde se teploty povrchu pohybují běžně pod Leidenfrostovou teplotou). Tento poznatek

by mohl souviset ze zkušeností ocelářských podniků, které zaznamenávají, že pro stejnou značku oceli a stejné parametry licího stroje vykazují předlitky různé vady a jejich četnost se v letní a v zimní sezoně statisticky rozchází. Výsledky článku predikují, že je tento jev způsoben parametry chladicí vody odebírané z okolních zdrojů, která má v letní a v zimní sezoně rozdílnou teplotu.



Obrázek 3.13: Výsledek výpočtu teplotního pole pro různé teploty chladicí vody [45]

Ekonomicky dohřívát chladicí vodu a udržovat jí na konstantní teplotě však nemá význam. Proto článek dále navrhuje využití odpadního tepla z ocelárny na přehřev chladicí vody [45]. Tím by byla zaručena její konstantní teplota po celý rok, což by mohlo vést ke zvýšení kvality odlévané oceli a lepší stabilitě procesu. Pro vyšší teploty chladicího média se navíc dle výsledků článku nabízí možnost snížení průtoků chladicí vody a tím dosáhnout její úspory, což opět spadá do ekologické optimalizace.

### 3.8 Celé texty článků

Dále následují plné texty předložených článků.

# OPTIMIZATION OF THE QUALITY OF CONTINUOUSLY CAST STEEL SLABS USING THE FIREFLY ALGORITHM

## OPTIMIZACIJA KAKOVOSTI KONTINUIRNO LITE JEKLENE PLOŠČE Z UPORABO ALGORITMA "FIREFLY"

Tomas Mauder, Cenek Sandera, Josef Stetina, Milos Seda

Brno University of Technology, Faculty of Mechanical Engineering, Technicka 2, Brno, Czech Republic  
ymaude00@stud.fme.vutbr.cz

Prejem rokopisa – received: 2010-10-20; sprejem za objavo – accepted for publication: 2011-03-21

The ambition to increase both the productivity and the product quality in the continuous casting process, led us to study new, effective mathematical approaches. The quality of the steel produced with the continuous casting process is influenced by the controlled factors, such as the casting speed or cooling rates. The appropriate setting of these factors is usually obtained with expert estimates and expensive experimental runs. This paper describes an algorithm for obtaining a black-box-type solution which maintains a high production rate and the high quality of the products. The core of the algorithm is our original numerical model of 2D temperature field designed for the real caster geometry. The mathematical model contains Fourier-Kirchhoff equation and includes boundary conditions. Phase and structural changes are modeled by the enthalpy computed from the chemical composition of the steel. The optimization part is performed with a recently created heuristic method, the so-called Firefly algorithm, in which the principles of searching for optimal values are inspired by the biological behavior of fireflies. Combining the numerical model and heuristic optimization we are able to set the controlled values and to obtain high-quality steel that satisfies the constraints for the prescribed metallurgical length, core and surface temperatures. This approach can be easily utilized for an arbitrary class of steel only by changing its chemical composition in the numerical model. The results of the simulations can be validated with real historical data in order to compare the relationship between the temperature field and the final product quality.

Key Words: continuous casting, Firefly algorithm, temperature field, enthalpy approach

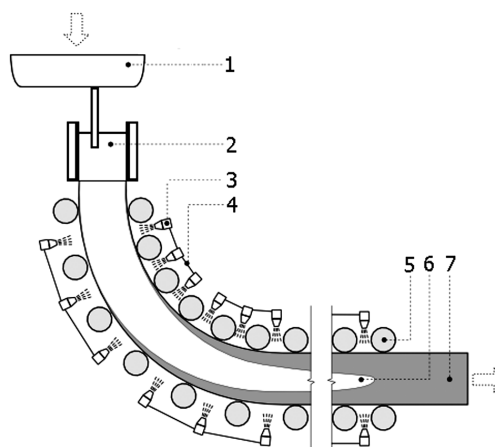
Ambicije za povečanje produktivnosti in kakovosti končnega proizvoda pri kontinuirnem ulivanju sta nas pripeljala do študija novih učinkovitih matematičnih prijemov. Na kakovost jekla, proizvedenega s kontinuirnim ulivanjem, vplivajo številni nadzorovani dejavniki, kot sta npr. hitrost ulivanja in ohlajanja. Ustrezno določanje teh dejavnikov je navadno povezano s strokovnimi ocenami in dragimi poizkusi. Prispevek opisuje algoritem za vrsto rešitev za ohranjanje visoke stopnje proizvodnje in visoke kakovosti izdelkov. Jedro algoritma je naš prvotni numerični model 2D-polja temperature, namenjen ulivalni geometriji. Ta matematični model vsebuje Fourier-Kirchhoffovo enačbo in tudi robne pogoje. Fazne in strukturne spremembe so bile modelirane z entalpijo, izračunano iz kemijske sestave jekla. Optimizacijski del je bil izveden z nedavno narejeno hevrstično metodo, s tako imenovanim algoritmom Firefly, kjer načela iskanja optimalnih vrednosti temeljijo na biološkem vedenju kresnic. Z združevanjem numeričnega modela in hevrstične optimizacije smo lahko predpisali nadzorovane vrednosti za izdelavo visokokakovostnega jekla, ki izpolnjuje predpisane pogoje za zagotovitev metalurške dolžine, ter temperature jedra in površine. Ta način je mogoče enostavno uporabiti za katero koli vrsto jekla le s spremembo kemične sestave v numeričnem modelu. Rezultate simulacij lahko potrdimo z resničnimi podatki iz preteklosti s primerjavo razmerja med temperaturnim poljem in kakovostjo končnega izdelka.

Ključne besede: kontinuirno litje, entalpija, algoritem Firefly, temperaturno polje

## 1 INTRODUCTION

Nowadays, continuous casting is the most common way of producing steel in the world. Every year, the steel industry processes millions of tons of liquid steel into semi-finished products such as slabs, blooms, and billets. A schematic representation of the continuous caster is shown in **Figure 1**. Molten steel (roughly 1550 °C) is poured down from a tundish into a water-cooled mould (primary cooling zone), where the steel obtains a solid shell. Afterwards, the steel is transported by rollers and cooled down by water sprays (secondary cooling zone). Groups of nozzles of sprays divide the secondary cooling zone into several coolant circuits. In the last zone, the steel surface is cooled down by free convection and radiation only (tertiary cooling zone).

Every steel company wants to produce steel as quickly as possible, while preserving the required



**Figure 1:** Scheme of continuous casting. 1 – tundish; 2 – mould; 3 – nozzle; 4 – coolant circuit; 5 – roller; 6 – liquid material; 7 – solid material

**Slika 1:** Shema kontinuirnega litja: 1 – vmesna ponova; 2 – kokila, 3 – šobe; 4 – hladilne šobe, 5 – valj, 6 – tekoči koren; 7 – trdna snov



quality<sup>1</sup>. There are a few ways to optimize the casting velocity and the output quality simultaneously. One possible method is to perform industrial trials, but this is very expensive and time-consuming. A better way is to use numerical simulations of the casting process and adjust these parameters to the optimal values. Previous studies were generally based on a simplified 2D temperature field model and were optimized by mathematical programming<sup>6</sup>, neural networks or a genetic algorithm.<sup>2</sup> These models describe the casting process very roughly and, therefore, their usage in real casters is not satisfactory.

Our original numerical model of the temperature field is designed for the real caster geometry. A modern heuristic method called the Firefly algorithm is used for the optimization of the model.

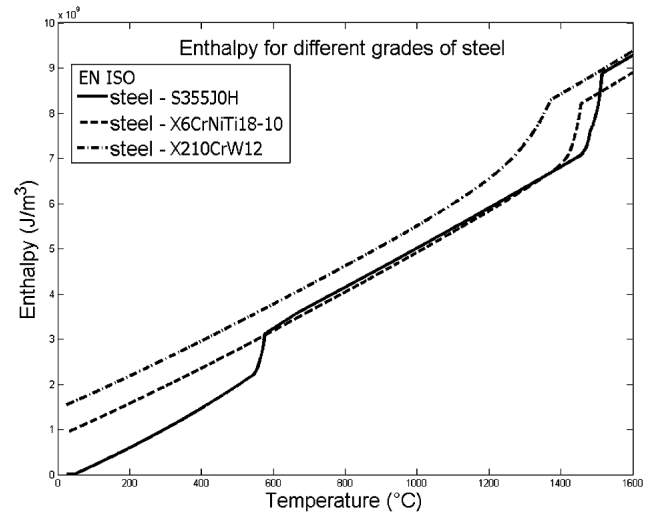
## 2 DEFINITION OF THE PROBLEM

The goal of the optimization is to improve the material properties of the final slab and increase the rate of production. With the aim to achieve this goal, we modified the casting process by controlling the casting speed and the cooling rates. The productivity is defined as the amount of cast material per unit time, thus, we maximize the casting speed under certain metallurgical criteria. The metallurgical criteria used in the optimization are formulated as a series of constraints that represent the quality of the slab products and the process feasibility. The criteria that must be met are the completeness of solidification before the unbending point (metallurgical length) and reaching the prescribed temperature in the exit area. The quality of the final material is influenced by the change of the surfaces and the core temperatures. The changes have to decrease in the whole profile and the temperature in the straightening area must be in the given range. The values for these constraints depend on the grade of cast steel.

## 3 MATHEMATICAL MODEL OF THE TEMPERATURE FIELD

All three basic mechanisms of heat transfer are incorporated into our model in a differential form. The conduction mechanism plays the dominant role inside the body of the cast steel, whereas convection and radiation take place only in the secondary and tertiary cooling zones, where they form the boundary conditions. The temperature field of the slab is described by the Fourier-Kirchhoff equation,<sup>3,4</sup> where the velocity component  $v_y$  (m/s) is considered only in the direction of casting. Phase and structural changes are included in the model by the use of a thermo-dynamical function of the volume enthalpy  $H$  (J/m<sup>3</sup>). The method is also called an enthalpy approach.<sup>3</sup>

$$\frac{\partial H}{\partial \tau} = \frac{\partial}{\partial x} \left( k \frac{\partial T}{\partial x} \right) + \frac{\partial}{\partial y} \left( k \frac{\partial T}{\partial y} \right) + v_y \frac{\partial H}{\partial y} \quad (1)$$



**Figure 2:** Relationship between the temperature and the enthalpy for three grades of steel

**Slika 2:** Razmerje med temperaturo in entalpijo za tri različna jekla

Equation (1) describes an unsteady-state 2D heat transfer (Fourier-Kirchhoff) written in Cartesian coordinates, where  $k$  (W/mK) is the thermal conductivity,  $T$  (K) is the temperature,  $H$  (J/m<sup>3</sup>) is the volume enthalpy,  $\tau$  (s) is the real time, and  $x$ ,  $y$ , are space coordinates. In order to have a well-defined problem, the initial and boundary conditions must be provided. The boundary conditions include the heat flux in the mould and under the rollers, forced convection under the nozzles and free convection and radiation in the tertiary cooling zone. The complete numerical model of the temperature field, including boundary conditions in Cartesian and cylindrical coordinates, can be found in.<sup>4</sup>

Equation (1) is discretized by the finite-difference method<sup>3,4</sup> using an explicit formula for the time derivative. The mesh for the finite-difference scheme is non-equidistant and its nodes are adapted to the real rollers and the positions of the nozzles. Equation (1) contains both enthalpy and temperature, so during the simulation the corresponding temperature must be calculated from the enthalpy for each node at each time step. **Figure 2** shows the relationship between the temperature and the enthalpy for three different grades of steel. This numerical model allows us to apply various enthalpy-temperature functions and thermal conductivity-temperature curves, and thus the temperature field can be calculated for various steels, only by defining their chemical composition.

## 4 OPTIMIZATION ALGORITHM

Our aim is to optimize the continuous casting process by processing its mathematical model. The only parameters we can control are the casting speed and the cooling rates. These parameters are included in the initial and boundary conditions of the model and they can acquire real values from a given continuous bound

interval. We need to find their values such that the final temperature field is the best possible. This problem belongs to the area of nonlinear constraint optimization and, therefore, it is usually impossible to obtain the exact solution. We use a method based on nature-inspired metaheuristics called the firefly algorithm.

The main principle is to maintain a group of fireflies where each of them represents one particular solution. These solutions must be comparable with each other in order to be able to decide which one represents a better solution and which one is worse. The algorithm starts with a number of randomly generated solutions (fireflies) and with their evaluations. The evaluation (also called the objective function) describes how much the solution is good and how much it violates the prescribed constraints. During the iteratively repeated algorithm steps, the worse fireflies move towards the better ones and at the end of the computation most of them are concentrated around the best discovered solution. A detailed description of these metaheuristics can be found in.<sup>5</sup>

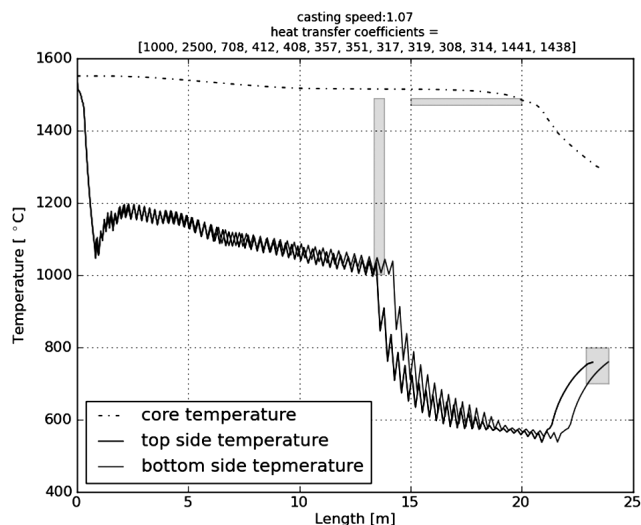
The firefly, in our implementation, is represented by a vector of fourteen real numbers, the first of which is the casting speed and the next thirteen numbers describe the cooling rates for thirteen cooling circles in the caster. Therefore, the search space of all possible solutions has fourteen independent dimensions and the fireflies moves there according to the aforementioned scheme. The evaluation function is defined as a weighted sum of optimized quantity (casting speed) and values representing the violations of the prescribed metallurgical criteria.

Each evaluation involves one simulation run of the model with parameters related to the actual firefly. This is quite time-consuming because the numerical simulations usually take a long time.

The firefly algorithm is not the only possible method for solving problems like this. It was chosen from a range of other heuristics because of its uncomplicated implementation and its appropriate performance in a real-valued optimization.

## 5 RESULTS AND DISCUSSION

We implemented the described heuristic algorithm in Python and the numerical model of the temperature field in MATLAB. The communication between them is provided through COM technology. The algorithm was tested on the geometry of a real caster with the steel number S355J0H. The objective function contains the weighted sum of the casting speed, the conditions for the length of the liquid material between 15 and 20 meters, the temperature in the bent part above 1000 °C, the decreasing trend of the temperature courses and the temperature in the exit part between 700 °C and 800 °C. The criteria of the metallurgical length and the exit temperature have to be fulfilled, and thus they have the



**Figure 3:** Surface and core temperature  
**Slika 3:** Temperatura površine in jedra

highest weight. The rest of the conditions have similar weights as each other.

After 10 iterations of 6 randomly chosen fireflies we obtained the result shown in **Figure 3**. It represents temperatures in the middle of the slab, and on its surfaces. The small oscillations are caused by alternating rollers and nozzles and they do not influence the quality of the material significantly.

The optimal speed was found to be 1.07 m/min and the metallurgical length is 19.9 m. If the metallurgical length was not on its maximum it would mean that there is a possibility for increasing the casting speed. But because our metallurgical length is almost 20 m, we have a good indication that we found at least a local extreme. The surface temperatures are above 1000 °C in the whole bent part (up to 13 m) and it keeps the material deformable before the straightening. The temperature in the last part increases, because there are no nozzles and the heat from the kernel is transported on the surface.

The obtained optimal solution fulfils all the prescribed conditions and the steel cast produced with this setting is of high quality and very economical.

## 6 CONCLUSION

This paper deals with suitable tools for optimization of the slab casting process. We have created an algorithm for the fast and effective casting of high-quality steel. The algorithm controls the cooling rates in the developed numerical model and optimizes it by using the so-called firefly algorithm. The obtained solution complies with all the specified criteria and therefore it can produce cheap final material. The whole method is very flexible and can be modified for an arbitrary grade of steel or quality conditions.

Further research will focus on making the algorithm more precise. This includes the 3D numerical model and

the specification of all the conditions that influence the final quality of the cast steel.

## ACKNOWLEDGEMENT

The authors gratefully acknowledge the financial support from the projects GA106/08/0606 and GA106/09/0940 funded by the Czech Science Foundation, Junior research project on BUT BD13002 and Specific research BD 13001002.

## 7 REFERENCES

- <sup>1</sup> A. S. Normanton, et al., Improving surface quality of continuously cast semis by an understanding of shell development and growth, Final report, Technical steel research series, Luxembourg, (2005), 349
- <sup>2</sup> C. A. Santos, J. A. Spim, A. Garcia, Mathematical modeling and optimization strategies (genetic algorithm and knowledge base) applied to the continuous casting of steel, *Engineering Applications of Artificial Intelligence*, 16 (2003), 511–527
- <sup>3</sup> D. M. Stefanescu, *Science and Engineering of Casting Solidification*, Second Edition, New York, Springer Science, (2009), 402
- <sup>4</sup> J. Stetina, F. Kavicka, J. Dobrovska, L. Cemek, M. Masarik, Optimization of a concasting technology via a dynamic solidification model of a slab caster. *Materials Science Forum*, (2005) 5, 475–479, 3831–3834
- <sup>5</sup> S. Lukasik, S. Zak, Firefly Algorithm for continuous constrained optimization tasks, *Computational Collective Intelligence. Semantic Web, Social Networks and Multiagent Systems Lecture Notes in Computer Science*, 5796 (2009), 97–106, DOI: 10.1007/978-3-642-04441-0\_8
- <sup>6</sup> T. Mauder, J. Novotny, Two mathematical approaches for optimal control of the continuous slab casting process, *Mendel 2010 – 16th International Conference on Soft Computing*, Brno, Brno University of Technology, 2010, 395–400

# Optimal Control Algorithm for Continuous Casting Process by Using Fuzzy Logic

Tomas Mauder,\* Cenek Sandera, and Josef Stetina

A supervision algorithm for controlling of continuous casting (CC) process is presented. The control strategy is based on the observation of temperature distribution through the casting strand. The algorithm is composed of two parts, an original 3D transient numerical model of the temperature field and the fuzzy-regulation model. The numerical model calculates and predicts the temperature distribution while the fuzzy-regulation model tracks the temperature in specific areas and tunes the casting parameters such as the casting speed, the cooling intensities in the secondary cooling, etc. The main goal is to keep surface and core temperatures in the specific ranges corresponding with the hot ductility of steel and adequately reacts on the variable casting conditions. The results show good and robust control behavior, fast response to dynamic system changes and general applicability for any CC process.

## 1. Introduction

Continuous casting (CC) technology originated almost 60 years ago, nowadays utilized in more than 95% of the world steel production. Through the years the product quality, production efficiency, operating safety, casting of special steels, alloys has been increased. These developments were allowed by equipment revamps, updates in installation setups, computer process, post-process control, better problem understanding by long-term experiments, computer simulations, etc. The report of Nortmanton et al.<sup>[1]</sup> shows that there is still a strong effort for optimization of the casting process in order to achieve better quality, high productivity in the environmental friendly operation.

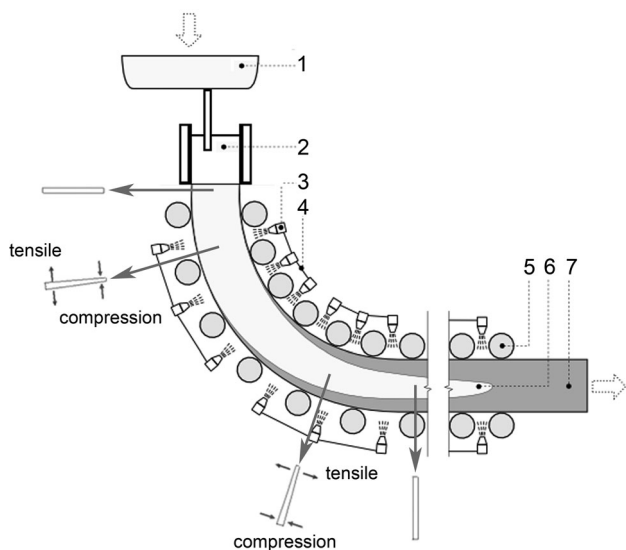
During the processing of the steel in a CC, there can arise many problems with quality. The solid shell is permanently subjected to thermal and mechanical stresses and it can give rise to cracks or the breakout of liquid steel through the solid shell. Birat et al.<sup>[2]</sup> presented the typical sources of the mechanical stresses: friction in the mold, ferrostatic force, poor adjustment of the casting speed, roll gaps, bending and straightening of the strand, etc. **Figure 1** shows CC installation and mechanical stresses in specific positions. Cracks caused by bending and straightening are influenced by the ductility of steel. Jansto<sup>[3]</sup> documented that the steel has reduced ductility over specific tempera-

ture ranges dependent on the steel composition, which has important implications for crack formation. Other important sources of stress are the temperature gradients set up by unexpected slowing or increasing of the rate of heat abstraction.

It is well known that the properties of the final material are highly dependent on the course of temperatures reached during the casting and overall temperature stability. However control of the CC process based on strand temperature distribution is a complex problem and cannot be achieved without proper knowledge of heat and mass transfer, solidification, micro and macrosegregation, crack formation, etc. Conducting of industrial trials is too expensive, time-consuming, and in some cases even impossible. Adjustment of the process by trial-and-error is out of the question, which makes the computer simulation the only suitable option. Computational models are nowadays a powerful and reliable tool to simulate different thermo-mechanical metallurgical processes; hence they are increasingly being used to investigate the steel industry processes, such as CC, hot rolling, cold rolling, heat treatment, etc. These models often include the combination of numerical and optimization algorithms, which can be done in many different ways and each of them has its advantages and drawbacks. The main attributes of these models should be as follows: the correct validated simulation to be able to run in real time, react on critical situations and dynamic system changes, store the data, optimize the cooling process, etc. This paper presents a coupling approach, which combines the original numerical model of temperature field and the original regulation algorithm. The main idea is based on regulation of the CC process by using fuzzy logic as a supervision monitoring system.

---

[\*] T. Mauder, C. Sandera, J. Stetina  
Faculty Mechanical Engineering, Brno University of Technology,  
Technicka 2, Brno, Czech Republic  
Email: mauder@fme.vutbr.cz



**Figure 1.** Scheme of the continuous casting and mechanical stresses during bending and straightening. 1 – tundish; 2 – mold; 3 – nozzle; 4 – cooling circuit; 5 – roller; 6 – liquid material; 7 – solid material.

From the physical point of view, the CC is the complex transient heat and mass transfer problem encompassing phase change by the solidification of steel.<sup>[4]</sup> This class of problem is generally referred to as phase change or Stefan problems. Through the years many authors published the steady-state and the transient numerical models of temperature field. However, most of them concern with the off-line simulation of the steady-state casting process and have a number of physical simplifications. Alizadeh et al.<sup>[5]</sup> proposed a 2D model and observed that the casting speed is the most effective parameter on mold heat removal, which means that it is the most important factor in control of the solidified shell thickness and slab temperature. Alizadeh et al.<sup>[5]</sup> also presented that the high superheat temperature may cause breakouts at the mold exit. Hardin et al.<sup>[6]</sup> presented a parametric study on more advanced transient 2D model, which allowed to observe the temperature response on the casting speed increase and decrease. One of the first 3D numerical model for the CC problem was introduced by Tieu and Kim<sup>[7]</sup> in 1997. The part of their work points on advantages of 3D in comparison to 2D numerical models. Wang et al.<sup>[8]</sup> developed a 3D model adapted to the Wu-Han Iron steelmaking plant. In order to increase the computation time Wang et al.<sup>[8]</sup> calculate heat transfer only in one quarter of the slab cross-section based on the axial symmetry. Gonzales et al.<sup>[9]</sup> extended the 3D numerical model by an inverse analysis procedure in order to properly estimate a heat flow in the mold. Another approach how to deal with 3D modeling of CC represents the so-called slice model, which neglects the heat transfer by conduction in the casting direction. This type of model

is presented, e.g., by Tambunan.<sup>[10]</sup> Rujiiu et al.<sup>[11]</sup> and Louhenkilpi et al.<sup>[12]</sup> created real-time transient 3D numerical models, which are able to operate directly in the steelmaking plant control system and they can collect the casting data. However, these models are based on simplified assumptions: simple geometry, constant thermophysical properties, average boundary conditions in the secondary cooling, use of empirical formulas for heat removal in the mold and secondary cooling areas, assuming plane symmetry, etc. These simplifications were mainly used because of computer power limitations, and the models therefore describe the casting process rather roughly. However, computational capabilities have progressed to the point where models used in the CC control include only minor physical simplifications and can provide more accurate results and eventually ensure a better steel quality. The numerical model presented in this paper is transient, fully three-dimensional and its geometry is designed according to the real caster. Boundary conditions were gained from large-scale experiments according to Raudensky et al.<sup>[13]</sup> and from real caster measurements, thermophysical properties of the steel were computed by the special solidification software IDS and the model runs faster than the real time even for fine mesh densities. The on-line version of the presented numerical model runs in EVRAZ VÍTKOVICE STEEL, a.s. plant, and was verified by the real temperature measurements acquired by pyrometers for a sufficient range of steel grades and casting conditions.

The numerical models can be supplemented by the optimization and the control algorithms. Previous works dealing with optimal control of CC process were optimized by mathematical programming or heuristic methods. Santos et al.<sup>[14]</sup> applied the genetic algorithm; Zhemping et al.<sup>[15]</sup> verified the usage of the ant colony algorithm; Zheng et al.<sup>[16]</sup> attempted to use the swarm optimization; Mauder et al.<sup>[17]</sup> applied the firefly algorithm; etc. These optimization concepts follow on iterative numerical model recalculation and progressive tuning of cooling parameters as a closed-loop system. Unfortunately, the numerical models in these works were often very simplified (which means with a short computation time), thus authors do not handle a number of optimization iteration (number of recalculation of the numerical model). The lack of this information complicates the potential usage of these optimization algorithms on complex numerical models. While the discussed algorithm based on regulation was designed mainly on precise 3D numerical models and is a special design to reach the optimum in small numbers of iteration. Some steelmakers control the CC process by conventional PID control systems, but PID control should not be used for nonlinear systems and systems with fast changes of the processing parameters. Furtmueller and del Re<sup>[18]</sup> discussed challenges and control issues in the CC and analyzed limitations of PID controlling. The presented regulation approach is based on fuzzy logic. Fuzzy logic is successfully run in many engineering and scientific

applications, therefore is natural to apply fuzzy logic to the CC control. Dussud et al.<sup>[19]</sup> applied the fuzzy logic on the mold level control and Tirian et al.<sup>[20]</sup> on the casting speed modification in order to predict the crack formation. The application of fuzzy control in this paper is more general since it is combined with the numerical model of temperature field. The regulator can react to an actual level of steel in the mold, to the casting temperature, metallurgical length, surface temperatures, and shell thickness under the mold. The optimal control is achieved by the modification of the casting speed and of the spraying intensity in secondary cooling. The presented fuzzy regulator behaves robustly and is designed for fast responses to dynamic system changes.

The basic idea of the fuzzy regulation strategy is composed of two goals: to increase the quality of final products and to maximize the casting speed in order to increase the productivity of casting. Steel quality is controlled by keeping the surface and core strand temperatures in the specific ranges corresponding to the hot ductility of steel in order to avoid surface and core defects.<sup>[3]</sup> Temperatures on the strand surfaces are monitored in specific locations. We have called these locations the “control points.” The inner quality is influenced by the position of the metallurgical length (the length of liquid material from the meniscus). Thus, the position of the metallurgical length should also be kept in some reasonable range. If temperatures in the control points and the metallurgical length are in the specific ranges the fuzzy regulator modifies the casting speed until maximal value is reached.

## 2. Numerical Model of Heat Transfer

The mathematical formulation of heat transfer and solidification to the temperature distribution and solid shell profile prediction is based on the governing equation of transient heat conduction also called the Fourier-Kirchhoff equation.<sup>[9,11]</sup> Three-dimensional heat transfer can be expressed as

$$\frac{\partial H}{\partial \tau} + v \frac{\partial H}{\partial z} = \nabla \cdot [k_{\text{eff}}(T) \nabla T] \quad (1)$$

where  $k_{\text{eff}}$  is the effective thermal conductivity ( $\text{W m}^{-1} \text{K}^{-1}$ );  $T$  is the temperature (K);  $H$  is the volume enthalpy ( $\text{J m}^{-3}$ );  $\tau$  is the time (s);  $v$  is the casting speed ( $\text{m s}^{-1}$ ), and  $z$  is the direction of casting (m). In order to take into account the convective heat transfer in the liquid and mushy zone due to the liquid flow, the effective thermal conductivity can be approximated by<sup>[21]</sup>

$$k_{\text{eff}} = k_s f_s + A k_l (1 - f_s) \quad (2)$$

Here,  $k_l$  and  $k_s$  are the thermal conductivities of the liquid and solid phases, respectively.  $f_s$  is the solid

fraction (–), and if  $f_s = 0$ , element is still liquid and only thermophysical properties of the liquid are considered, and if  $f_s = 1$ , the element is completely solid.  $A$  is a constant, which has a recommended value according to the Louhenkilpi et al.<sup>[22]</sup> between 1 and 8. If the constant  $A$  is 1, there is no increased heat transfer in the mushy or liquid region due to convection. By the many computations and verifications for the slab casters, we have determined a value of  $A \approx 1.5$ .

### 2.1. Phase Change

When the molten steel is solidified into solid steel, a large amount of heat (latent heat) is released. The latent heat must be taken into account in order to obtain an accurate result. Muhieddine et al.<sup>[23]</sup> described several methods concerning to simulation of solidification problems, including the temperature recovery method, specific heat capacity method, and the enthalpy method. Li et al.<sup>[24]</sup> applied front tracking method, but only for 2D problem. To decide which method is better is difficult and it depends on particular problem. In presented numerical model, the enthalpy method was chosen because its feature is that the evaluation of the latent heat is accounted by the enthalpy (1). The relation between the enthalpy and temperature can be defined in terms of the latent heat release characteristic of the phase-change material by<sup>[4]</sup>

$$H = \int_0^T \left( \rho(\xi) c(\xi) - \rho(\xi) \Delta H \frac{\partial f_s}{\partial \xi} \right) d\xi \quad (3)$$

where  $\Delta H$  is the latent heat ( $\text{J kg}^{-1}$ );  $\rho$  is the material density ( $\text{kg m}^{-3}$ );  $c$  is the specific heat capacity ( $\text{J kg}^{-1} \text{K}^{-1}$ ). On equilibrium solidification, it is assumed that complete diffusion occurs between the solid and liquid states during solidification. Tambunan<sup>[25]</sup> summarized several models that are generally used to evaluate the relationship between the solid fraction and temperature, such as lever rule model, Scheil model, Brody–Flemings model, linear model, and nonlinear models. If there is not any explicit relation between the solid fraction and temperature or the solid fraction cannot be easily evaluated as a function of temperature because phase diagrams are not known, the linear model is generally used, which yields

$$f_s = \frac{T_1 - T}{T_1 - T_s}, \quad T_s \leq T \leq T_1 \quad (4)$$

where  $T_s$  is the solidus temperature and  $T_1$  is liquidus temperature. In the proposed numerical model, the Equation 3 is substituted by an enthalpy-temperature function computed by the solidification analyses package IDS (see Section 2.3).

## 2.2. Initial and Boundary Conditions

In order to have a well-posed problem, initial and boundary conditions must be provided. The initial condition can be expressed as

$$T(x, y, z, \tau) = T_0(x, y, z) \quad (5)$$

where  $T_0$  is the initial temperature distribution and can be equal to the casting temperature  $T_{\text{cast}}$ .

Determination of the boundary conditions has to be made properly, because boundary conditions highly influence the numerical result. This section describes in more detail boundary conditions used by the presented numerical model.

Boundary conditions include the meniscus temperature, heat flux in the mold and under the rollers, forced convection under the nozzles, and free convection and radiation in the tertiary cooling zone.

Temperature in meniscus

$$T(x, y, z) = T_{\text{cast}} \quad (6)$$

In exit area

$$-k \frac{\partial T}{\partial n} = 0 \quad (7)$$

In mold and beneath the support rollers

$$-k \frac{\partial T}{\partial n} = \dot{q} \quad (8)$$

In secondary and tertiary zone

$$-k \frac{\partial T}{\partial n} = \text{htc}(T - T_{\text{water}}) + \sigma \varepsilon (T^4 - T_{\text{amb}}^4) \quad (9)$$

where  $T_{\text{water}}$  is the cooling water temperature;  $T_{\text{amb}}$  is the ambient temperature; htc is the heat transfer coefficient ( $\text{W m}^{-2} \text{K}^{-1}$ );  $\sigma$  is the Stefan–Boltzman constant ( $\text{W m}^{-2} \text{K}^{-4}$ ), and  $\varepsilon$  is the emissivity of the slab surface (–).

In ref.,<sup>[5–12]</sup> a large number of empirical relationships for determination of boundary condition through the caster can be found. Unfortunately, there is a lack of informations such as rate of water flow in mold walls, distance and impact angel between nozzle and strand surface, influence of Leidenfrost effect, influence of strand temperature to the heat transfer coefficient, etc. The more accurate way is using laboratory experiments and operating temperature measurement.

Heat removal in the mold walls (Equation 8) can be determined from measurement of cooling water temperatures and flow rate using the following energy balance

$$\dot{q}_{\text{mold}} = \frac{\dot{V}_{\text{water}} \rho_{\text{water}} c_{\text{water}} (T_{\text{out}} - T_{\text{in}})}{S_{\text{mold}}} \quad (10)$$

where  $V_{\text{water}}$  is the water volume flow ( $\text{L s}^{-1}$ ) and  $S_{\text{mold}}$  is the mold area ( $\text{m}^2$ ). Heat flux in the real mold varies along the mold length and width and drops mainly near the corners. The heat flux layout can be compiled from the average value using additional information like a matrix of thermocouples in the mold wall.

Heat flux in the roller contact area depends mainly on the roll contact length in the casting direction. In the case that the rollers have internal water cooling, the heat flux can be described similar as in the mold area by heat balance.<sup>[10]</sup> Otherwise, the assumption can be made that the heat removal from slab to the roller is equal to the heat removal from roller to surroundings. Then the heat flux can be summarized by the following formula

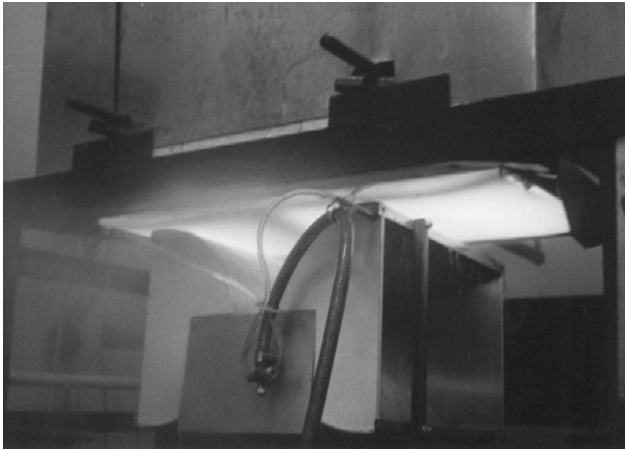
$$\dot{q}_{\text{rol}} = \frac{\pi(l/2)d}{S_{\text{rol}}} \text{htc}_{\text{rol}}(T_{\text{rol}} - T_{\text{amb}}) + \varepsilon \sigma (T_{\text{rol}}^4 - T_{\text{amb}}^4) \quad (11)$$

where  $d$  is the roller diameter (m);  $S_{\text{rol}}$  is the roller surface ( $\text{m}^2$ ), and  $T_{\text{rol}}$  is the roller surface temperature.

The domain between the rollers can be divided into four different cooling regions: roller contact area, pre-nozzle area, spraying area, after-spray, and pool-water area. The heat transfer coefficient in the pre-nozzle and the post-nozzle area involve mainly free convection and radiation. The heat transfer coefficient for these areas as well as for the tertiary cooling zone can be approximated by the empirical formula by<sup>[6]</sup>

$$\text{htc}_{\text{nat}} = 0.84(T_{\text{surf}} - T_{\text{amb}})^{1/3} \quad (12)$$

In the spraying area, the strand is cooled by the spray of water or water–air mixture. Nozzle parameters like air and water flow, nozzle position, and impact angles have an effect on the cooling efficiency. Totten et al.<sup>[21]</sup> showed several empirical formulas showing how to deal with the heat transfer coefficient beneath the nozzle. However, these empirical formulas include many constants and parameters and their correct determination for a particular cooling setup is difficult. The advantage of model discussed in this paper is that obtains its heat transfer coefficients from measurements of the spraying characteristics of all nozzles used by the caster on a so-called hot plate in the experimental laboratory, according to ref.<sup>[13]</sup>. The experiment is shown in Figure 2 where the nozzle is placed between two rollers and moves under the test plate and sprays the surface. A sufficient range of operational pressures of water and a sufficient range of casting speeds of the strand (i.e., casting speed) were measured. Heat transfer coefficients obtained by the inverse heat conduction problem are entered into a database of boundary conditions from which (based on interpolation) the model determines the appropriate heat transfer coefficient beneath the nozzle for the required temperature of the surface of the slab, the operational pressure of the water, and for the required casting speed. This approach represents a unique combination of experimental



**Figure 2.** Laboratory experiment on hot plate.

measurement in a laboratory and a numerical simulation for the calculation of the nonlinear boundary conditions.

### 2.3. Thermophysical Properties

The thermophysical parameters such as thermal conductivity, density, specific heat capacity, and enthalpy are all strong functions of temperature. Generally, there are three common ways how to determine them. Many authors use the empirical relationships, which can be applied for certain steel grades and temperature ranges. The second possibility is the real material measurement on small steel samples via differential thermal analysis or differential scanning calorimetry. The results are much better than in previous approaches, but the expensiveness of these measurements and large numbers of different steel grades cast on CC makes it unacceptable. The last way to estimate thermophysical parameters are the solidification analysis packages. The results of these packages are acceptable and validated for a large scale of steel grades. In this paper, the

thermophysical parameters are computed from the specific chemical composition of the steel by using the solidification analysis package IDS.<sup>[26]</sup>

The results for steel grade S355J0H with average chemical composition are in **Figure 3**. This steel was chosen purposely because it represents frequently cast low-carbon steel. All results in this paper were calculated for this particular steel. **Figure 3** shows the nonlinear thermophysical properties, which make the numerical simulation more complex but in the same time more realistic.

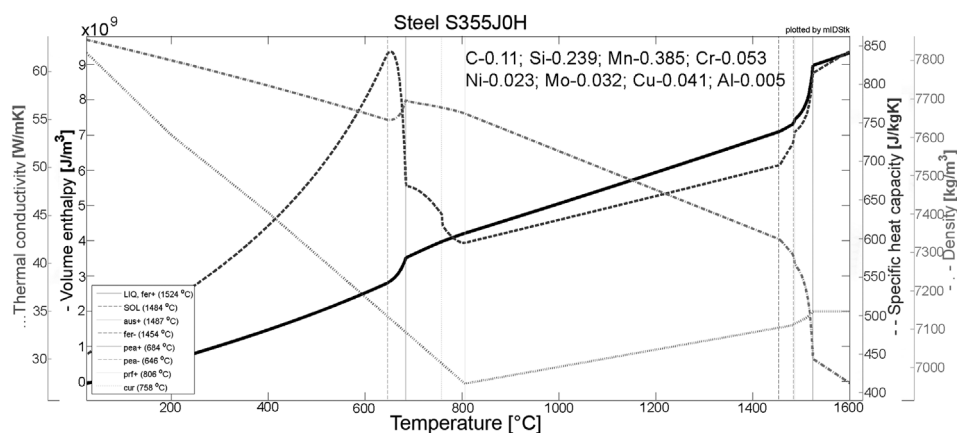
### 2.4. Geometric Conditions

During the simulation, the Equation 1 is solved numerically. All geometric conditions are taken from the real slab caster operated in the EVRAZ VÍTKOVICE STEEL, a.s. The computing domain for numerical validation was chosen for frequently cast slab cross-section 1530 mm × 250 mm. The caster geometry is as follows: the mold length of 900 mm; radius of 8000 mm; length of secondary cooling after unbending point of 8500 mm; length of tertiary cooling of 2000 mm. The secondary cooling zone is divided into 13 independent regulation zones (cooling circuits) according to **Table 1**. The circuits 1, 3, 4, and 5 influenced both the top and the bottom surfaces, while zones 6, 8, 10, and 12 spraying top surface and zones 7, 9, 11, and 13 spraying bottom surface.

### 2.5. Numerical Discretization

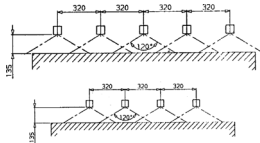
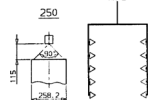

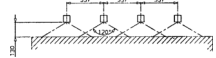
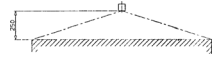
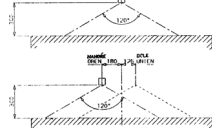
In this study, we propose non-uniform Cartesian and cylindrical grids as the spatial domain discretization and finite difference method for numerical solution of the governing Equation 1.

There are generally two approaches for the time domain discretization, implicit and explicit schemes. The former has no restriction on its time stepping. However, in each



**Figure 3.** IDS results for steel S355J0H.



Regulation circuit	Type of nozzle	Number of nozzles	Nozzle configuration
1	148.638.30.43	18	
2	660.766.30	10	
3	148.638.30.43	32	
4	148.638.30.43	24	
5	100.728.30.24	12	
6	100.638.30.24	12	
7	100.638.30.24	12	
8	100.638.30.24	12	
9	100.638.30.24	12	
10	100.638.30.24	10	
11	100.638.30.24	10	
12	100.538.30.24	24	
13	148.538.30.24	24	

**Table 1.** Type of nozzles in the secondary cooling.

time step one has to solve a global system of nonlinear equations. The solution of such a system of equations usually takes high computational cost and memory. Also, the implementation of implicit methods is usually a difficult task. The latter has a local nature and is easy to implement. However, it suffers from the severely restricted time step due to stability requirements. It seems that in spite of large time increment, the computational efficiency of implicit methods is essentially not better than explicit methods for solidification modeling. Tavakoli and Davami<sup>[27]</sup> summarize the advantages and the drawbacks of implicit and explicit schemes according to the following properties: efficiency, robustness, adjustability, accuracy, simplicity of implementation, and scalability. From the revue, it is obvious that in this case (heat transfer with phase change/solidification), the performance of the implicit method is not better than that of the explicit ones

because the problem is nonlinear. The best results were reached by the alternating direction explicit scheme (ADE) proposed by Larkin,<sup>[28]</sup> which is modification of Saul'yev's method. Unlike the classic explicit scheme, the ADE is more stable (Tavakoli and Davami<sup>[27]</sup> shows that in some cases unconditionally), which allows larger time steps. The ADE scheme is asymmetric and the governing equation is solved independently in the downward (−) and upward (+) direction. Final temperature in node  $i, j, k$  for each time step is averaged from results  $T_{i,j,k}^+$  and  $T_{i,j,k}^-$ . Tavakoli and Davami<sup>[29]</sup> modified and successfully applied the ADE scheme on a stationary casting solidification process. This problem is a simplified CC problem described by Equation 1 where the second term on the left hand side is neglected. The following formulations in Equation 14–18 generalize the ADE scheme for the CC process. The finite difference method with the ADE formula for a uniform

space and time steps and for temperature-invariant physical properties can be described by

$$H_{i,j,k}^{n+1} \psi^\pm = H_{i,j,k}^n + \Delta\tau \left[ QX^\pm + QY^\pm + QZ + v \frac{H_{i,j,k-1}^{n+1}}{\Delta z_{k-1}} \right] \quad (14)$$

where

$$\psi^+ = 1 + \frac{1}{C_{i,j,k}^n} \left[ \frac{k_{i-1/2,j,k}^n}{\Delta x^2} + \frac{k_{i,j-1/2,k}^n}{\Delta y^2} + \frac{k_{i,j,k-1/2}^n}{\Delta z^2} + v \frac{\Delta\tau}{\Delta z} \right]$$

$$\psi^- = 1 + \frac{1}{C_{i,j,k}^n} \left[ \frac{k_{i+1/2,j,k}^n}{\Delta x^2} + \frac{k_{i,j+1/2,k}^n}{\Delta y^2} + \frac{k_{i,j,k-1/2}^n}{\Delta z^2} + v \frac{\Delta\tau}{\Delta z} \right] \quad (15)$$

The heat flux in direction  $x$  can be expressed as

$$QX^+ = k_{i-1/2,j,k}^n \frac{H_{i-1,j,k}^{n+1}}{\Delta x^2 C_{i-1,j,k}^n} + k_{i+1/2,j,k}^n \frac{T_{i+1,j,k}^n}{\Delta x^2} - k_{i+1/2,j,k}^n \frac{T_{i,j,k}^n}{\Delta x^2}$$

$$QX^- = k_{i+1/2,j,k}^n \frac{H_{i+1,j,k}^{n+1}}{\Delta x^2 C_{i+1,j,k}^n} + k_{i-1/2,j,k}^n \frac{T_{i-1,j,k}^n}{\Delta x^2} - k_{i-1/2,j,k}^n \frac{T_{i,j,k}^n}{\Delta x^2} \quad (16)$$

where

$$k_{i+1/2,j,k}^n = \left( \frac{0.5}{k_{i+1,j,k}^n} + \frac{0.5}{k_{i,j,k}^n} \right)^{-1} \quad k_{i-1/2,j,k}^n = \left( \frac{0.5}{k_{i-1,j,k}^n} + \frac{0.5}{k_{i,j,k}^n} \right)^{-1} \quad (17)$$

The axis  $y$  and  $z$  can be expressed analogously. The index  $n + 1$  is associated to the future time,  $n$  is the index corresponding to the actual time,  $\Delta\tau$  is the increment of the time,  $x$ ,  $y$ , and  $z$  are the directions,  $\Delta x$ ,  $\Delta y$ , and  $\Delta z$  are increments in the directions,  $i$ ,  $j$ , and  $k$  are the positions. The  $C$  is the apparent heat capacity ( $\text{J kg}^{-1} \text{K}^{-1}$ ) and can be describe by<sup>[4]</sup>

$$C(T) = \frac{\partial H}{\partial T} = \rho(T)c(T) - \rho(T)\Delta H \frac{\partial f_s}{\partial T} \quad (18)$$

The stability of the presented approach is higher than the well-known explicit stability condition

$$\Delta\tau \leq \frac{1}{(2k/\rho c)((1/\Delta x^2) + (1/\Delta y^2) + (1/\Delta z^2)) + (v/\Delta z)} \quad (19)$$

### 2.6. Mesh Size

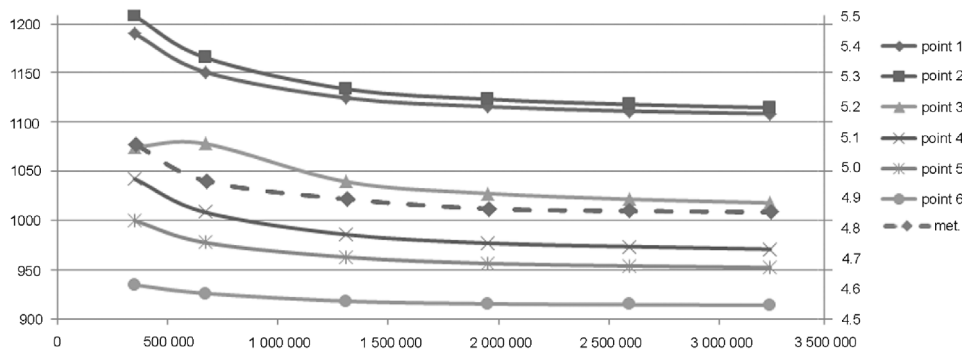
The numerical model has non-equidistant mesh in all directions. The reason for this is that the largest temperature gradients are near the surface. In axis  $z$ , the nodes are adapted to the real rollers and nozzles positions to get more accurate determination of boundary conditions.

Between the numerical results accuracy (fineness of mesh) and speed of simulation there has to be a compromise. In the finite difference method, a finer mesh typically results in a more accurate solution. The results should not be affected by changing the size of the mesh. The formal method of establishing mesh convergence requires a curve of a critical result parameter (temperatures) in a specific fixed location, to be plotted against some measure of mesh density. Several convergence runs were tested. The results in **Figure 4** can be used to indicate when convergence is achieved, or how far away the most refined mesh is from full convergence. In  $x$  axis is the number of elements, in  $y$ -left axis is the temperature in several points on the top surface (at the end of each cooling circuit) and in the  $y$ -right axis is the value of the metallurgical length.

This study shows that the number of elements should be at least 2 000 000. Finer mesh does not affect the results significantly.

### 2.7. Software Implementation and Parallel Computation

The core of numerical model is programmed in C++, while the graphical output and the data transfer are solved by MATLAB<sup>®</sup>. In cooperation with IDS, the model allows the user to apply various enthalpy-temperature functions, thus the temperature field can be calculated for various



**Figure 4.** Temperatures and metallurgical length for different mesh densities.

steel grades by describing their chemical composition. The temperature is calculated in each time step from the enthalpy by the binary searching algorithm.

The explicit schemes easily allow the parallel decomposition. Nowadays, the computation on multiple processors is the common standard in the numerical codes and computation on the graphic processing unit GPU can decrease even more the computation time. Klimes and Stetina<sup>[30]</sup> dealing with the numerical model of the temperature field for CC process solved by the GPU. Their results clearly define the computing efficiency and better optimization possibility.

### 2.8. Numerical Model Validation

The numerical model of the temperature field without a proper validation cannot be used for the real casting process control. The presented model is validated by surface temperature measurement provided by two pyrometers. Special water-cooled pyrometers installed by SMS Demag were used in two caster locations 12677 and 20909 mm from the meniscus on the top surface (see Figure 5). The unevenly oxidized surface of strand affects the emissivity of surface and makes the non-contact temperature measurement difficult. Therefore, the data from the pyrometers before the use for numerical model validation have to be statistically processed. The median filtering and averaging of measured data through the casting sequence were used. The temperature validation contains a large number of simulations for different steel grades, size of slab, and casting conditions. The real history data was selected from castings provided in 2011 and 2012.

Figure 5 shows the temperatures history on selected points (top surface, bottom surface, corner, and core) through the caster obtained by simulation and the comparison with pyrometer measurement.

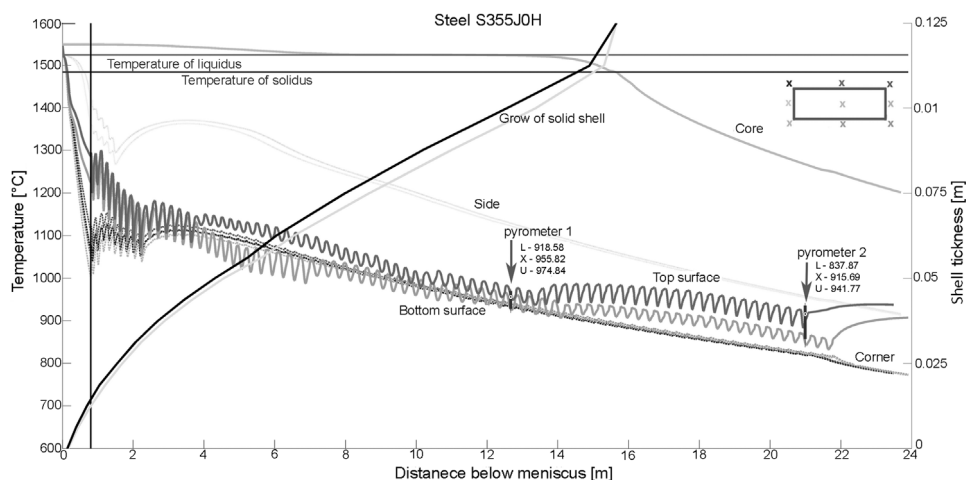


Figure 5. Temperature distribution and verification by two pyrometers.

The casting conditions were the following: casting speed  $0.79 \text{ m min}^{-1}$ , casting temperature  $1549 \text{ }^\circ\text{C}$ , average heat flux in mold  $795594.4 \text{ W m}^{-2}$ , cooling rates in cooling circuits 1–13 (70.7; 48.1; 93.7; 72.4; 78.3; 38.9; 78.4; 40.3; 51.2; 29.4; 38.8; 49.0; and  $78.5 \text{ L min}^{-1}$ ). The results from many simulations show a good agreement between the numerical results and the pyrometer measurements.

The presented transient 3D numerical model runs faster than real time and includes more than 2 000 000 space elements, has nonlinear boundary conditions, nonlinear thermophysical properties and was validated for large scale of casting conditions. The on-line version of the presented numerical model runs in control system in EVRAZ VÍTKOVICE STEEL, a.s.

### 3. Fuzzy Logic Regulator

The numerical model of temperature field can calculate the temperature distribution of the strand for given casting parameters such as initial temperature distribution, intensity of cooling, etc. The problem looking for optimal input parameters ensuring a known (desire) temperature distribution is called the inverse problem. In Section 1, some literature dealing with the optimization of casting process was mentioned.<sup>[8–11]</sup> The algorithms based on the black-box approach such as genetic algorithms, neural networks, etc. are only applicable for steady-state simulations because they require a large number of numerical model evaluations for different casting parameters. In the transient processes, such as CC process, reaction on specific or nonstandard situations in the optimal way, it is essential to ensure high quality of cast steel. There are several well-known regulation algorithms such as PID control systems, model predictive control, fuzzy regulation, etc. These approaches have some advantages but also drawbacks: PID control systems should not be used for

nonlinear systems and systems with fast changes of processing parameters.<sup>[18]</sup> The model predictive control needs several feed-forward evaluations of the numerical model at the same time, which can be a computation problem for complex numerical models without massive parallelization.<sup>[30]</sup>

The past few years have witnessed a rapid growth in the number and variety of applications of fuzzy logic. Fuzzy logic techniques have been used in image-understanding applications, detection of edges, feature extraction, classification, clustering, regulation systems, etc.

This section proposes the idea of how to optimally control the casting process by using fuzzy logic. The optimization/regulation algorithm was created with the aim to optimize parameters of the caster for a given particular grade of steel. **Figure 6** shows the block scheme of fuzzy regulator and numerical model. The fuzzy regulator operates as a supervision system and adjusts numerical model casting parameters in a closed-loop.

An essential aspect of fuzzy control is the defining and combining linguistic variables and linguistic rules. Four linguistic variables were created. The “error” presents the temperature difference at a particular control point; the “impact” represents the mean distance between a control point and the adjusting cooling circuit; “total error” is calculated as a sum of all “errors;” and the “metallurgical length” represents the actual position of a solidification point. The linguistic rules are in the form that IF  $x$  is A AND  $y$  IS B, THEN  $z$  IS C. So for instance, IF the actual error of the controlled temperature IS “big” AND the impact IS “big,” THEN the modification of cooling intensity IS also “big.” Similar fuzzy rules are applied for each circuit and for modification of the casting speed. By evaluation of these simple rules the optimal values can be found. Membership functions for all linguistic variables are trapezoidal-shaped uniformly distributed through the corresponding intervals. As a defuzzification method

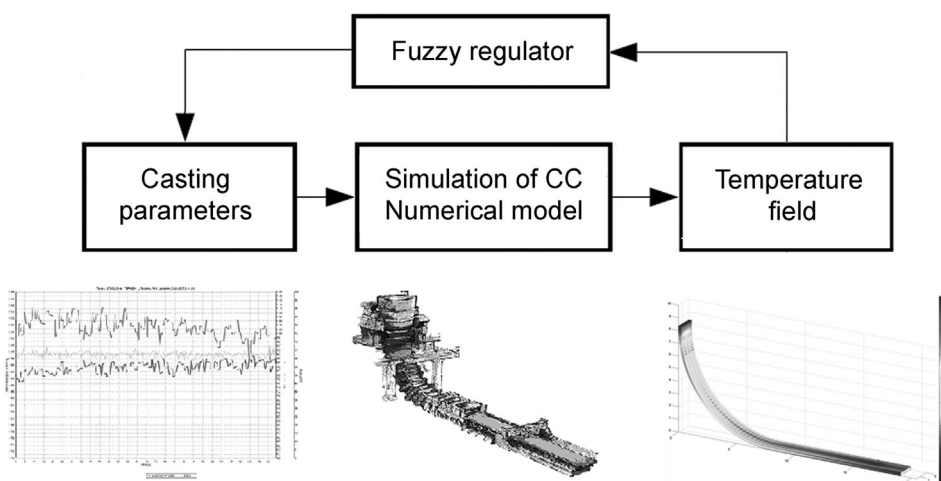
the standard center of gravity was chosen. If there is a requirement for faster reaction, for instance, the on-line regulation case, the user can choose for defuzzification a different method, such as the largest or smallest (absolute) value of maximum. However, the regulation will be compressed although less stable.

For the detailed explanation of fuzzy sets and fuzzy logic we recommend reading Nguyen and Walker.<sup>[31]</sup>

### 3.1. Input and Output Parameters

The input for regulation algorithm is the final temperature field (output from the numerical model), specifically the temperatures in control points and the value of metallurgical length. The control points can be placed anywhere at the strand surface. The control of secondary cooling is divided into several cooling circuits (13 in this case) and from the regulation point of view the most “interesting” surface temperatures are in front of and behind the circuits. In the presented case, the control points are placed behind each circuit, which also helps to easily create the linguistic rules and the linguistic variables for fuzzy logic decisions.

The regulator output is presented by the casting speed and intensity of cooling in the secondary cooling zone. Regulator search for the optimal state, which represent the state where the casting speed is maximal (highest productivity) and all constraints are fulfilled. The constraints can be separated into two groups. Some constraints are given by technical parameters, such as maximal and minimal water flow for a particular cooling circuit given by pump limits and nozzle properties, limits for casting speed given by caster construction, etc. Other constraints can be set by the user, such as temperature limits for a particular control point, limits for metallurgical length, etc.



**Figure 6.** Block scheme of the regulation approach.

### 3.2. Linguistic Rules

When the algorithm starts, the initial value for each parameter is drawn uniformly from the permitted range and put into the model and consequently evaluated by its simulation. From the computed result, the algorithm extract temperatures in the controlled points and by comparison with the prescribed values to determine their errors. The metallurgical length is also evaluated and checked with its boundaries. With all this information, the algorithm infers modifications for each parameter.

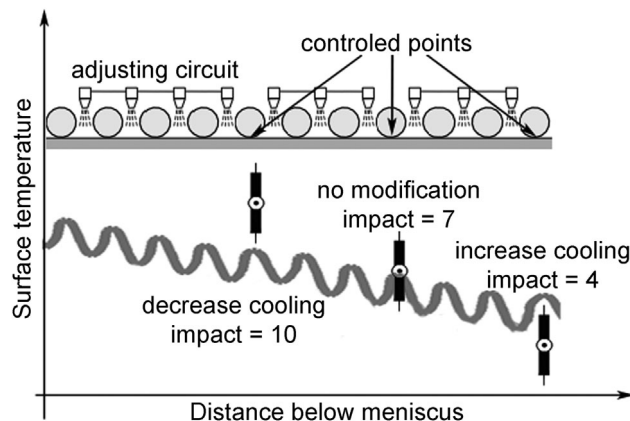
The temperatures in the controlled points are influenced by all previous cooling circuits in the long-term view. However in short term, the controlled points are mainly influenced by the closest cooling circuits (depending on casting speed). Simply, the closer cooling circuit has a bigger influence on the controlled point. This is described by the impact value determined in the range from 0 to 10. Linguistic variables error and impact are represented by linguistic terms such as “small,” “medium,” “big,” etc. The regulator evaluates the errors and impacts by the following linguistic rules: “IF *error* IS *adj1* AND *impact* IS *adj2* THEN *modification* IS *adj3*.” The linguistic rules and linguistic terms for cooling modification are described in Table 2. The abbreviations in Table 2 stand for VerySmall, Small, Medium, OK, Big, VeryBig, MOre, LittleMore, LittleLess, Less, and Nothing.

One circuit can get several different modifications from following controlled points proportional to the impact. Some modification can require increasing of cooling, the other decreasing. The algorithm uses the value for modification as a weight sum of these values. Figure 7 shows the situation when the adjusting circuit has from three control points three different modifications (decrease cooling, no modification, and increase cooling). The situation likely ends with cooling decrease, because the impact from the first control point is 10. But cooling decrease will be very slight.

If the maximal absolute value of all the temperature errors (total error) does not exceed a given limit, the algorithm computes modification of the casting speed. The

adj2/adj1	VS	S	M	B
S	VS	VS	S	S
M	VS	VS	S	M
B	VS	S	M	B
adj4/adj 5	VS	S	OK	B
S	MO	LM	LM	LL
M	LM	N	N	N

**Table 2.** The dependences of adjective 3 on adjectives 1 and 2 and dependences of adjective 6 on adjectives 4 and 5.



**Figure 7.** Scheme of modification and impact parameter.

reason that this limit was introduced is because when the total error is too big, i.e., the solution is far from the optimal, we have no idea whether the speed is high or not, and it is better to stabilize the process and then infer the speed modification. Linguistic terms for the casting modification are “more,” “little more,” “nothing,” “little less,” “less.” The rules for modification of the casting speed are in the form: “IF *total\_error* IS *adj4* AND *metallurgical\_length* IS *adj5* THEN *modification* IS *adj6*.” The linguistic rules and linguistic terms for casting speed modification are described in the Table 2.

### 3.3. Software Implementation

The regulation algorithm is developed in MATLAB® by using Fuzzy Logic Toolbox™. The communication between regulation algorithm and the numerical model of temperature field is also provided by MATLAB®.

The algorithm for adjusting of the cooling intensity and the casting speed is expressed by the pseudo-code in the Figure 8.

The presented fuzzy algorithm can be used for both the steady-state and transient numerical simulations. It means that an optimal cooling intensity can be found for static parameters as well as an optimal reaction on a dynamic change of processing parameters.

## 4. Results and Discussion

The fuzzy regulator was tested for many different fuzzy parameters, for different temperature and casting speed constraints, for different caster and slab geometries, and for different steel grades. This section shows an example of the setting of constraints and related results.

The expertly defined temperature ranges in the controlled points for presented caster are shown as black boxes in Figure 9. For instance, the temperature interval in

```

1. [Initialize.]
   Set position for controlling_points (1,...,n).
2. [Define.]
    $\forall$  cooling_circuit[j]  $\rightarrow$  max_flow[j].
    $\forall$  controlling_point[i]  $\rightarrow$  range[i], impact[i],[j] (0 - 10).
3. [Generate.]
    $\forall$  circuit[j] randomly generate starting values
   (0 - max_flow[j]).
4. [Run.]
   Run numerical model  $\rightarrow$  error[i], metallurgical_length.
5. [While.]
    $\forall$  controlling_point[i]  $\notin$  range[i].
   for j = 1 : m
     modification[i],[j] = fuzzy logic flow protocol;
     (error[i],[j], impact[i],[j]).
     max_modification[j] = maxi {modification[i],[j]};
     new_flow[j] = old_flow[j] + max_modification[j] * max_flow[j];
   end for.
   max_error = maxi {error[i],[j]}.
   speed_modification = fuzzy logic speed protocol (max_error,
   metallurgical_length).
   new_casting_speed = old_casting_speed * speed_modification.
   Run numerical model  $\rightarrow$  new_error[i], new_metallurgical_length.
6. [End While.]
7. [Output.] Optimal flow  $\forall$  circuit[j], Optimal casting_speed.

```

**Figure 8.** Pseudo-code of fuzzy control algorithm.

the first control point is 1200–1300 °C and for the last one 700–800 °C. These intervals are set according to recommendations from the steel plant. Jansto<sup>[31]</sup> suggested that the temperature in the unbending point (control point 9 on top surface and 10 on bottom surface) should be higher than 1000 °C according to mechanical stresses caused by straightening and the hot ductility of steel for low-carbon steels. The rest of the cooling points are set to get a smooth decreasing surface temperature. The metallurgical length limit for slab cross-section 1530 mm × 250 mm is set between 15 and 20 m (resulting from practice). The water flow limits for each cooling circuit were taken from the caster specifications (28–139; 40–60; 51–171; 38–128; 50–148; 26–112; 26–112; 26–112; 26–112; 24–94; 24–94; 31–148; and 31–148) L min<sup>-1</sup>.

The value of impacts of each circuit to the controlled point is chosen according to the distance from the cooling circuits. The closest circuit has an impact value of 10, the previous circuit 7, etc. (These values should be chosen with consideration of the caster geometry). In order to get as smooth as possible, the regulator reactions the impact can be a function of the casting speed.

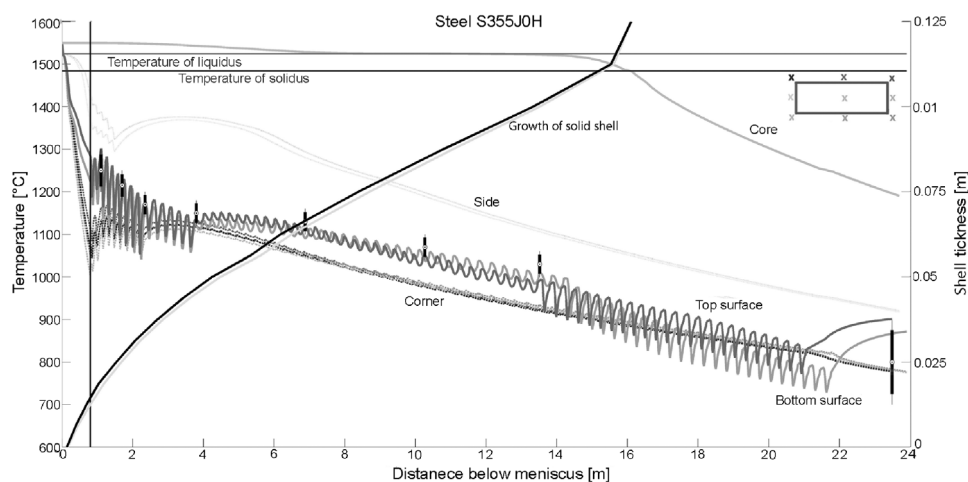
The results for the presented steel are summarized in **Table 3** and depicted in the Figure 9. The black boxes present the allowed temperature intervals in control points placed on the top surface.

The obtained solution fulfills all the prescribed conditions and the value for a metallurgical length of approximately 19.9 m (close to the upper limit of 20 m) suggests that at least local optimum was discovered. This means that the casting speed is very close to its maximal value (maximal productivity).

The cooling intensity for zones 6–11 reaches its minimal allowed values. This means that even a better solution possibly exists. The calculations were done for many different steel grades cast in EVRAZ VÍTKOVICE STEEL, a.s. The plant decided based on the model results to replace the Lechler nozzle 100.638.30.24 in the cooling circuits 6, 8, and 10 at the top surface by the smaller Lechler nozzle 100.528.30.24. Due to the nozzle replacement, the surface temperature at the unbending point has increased by approximately 100 °C, which positively influences on the quality of steel. Moreover, there have also been attained significant savings of water consumption. More detailed information can be found in ref.<sup>[32]</sup>.

#### 4.1. Relationship between Casting Speed and Cooling Intensity

Other useful information can be obtained via the presented algorithm, the relationship between casting speed and cooling intensity. Unfortunately, the actual state



**Figure 9.** Temperature distribution after fuzzy regulation.

Cooling circuit no.	1	2	3	4	5	6
Water flow [L min <sup>-1</sup> ]	133	50	123	94	82	26
Cooling circuit no.	7	8	9	10	11	12
Water flow [L min <sup>-1</sup> ]	30	26	26	24	24	119
Cooling circuit no.	13	Casting speed		Metallurgical length		
Water flow [L min <sup>-1</sup> ]	139	0.81 [m min <sup>-1</sup> ]		19.9935 [m]		

**Table 3.** Casting parameters after optimization.

in many steel works is still that the setting of the cooling intensity follows a simple linear function of the casting speed. When the user fix the casting speed in particular values the algorithm finds the corresponding cooling intensities. The data obtained from many simulations were fitted by various linear regression models (linear, polynomial, etc.); the most promising one of them was the model in the quadratic form

$$y = \beta_0 + \beta_1 x + \beta_2 x^2 \quad (20)$$

The results on four selected cooling circuits are demonstrated in **Figure 10**.

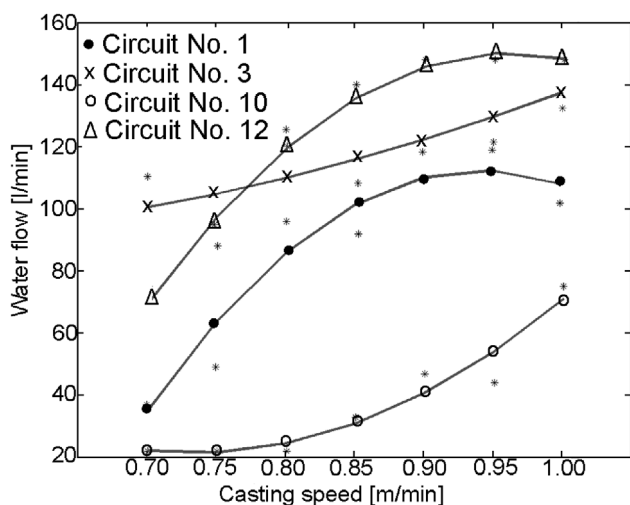
$R^2$  is the coefficient of determination and indicates how well data points are fit by a statistical model. The  $R^2$  values for presented cooling circuits 1, 3, 10, and 12 in **Figure 10** are 0.785, 0.428, 0.926, and 0.974. The values close to 1 suggest that the data are well fitted. For instance the  $R^2$  value shows that the cooling circuit no. 3 can be fitted by simple linear function but the remainder of cooling circuits should be controlled by a polynomial function.

The steelmakers operating with CC are forced by the customer demands to cast different slab cross-sections. The width of the slab is generally from 800 to 1600 mm and

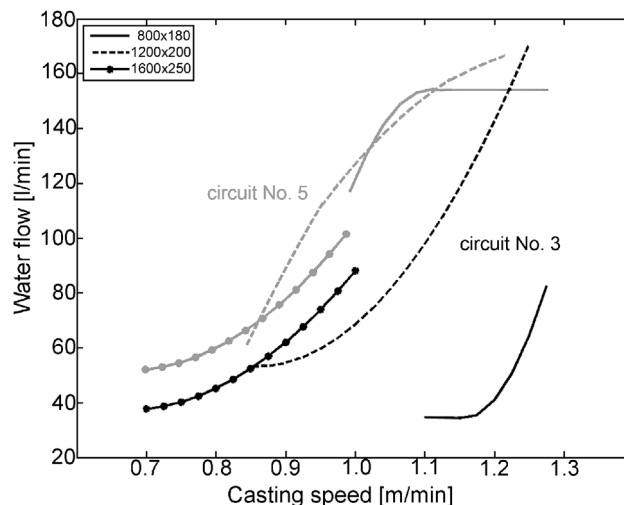
thickness of slab from 180 to 250 mm depending on the caster's installation. Each slab cross-section has typical defects. In order to avoid these defects, the caster should be set up with the consideration of the slab cross-section. The same analysis was used for the three frequently cast slab cross-sections, 1600 mm × 250 mm, 1200 mm × 200 mm, 800 mm × 180 mm. The results for two representative cooling circuits are shown on **Figure 11**.

The regulator will establish an infeasible solution in the case when the user sets the casting speed for which all constraint cannot be fulfilled; for instance, in the situation where all temperatures in the control points are in allowed limits but the metallurgical length is not. In this case, the regulator suggests that the casting speed should be increased or decreased, respectively.

Results from **Figure 11** are free of infeasible solutions, which give us the recommended range for the casting speed. For instance, the fuzzy control algorithm finds for the slab cross-section 1600 mm × 250 mm, the casting speed interval between 0.7 and 1.0 m min<sup>-1</sup>. This result was different than the casting limits presented by the casting equipment. The most flexible casting speed range has the slab 1200 mm × 200 mm while the most critical interval has the slab 800 mm × 180 mm and probably it



**Figure 10.** Regression cooling curves for selected cooling circuits.



**Figure 11.** Optimal cooling curves for cooling circuit no. 3 and 5.

needs a special treatment. There are more reasons for this, but we should realize that the presented caster was mainly built with the aim of casting a larger cross-section.

The fuzzy control algorithm can also react on casting temperature variations. Thus, the cooling intensity in the secondary cooling can be a function of the casting speed, cross-section of slab and the casting temperature.

#### 4.2. Efficiency of the Fuzzy Regulator

The most important indicator of iterative optimization algorithms is usually the number of evaluations of the problem. The evaluation of the numerical model is very time consuming and therefore each repetition can significantly prolong the computations. For steady-state simulation, our algorithm was able to find the optimal parameters in less than 30 evaluations on average. The tests were run several times for different grades of steel and with completely random initial states and the number of evaluations never exceeded 50. The result from Figure 9 was obtained after 27 evaluations. The fuzzy regulator can control casting parameters in transient simulations and combined with the numerical model, which runs on the parallel GPU can be used efficiently as an on-line supervision system for any CC process.

### 5. Conclusions

In this work, the usefulness of an original supervision system for optimal control of the CC process was presented. This system is composed of two parts, an original complex and a validated 3D transient numerical model of temperature field and the regulator based on fuzzy logic. The fuzzy regulator was created to establish appropriate cooling intensities for different casting speed and casting temperature conditions; to optimally react on dynamic changes of process parameters; and avoid and prevent liquid steel breakouts by monitoring of the position of metallurgical length. The regulator was tested for different casting conditions and parameters setting. The main advantage is a small number of evaluations before the optimal solution is reached. The system concept was universally designed in order to optimally control any slab or billet CC process and can be used for maximizing of productivity and increasing of final steel quality.

#### Acknowledgement

This work is an output of research and scientific activities of NETME Centre, regional R&D centre built with the financial support from the Operational Programme Research and Development for Innovations within the project NETME Centre (New Technologies for Mechanical

Engineering), Reg. No. CZ.1.05/2.1.00/01.0002 and, in the follow-up sustainability stage, supported through NETME CENTRE PLUS (LO1202) by financial means from the Ministry of Education, Youth and Sports under the “National Sustainability Programme I.”

Received: June 10, 2014;

Published online: February 5, 2014

**Keywords:** fuzzy regulation; optimal control; continuous casting; secondary cooling

#### References

- [1] A. S. Normanton, V. Ludlow, A. W. Smith, *Improving Surface Quality of Continuously Cast Semis by an Understanding of Shell Development and Growth, Final Report*, Technical Steel Research Series, Luxembourg **2005**, p. 349.
- [2] J. P. Birat, in *The Making, Shaping, Treating of Steel: Casting Volume*, 11th ed. (Ed: A. W. Cramb), The AISE Steel Foundation, Pittsburgh, PA, USA **2003**, p. 1000.
- [3] G. S. Jansto, *METAL 2013 Conf. Proc.*, Ostrava, Tanger s.r.o., **2013**, pp. 32–39.
- [4] D. M. Stefanescu, *Science and Engineering of Casting Solidification*, 2nd ed., Springer Science, New York **2009**, p. 402.
- [5] M. Alizadeh, H. Edris, A. Shafyei, *Int. J. ISSI* **2006**, 3, 7.
- [6] R. A. Hardin, K. Liu, A. Kapoor, C. Beckermann, *Metall. Mater. Trans. B* **2003**, 34, 297.
- [7] A. K. Tieu, I. S. Kim, *Int. J. Mech. Sci.* **1997**, 39, 185.
- [8] H. Wang, G. Li, Y. Lei, Y. Zhao, O. Dai, J. Wang, *ISIJ Int.* **2005**, 45, 1291.
- [9] M. Gonzalez, M. B. Goldschmit, A. P. Assanelli, *Metall. Mater. Trans. B* **2003**, 34, 455.
- [10] B. Tambunan, *Seminar Nasional MIPA 2005 Proc.*, Universitas Indonesia Depok.
- [11] L. Rujiiu, Z. Zhenshan, C. Tianyou, *The Ninth Int. Conf. Electronic Measurement & Instruments Proc., Beijing* **2009**, pp. 545–550.
- [12] S. Louhenkilpi, M. Makinen, S. Vapahti, *Mater. Sci. Eng. A* **2005**, 413–414, 135.
- [13] M. Raudensky, M. Hnizdil, J. Hwang, S. Lee, S. Kim, *Mater. Technol.* **2012**, 46, 311.
- [14] C. A. Santos, J. A. Spim, A. Garcia, *Eng. Appl. Artif. Intell.* **2003**, 16, 511.
- [15] J. Zhemping, B. Wang, Z. Xie, Z. Lai, *Proc. 2007 IEEE Int. Conf. Integration Technol.*, IEEE, Shenzhen, China **2007**, pp. 558–562.
- [16] P. Zheng, J. Guo, X. J. Hao, *IEEE Int. Conf. on Industrial Technology*, IEEE, Hammamet, Tunisia **2004**, pp. 1156–1161.
- [17] T. Mauder, C. Sandera, J. Stetina, M. Seda, *Mater. Technol.* **2011**, 45, 347.



- [18] C. Furtmueller, L. del Re, *Proc. of the 17th World Congress The International Federation of Automatic Control*, Seoul, Korea, **2008**, pp. 700–705.
- [19] M. Dussud, S. Galichet, L. P. Faulloy, *IEEE Trans. Control Syst. Technol.* **1998**, *6*, 246.
- [20] G. O. Tirian, C. B. Pinca, D. Cristea, M. Topor, *WSEAS Trans. Syst. Control* **2010**, *5*, 133.
- [21] G. E. Totten, C. E. Bates, N. A. Clinton, in *Handbook of Quenchants and Quenching Technology* (Ed: M. T. Haddad), ASM International, USA **1993**, p. 507.
- [22] S. Louhenkilpi, M. Uoti, H. Kttönen, S. Vapalahti, *Welding and Advanced Solidification Processes X*, Minerals, Metals, & Materials Society, Florida, USA **2003**, pp. 733–740.
- [23] M. Muhieddine, É. Canot, R. March, *IJFV Int. J. Finite* **2006**, *3*, 20.
- [24] Ch.Y. Li, S. V. Garimella, J. E. Simpson, *Numer. Heat Transf. B* **2003**, *43*, 117.
- [25] B. Tambunan, *Seminar National MIPA 2005, Proceedings, 2005, Depok Indonesia, FMIPA*, p. 7.
- [26] J. Miettinen, *IDS Solidification Analysis Package for Steels: User Manual of DOS Version 2.0.0*, Helsinki University of Technology, Helsinki, Finland **1999**, p. 22.
- [27] R. Tavakoli, P. Davami, *Metall. Mater. Trans. B* **2007**, *38*, 121.
- [28] B. K. Larkin, *Math. Comput.* **1964**, *18*, 196.
- [29] R. Tavakoli, P. Davami, *Commun. Numer. Methods Eng.* **2008**, *24*, 1723.
- [30] L. Klimes, J. Stetina, *Conf. Proc. of 22nd Conf. on Metallurgy and Materials*, Ostrava, Tanger, s.r.o., **2013**, pp. 34–39.
- [31] H. T. Nguyen, E. A. Walker, *A First Course in Fuzzy Logic*, CRC Press, New York, USA **1999**, p. 392.
- [32] J Stetina, et al. *Mater. Technol.* **2013**, *47*, 311.

# Assessment of Basic Approaches to Numerical Modeling of Phase Change Problems—Accuracy, Efficiency, and Parallel Decomposition

**Tomas Mauder**<sup>1</sup>

Department of Thermodynamics,  
Brno University of Technology,  
Brno 616 00, Czech Republic  
e-mail: mauder@fme.vutbr.cz

**Pavel Charvat**

Department of Thermodynamics,  
Brno University of Technology,  
Brno 616 00, Czech Republic  
e-mail: charvat@fme.vutbr.cz

**Josef Stetina**

Department of Thermodynamics,  
Brno University of Technology,  
Brno 616 00, Czech Republic  
e-mail: stetina@fme.vutbr.cz

**Lubomir Klimes**

Department of Thermodynamics,  
Brno University of Technology,  
Brno 616 00, Czech Republic  
e-mail: klimes@fme.vutbr.cz

*The fast and accurate modeling of phase change is of a significant importance in many processes from steel casting to latent heat thermal energy storage. The paper presents a numerical case study on the transient 3D heat diffusion problem with phase change. Three different approaches to modeling of the solid–liquid phase change in combination with four commonly used numerical schemes are compared for their efficiency, accuracy, applicability, simplicity of implementation, and robustness. The possibility of parallel decomposition of the approaches is also discussed. The results indicate that the best accuracy was achieved with the second-order implicit methods, and the best efficiency was reached with the simple explicit methods. [DOI: 10.1115/1.4036081]*

## Introduction

The phase change phenomena are multidimensional transient nonlinear heat transfer problems that are encountered in many technical applications from metal production to latent heat thermal energy storage. Although the analytical methods provide an exact solution and they are mathematically elegant, due to their limitations, the analytical solutions are mainly available for 1D cases in the infinite or semi-infinite regions with simple initial and boundary conditions and the constant thermal properties of the material undergoing a phase change. Hence, the analytical solutions cannot be applied to multidimensional problems with complex boundary conditions. Ockenden and Hodgkin [1] presented an extensive review of the analytical and numerical techniques used in the phase change analyses. With the rise of high-speed computers, advanced numerical methods have become the most economical and fastest approach

to acquiring solutions for the processes involving a phase change. Many numerical schemes have been proposed for one-dimensional (1D), two-dimensional (2D), and three-dimensional (3D) cases.

The accuracy of these numerical schemes generally depends on the particular method and on the grid spacing. Tavakoli and Davami [2] summarized the advantages and drawbacks of implicit and explicit schemes in solidification problems. The results presented by the authors were for a simple geometry, Dirichlet boundary conditions, and constant thermal diffusivity. The conclusions thus cannot be generally applied to complex nonlinear problems. For instance, the alternating direction implicit scheme proposed by Douglas and Gunn [3] is generally claimed to be unconditionally stable for 3D cases, but there is no proof that this is also valid for the heat diffusion problems with phase change and with nonlinear thermophysical terms.

The choice of the method for simulation of phase change phenomena is another factor with the strong influence on the suitability of selected approach. Tavakoli and Davami [2] presented results for the temperature recovery method but they did not compare their results with other methods. Muhieddine et al. [4] described the differences in the results of the effective heat capacity method and the enthalpy method for the 1D ice–water melting problem. In this work, the effective heat capacity method provided better results but only simple explicit numerical scheme was used. On the other hand, it is known that effective heat capacity method without modification is generally not very suitable for implicit schemes [5].

The present paper deals with the assessment of the combination of four most common approaches to numerical discretization of multidimensional heat diffusion problems and three approaches to addressing phase change (latent heat). The main goal of the study was to find the most suitable approach which ensures high accuracy, robustness, adjustability, efficiency, and the possibility of parallel decomposition for massive parallel computing. The simulations were carried out in MATLAB.

## Numerical Model of Heat Transfer With Phase Change

The mathematical description of the transient 3D heat transfer problem with phase change is based on the following governing equation:

$$c_p \rho \frac{\partial T}{\partial \tau} = \nabla \cdot [k \nabla T] + \rho \Delta H \frac{\partial f_s}{\partial \tau} \quad (1)$$

The main issue here is how the latent heat is actually released in practice and thus how the latent heat should be taken into account in the mathematical models. There are two basic approaches to this problem. The first approach involves domain techniques (also called interface capturing methods) where the solid and liquid phases constitute the same medium with the average thermal properties defined at each node as a function of temperature. The problem is reformulated in a way that the interface condition, which ensures the balance between two phases, is implicitly incorporated as a new term in the governing equation Eq. (1). The modified equation is then solved in the entire domain [6]. The second approach involves the front-tracking (or interface-tracking) methods. In the front-tracking methods, the accurate position of the interface between the two phases (the solid and the liquid phases are treated as two separate media) is determined explicitly at each time-step, and the release or absorption of latent heat is dealt with as a special boundary condition, which balances the domains of two phases [7].

The domain methods are computationally simple, easy to use, and they are better suited for the nonisothermal transformations. However, the phase boundary is not explicitly defined which means that in this respect they are less accurate than the front-tracking methods. The domain methods include the temperature recovery method, the effective heat capacity method, the enthalpy method, and other hybrid variants (modifications) of these three methods. The front-tracking methods are more computationally complicated, especially for 3D cases, and they are more often used

<sup>1</sup>Corresponding author.

Contributed by the Heat Transfer Division of ASME for publication in the JOURNAL OF HEAT TRANSFER. Manuscript received June 27, 2016; final manuscript received January 27, 2017; published online April 11, 2017. Editor: Portonovo S. Ayyaswamy.

for the isothermal transformations. As most phase change material (PCM) exhibit a nonisothermal transformation and detailed simulations require 3D formulation, the present paper focuses on the domain methods.

**Solidification Methods.** Three solidification methods are compared in this study, the enthalpy method, the effective heat capacity method, and the temperature recovery method. The enthalpy method has some advantages in comparison to other methods for modeling of phase change. It ensures energy conservation at all times, since the enthalpy is a direct dependent variable in the energy equation. However, the enthalpy method is more difficult to implement mainly for the implicit numerical scheme. The enthalpy method was comprehensively discussed by Voller [8]. The effective heat capacity method [9] is probably the most commonly used method in phase change modeling. Since the specific heat can be regarded as the temperature-dependent property, the implementation in a computer model is quite easy. The main disadvantage of the effective heat capacity method lies in the discontinuity of specific heat at both the liquidus and solidus temperatures. There are several sources in the literature for developing various versions of the effective heat capacity method. A review on the methods was presented by Lewisa and Ravindran [10]. The temperature recovery method was first reported by Dusanberre [11] for isothermal transformation. Since then the temperature recovery method was also applied for nonisothermal transformations with minor modification [12]. The main advantage of this method, over the effective heat capacity method, is that the phase change is not complete until all the latent heat of transformation has been released or absorbed, which means that the conservation of energy is ensured. Also, this method is computationally economic and easy to implement. However, the method has been shown to be very sensitive to the size of the time-step, and the errors in the approximation are larger in the vicinity of the mushy zone than in the single phase regions. The formulations of Eq. (1) for the three solidification methods are in Table 1.

A well-known weakness of the domain methods for numerical simulations of the phase change problems is the convergence and accuracy of the calculated temperature field for small Stefan numbers. The Stefan number is defined as the ratio of sensible heat to latent heat [13]. The problems with convergence and accuracy are the result of the increasing nonlinearity with the decreasing Stefan number. Note that with the decreasing Stefan number (increasing latent heat), the speed of the phase change front decreases, and so the accuracy of the predicted front position is increased. At the same time, the numerical oscillation in the predicted temperature history is also increased (due to increasing nonlinearity). This was demonstrated by Voller [14] for three Stefan numbers (0.1, 1, and

10). Thus, when considering an approach to phase change modeling, it is also necessary to assess its behavior for small Stefan numbers.

The cases presented in this paper were defined with respect to small Stefan numbers (from 0.1 to 1). If a method is accurate for small Stefan numbers, it will very likely be accurate for larger Stefan numbers. The validation of the numerical schemes was done by the comparison of numerical results with the 1D analytical solution of the two-phase Stefan solidification problem [15].

**Time Discretization.** Four commonly used numerical schemes were investigated in order to find the most efficient numerical procedure for the transient multidimensional heat diffusion with phase change. These were the simple explicit (SE) scheme, the alternating direction explicit (ADE) scheme, the simple implicit (SI) scheme, and the alternating direction implicit (ADI) scheme. The SE scheme is basic straightforward easily implementable method for time discretization. However, the stability condition limits the time-step size of the SE scheme. The scheme has the second-order accuracy in space and the first-order accuracy in time [16]. The SI scheme also has the second-order accuracy in space and the first-order accuracy in time [16]. In case of linear problems, the SI scheme is unconditionally stable for a 1D case as well as for multidimensional cases. The internal iterations are required in case of the nonlinear problems in order to correct the results. In order to solve Eqs. (1)–(4) implicitly, one has to solve a system of linear equations at each time-step [16]. For multidimensional cases, the principle of superposition of heat conduction can be expressed as a product of one-dimensional conductions. Thus, the problem can be split into separate one-dimensional problems along the main axes which can be solved very effectively by the Thomas algorithm [17]. This approach is also called the line-by-line method [18]. The ADE scheme was developed in order to utilize the benefits of both explicit and implicit schemes. The ADE scheme was originally formulated by Larkin [19]. A better modification of ADI scheme presented by Barakat and Clark [20] uses two intermediate values to calculate enthalpy  $H$ . The computing demands are higher than in case of the SE scheme, because the ADE requires two calculations at each time-step (downstream and upstream). For nonlinear cases, the internal iterations are needed in order to achieve correct result. The Douglas and Gunn ADI scheme developed in 1964 is unconditionally stable and retains the second-order accuracy when applied to 3D problems [21]. Unlike the Crank–Nicolson scheme, the ADI separates the implicit calculation into one-dimensional problems, similarly as in case of the line-by-line method in the SI scheme. Wang and Chen [22] compared the runtime and the memory usage between the Crank–Nicolson and the ADI schemes in dependence on the

**Table 1 Governing equations for different solidification schemes**

Solidification methods	Governing equation	Latent heat formulation
Enthalpy method	$\frac{\partial H}{\partial \tau} = \nabla \cdot [k \nabla T]$	$H = \int_0^T \left( c_p \rho - \rho \Delta H \frac{\partial f_S}{\partial \xi} \right) d\xi \quad (2)$
Effective heat capacity	$C_{\text{eff}} \frac{\partial T}{\partial \tau} = \nabla \cdot [k \nabla T]$	$C_{\text{eff}} = \frac{\partial H}{\partial T} = c_p \rho - \rho \Delta H \frac{\partial f_S}{\partial T} \quad (3)$
Temperature recovery	$c_p \rho \frac{\partial T}{\partial \tau} = \nabla \cdot [k \nabla T]$	$T = \begin{cases} T & T < T_S \\ T_L - ((H_2 - H_1)/\Delta H) (T_2 - T_1) & T_S \leq T \leq T_L \\ T & T > T_L \end{cases} \quad (4)$

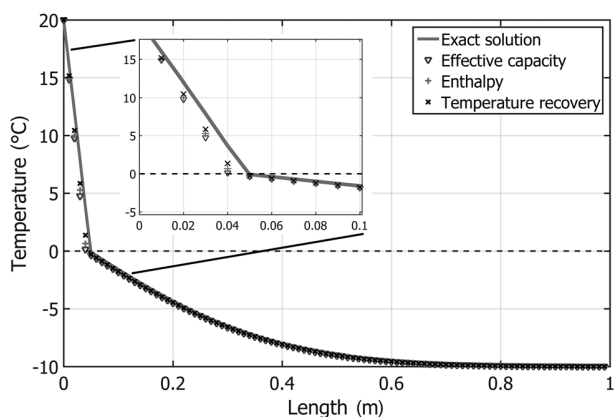


Fig. 1 Results of 1D simulations

number of nodes. From their results, it is obvious that for large-size problems the ADI scheme is much more efficient than the Crank–Nicolson scheme.

## Results and Discussion

The first set of calculations was carried out with the aim to find the most accurate scheme in comparison to analytical solution. The analytical solution exists only for the isothermal phase change. On the other hand, only the temperature recovery method was originally formulated for the isothermal phase change. For this reason, the phase change temperature interval of  $\pm 0.1^\circ\text{C}$  was considered for the enthalpy method and the effective heat capacity method in the isothermal case.

The second set of calculations dealt with the stability, robustness, and efficiency of the investigated methods for a 3D nonisothermal phase change problem. The thermophysical properties of phase change material Rubitherm RT 28HC (mean phase change temperature of  $28^\circ\text{C}$ ) were considered in this case [23].

The last part of the investigations focused on the suitability of the presented approaches for parallel computing and shows the efficiency of massive parallelization.

**One-Dimensional Isothermal Case.** The analytical solution for the Stefan two-phase (ice–water) melting problem [15] was used for validation of numerical results. The time of simulation was 50 h. According to stability condition, the time scale was divided into 18,000 time-steps for SE scheme (time-step of 10 s). There is no time-steps restriction for the SI and the ADI schemes, but smaller time-steps lead to more accurate solutions.

Two criteria were used for the comparison of the tested schemes—accuracy and efficiency. The accuracy was determined by comparing the numerical results with the analytical solution. All schemes were calculated with the same time-step of 10 s. The second criterion was the wall-clock time of simulations

Table 2 Accuracy and efficiency for 1D case

Numerical scheme	Enthalpy method	Effective heat capacity	Temperature recovery
Accuracy—mean errors ( $^\circ\text{C}$ )			
SE	0.0223	0.0246	0.0063
ADE	0.0171	0.0253	0.0064
SI	0.0205	0.0244	0.0065
ADI	0.0114	0.0152	0.0061
Efficiency—computation time (s)			
SE	105.3589	19.6155	22.3065
ADE	18.1816	5.3682	25.8898
SI	4.5980	2.9712	8.0800
ADI	11.2641	6.0630	24.4115

(efficiency). In this comparison, the same level of accuracy was set for all approaches, leading to different numbers of time-steps and thus different wall-clock computation times for each approach.

The Dirichlet boundary condition  $T(x=0) = 20^\circ\text{C}$  and the adiabatic wall boundary condition for  $x=N$  were used. The initial temperature  $T_0 = -10^\circ\text{C}$  was considered.

The accuracy of the numerical schemes in comparison with the analytical solution can be evaluated in terms of the mean temperature error over all nodes. The results for all solidification methods were averaged through the numerical schemes and compared with Stefan analytical solution, see Fig. 1. The smallest mean error was obtained for the temperature recovery method (Table 2).

Good results were generally achieved with the ADI scheme for all phase change methods. Such outcome could be expected as only the ADI scheme has the second-order accuracy in both time and space. Very good results were achieved with the temperature recovery method. This result could also be expected, because only temperature recovery method can calculate isothermal phase change directly without the artificial introduced phase change temperature interval (mushy zone). On the other hand, the accuracy of all approaches would be satisfactory for most practical applications.

In the efficiency comparison, the initial number of time-steps was 100 for all methods. If the mean error after calculation was higher than  $0.02^\circ\text{C}$ , the calculation started again with the number of time-steps increased by 10. The computational efficiency for 1D problem can be seen in Table 2.

The best results were obtained for the SI scheme. The most efficient method for phase change modeling was the effective heat capacity method. The ADI scheme was also quite efficient. It needs to be emphasized that the implicit methods are more difficult to implement than the explicit methods (because of a system of linear equations). The simplicity of implementation plays an important role, and it should be taken into account. From this point of view, very good results were reached for the combination of the ADE scheme with the effective heat capacity method and the temperature recovery method.

**Three-Dimensional Nonisothermal Case.** The main question was whether the conclusions obtained in case of the 1D problem also apply for a 3D problem. The 3D case was a cube of PCM with the dimensions of  $1\text{ m} \times 1\text{ m} \times 1\text{ m}$ . Three mesh sizes were used: very-coarse-mesh with  $10 \times 10 \times 10$  nodes, coarse-mesh with  $20 \times 20 \times 20$  nodes, and the fine-mesh with  $50 \times 50 \times 50$  nodes. The results for different mesh sizes give some guidance about the robustness of a particular scheme. The time of simulation was 50 h. The initial temperature above the mushy zone ( $T_0 = 40^\circ\text{C}$ ) was used. The Dirichlet boundary condition was  $T(x=0, x=Nx, y=0, y=Ny) = 10^\circ\text{C}$ , and the adiabatic wall boundary condition was specified at  $z=0$  and  $z=Nz$ .

As there is no analytical solution for the 3D case, the assessment of the accuracy of the examined schemes was difficult. Experimental data can generally be used for validation of the simulation models; however, in the studied case, the uncertainty of experimental data would be much higher than the differences between the numerical results of different numerical schemes. We therefore proceeded as follows. The ADI scheme was found to be the most accurate among the examined schemes for the 1D problem. The first calculation was done with the ADI scheme, and the very short time-step of 0.1 s was used. The results calculated in this way served as the reference temperature field for accuracy comparison. The efficiency was evaluated in the same way as in case of the 1D problem. The mean error between the actual solution and the very-fine-mesh ADI solution was set to  $0.02^\circ\text{C}$ .

The efficiency results for the 3D problem are shown in Table 3. The best efficiency was reached with the enthalpy method. For the simulated 3D problem, the enthalpy method was the most stable

**Table 3 Efficiency—computation time for 3D case**

Numerical scheme	Efficiency—computation time (s)		
	Enthalpy method	Effective heat capacity	Temperature recovery
Very-coarse-mesh			
SE	1.93	<b>1.10</b>	8.66
ADE	1.81	6.51	2.82
SI	9.55	14.05	11.40
ADI	7.47	15.36	9.16
Coarse-mesh			
SE 1CPU/12CPU	<b>11.54/135.28</b>	21.35	71.98
ADE	27.02	80.87	79.10
SI	83.38	309.74	333.35
ADI 1CPU/12CPU	41.80/58.61	176.85	271.61
SE GPU	18.67	—	—
Fine-mesh			
SE 1CPU/12CPU	887.14/1 122.13	1051.11	1926.70
ADE	2359.07	3461.83	4331.50
SI	3251.27	7929.16	9517.30
ADI 1CPU/12CPU	714.73/824.32	6109.06	7809.40
SE GPU	<b>97.72</b>	—	—
Very-fine-mesh			
SE 1CPU/12CPU	54 362.19/35 124.51	—	—
ADI 1CPU/12CPU	36 210.45/32 416.32	—	—
SE GPU	<b>972.49</b>	—	—

The shortest computation times (best cases) are in bold print.

and the most efficient one, while the temperature recovery method performed the worst. As can be seen in Table 3, the behavior of numerical schemes for coarse and fine-mesh was quite similar. Thus, we can say that all approaches are robust. The SE scheme was the most efficient, but the ADE scheme also reached good results in comparison with the implicit schemes.

**Parallel Calculations.** The time required for the calculation (efficiency) is one of the most important factors for selection of a numerical scheme. For instance, the online solidification models are widely used in the industry for the monitoring and control of metal casting processes. These models need to calculate the 3D temperature fields with a very-fine-mesh (more than  $1 \times 10^6$  nodes) in real-time [24]. Thus, parallel possibility for the online numerical codes is essential.

The SE scheme is parallel in its nature because the temperature field is calculated only from previous results. It means that the space dimensions can be decomposed into arbitrary number of

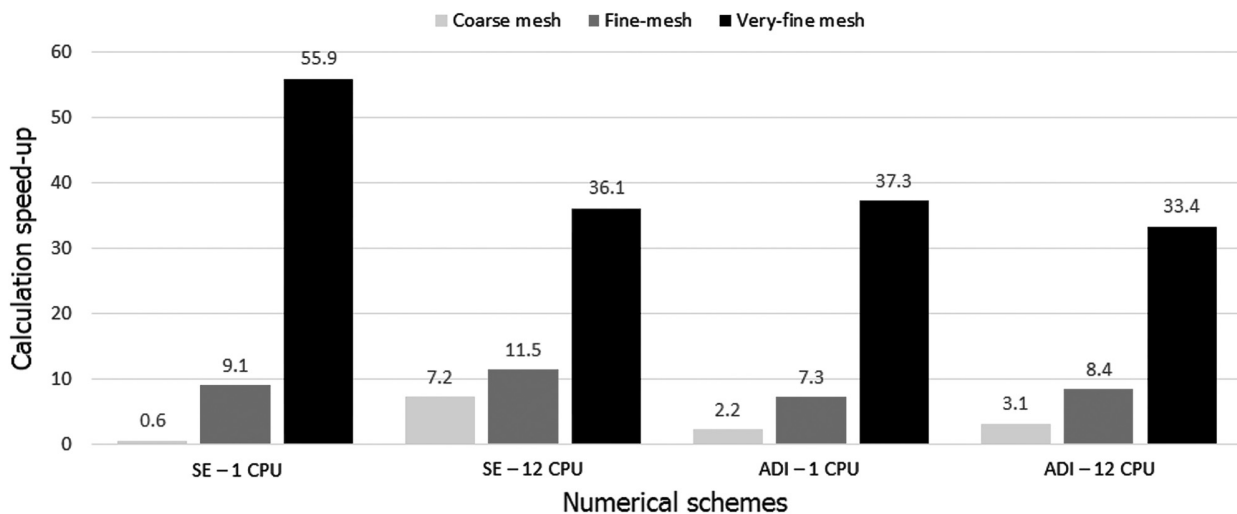
processors. The ADE scheme has to be calculated gradually in the predetermined order. The calculation of the ADE scheme can only be separated to upstream and downstream directions. Thus, massive parallelization of the ADE is not an option. The SI scheme, similarly to the ADI scheme, can be parallelized in the following way. The first step deals with the implicitly determined  $x$  axis which is calculated through the  $y$  and  $z$  axes in the loop. This loop can be easily parallelized. At step two, the implicitly determined  $y$  axis is calculated along the  $x$  and  $z$  axes in the loop, which can also be parallelized, etc.

A significant amount of time in the parallel computing is consumed for data transfer between the central processing unit (CPU) workers. For the small size problems, this amount of time can be even larger than the numerical calculation itself, and the parallel decomposition would not be effective. Another approach can be chosen if the solved problem is very large, and the number of CPU workers is not enough. Unlike a traditional CPU, including no more than a handful of cores, a graphic processor unit (GPU) has a massively parallel array of integer and floating-point processors, as well as high-speed memory. Several GPU applications were published in relation to heat transfer problems, e.g., Ref. [25].

Considering the obtained results and the mentioned conclusions, only two numerical schemes were used for parallel computing: the SE (with the best parallel possibility) and the ADI (the most accurate one). All three presented methods for phase change modeling can be parallelized. Since the enthalpy method was found to be the most effective for 3D problems, it was used in parallel computations.

The calculations for comparison of parallelization efficiency were performed on 1CPU, 12CPU, and GPU units. The 3D simulations were run for three types of meshes (coarse-mesh with  $20 \times 20 \times 20$  nodes, fine-mesh with  $50 \times 50 \times 50$  nodes, and the very-fine-mesh with  $100 \times 100 \times 100$  nodes). The results are shown in Table 3.

The assumption that the data transfer can significantly influence the execution time in case of small size problems was confirmed by the results. The parallel computation on 12CPU and GPU brings significant time saving in comparison to 1CPU calculation for the fine meshes. For the very-fine-mesh and for the SE scheme, the speedup in calculation time was 1.54 on 12CPU cores and 21.11 on GPU. The speedup for the ADI scheme between 1CPU and 12CPU cores was only 1.15. The results indicate that the massive parallelization technique via GPU overcomes the performance of traditional CPUs. Since the SE scheme is the only one among the examined schemes that allows massive parallelization, it is also the most effective one. The speedup in the calculation time on GPU comparing with CPUs can be seen in Fig. 2.



**Fig. 2 GPU speedup**

## Conclusion

The accuracy, effectiveness, robustness, and parallel possibility of basic numerical schemes for the solution of 1D and 3D heat conduction problem with phase change were investigated.

A set of calculations was conducted in order to validate the numerical models with the 1D analytical solution of the Stefan problem. The most accurate approach in this test was the combination of the ADI scheme with the temperature recovery method. The most efficient method for the 1D problem was the SI scheme with the effective heat capacity method. The ADE scheme also achieved good results, and it provided a very good alternative considering easy implementation of this scheme.

The 3D problem was calculated consequently for four mesh sizes. All tested schemes can be considered robust for different mesh sizes. The enthalpy method was found to be the most stable one for the 3D problems. The SE scheme and the ADE scheme were the most efficient numerical schemes for 3D calculation.

Finally, the parallel decomposition on multiple CPUs and on the GPU was tested. The results show that the parallel calculations were only able to speed up the computations in case of fine meshes, because certain execution time is needed for data transfer. The best results were achieved with the SE scheme on GPU. The average speedup was 9.1 for the fine-mesh and 40.6 for the very-fine-mesh in comparison with the one-core and multicore CPU approaches.

It can be concluded from the results that all tested phase change methods and all investigated numerical schemes can be used for phase change problems. At present, the most potential for practical applications has the methods capable of calculating 3D problems with fine meshes in real-time. From this point of view, the best presented approach is the combination of the SE numerical scheme with the enthalpy method which allows for the massive parallelization, despite the fact that the stability condition restricts the size of the time-step in this scheme.

## Acknowledgment

The presented research was supported by the Czech Science Foundation (GACR) under Contract No. 15-11977 S.

## Nomenclature

$c_p$	= specific heat capacity (J/(kg K))
$C_{\text{eff}}$	= apparent/effective heat capacity (J/(m <sup>3</sup> K))
$f_s$	= solid fraction (0–1)
$H$	= volume enthalpy (J/m <sup>3</sup> )
$k$	= thermal conductivity (W/(m K))
$T$	= temperature (°C; K)
$T_L$	= liquidus temperature (°C; K)
$T_S$	= solidus temperature (°C; K)
$\Delta H$	= latent heat (J/kg)
$\rho$	= density (kg/m <sup>3</sup> )
$\tau$	= time (s)

## References

- [1] Ockenden, J. R., and Hodgkin, W. R., 1975, *Moving Boundary Value Problems in Heat Flow and Diffusion*, Oxford University Press, Oxford, UK.
- [2] Tavakoli, R., and Davami, P., 2007, "Unconditionally Stable Fully Explicit Finite Difference Solution of Solidification Problems," *Metall. Mater. Trans. B*, **38**(1), pp. 121–142.
- [3] Douglas, J., and Gunn, J. E., 1964, "A General Formulation of Alternating Direction Methods—Part I: Parabolic and Hyperbolic Problems," *Numer. Math.*, **6**(1), pp. 428–453.
- [4] Muhieddine, M., Canot, É., and March, R., 2009, "Various Approaches for Solving Problems in Heat Conduction With Phase Change," *Int. J. Finite*, **3**, pp. 1–20.
- [5] Liu, Y.-Ch., and Chao, L.-S., 2006, "Modified Effective Specific Heat Method of Solidification Problems," *Mater. Trans. J.*, **47**(11), pp. 2737–2744.
- [6] Zhang, Y., Du, K., He, J. P., Yang, L., and Li, Y. J., 2014, "Impact Factors Analysis of the Enthalpy Method and the Effective Heat Capacity Method on the Transient Nonlinear Heat Transfer in Phase Change Materials (PCMs)," *Numer. Heat Transfer A*, **65**(1), pp. 66–83.
- [7] Li, Ch.-Y., Garimella, S. V., and Simpson, J. E., 2003, "Fixed-Grid Front-Tracking Algorithm for Solidification Problems—Part I: Method and Validation," *Numer. Heat Transfer, Part B*, **43**(2), pp. 117–141.
- [8] Voller, V., 1983, "An Explicit Numerical Method to Track a Moving Phase Change Front," *Int. J. Heat Mass Transfer*, **26**(1), pp. 147–150.
- [9] Hashemi, T. H., and Slepcevic, C. M., 1968, "A Numerical Method for Solving Two-Dimensional Problems of Heat Conduction With Change of Phase," *Chem. Eng. Prog. Symp. Ser.*, **63**, pp. 34–41.
- [10] Lewisa, R. W., and Ravindran, K., 2000, "Finite Element Simulation of Metal Casting," *Int. J. Numer. Methods Eng.*, **47**(1–3), pp. 29–59.
- [11] Dusinberre, G. M., 1945, "Numerical Methods for Transient Heat Flows," *Trans. ASME*, **67**, pp. 703–712.
- [12] Mochnacki, B., and Lara, S., 2003, "Application of Generalized Finite Difference Method in Numerical Modelling of Moving Boundary Problems," *Sci. Res. Inst. Math. Comput. Sci.*, **2**(1), pp. 129–143.
- [13] Minkowycz, W. J., Sparrow, E. M., Schneider, G. E., and Pletcher, R. H., 1988, *Handbook of Numerical Heat Transfer*, Wiley, New York.
- [14] Voller, V. R., 1996, "An Overview of Numerical Methods for Solving Phase Change Problems," *Advances in Numerical Heat Transfer*, Vol. 1, W. J. Minkowycz and E. M. Sparrow, eds., Taylor & Francis, London, pp. 341–375.
- [15] Hahn, D. W., and Ozisik, M. N., 2012, *Heat Conduction*, 3rd ed., Wiley, Hoboken, NJ.
- [16] Yang, W. Y., Cao, W., Chung, T.-S., and Morris, J., 2005, *Applied Numerical Methods Using Matlab*, Wiley, Hoboken, NJ.
- [17] Otto, S. R., and Denier, J. P., 2005, *An Introduction to Programming and Numerical Methods in MATLAB*, Springer-Verlag, London.
- [18] Patankar, S. V., 1980, *Numerical Heat Transfer and Fluid Flow*, McGraw-Hill, New York.
- [19] Larkin, B. K., 1964, "Some Stable Explicit Difference Approximations to the Diffusion Equation," *Math. Comput.*, **18**(86), pp. 196–202.
- [20] Barakat, H. Z., and Clark, J. A., 1966, "On the Solution of Diffusion Equation by Numerical Methods," *ASME J. Heat Transfer*, **88**(4), pp. 421–427.
- [21] Warming, R. F., and Beam, R. M., 1979, "An Extension of A-Stability to Alternating Direction Implicit Methods," *BIT Numer. Math.*, **19**(3), pp. 395–417.
- [22] Wang, T.-Y., and Chen, Ch. C.-P., 2002, "3-D Thermal-ADI: A Linear-Time Chip Level Transient Thermal Simulator," *IEEE Trans. Comput.-Aided Des. Integr. Circuits Syst.*, **21**(12), pp. 1434–1445.
- [23] Rubitherm Technologies GmbH, 2016, Data sheet RT28HC, Berlin, accessed Dec. 8, 2016, <http://www.rubitherm.eu/>
- [24] Mauder, T., Sandera, C., and Stetina, J., 2015, "Optimal Control Algorithm for Continuous Casting Process by Using Fuzzy Logic," *Steel Res. Int.*, **86**(7), pp. 785–798.
- [25] Fu, W. S., Wang, W. H., and Huang, S. H., 2012, "An Investigation of Natural Convection of Three Dimensional Horizontal Parallel Plates From a Steady to an Unsteady Situation by a CUDA Computation Platform," *Int. J. Heat Mass Transfer*, **55**(17–18), pp. 4638–4650.

Article

# High Quality Steel Casting by Using Advanced Mathematical Methods

Tomas Mauder \* and Josef Stetina

Energy Institute, Brno University of Technology, 616 69 Brno, Technicka 2, Czech Republic; stetina@fme.vutbr.cz

\* Correspondence: mauder@fme.vutbr.cz; Tel.: +420-541-14-3252

Received: 15 November 2018; Accepted: 30 November 2018; Published: 4 December 2018



**Abstract:** The main concept of this paper is to utilize advanced numerical modelling techniques with self-regulation algorithm in order to reach optimal casting conditions for real-time casting control. Fully 3-D macro-solidification model for the continuous casting (CC) process and an original fuzzy logic regulator are combined. The fuzzy logic (FL) regulator reacts on signals from two data inputs, the temperature field and the historical steel quality database. FL adjust the cooling intensity as a function of casting speed and pouring temperature. This approach was originally designed for the special high-quality high-additive steel grades such as higher strength grades, steel for acidic environments, steel for the offshore technology and so forth. However, mentioned approach can be also used for any arbitrary low-carbon steel grades. The usability and results of this approach are demonstrated for steel grade S355, where the real historical data from quality database contains approximately 2000 heats. The presented original solution together with the large steel quality databases can be used as an independent CC prediction control system.

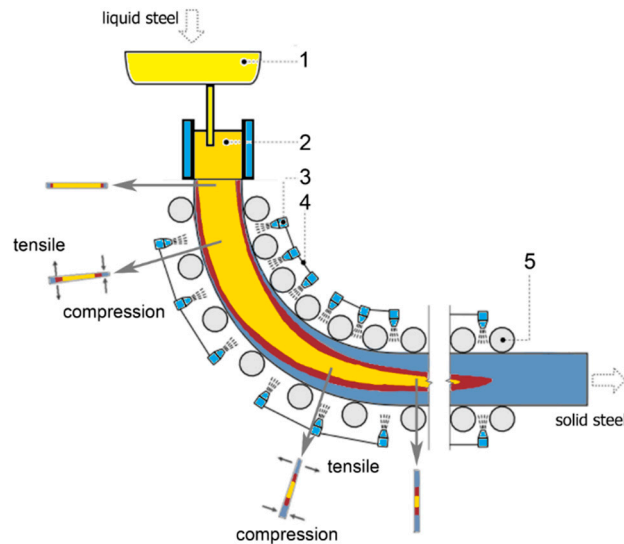
**Keywords:** continuous casting; fuzzy logic; optimal cooling; steel quality prediction

## 1. Introduction

The continuous casting technology is a well-known predominant process how the steel is produced in the world. CC is already fully-grown technology and successfully casting million tonnes of classic low-carbon and low-alloy steel grades per year. In spite of this fact, casting of special high-strength grades, steels for acidic environment, steels for the offshore technology, high alloyed tool steels, can be still challenging in order to ensure a constant steel quality through the whole casting process. Flick and Stoiber [1] described present issues and future trends in the CC technology. The quality of the steel is still a discussed topic. In CC the solid shell is permanently subjected to thermal and mechanical stresses and it can give rise to crack formation, see Birat et al. [2]. Figure 1 shows CC installation and mechanical tensile/compression stresses in specific locations. The rejected slabs, by the quality control system, which need to be scrapped is very uneconomic. The breakdown situation caused by a low quality of these steels could have a catastrophic effect on material and human losses. This quality issue can be handled by using the advanced numerical modelling methods, optimization-regulation techniques and statistical evaluations of the real casting data.

Historically, there are many papers which combine the numerical modelling and optimization-regulation approaches, such as Santos et al. [3] who applied the genetic algorithm, Zhemping et al. [4] verified the usage of the ant colony algorithm, Zheng et al. [5] attempted to use the swarm optimization on 2-D solidification model, Mauder and Novotny [6] showed the possibility of using classical mathematical programming method and compared the results with simple Nelder-Mead algorithm, Ivanova [7] constructed basic predictive control algorithm for 2-D solidification model and so forth. Rao et al. [8] publish a comprehensive review dealing with parameters optimization of selected casting processes. Unfortunately, these works are far from the use on the real casting process,

because they often calculate very simplified solidification models (simple geometry, 2-D mesh, simple boundary conditions, contain a small steel database, etc.) and it is proven that the numerical results of these models in compare with the 3-D fine-mesh validated solidification models are poor, see Mosayebidorcheh and Bandpy [9]. Moreover, the optimization algorithms are often based on black-box approach that generally needs a large number of optimization iterations before the optimal solution is found. This is not a problem in the case of simple solidification models, which calculates the temperature field very fast. However, in the case of the complex 3D numerical simulations it is not possible to use these optimization algorithms for the real time control.



**Figure 1.** Scheme of the continuous casting and mechanical stresses during bending and straightening. 1—tundish; 2—mould; 3—nozzle; 4—cooling circuit; 5—roller.

This paper describes both, the original 3-D solidification model, the so-called Brno Dynamic Solidification Model<sup>®</sup> (BrDSM) and advanced optimal control algorithm based on the fuzzy logic (FL-BrDSM). This unique combination represents a tool for achievement of high steel quality products. Besides of the numerical and fuzzy regulation models, special attention must be concentrated to proper setting of thermophysical parameters of investigated steel grade, experimental measurement of boundary conditions and statistical evaluations of the real casting data.

Presented approach is demonstrated on the real radial slab caster with twelve cooling loops in the secondary cooling for the special grade of steel S355. This steel was selected expediently because it is mainly used for shipbuilding projects, marine mechanical systems and deep-water ocean offshore structural projects where the quality of steel S355 plates is essential. The mechanical properties for these grades of steel are specified by the European Standards.

## 2. Solidification Model—BrDSM

The core of presented approach is the 3-D transient solidification model. The computing precision, accuracy, robustness and fast computational times are essential. In order to reach these specifications a suitable numerical scheme should be selected. Numerical mesh independence tests as well as tests of the calculation speed on different CPU/GPU and mainly a properly validation on the real casting data were made.

The transient 3-D solidification model is based on Fourier-Kirchhoff Equation [2] which can be expressed as:

$$\frac{\partial(h\rho)}{\partial\tau} + v_{cast}\frac{\partial(h\rho)}{\partial z} = \nabla \cdot (k_{eff}\nabla T), \quad (1)$$



with boundary conditions:

$$T(x, y, z)|_{z=0} = T_{pouring} \quad \text{the meniscus,} \quad (2)$$

$$-\lambda \frac{\partial T}{\partial n} = 0 \quad \text{the exit area,} \quad (3)$$

$$-\lambda \frac{\partial T}{\partial n} = \frac{\dot{m}_{water} c_{water} (T_{out} - T_{in})}{S_{mold}} \quad \text{in the mould,} \quad (4)$$

$$-\lambda \frac{\partial T}{\partial n} = \frac{\pi(l/2)d_{rol} htc_{rol} (T_{rol} - T_{amb}) + \sigma \varepsilon (T_{rol}^4 - T_{amb}^4)}{S_{rol}} \quad \text{beneath the rollers,} \quad (5)$$

$$-\lambda \frac{\partial T}{\partial n} = htc(T - T_{water}) + \sigma \varepsilon (T^4 - T_{water}^4) \quad \text{beneath the spray cooling,} \quad (6)$$

$$-\lambda \frac{\partial T}{\partial n} = 0.84(T - T_{amb})^{4/3} + \sigma \varepsilon (T^4 - T_{amb}^4) \quad \text{within the solidified shell free surface.} \quad (7)$$

$k_{eff}$  is the effective thermal conductivity (W/mK);  $T$  is the temperature (K);  $T_{pouring}$  is the pouring temperature (K);  $h$  is the specific enthalpy (J/kg);  $\rho$  is the density (kg/m<sup>3</sup>);  $\tau$  is the time (s);  $v_{cast}$  is the casting speed (m/min);  $z$  is the direction of casting (m),  $T_{rol}$  is the roller temperature;  $T_{water}$  is the cooling water temperature;  $T_{amb}$  is the ambient temperature;  $\dot{m}_{water}$  is the mass water flow in the mould (kg/s);  $c_{water}$  is the specific heat capacity of water (J/kgK);  $htc$  is the heat transfer coefficient beneath spraying surface (W/m<sup>2</sup>K);  $\sigma$  is the Stefan-Boltzman constant (W/m<sup>2</sup>K<sup>4</sup>) and  $\varepsilon$  is the emissivity of the slab surface (-).

The latent heat released during the solidification in Equation (1) is substituted by the enthalpy  $h$  and can be expressed as:

$$h = \int_0^T \left( c(\zeta) - \Delta H \frac{\partial f_s}{\partial \zeta} \right) d\zeta, \quad (8)$$

where  $\Delta H$  is the latent heat (J/kg) and  $f_s$  is the solid fraction (-). The Enthalpy method was used for modelling the solidification process, see Mauder et al. [10]. The Enthalpy method is robust method because it ensures energy conservation and there is no discontinuity at either the liquidus or the solidus temperatures because the solidification/melting path is characterized strictly by decreasing/increasing enthalpy. In the Equation (1) the enthalpy is calculated in the first step as the primary variable and the temperature is calculated from a defined enthalpy-temperature relationship in the second step Equation (8).

In the presented solidification model, Equation (8) is substituted by an enthalpy-temperature function obtained by the InterDendritic Solidification (IDS) package created by the Miettinen [11]. The IDS allows calculation of enthalpy, thermal conductivity, density and other thermophysical parameters as a function of temperature from 1600 °C–0 °C.

Fluid flow of the liquid steel can be calculated by the computational fluid dynamics (CFD) techniques. However, computational times are even with the use of new modern modelling approaches far from the real duration of the simulated process. The influence of heat transfer by the fluid flow is account in the effective thermal conductivity term  $k_{eff}$ . The thermal conductivity is increased by the flow of liquid steel at different distances from the meniscus, where  $k_{eff}$  is represented by Zhang et al. [12] as follows:

$$k_{eff} = \begin{cases} k & T \leq T_{sol} \\ 4k + \frac{3k(T - T_{liq})}{(T_{pouring} - T_{liq})} & T \geq T_{liq} \wedge 0 \leq z \leq 1 \text{ m} \\ k + \frac{3k(T - T_{sol})}{(T_{liq} - T_{sol})} & T_{sol} \geq T \geq T_{liq} \wedge 0 \leq z \leq 1 \text{ m} \\ k + \frac{k(T - T_{liq})}{(T_{pouring} - T_{liq})} & T \geq T_{liq} \wedge 1 \text{ m} \leq z \leq 3 \text{ m} \\ k & z \geq 3 \text{ m,} \end{cases} \quad (9)$$

where  $k$  is the thermal conductivity (W/mK);  $T_{sol}$  is the temperature of solidus (K);  $T_{liq}$  is the temperature of liquidus (K); and  $z$  is the distance from the meniscus (m).

The heat transfer in the mould region described by Equation (4) is calculated from the heat balance between heat removal from the mould walls and internal water cooling in-out temperature difference. The real data comes directly from the measurement of cooling water temperatures and flow rates, which are affected by the casting speed and steel carbon content.

The situation beneath the rollers Equation (5) also comes from the heat balance assumption. The removed heat from the slab surface is equal to the heat, which is radiated to the surroundings by the rollers. In the case of internal cooled rollers, Javurek et al. [13] published a paper on how to determine boundary conditions in the case of dry casting.

In the spraying area, the strand is cooled by the water or water–air mixture sprays. Nozzle parameters like air and water flow, nozzle position and impact angles have an effect on the cooling efficiency, the  $htc$  from the Equation (6) respectively. Totten et al. [14] showed several empirical formulas describing how to deal with the heat transfer coefficient beneath the nozzle. However, these empirical formulas include many constants and parameters and their correct determination for a particular cooling setup is difficult. Proper determination of boundary conditions is crucial in case to obtain a real results, see Lopez et al. [15].

The advantage of the model discussed in this paper is that it obtains its heat transfer coefficients from measurements of the spraying characteristics of all nozzles used by the caster on a so-called hot plate in the experimental laboratory, according to Raudensky et al. [16]. Thus, the model takes  $htc$  as a function of water flow, casting speed, surface temperature, air pressure and can be expressed mathematically as:

$$htc = f(\dot{m}_{water}, v_{cast}, T_{surface}, p_{air}). \quad (10)$$

### 3. Numerical Formulation and Massive Parallelization

There are several discretization schemes how to solve the Equations (1)–(7). After large-scale numerical studies two numerical schemes proved to be good candidates for solving the case of 3-D transient heat transfer problem with solidification phenomena, Simple Explicit (SE) and Alternating Direction Implicit (ADI), see Mauder et al. [10]. The ADI scheme proposed by Douglas and Gunn is unconditionally stable and retains the second-order accuracy when applied to 3-D problems. However, ADI scheme has very limited possibility of parallelization on multiple CPU and massive parallelization on GPU is out of question. In the case of complex 3-D solidification-optimization models, the requirement for the real time control can be reached only by the use of the massive parallelization techniques. In Table 1 there are computation times for ADI and SE schemes tested on three different types of meshes (coarse-mesh with 10 000 nodes, fine-mesh with 125,000 nodes and the very-fine mesh with 1,000,000 nodes) on Intel(R) Core(TM) i7-3770 CPU @ 3.4GHz 16GB RAM. More information about efficiency, robustness and accuracy of the examined numerical schemes can be found in Mauder et al. [10].

**Table 1.** Computation time for non-parallel and parallel solution (s).

Numerical Scheme	Computational Time (s)		
	Coarse mesh	Fine-mesh	Very-fine mesh
SE—1 CPU	11.54	887.14	54,362.12
SE—12 CPU	135.28	1122.13	35,124.54
ADI—1 CPU	41.81	714.73	36,210.41
ADI—12 CPU	58.61	824.32	32,416.32
SE—GPU	18.67	97.72	972.49

This is the reason why the numerical core in presented solidification model is created by SE scheme. On the one hand, SE has its limitation in the form of stability condition, thus for fine meshes

the time step has to be very small. However, due to the use of massive parallelization on GPU this issue is compensated. The calculation on GPU is more than 50 times faster for very-fine meshes. The SE scheme applied to Equation (1) can be in the form:

$$h_{i,j,k}^{n+1} \rho_{i,j,k}^{n+1} = h_{i,j,k}^n \rho_{i,j,k}^n + \Delta\tau [\dot{Q}x + \dot{Q}y + \dot{Q}z] - \Delta\tau v_{cast} \frac{h_{i,j,k+1}^n \rho_{i,j,k+1}^n - h_{i,j,k}^n \rho_{i,j,k}^n}{\Delta z_{k-1}}, \quad (11)$$

where:

$$\dot{Q}_\Psi = 2 \frac{\left(\frac{0.5}{k_{\xi+1}^n} + \frac{0.5}{k_{\xi}^n}\right)^{-1} \frac{T_{\xi+1}^n - T_{\xi}^n}{\Delta\Psi_{\xi}} - \left(\frac{0.5}{k_{\xi-1}^n} + \frac{0.5}{k_{\xi}^n}\right)^{-1} \frac{T_{\xi}^n - T_{\xi-1}^n}{\Delta\Psi_{\xi-1}}}{\Delta\Psi_{\xi} + \Delta\Psi_{\xi-1}} \quad \Psi \in \{x, y, z\} \quad \xi \in \{i, j, k\}. \quad (12)$$

The index  $n + 1$  is associated to the future time;  $n$  is the index corresponding to the actual time;  $\Delta\tau$  is the increment of the time;  $x, y$  and  $z$  are the directions;  $\Delta\Psi$  are increments in the directions and  $\xi$  are the positions. The time step  $\Delta\tau$  has to fulfil a well-known stability condition:

$$\Delta\tau \leq \frac{1}{\left(\frac{2k(T)}{\rho(T)c(T)}\right) \left(\sum_{\Psi} \frac{1}{\Delta\Psi^2}\right) + \frac{v_{cast}}{\Delta z}}. \quad \Psi \in \{x, y, z\} \quad (13)$$

The numerical model has a non-equidistant mesh in all directions. The reason for this is that the largest temperature gradients are near the surface. In axis  $z$  (direction of casting) the nodes are adapted to the real rollers and nozzles positions to get more accurate determination of boundary conditions in secondary cooling zone. Mesh independence test in Figure 2 indicates when the convergence is achieved. In  $x$  axis is the number of elements, in  $y$ -left axis is the temperature in several points on the top surface (distance from meniscus 1, 2, 4, 10, 15, 20 m) and in the  $y$ -right axis is the value of the metallurgical length. This study shows that the number of elements should be at least 2 500,000. Finer mesh do not affected the results significantly. These results with respect the results obtained in Table 1 show again the needs of SE GPU parallel scheme in order to calculate complex 3-D solidification model in the real time.

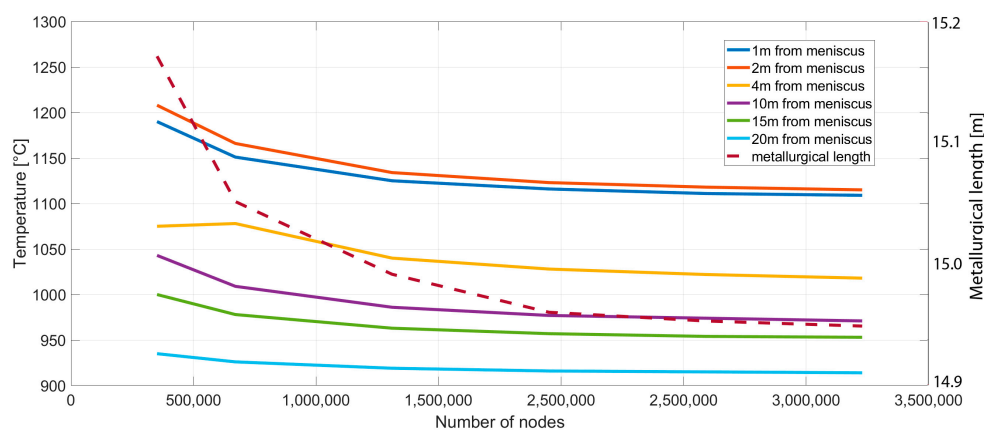


Figure 2. Temperatures and metallurgical length for different mesh densities.

The mesh decomposition is sketched out in Figure 3. The primary mesh is created on CPU, then is divided into many sub-meshes (regions). The boundary conditions and initial condition are set on CPU. Further, numerical regions are separately send to the GPU units where Equations (10) and (11) are calculated. After the temperatures in future time step are calculated, the values in separated regions are send back to CPU where boundary conditions are recalculated and again send to the GPU. This loop is repeated until final temperature field is reached.

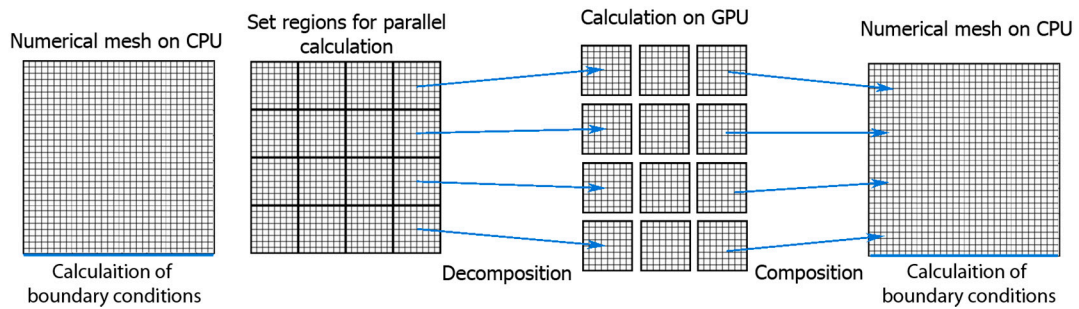


Figure 3. Numerical mesh CPU-GPU decomposition.

#### 4. Fuzzy Logic Regulator—FL-BrDSM

The BrDSM can calculate the temperature distribution of the strand in real time for given casting parameters such as the initial temperature distribution, intensity of cooling, speed of casting and so forth. The problem is how to set input parameters in the optimal way to get a required (optimal) temperature distribution. This is referred to as an inverse problem. For this reason, supervision-system/optimal-regulator based on fuzzy logic has been created. The FL regulator treats the solidification model as a black-box and when the FL regulator changes input parameters such as casting speed and intensity of cooling, the black-box returns the final temperature field for new input parameters. Based on the temperature field the FL regulator adjusts input parameters and repeats the process in a closed-loop until the optimal solution is found.

Several regulation approaches have been tested in the past, such as PID regulation, FL regulation, Model Predictive Control (MPC) regulation and their combinations. The most promising regulation outcome for dynamic changes in process parameters was reached by using a combination of MPC and FL regulation, see Stetina et al. [17]. This approach generally requires a large number of iterations because several future scenarios are calculated. For the real time simulation, this is possible only with use of GPU solidification model.

The most important parameters for the MPC/FL regulator are so called optimal surface temperature intervals. These temperature intervals should guarantee smooth temperature (cooling) profiles and high quality of final steel with zero or minimum surface defects. The optimal cooling strategy is to keep the surface temperatures in these intervals, see Figure 4. These intervals are set by the user and they are distinct for different grades of steel. In Section 5 is discussed how to set these intervals.

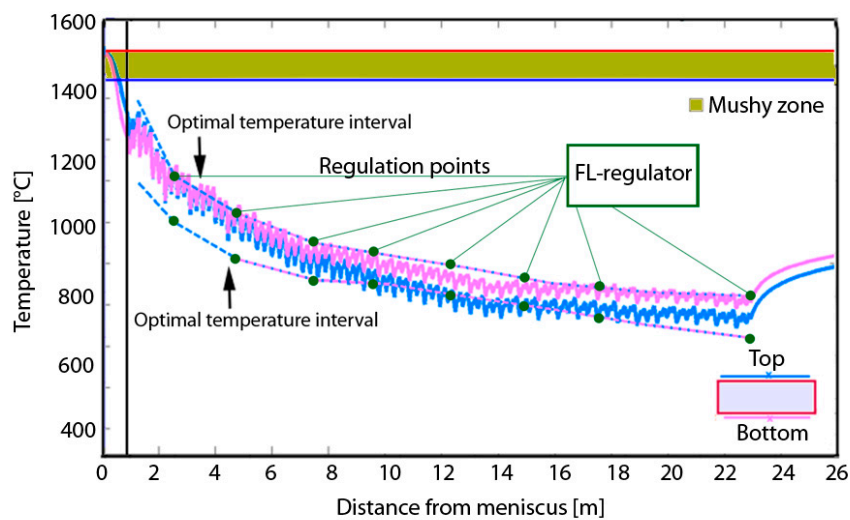


Figure 4. Optimal temperature intervals.

FL regulator extracts temperatures in the regulation points from the computed result (output from BrDSM) and by compare them with the prescribed temperature values to determine their errors. With all the temperature information, the FL regulator infers modifications for each cooling circuits. The temperatures in the regulation points are influenced by all previous cooling circuits, which should be taken account. The closer cooling circuit has a bigger influence on the regulation point, thus artificial parameter so call impact parameter in the range from 0 to 10 is created. The regulator evaluates the errors and impacts by the fuzzy rules. These rules give the value of modification for each cooling circuit. One circuit can get several different modifications from following control points proportional to the impact. Some modifications can require increase of cooling, the other decrease of cooling. The algorithm uses the final value for modification of one cooling loop as a sum of these values.

Membership functions for all fuzzy statements are trapezoidal-shaped uniformly distributed through the corresponding interval. These intervals are professionally/expertly set based on caster geometry and another caster parameters. As a defuzzification method, the standard centre of gravity was chosen.

The combination of the FL regulator with the GPU solidification model can predict future temperature states and it works like the MPC system. The detailed description of the FL regulator including linguistic variables and linguistic rules, input and output data and so forth, is described in Mauder et al. [18].

## 5. Steel S355 and Real Casting Data

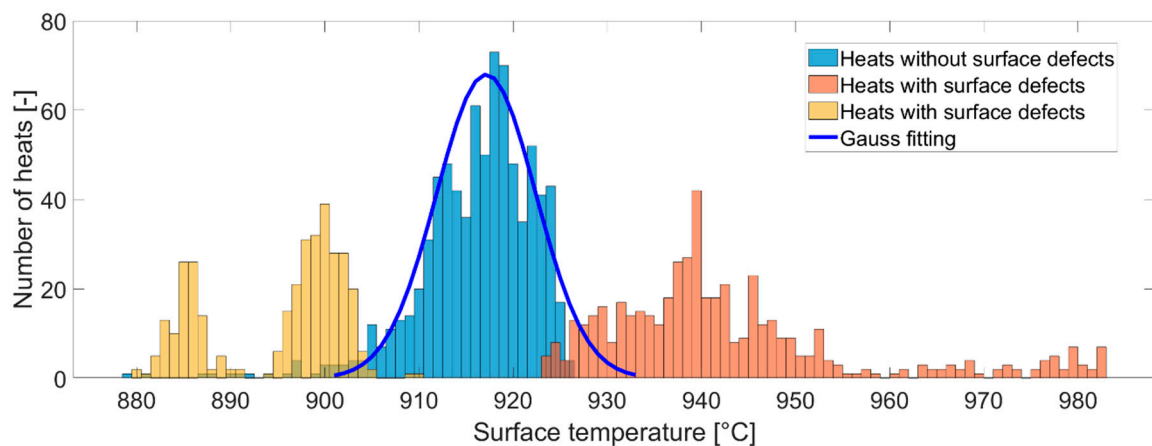
A frequent occurrence of surface defects in slabs of the cast steel grade S355 was the reason for statistical and numerical investigation. The importance of high quality of the steel S355 was mentioned in the introduction. The chemical composition is listed in Table 2.

**Table 2.** Chemical composition of steel S355.

Weight Fraction	Ni	Mn	Mo	Si	Nb	Ti	Cu
wt%	max 0.300	1.400–1.550	max 0.080	0.5	max 0.060	max 0.020	max 0.200
Weight Fraction	V	Al	P	C	Cr	S	Ca
wt%	max 0.020	0.020–0.060	0.030	0.160–0.180	max 0.200	0.020	0.002

Three typical defects were found: transverse facial cracks, star cracks and longitudinal facial cracks. The most common defects were the star cracks. These defects primarily appear at the top surface of the strand and possible causes for these defects are hard cooling and tensile stresses at the straightening area [2]. Therefore, the top surface of the strand and the temperatures at the straightening area were investigated.

The real casting data were statistically evaluated from approximately 2000 heats cast in 2011 and 2012 in EVRAZ VITKOVICE STEEL machinery in the Czech Republic. The evaluation of the statistical hypothesis shows that the surface temperature in the unbending point significantly influences the surface quality of slabs. The heats were divided into two groups. Heats where surface defects were found and heats without surface defects. The surface temperature was measured by a pyrometer at the straightening area. The results in a form of histogram are shown in Figure 5. The heats without surface defects were fitted by the Gauss curve to obtain optimal temperature intervals at unbending point.



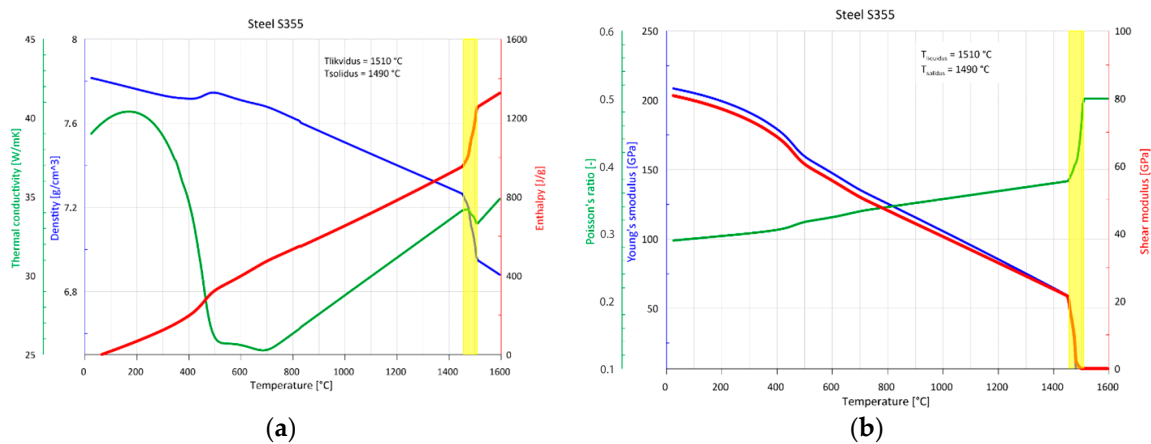
**Figure 5.** Surface temperatures in unbending point with and without defects.

Hypothesis tests show that we cannot reject the hypothesis on the 5% level of significance stating that the surface temperature at the straightening area influences the presence of surface defects. This leads back to the following idea: if we will keep the surface temperature in some range, the occurrence of surface defects would be minimized. The optimal temperature intervals at unbending point were set according to the statistical results from heats without defects  $916.03 \pm 6.89$  °C.

There are three pyrometers distributed on the examined caster. First one at end of the mould, the second one at unbending point (Figure 5) and the last one at the end of tertiary cooling zone. The most significant area is at unbending point from the perspective of cracks. However, smooth decreasing of surface temperatures through the casting process has positive influence on the final steel quality. Thus, the optimal temperature intervals for the fuzzy regulator were obtained by the curve fitting of these three points using following function:

$$y = xa^b + c, \quad (14)$$

where  $y$  is the temperature,  $x$  is distance from the meniscus and constant  $a$ ,  $b$  and  $c$  were found by using curve fitting tool. These constants have to be found for each grade of steel separately. Optimal temperature intervals obtained this way are used as the input parameters for FL-BrDSM. Thermophysical properties for the steel grade S355 as functions of the temperature were calculated using the InterDendritic Solidification (IDS) thermodynamic-kinetic package (version 1.3.1, Helsinki University of Technology, Helsinki, Finland). The results are presented in Figure 6a. The solidification model of the IDS is a so-called “grey box”, that is, it combines empirical or semi-empirical submodels with physically conceived submodels. The IDS model has been created at Aalto University in Helsinki [11] and is further developed, see Louhenkilpi et al. [19]. The IDS model consists of two main submodels for the simulation of interdendritic solidification (solves solidification from liquidus temperature to 1000 °C, i.e., the formation of, for example, ferrite or austenite) and simulation of solid state austenability (solves solidification from 1000 °C to temperature, 25 °C, that is, the formation of proeutectoid ferrite, cementite, perlite, bainite and martensite). The model also supports basic calculations of properties that influence the strength behaviour of steel and can serve as a basis for predictive crack criteria, see Figure 6b).

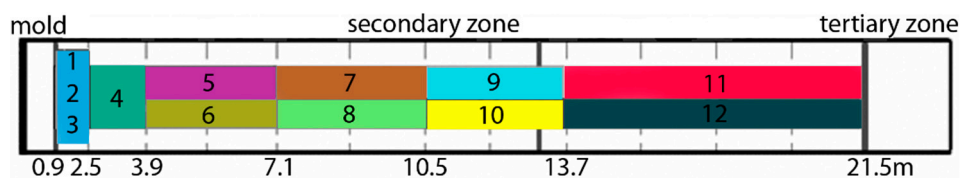


**Figure 6.** Temperature dependent physical properties for the steel grade S355, (a) thermophysical properties; (b) Mechanical properties.

## 6. Results and Discussion

The input parameters for the FL-BrDSM were: the thermophysical properties of steel grade S355 (from IDS); optimal surface temperature intervals (from statistical evaluation); speed of casting (set by the user); meniscus temperature (from historical/actual casting data in case of offline/online simulation); heat fluxes at the mould (from historical/actual casting data as a function of casting speed); and maximal and minimal water flows at the secondary cooling (from the caster specification). The output parameters for the FL-BrDSM were the temperature field (from BrDSM) and the optimal cooling intensity at the secondary cooling zone (from the FL regulator).

The geometry of the investigated CC machine is as follows: a mould length of 900 mm; a radius of 8000 mm; a length of secondary cooling after an unbending point of 8500 mm; length of tertiary cooling of 2000 mm. The secondary cooling zone is divided into 12 independent cooling loops according to Figure 7. For more detailed caster description see Mauder et al. [18].



**Figure 7.** Position of cooling loops.

Firstly, the FL regulator was tested for static process parameters. The optimal temperature field for the average casting speed 1.7 m/min is shown in Figure 8. The cross-section size of the slab was 1530 mm × 250 mm and the numerical mesh was created from over 1.5 million nodes. Because the CC is a dynamic process and the casting speed varies in time, it is necessary to keep surface temperatures at constant values in order to achieve a high steel quality. Thus, optimization was carried out for two different casting speeds in order to obtain the optimal relationship between cooling intensities and the casting speed, see Table 3. These results can be used for the real CC process in case of steel grade S355 casting.

The cooling intensity in loops 9 and 11 (last two loops at top surface) reaches its minimal allowed values for casting speed of 1.5 m/min. This means that for lower values of casting speed is even a better solution possibly exists. The last two cooling loops at top surface should therefore be replaced by smaller nozzles, which can operate smaller water flows (soft cooling). Moreover, significant savings of water consumption can be reached. In the case of casting speed 1.9 m/min, the maximal allowed cooling intensity values (physical limitations of pumps) were reached. This casting speed should not

be exceeded, otherwise the surface temperature increases over the optimal temperature interval and the number of defects may rise.

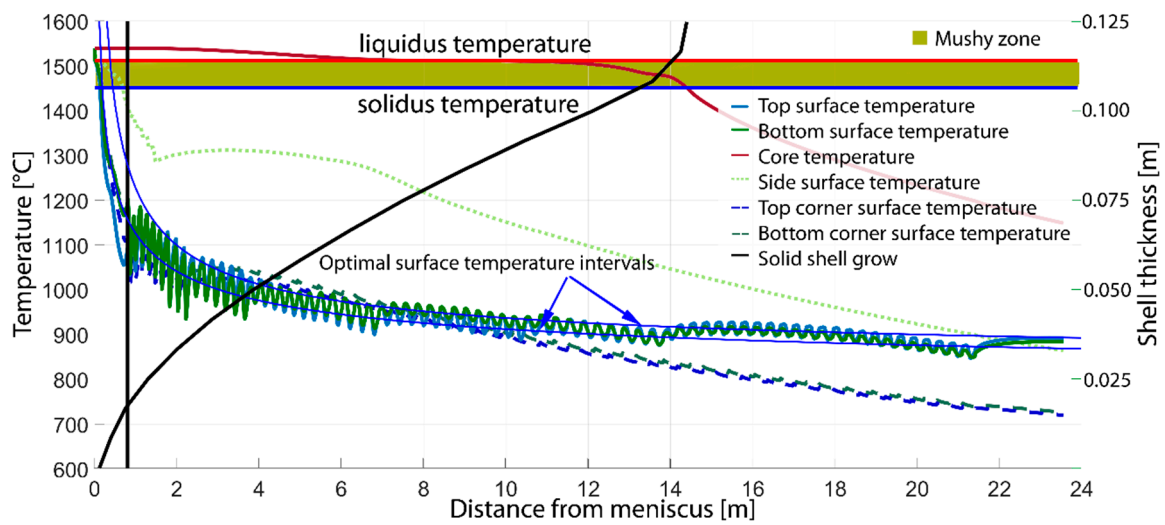


Figure 8. Optimal temperature field after fuzzy regulation.

Table 3. Optimal cooling intensities for cooling loops and different casting speeds.

Casting Speed (m/min)	Loop 1 (L/min)	Loop 2 (L/min)	Loop 3 (L/min)	Loop 4 (L/min)	Loop 5 (L/min)	Loop 6 (L/min)
1.5	96.6	125.4	103.9	124.6	65.3	98.5
1.9	98.1	132.6	109.5	146.3	98.3	103.3
Casting Speed (m/min)	Loop 7 (L/min)	Loop 8 (L/min)	Loop 9 (L/min)	Loop 10 (L/min)	Loop 11 (L/min)	Loop 12 (L/min)
1.5	32.0	65.7	22.0	34.7	31.2	43.7
1.9	46.9	85.7	26.7	58.3	99.5	106.2

Another set of simulations were carried out for dynamic changes in process parameters such as casting speed or casting temperature. The following results show 1 h casting process where a drop of the casting speed from 1.9 to 1.2 m/min at time 30 min and the increase of the casting speed from 1.2 to 1.9 m/min occurs at time 40 min. The Figure 9 shows the response in cooling intensities for all 12 cooling loops on casting speed drop calculated by FL regulator. Because MPC were used, several future scenarios were calculated and optimal dynamic changes were found. The value of temperature errors after each regulation points (surface temperatures after each cooling loop) are shown in Figure 10. The maximal temperature error was approximately 20 °C but average temperature error was less than 10 °C. This can be consider as a very good regulation results.

Static and dynamic simulations proved regulation possibilities of the presented FL-BrDSM solution. The computation time without GPU was 27.25 min for static and 47.20 min for dynamic simulation. With GPU approach, the computation time was less than 1 min and 2 min in case of dynamic simulation respectively. This declares that there is no problem to solve complex fine-mesh (more than 3 million nodes) 3D transient solidification models and their optimal regulation in the real time on the real CC machine.



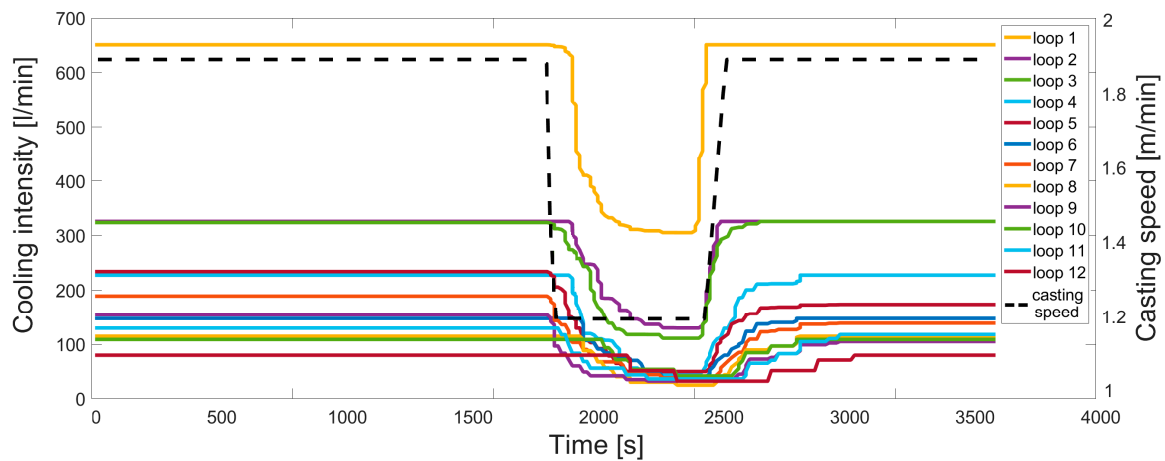


Figure 9. Dynamic response of FL regulator to casting speed drop.

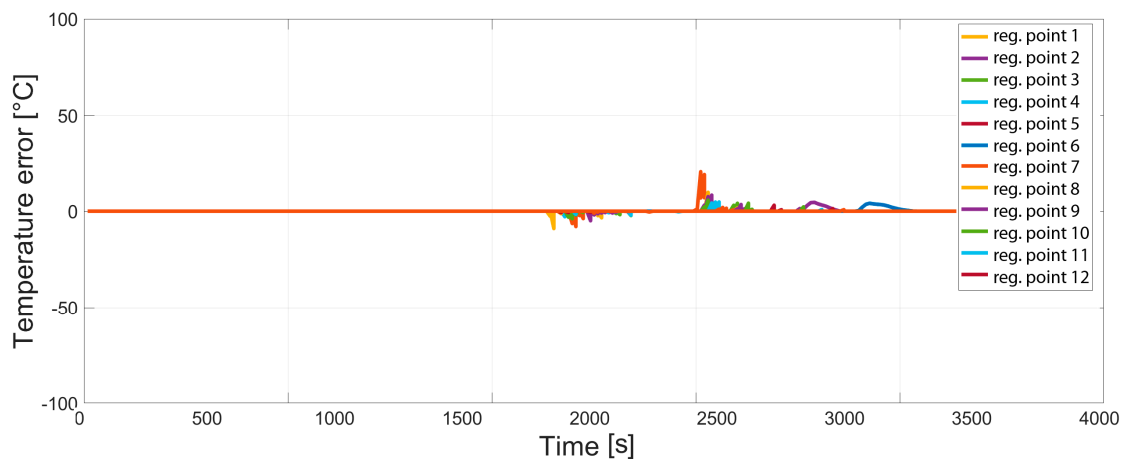


Figure 10. Surface temperature errors after each cooling loop.

## 7. Conclusions

The FL-BrDSM was tested for many different fuzzy parameters, for different casting temperatures and casting speeds constraints, for different caster and slab geometries and for different steel grades. This paper is focused on the quality improvement of the steel grade S355 and demonstration of the FL-BrDSM. The first part of the work was focused on detail description of solidification model and its GPU version. Then FL regulator was described. Last part of the work was statistical evaluation of real historical casting data for steel grade S355. The influence of the surface temperature at the straightening area to the occurrence of surface defects was statistically evaluated as significant. From the statistic results the optimal (recommended) temperature field was obtained and used as the input to the FL-BrDSM. For different casting speeds the optimal cooling intensities were found. The control of the CC process using recommended cooling curves can decrease the number of surface defects. The dynamic simulation shows real time regulation possibilities in the case of casting speed drop. The same approach can be applied for any grade of steel. The main advantage of the presented approach is a small number of evaluations before the optimal solution is reached and its overall versatility. This also allows for the on-line real-time regulation of a real CC process.

**Author Contributions:** Conceptualization, T.M. and J.S.; Methodology, J.S.; Software, T.M.; Validation, T.M. and J.S.; Formal Analysis, J.S.; Investigation, T.M.; Resources, T.M.; Data Curation, J.S.; Writing-Original Draft Preparation, T.M.; Writing-Review & Editing, T.M.; Visualization, T.M.; Supervision, J.S.; Project Administration, J.S.; Funding Acquisition, J.S.

**Funding:** This research was funded by the project NETME+, LO1202, with the financial support from the Ministry of Education, Youth and Sports of the Czech Republic under the “National Sustainability Programme I and APC was funded by the Open Access fond Brno University of Technology.

**Acknowledgments:** The authors gratefully acknowledge funding from the Open Access fond Brno University of Technology and Specific research on BUT FSI-S-17-4444.

**Conflicts of Interest:** The authors declare no conflict of interest. The funders had no role in the design of the study; in the collection, analyses, or interpretation of data; in the writing of the manuscript and in the decision to publish the results.

## References

1. Flick, A.; Stoiber, C. Trends in continuous casting of steel: Yesterday, today and tomorrow. In Proceedings of the METEC InSteelCon, Düsseldorf, Germany, 27 June–1 July 2011; pp. 80–91.
2. Birat, P.; Chow, C.; Emi, T.; Emling, W.H.; Fastert, H.P.; Fitzel, H.; Flemings, M.C.; Gaye, H.R.; Gilles, H.L.; Glaws, P.C.; et al. *The Making, Shaping and Treating of Steel: Casting Volume*, 11th ed.; The AISE Steel Foundation: Pittsburgh, PA, USA, 2003; p. 1000, ISBN 978-0-930767-04-4.
3. Santos, C.A.; Spim, J.A.; Garcia, A. Mathematical modeling and optimization strategies (genetic algorithm and knowledge base) applied to the continuous casting of steel. *Eng. Appl. Artif. Intell.* **2003**, *16*, 511–527. [[CrossRef](#)]
4. Zhemping, J.; Wang, B.; Xie, Z.; Lai, Z. Ant Colony Optimization Based Heat Transfer Coefficient Identification for Secondary Cooling Zone of Continuous Caster. In Proceedings of the IEEE International Conference Industrial Technology, Shenzhen, China, 20–24 March 2007; pp. 558–562. [[CrossRef](#)]
5. Zheng, P.; Guo, J.; Hao, X.-J. Hybrid Strategies for Optimizing Continuous Casting Process of Steel. In Proceedings of the IEEE International Conference Industrial Technology, Hammamet, Tunisia, 8–10 December 2004; pp. 1156–1161. [[CrossRef](#)]
6. Mauder, T.; Novotny, J. Two mathematical approaches for optimal control of the continuous slab casting process. In Proceedings of the Mendel 2010—16th International Conference on Soft Computing, Brno, Czech Republic, 26–28 June 2010; pp. 395–400, ISBN 978-80-214-4120-0.
7. Ivanova, A.A. Predictive Control of Water Discharge in the Secondary Cooling Zone of a Continuous Caster. *Metallurgist* **2013**, *57*, 592–599. [[CrossRef](#)]
8. Rao, R.V.; Kalyankar, V.D.; Waghmare, G. Parameters optimization of selected casting processes using teaching-learning-based optimization algorithm. *Appl. Math. Modell.* **2014**, *38*, 5592–5608. [[CrossRef](#)]
9. Mosayebidorcheh, S.; Bandpy, M.G. Local and averaged-area analysis of steel slab heat transfer and phase change in continuous casting process. *Appl. Thermal Eng.* **2017**, *118*, 724–733. [[CrossRef](#)]
10. Mauder, T.; Charvat, P.; Stetina, J.; Klimes, L. Assessment of Basic Approaches to Numerical Modeling of Phase Change Problems—Accuracy, Efficiency, and Parallel Decomposition. *J. Heat Transf.* **2017**, *139*, 5. [[CrossRef](#)]
11. Miettinen, J. *IDS Solidification Analysis Package for Steels: User Manual of DOS Version 2.0.0*; Helsinki University of Technology: Helsinki, Finland, 1999; p. 22, ISBN 9512246600.
12. Zhang, J.; Chen, D.F.; Zhang, C.Q.; Wang, S.G.; Hwang, W.S.; Han, M.R. Effects of an even secondary cooling mode on the temperature and stress fields of round billet continuous casting steel. *J. Mater. Process. Technol.* **2015**, *222*, 315–326. [[CrossRef](#)]
13. Javurek, M.; Ladner, P.; Watzinger, J.; Wimmer, P. Secondary cooling: Roll heat transfer during dry casting. In Proceedings of the METEC ESTAD, Düsseldorf, Germany, 15–19 June 2015; p. 8.
14. Totten, G.E.; Bates, C.E.; Clinton, N.A. *Handbook of Quenchants and Quenching Technology*; Haddad, M.T., Ed.; ASM International: Materials Park, OH, USA, 1993; p. 507, ISBN 0-87170-448-X.
15. Ramírez-López, A.; Muñoz-Negrón, D.; Palomar-Pardavé, M.; Romero-Romo, M.A.; Gonzalez-Trejo, J. Heat removal analysis on steel billets and slabs produced by continuous casting using numerical simulation. *Int. J. Adv. Manuf. Technol.* **2017**, *93*, 1545–1565. [[CrossRef](#)]
16. Raudensky, M.; Hnizdil, M.; Hwang, J.Y.; Lee, S.H.; Kim, S.Y. Influence of Water Temperature on The Cooling Intensity of Mist Nozzles in Continuous Casting. *Mater. Tehnol.* **2012**, *46*, 311–315; ISSN 1580-2949
17. Stetina, J.; Mauder, T.; Klimeš, L. Utilization of Nonlinear Model Predictive Control to Secondary Cooling during Dynamic Variations. In Proceedings of the AISTech, Pittsburgh, PA, USA, 16–19 May 2016; p. 14.

18. Mauder, T.; Sandera, C.; Stetina, J. Optimal control algorithm for continuous casting process by using fuzzy logic. *Steel Res. Int.* **2015**, *86*, 785–798. [[CrossRef](#)]
19. Louhenkilpi, S.; Laine, J.; Miettinen, J.; Vesanen, R. New Continuous Casting and Slab Tracking Simulators for Steel Industry. *Mater. Sci. Forum* **2013**, *762*, 691–698. [[CrossRef](#)]



© 2018 by the authors. Licensee MDPI, Basel, Switzerland. This article is an open access article distributed under the terms and conditions of the Creative Commons Attribution (CC BY) license (<http://creativecommons.org/licenses/by/4.0/>).

Article

# Comparison of Optimization-Regulation Algorithms for Secondary Cooling in Continuous Steel Casting

Michal Brezina , Tomas Mauder , Lubomir Klimes \*  and Josef Stetina

Faculty of Mechanical Engineering, Brno University of Technology, Technická 2896/2,  
616 69 Brno, Czech Republic; Michal.Brezina1@vutbr.cz (M.B.); mauder@fme.vutbr.cz (T.M.);  
stetina@fme.vutbr.cz (J.S.)

\* Correspondence: klimes@fme.vutbr.cz; Tel.: +420-541-143-243

**Abstract:** The paper presents the comparison of optimization-regulation algorithms applied to the secondary cooling zone in continuous steel casting where the semi-product withdraws most of its thermal energy. In steel production, requirements towards obtaining defect-free semi-products are increasing day-by-day and the products, which would satisfy requirements of the consumers a few decades ago, are now far below the minimum required quality. To fulfill the quality demands towards minimum occurrence of defects in secondary cooling as possible, some regulation in the casting process is needed. The main concept of this paper is to analyze and compare the most known metaheuristic optimization approaches applied to the continuous steel casting process. Heat transfer and solidification phenomena are solved by using a fast 2.5D slice numerical model. The objective function is set to minimize the surface temperature differences in secondary cooling zones between calculated and targeted surface temperatures by suitable water flow rates through cooling nozzles. Obtained optimization results are discussed and the most suitable algorithm for this type of optimization problem is identified. Temperature deviations and cooling water flow rates in the secondary cooling zone, together with convergence rate and operation times needed to reach the stop criterium for each optimization approach, are analyzed and compared to target casting conditions based on a required temperature distribution of the strand. The paper also contains a brief description of applied heuristic algorithms. Some of the algorithms exhibited faster convergence rate than others, but the optimal solution was reached in every optimization run by only one algorithm.

**Keywords:** continuous casting; secondary cooling; numerical modeling; thermal-solidification model; heuristic optimization



**Citation:** Brezina, M.; Mauder, T.; Klimes, L.; Stetina, J. Comparison of Optimization-Regulation Algorithms for Secondary Cooling in Continuous Steel Casting. *Metals* **2021**, *11*, 237. <https://doi.org/10.3390/met11020237>

Academic Editor: Miha Kovačič  
Received: 30 December 2020  
Accepted: 25 January 2021  
Published: 1 February 2021

**Publisher's Note:** MDPI stays neutral with regard to jurisdictional claims in published maps and institutional affiliations.



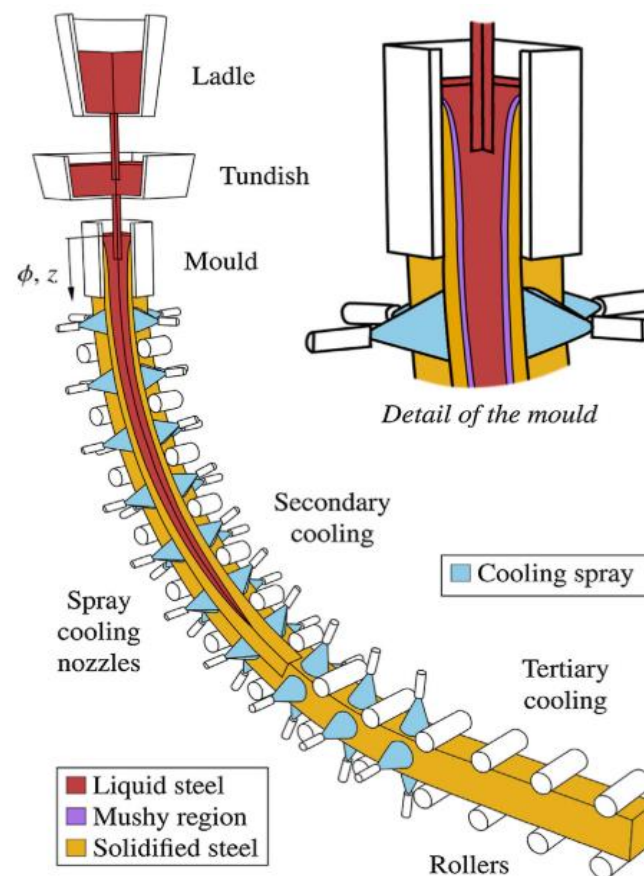
**Copyright:** © 2021 by the authors. Licensee MDPI, Basel, Switzerland. This article is an open access article distributed under the terms and conditions of the Creative Commons Attribution (CC BY) license (<https://creativecommons.org/licenses/by/4.0/>).

## 1. Introduction

The use of the continuous steel casting process has been experiencing a constant growth since the 1950s, when the ingot casting was replaced by the new method, which could satisfy increasing demands towards higher steel quality and production rate. Since those days, the continuous casting (CC) method evolved to a dominant steel production process. To avoid casting of semi-products with defects such as cracks, the casting regulation in real time is a necessity. Heat withdrawal from the strand can be now controlled by mathematical numerical models, even the real-time decisions during the casting process can be made owing to sophisticated code structure [1].

The CC of steel can be done with horizontal, vertical, or radial continuous casting machines (CCMs). The last-mentioned machine is the most used type worldwide as it overcomes the drawbacks of the other two machines [2]. That is the reason why the radial CC is also considered in this study. The CCM (see Figure 1) is a complex machine composed of many parts, which are usually divided to sections of the primary cooling zone (mold), the secondary cooling zone (water-air nozzle cooling), the tertiary cooling zone (radiation only with no nozzles), the cutting section and the chill zone where the cast

semi-products (billet, bloom, slab, etc.) rest until they are further proceeded. Some of these parts contribute to the heat withdrawal from a strand and these must be implemented in the numerical heat transfer and solidification model. As the process is transient, the initial and boundary conditions need to be specified for a precise prediction of the heat withdrawal and the temperature distribution. In the primary cooling zone referred to as the mold, heat transfer is governed mainly by heat conduction across the interfacial gap between the strand and the mold wall. In the secondary cooling zone, the most challenging task is to precisely describe heat transfer and its phenomena, including water-spray cooling, droplets impingement to the surface of the strand and liquid film boiling that may occur at the strand surface.



**Figure 1.** Radial continuous casting machine (CCM) depicting primary, secondary and tertiary cooling zones [3] (with the permission of Elsevier).

The main objective of this paper is to investigate and compare some of the well-known heuristic approaches coupled with a solidification model in terms of the computational efficiency, robustness, and accuracy to the CC problem. This approach makes it possible to appropriately assess the efficiency and accuracy of individual optimization algorithms, reducing a direct influence of the heat transfer and solidification model of the CC since the model is identical in all considered cases with distinct optimization algorithms. According to the literature survey focusing on minimization of the occurrence of defects in CC (mainly defects in secondary cooling), the target strand surface temperatures along the caster were set in this respect. The optimization problem was formulated to find adequate cooling intensities (water flow rates in secondary cooling) for all the cooling nozzles in order to reach specified ranges of the target surface temperature.

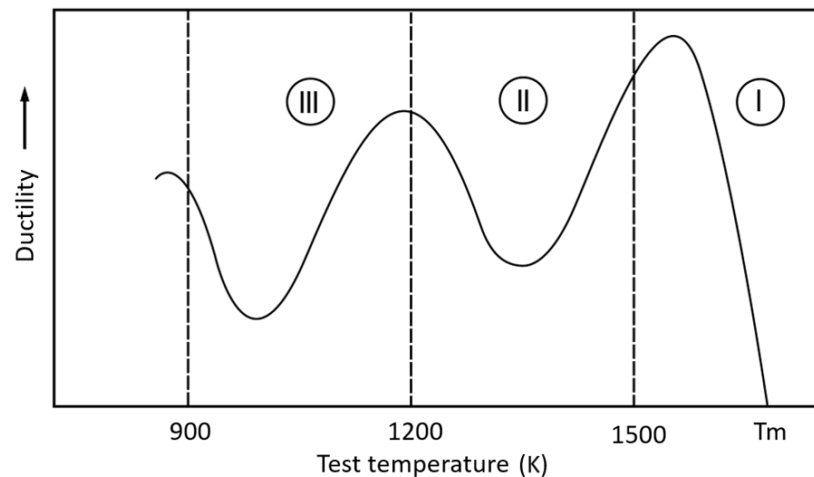
### 1.1. Conditions towards High-Quality Steel Casting

A crucial question is how to maximize the steel quality and productivity with the minimal cost. One of the main causes of crack formation is the exceeding maximum allowable mechanical strain and stress, which the cast steel grade can withstand. A literature survey on metallurgical problems and crack formations in continuous steel casting affecting the quality of steel, particularly in the secondary cooling zone, is presented below. Some of these properties can be implemented to the solidification thermal model, but to evaluate all of them, the stress-strain, fluid flow, segregation models and their coupling need to be considered [1]. Brimacombe [4] summarized fundamentals of steel and identified different types of cracks. The knowledge base about the high-quality casting was set. The serious problem in CC—the breakout of the liquid steel below the mold—can be initialized with a too high temperature of the liquid steel in the tundish [5]. As a result, the mold does not provide a sufficient cooling rate to create the necessary solidified shell at the surface of the strand. Nevertheless, if the shell would withstand the hydrostatic pressure of the liquid steel, the whole casting would be shifted in terms of the optimal temperature intervals along the CCM this would also affect the steel quality of the strand. Moreover, the origin of cracks caused by bending and straightening (unbending) processes is also influenced by the temperature-dependent ductility of steel [6].

The crack formation including centerline, intermediate, triangle, midway cracks, etc. is particularly triggered by an improper setup of primary and secondary cooling intensities, excessive oscillation of the mold and excessive gaps between supporting rollers, especially in slab casting [7]. The most frequent surface defects are transversal cracks, which are particularly initialized by deep oscillation marks followed by the tension generated by bulging, bending, and straightening of the strand. Another cause for developing mechanical strain can be poor accuracy of arcing between the segments and abnormal roll-gap shrinkage, which leads to excessive bulging. There is also an influence of the thermal stress, which results from an uneven cooling of the strand shell in the secondary cooling zone. Kulkarni and Babu [8] considered coupled thermal and mechanical conditions and proposed 17 quality criteria, which allow for the reduction of occurrence of defects during the casting process. This approach of optimization needs both thermal and mechanical models to be coupled. From studies of Cheung et al. and Kong et al. [9,10], it is known that the temperature regeneration between cooling sections should be less than 150 °C to avoid stress due to bulging and reheating in the secondary cooling zone. Reheating beyond 150 °C/m leads to a high probability of forming intermediate cracks. Surface cracks are formed if the surface temperature decreases into a zone of low steel ductility, which depends on steel grade; Santos et al. [11] identified it as being under around 850 °C. Cheung et al. [12] discussed the formation of cracks in steel casting and contributed to high-quality casting knowledge base with other optimal casting conditions. The authors discussed the centerline segregation and its impact to the crack formation while the centerline of the strand was liquid in the unbending part and pointed out that the center solidification of the strand must be completed before the point where a high deformation is applied (unbending point).

Brimacombe and Sorimachi [6] documented that the steel has reduced ductility over specific temperature ranges (Figure 2) dependent on the steel composition, which has important implications for the crack formation. Kim et al. [13] mentioned the so-called reduced ductility regions, namely zero ductility temperatures (ZDTs) and liquid impenetrable temperatures (LITs). Internal cracks detected in strands mainly originate in the mushy zone where the solid fraction of steel reaches 0.9 and 0.99 value for the LITs and ZDTs, respectively. These LIT and ZDT zones are sensitive for cracking because the steel is brittle in these temperature zones and has a higher tendency to hot cracking, and thus, it has a higher tendency towards the creation of defects [14]. The problem of crack formation in these locations is that the dendrite arms are dense enough to prevent the liquid steel to fill in gaps [15]. A lower solidification temperature is observed in these areas, which is a consequence of micro-segregation, and together with the shrinkage, the steel is more

prone to cracking while the tensile stress can reach lower values and cause cracking. The LITs and ZDTs are functions of chemical compositions and vary for different steel grades. Steel grades with larger temperature differences between the LIT and ZDT have a higher tendency to hot cracking and thus have a higher tendency to form defects such as internal cracks in the CC.



**Figure 2.** Schematic representation of temperature regions with reduced ductility redrawn from [16] (with the permission of Elsevier). For further details, see [16].

### 1.2. Numerical Modeling of Thermal Behavior in CC

In the steel CC, many numerical models have been used since the computational technique developed significantly. In the available literature, a number of implementations using the finite difference, finite volume or finite element methods can be found. In some previous works (e.g., by Fic et al. [17]), models with rather unrealistic assumptions of steel undergoing the phase change at a constant temperature were considered. The user-friendly packages that can predict variable-dependent thermophysical and mechanical properties were introduced in [18,19] and enabled more accurate modelling. Meng and Thomas [20] developed a 1D transient heat transfer model of the strand coupled with a 2D steady-state heat transfer model of the mold. Metallurgical phenomena such as the slag behavior in the mold and effects of oscillation marks were examined. Alizadeh et al. [21] proposed a 2D model and observed that the casting speed is the most effective parameter to heat removal in the mold, which means that it is the most important factor in control of the solidified shell thickness and strand temperature. Hardin et al. [22] presented a parametric study on more advanced transient 2D model, which allowed to observe the temperature response on the casting speed changes. One of the first 3D solidification model was introduced by Tieu and Kim [23] in 1997. The part of their work points to advantages of the 3D approach in comparison to 2D models. Another approach towards 3D heat transfer in the CC process is to use the so-called slice model, which neglects the heat transfer by conduction in the casting direction. This type of the solidification model is presented, for example, by Tambunan [24].

Due to limitations in terms of the computational performance, these models are often simplified: They use a simple geometry, constant thermophysical properties, average boundary conditions, use of empirical formulas for heat removal in the mold and secondary cooling, simulate only one quarter of the strand cross-section, etc. However, computational capabilities have progressed to the point where models used in the CC control include only minor physical simplifications, can provide more accurate results and can be used for steel quality optimization in real processing time. Utilizing the GPU-based model [3] enabled to overstep large numbers of shortcomings and resulted in a significantly reduced computing time while compared to CPU-based models.

### 1.3. Optimization and Regulation Algorithms in CC

To reach the optimal temperature intervals for a particular grade of steel and to react to dynamical changes such as an abrupt change of the casting speed, the solidification model must be coupled with optimization and control algorithms. One-dimensional mold cooling optimizations were among the very first optimization approaches which examined break outs at the mold exit due to the inappropriate shell thickness. During the two decades of the twenty-first century, computational techniques and performance experienced an exponential increase and simulation results can be obtained in the fraction of time that was needed two decades ago. This allowed many optimization algorithms to develop and get into practice. There are many papers which combine numerical modelling and optimization-regulation approaches in CC, such as Santos et al. [11], who applied the genetic algorithm and determined the optimum settings of water flow rates in different sprays zones. Optimized cooling conditions of mold and secondary cooling zones resulted in a shorter metallurgical length with the same quality [9]. Ji et al. [25] verified the use of the ant colony algorithm and Zheng et al. [26] used swarm optimization. Rao et al. [27] published a comprehensive review dealing with parameter-based optimization of selected casting processes. The authors pointed out that various optimization techniques such as simulated annealing [28], genetic algorithm [29] and particle swarm optimization [30] applied to the CC process does not always find the optimal solution. To control the casting process, these supervision systems include regulation algorithms such as the PID regulation which exhibit a slower response against a very fast regulation using fuzzy logic [31]. Mauder et al. in [31] introduced a 3D fully-transient and advanced optimal control algorithm based on the fuzzy logic that enabled a smooth regulation of cooling nozzles to the casting speed change.

Unfortunately, these works often needed a large number of optimization iterations before the optimal solution was found. It is; therefore, impossible to compare these approaches to each other since every author used his/her own specific solidification model and other specific conditions and setup. This drawback was the motivation for the present paper. In this paper, five optimization algorithms and their performance applied to the optimization of the CC are compared in terms of the heuristic search of appropriate water flow rates through cooling nozzles to reach the target temperature distribution of the strand, which would satisfy requirements towards a higher steel quality.

## 2. Slice Solidification Model

The mathematical formulation of heat transfer and solidification to the temperature distribution and solid shell profile prediction is based on the governing equation of transient heat conduction, called the Fourier-Kirchhoff equation [32]. To decrease the computational time in solving the optimization problem requiring a large number of evaluations of the model with various casting parameters, the 3D Fourier-Kirchhoff equation can be reformulated for the so-called 2.5D moving slice model neglecting conduction heat transfer in the casting direction ( $z$ ). The heat transfer equation for the 2.5D slice model formulated with the enthalpy approach reads

$$\frac{\partial H}{\partial t} = \frac{\partial}{\partial x} \cdot \left[ k_{\text{eff}}(T) \frac{\partial T}{\partial x} \right] + \frac{\partial}{\partial y} \cdot \left[ k_{\text{eff}}(T) \frac{\partial T}{\partial y} \right] + v \frac{\partial H}{\partial z}, \quad (1)$$

where  $k_{\text{eff}}$  is the effective thermal conductivity ( $\text{W} \cdot \text{m}^{-1} \cdot \text{K}^{-1}$ ),  $T$  is the temperature (K),  $H$  is the volume enthalpy ( $\text{J m}^{-3}$ ),  $t$  is the time (s) and  $x$ ,  $y$ , and  $z$  are spatial coordinates. Fluid flow of the liquid steel can be calculated by the computational fluid dynamics (CFD) techniques. However, computational time of such simulations is too excessive for real-time applications. The influence of fluid flow can be accounted in a simplified way by means of the effective thermal conductivity  $k_{\text{eff}}$ . Increasing heat transfer due to convection in the flow of liquid steel at different distances from the meniscus can be considered by an increased effective thermal conductivity as proposed by Zhang et al. [33]. For more information



about the solidification model in terms of equations, initial and boundary conditions, see the previous works of the co-authors of this paper [3,31].

The advantage of the model applied in this paper, when compared to models using empirical formulas for the heat transfer coefficient under the water-air cooling nozzles, is the use of experimentally measured characteristics of all nozzles used at the caster. As a result of many years of experience with computational inverse heat transfer in the heat transfer and fluid flow laboratory at Brno University of Technology, the heat transfer coefficient characteristics of nozzles can be experimentally determined with the use of a so-called hot plate and used in solidification numerical models [34]. In general, the heat transfer coefficient ( $htc$ ) of each nozzle is determined as a function of the casting speed, water mass flow rate, air pressure and the surface temperature and it can be expressed as

$$htc = f(v_{\text{cast}}, \dot{m}_{\text{water}}, p_{\text{air}}, T_{\text{surf}}). \quad (2)$$

The purpose of the slice model is to provide a thermo-solidification 2.5D analysis for a slice perpendicular to the longitudinal strand axis, see Figure 3. The whole casting strand (in this paper, the length from the meniscus to the cutting torch is considered 27.2 m) is divided into a number of slices having a defined thickness. In this paper, it was decided to set the slice thickness to 25 mm. The thickness of the slice needs to be chosen properly to achieve a sufficient precision of the boundary conditions describing heat withdrawal from the strand. The initial slice starts at the meniscus in the mold and moves downwards through the whole caster until it reaches the cutting part of the CCM. The explicit finite difference method was used in the thermal numerical model. Thus, the maximum numerical time step had to be defined to avoid numerical oscillations in the explicit calculation. The time step of the explicit scheme needs to be smaller than the wall-clock time required by the slice for its movement to the following position in the casting direction. The required time to move the slice to the following position was determined as a ratio between the thickness of the slice and the casting speed. New temperature field of the moving slice is initially set to the final temperature field of the previous slice and the boundary conditions corresponding to the slice location are applied for the evaluation of heat transfer. This type of 2.5D slice model significantly reduces the computational time in contrast to the fully 3D model, where the complete temperature distribution of the strand is calculated in each time step.

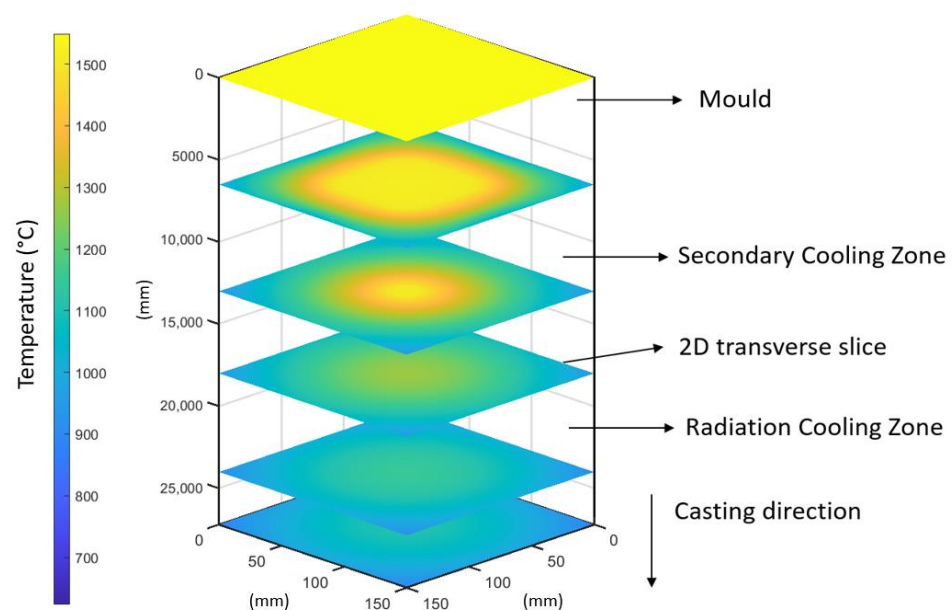


Figure 3. Idea of the 2.5D slice model.

### Thermophysical Properties

A low-carbon steel grade 18CrNiMo7-6 and a billet having the cross-section of 150 mm × 150 mm were considered in this paper. The thermophysical properties of the steel grade were determined in the temperature range from 1600 °C to the room temperature by means of the solidification analysis package IDS (version 1.3.1, created at Helsinki University of Technology, Laboratory of Metallurgy) [19]. The temperature-dependent enthalpy and other thermophysical properties (density, specific heat, thermal conductivity) identified with the IDS for the steel grade 18CrNiMo7-6 are shown in Figure 4.

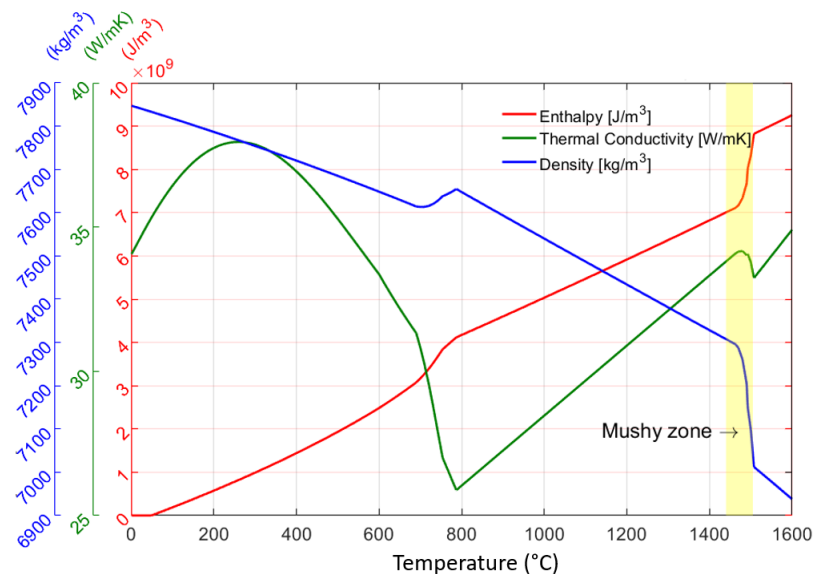


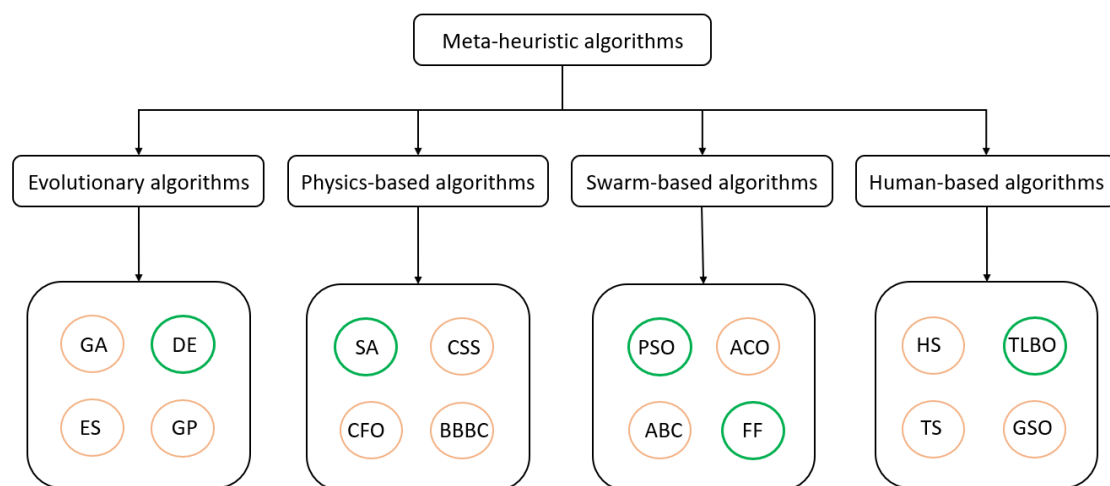
Figure 4. Thermophysical properties of structural steel 18CrNiMo7-6.

### 3. Optimization Approach

The 2.5D slice solidification model predicts the temperature distribution of the strand under certain values of the casting parameters, such as the casting speed, heat withdrawal in the mold, the secondary cooling intensity, etc. The problem is how to set these input parameters in a way to get a high-quality steel with a minimum occurrence of defects. This is referred to as an inverse problem and, to solve this issue, optimization algorithms need to be used. The solidification model is based on the discretization of Equation (1), which generally leads to millions of nonlinear finite-difference equations. A direct optimization approach with mathematical programming methods is not applicable, as the computational complexity and computation time grow exponentially with the size of the numerical mesh. Thus, it is needed to separate the optimization algorithm and the solidification model, which is referred to as the so-called black-box approach. In this approach, the optimization algorithm controls input parameters (speed of casting, intensity of water spray cooling, etc.) to the solidification model. The solidification model predicts the temperature distribution under the particular casting parameters and provides it to the optimization algorithm. Based on the temperature distribution, the optimization algorithm evaluates the objective function, somehow modifies input casting parameters and repeats the described process in a closed loop until the optimal solution is found. The computational efficiency of the optimization algorithm is usually assessed from the viewpoint of the number of iterations, which the algorithm needs to reach the optimal solution [35].

To deal with complex computational problems such as the CC, some optimization algorithms have been inspired by biological mechanisms in the nature. The nature acts as a source of concepts and principles for designing artificial computing systems [36]. So-called nature-inspired meta-heuristic algorithms attempt to solve optimization problems by mimicking biological or physical phenomena. Meta-heuristics can be grouped in four main categories based on the applied techniques, population and convergence logic used

to reach the optimal solution (see Figure 5): evolution-based, physics-based, swarm-based and human-based methods [37]. Laws of the natural evolution inspired the evolutionary-based methods. A randomly generated population starts the optimization process and evolves over subsequent generations with the combination of the best individuals to form the next generation of individuals [38]. The nature-inspired operations over individuals for the creation of the next generation are the mutation, crossover, elitism and many more, depending on a particular algorithm. On the other hand, algorithms imitating the physical rules, such as the simulated annealing algorithm employing the logic of annealing characteristics in metal processing and steel cooling, has usually only a single population. The algorithms mimicking the social behavior of individuals living in groups are called swarm-based algorithms. These algorithms usually include less operations compared to evolutionary-based approaches. Hence, they are easier for implementation and preserve search-space information over subsequent iterations, while evolution-based algorithms discard any information once a new generation of the population is formed. In human-based algorithms, the search process is divided into two phases: an initial exploration of the space and a consequent local exploitation.



**Figure 5.** Classification of metaheuristic optimization methods and the selection of used algorithms in this paper (in green circles): Genetic algorithm (GA), differential evolution (DE), evolution strategy (ES), genetic programming (GP), simulated annealing (SA), charged system search (CSS), central force optimization (CFO), big-bang big-crush (BBBC), particle swarm optimization (PSO), ant colony optimization (ACO), artificial bee colony (ABC), firefly (FF) algorithm, harmony search (HS), teaching learning-based optimization (TLBO), tabu search (TS), group search optimizer (GSO).

Optimization algorithms applied in this paper were selected in a way to examine at least one representative algorithm from each group of the metaheuristics. The simulated annealing (SA) algorithm was chosen from the physics-based algorithms. The vector-based differential evolution (DE) method as a representative of evolution-inspired algorithms was chosen, particularly due to its very good convergence [39]. The particle swarm optimization (PSO) and the firefly (FF) algorithm are the representatives of swarm-based algorithms since the PSO was proven to be very competitive with evolutionary and physically based algorithms [40] and the FF algorithm was already successfully applied in the CC optimization by the authors of the present paper [41]. The last considered algorithm is the teaching-learning-based optimization (TLBO) from the category of the human-based algorithms and can be considered as the most recent algorithm among the algorithms applied in this paper.

The description of main ideas of these algorithms is provided in the following section and further information can be found in [40]. One of the crucial issues of meta-heuristics is a determination and proper tuning of their parameters. In the group of considered five meta-heuristics, the TLBO is an only parameter-less method, thus no parameter of the

method needs to be determined. This can be beneficial in cases with rather simpler and fast optimization tasks, but the disadvantage is that the only option how to tune the algorithm is a proper selection of the random walk. Randomization is usually achieved with the use of pseudo-random numbers, based on some common stochastic processes, such as the Lévy flights or the Markov chain [40].

### 3.1. Simulated Annealing (SA)

The SA is one of the earliest and most popular metaheuristic algorithms developed in 1983 by Kirkpatrick et al. [42]. The SA is a trajectory-based, random-search technique for global optimization. It mimics the annealing process in materials processing when a metal cools and solidifies into a crystalline state with the minimum energy and growing crystals to reduce defects in the metallic structure. The annealing process involves a careful control of the temperature and its cooling rate, often referred to as the annealing schedule. The advantage of the SA against the deterministic methods is its ability to avoid being trapped in a local optimum solution. In this paper, the geometric cooling schedule and the temperature  $T$  during the annealing process is

$$T = T_0 \alpha^t, \quad (3)$$

with a stabilizing parameter  $\alpha$  and an initial temperature  $T_0$ . In most practical applications,  $\alpha \in [0.7, 0.99]$  is frequently used [40]. If a new value of the objective function is worse than the previous one, the algorithm accepts the new solution only if the randomly generated number  $r$  from the uniform distribution  $[0, 1]$  satisfies the condition

$$p = e^{[-\frac{\Delta f}{T}]} > r \quad (4)$$

where  $\Delta f$  is the difference of the values of the objective function. This setting leads to faster stabilization and a more extensive local search.

### 3.2. Differential Evolution (DE)

The DE algorithm was initially developed in 1997 by Storn and Price [43]. The DE is a vector-based meta-heuristic algorithm, which has good convergence properties. This algorithm has some similarity to pattern search and genetic algorithms due to its use of crossover and mutation. The DE generates vectors of new parameters by adding the weighted difference between two population vectors to a third vector as

$$v_i^{t+1} = x_p^t + F(x_q^t - x_r^t), \quad (5)$$

where  $F \in [0, 2]$  is a mutation parameter referred to as the differential weight. The setup of  $F \in [0.7, 0.9]$  is recommended as a good first choice [40]. Parameters of the mutated vector are then mixed with parameters of another predetermined vector to form the trial vector as

$$u_{j,i}^{t+1} = \begin{cases} v_{j,i}^{t+1} & \text{if } r_i \leq C_r, \\ x_{j,i}^t & \text{otherwise,} \end{cases} \quad j = 1, 2, \dots, d. \quad (6)$$

The parameter controlling the crossover probability  $C_r \in [0, 1]$  is recommended to be  $C_r = 0.5$  [40], thus the  $j$ -th component has a 50% probability to be mutated, while the  $r_i \in [0, 1]$  is a uniformly distributed random number. If the value of the objective function of the trial vector is better than the target vector, the trial vector replaces the target vector as

$$x_i^{t+1} = \begin{cases} u_i^{t+1} & \text{if } f(u_i^{t+1}) \leq f(x_i^t), \\ x_i^t & \text{otherwise.} \end{cases} \quad (7)$$

Each population vector serves once as the target vector. It is recommended that the population size should depend on the dimensionality of the problem [40].

### 3.3. Particle Swarm Optimization (PSO)

The PSO was developed by Kennedy and Eberhart in 1995 [44] and became one of the most widely used swarm-intelligence based algorithms due to its simplicity and flexibility. The behavior of the algorithm is based on the stochastically-drawn movement of particles in the space while they are attracted to the current best particle  $x_i^{*(t)}$  and to the current global best particle  $g^*$  over the populations as

$$v_i^{t+1} = v_i^t + \alpha \varepsilon_{i,1} (g^* - x_i^t) + \beta \varepsilon_{i,2} (x_i^{*(t)} - x_i^t), \quad (8)$$

where  $\alpha$  and  $\beta$  are learning and acceleration parameters, respectively, which are typically equal to 2 [40]; and  $\varepsilon_{i,1}$  and  $\varepsilon_{i,2}$  are random uniformly-distributed vectors having the values between 0 and 1. In each step, the particles are moved to new positions no matter if the new positions are better or not in terms of the value of the objective function as

$$x_i^{t+1} = x_i^t + v_i^{t+1}. \quad (9)$$

Many improvements of the PSO have been published, including, for example, an accelerated PSO (APSO) [45] with an enhanced scheme allowing a better convergence rate.

### 3.4. Firefly (FF) Algorithm

Due to similarities between the PSO and the FF algorithm, the FF method received negative feedback within the research community. The inspiration between flashing patterns and the behavior of fireflies gave rise to the firefly algorithm proposed by Xin-She Yang [46] in 2010. A new position of a firefly in each generation is determined as

$$x_i^{t+1} = x_i^t + \beta (x_j^t - x_i^t) + \alpha \varepsilon, \quad (10)$$

where the new position of the current firefly is determined by an attractiveness parameter  $\beta$  and a randomization parameter  $\alpha$ . In this paper, the geometric annealing schedule is implemented, which reads

$$\alpha = \alpha_0 \theta^t, \quad (11)$$

meaning that with the increasing number of generations, the randomness involved in the algorithm decreases. The attractiveness between fireflies is modeled as

$$\beta = \beta_0 e^{-\gamma r_{ij}^2}, \quad (12)$$

where  $\beta_0$  is the attractiveness at the distance  $r_{ij} = 0$ ,  $\gamma$  is the light absorption coefficient and  $r_{i,j}$  is the Cartesian distance between the two fireflies  $i$  and  $j$ . The term for attractiveness is more significant for those fireflies that are closer to each other.

### 3.5. Teaching Learning-Based Optimization (TLBO)

The TLBO approach is one of the recently developed optimization algorithms [47]. This method exhibits great performance, which was assessed in [48]. The TLBO is a parameter-less algorithm, which consists of two phases. The first one is called the teacher phase, in which the group of learners (population) is normally distributed (with an obtained mean  $x_{\text{mean},i}$ ) and learns from the teacher who is the learner with the best fitness among the whole population  $x_{\text{teacher},i}$ . In this phase, the learners attempt to get their values of the objective function towards the teacher's value of the objective function as

$$D_i = r_i (x_{\text{teacher},i} - T_F x_{\text{mean},i}), \quad (13)$$

where  $r_i$  is a random number within the range [0, 1] and  $T_F$  is the teaching factor defined as a heuristic step which can be either 1 or 2. The difference modifies the current vector and forms the new vector as

$$x_{\text{new},i} = x_{\text{old},i} + D_i. \quad (14)$$

$x_{\text{new},i}$  is accepted if it leads to better objective function, otherwise it remains unchanged and equals to vector of a previous generation  $x_{\text{old},i}$ . The second phase is called the learner phase, in which the learner shares knowledge and interacts with other different learners to further improve his/her performance. In this phase, the obtained new vector in teacher phase is set to  $x_{\text{old},i}$ , while  $x_j$  is a randomly selected vector ( $i \neq j$ ) from the learners and the new vector is

$$x_{\text{new},i} = \begin{cases} x_{\text{old},i} + r_i(x_{\text{old},i} - x_j), & \text{if } f(x_{\text{old},i}) < f(x_j) \\ x_{\text{old},i} - r_i(x_{\text{old},i} - x_j), & \text{if } f(x_{\text{old},i}) > f(x_j) \end{cases}, \quad (15)$$

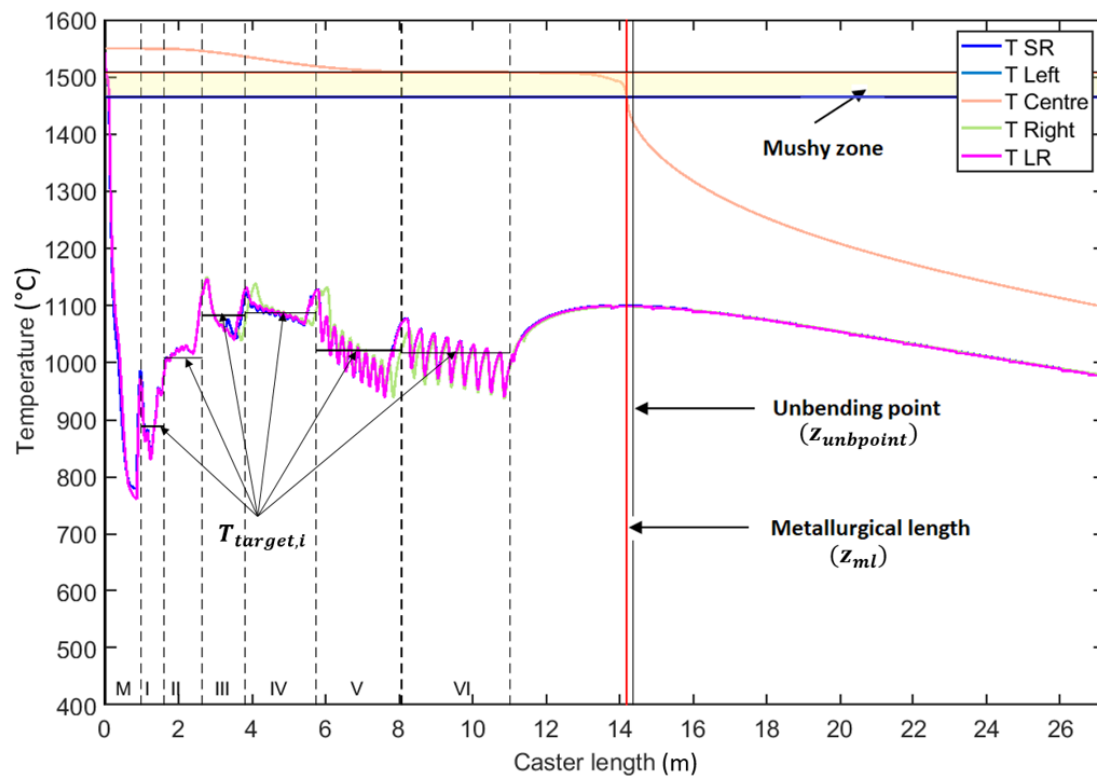
where  $r_i$  is a random number within the range [0, 1]. Finally, the new vector  $x_{\text{new},i}$  is accepted if it provides a better value of the objective function value.

#### 4. Results and Discussion

The computational model was set up with the geometry and configuration of the radial CCM operated in Trinec Iron and Steelworks in the Czech Republic. The CCM produces steel billets with the cross section of 150 mm × 150 mm, it has a tube-based water-cooled mold and the secondary cooling zone incorporates 178 water cooling nozzles. The length of the mold is 1000 mm and the radius of the radial part of the CCM is 8900 mm. The straightening of the curved strand starts at the distance of 14,255 mm from the meniscus (called the unbending point), where the strand is assumed to be fully solidified in order to withstand high tensile strain in this location. The secondary cooling zone is divided into six sections, each independently controlled and having a different set of cooling nozzles. The casting speed is set to 2.78 m/s and does not vary during the optimization. The target temperature distribution and cooling profile of secondary cooling zone was assumed as shown in Figure 6 (based on operational experience) and the optimization problem can be formulated as

$$\begin{aligned} \min \sum_{i=1}^d T_{\text{err},i} &= \sum_{i=1}^d (T_{\text{target},i} - T_{\text{calc},i}) \\ \text{Subjected to: } & z_{\text{ml}} < z_{\text{unbpoint}} \\ & T_{\text{unbending}} > T_{\text{unbending,min}} \\ & T_{\text{calc},i} > T_{\text{calc},i,\text{min}} \\ & \dot{V}_{\text{loop},i,\text{min}} \leq \dot{V}_{\text{loop},i} \leq \dot{V}_{\text{loop},i,\text{max}} \\ \text{Stop criterium: } & \sum_{i=1}^d T_{\text{err},i} < T_{\text{err,max}} \end{aligned} \quad (16)$$

where the objective function is the sum of average surface temperature errors in individual loops,  $d$  is the number of cooling loops,  $T_{\text{target},i}$  is the target average surface temperature in the  $i$ -th section of secondary cooling zone,  $T_{\text{calc},i}$  is the calculated average surface temperature in the  $i$ -th section of the secondary cooling zone,  $T_{\text{err,max}}$  is the maximum allowable surface temperature error set to 50 °C,  $z_{\text{ml}}$  is the metallurgical length,  $z_{\text{unbpoint}}$  is the location of the unbending point of the CCM and  $T_{\text{unbending}}$  is the average surface temperature at the unbending point. According to [11,12], the surface temperature at the unbending point  $T_{\text{unbending}}$  must be higher than  $T_{\text{unbending,min}}$  (which is considered 1100 °C in this work) and the average surface temperature in each secondary cooling zone  $T_{\text{calc},i}$  must be higher than  $T_{\text{calc},i,\text{min}}$  (which is considered 850 °C in this work) to avoid brittle regions with reduced ductility. Water flow rates  $\dot{V}_{\text{loop},i}$  through the cooling loops in the secondary cooling zone are also limited as specified in Table 1.



**Figure 6.** Considered target temperature distribution along the CCM for the steel grade 18CrNiMo7-6, with the longitudinal temperature profiles depicted in the middle of strand faces T SR (small radius), T LR (large radius), T Left (left side), T Right (right side) and T Centre being the temperature in the core of strand.

**Table 1.** Considered target water flow rates in the secondary cooling zone for given casting speed 2.78 m/s.

Value	Water Flow Rates						Total (l/min)
	Loop 1 (l/min)	Loop 2 (l/min)	Loop 3 (l/min)	Loop 4 (l/min)	Loop 5 (l/min)	Loop 6 (l/min)	
Minimum	0	0	0	0	0	0	0
Target	160	170	120	120	100	75	745
Maximum	300	250	140	140	140	100	1070

The aim of optimization was to determine casting conditions under which the sum of the average zone surface temperature errors is less than 50 °C. This accounts for about 8 °C of the temperature deviation per section in average, which is a rather hard condition to be achieved. In this work, the target water flow rates through the cooling loops in the secondary cooling zone were assumed as presented in Table 1 for the casting speed 2.78 m/s. In case of all optimization algorithms, the maximum number of algorithm-related operations was set to 1000. This means that the SA with a steady population was allowed to develop into 1000 generations. However, in swarm-based algorithms, such as the FF or the PSO, the population (including 10 individuals) was allowed to develop only into 100 generations. In this work, the population size was set identically to the number of generations applied in swarm-based algorithms (the FF and the PSO). In case of the DE, the number of individuals is recommended to be dependent on the dimensionality of a problem [40]. This recommendation was neglected, and the DE algorithm included the same number of individuals and maximum number of generations, such as were in FF and PSO. In the TLBO, the number of students was set to 10 individuals; however, due to the two-phase optimization approach (teacher and student phases), the maximum of

50 generations was established, whereas there were two evaluations of the solidification model for one individual in one generation. The recommended values of parameters for the SA, the DE and the PSO algorithms were defined in the previous chapter and the main parameters and their values applied in this work are listed in Table 2. The random walks involved in all algorithms were simulated in terms of the uniform distribution.

**Table 2.** Used optimization parameters.

Algorithm	Parameters of Optimization and Their Values
SA	$T_0 = 150, \alpha = 0.8, \gamma = 1$
DE	$F = 0.8, C_r = 0.5$
FF	$\beta_0 = 1, \alpha = 0.1, \gamma = 0.001, \theta = 0.98$
PSO	$\alpha = 2, \beta = 2$
TLBO	-

The 2.5D slice thermal-solidification numerical model, which was described in the foregoing section, was capable to simulate the temperature distribution of the cast strand in approximately 15 s on a PC with Intel(R) Core(TM) i7-3770 CPU @ 3.4GHz and 16 GB RAM. The size of the computational mesh 2.5 mm  $\times$  2.5 mm was set according to the mesh independency test mentioned above and with respect to appropriate treatment with boundary conditions, which were applied to all computational slices of thickness 25 mm. The majority (about 73%) of the computational time required by the numerical model is spent with a determination of boundary conditions, especially with the distribution of the heat transfer coefficients under cooling nozzles. As metaheuristics are random-based algorithms and a repeated execution of a particular algorithm under identical setup does not in general lead to the same result, the optimization study in this work included 500 runs with 100 runs per each algorithm. The maximum number of operations available to an algorithm per one run was considered 1000, as explained above, which gives the overall maximum of 500,000 evaluations of the heat transfer and solidification model. This approach was used to assess the stability of algorithms in terms of the optimal solution. The flow block diagram representing the introduced optimization process is shown in Figure 7.

According to Table 3 with the results, the overall best solutions were achieved with the use of the DE algorithm. In this case, the temperature error was 11.37 °C, with a slightly higher (by about 2.4 l/min) overall water flow rate through the secondary cooling zone when compared to the target solution. The only algorithm which achieved a solution with a lower overall water flow rate through the secondary cooling zone was the FF, as its best solution exhibits about a 2% lower water flow rate than the target solution. As for the temperature error of the FF for its best solution, it is about 21.4 °C, which is similar to those of the SA, the PSO and the TLBO. The highest mean-value water flow rate of about 756.6 l/min was achieved with the PSO algorithm. Figure 8 demonstrates the water flow rates for the best solution within the set of 100 runs. A fairly similar behavior in the first cooling loop for each metaheuristic algorithm can be seen, nevertheless the other cooling loops exhibit some minor deviations against the target water flow rates.

The overall results listed in Table 4 show that the only algorithm exhibiting a worse convergence rate than other algorithms is the PSO algorithm, with only 78 of 100 runs reaching the stop criterium. In case of the SA, the DE, the FF and the TLBO algorithms, the stop criterium was in the majority of runs reached. The FF algorithm reports even a 100% convergence success. The lowest mean-value and median-value number of operations performed by the algorithm to reach the solution was in case of the DE algorithm, which also exhibits the smallest variation of the number of generations needed to converge in each run, as depicted in Figure 9 where the median, the lower and upper quartiles for the number of operations are shown. The best (lowest) median value for the number of operations was achieved in case of the SA algorithm. On the other hand, the worst behavior in terms of the required number of operations was observed in case of the FF algorithm. This can be attributed to the geometric annealing schedule with an initial larger exploration



and gradually increasing exploitation. The minimum number of operations needed to reach the solution was achieved for the SA, the DE and the PSO with 70, 68 and 73 operations per run, respectively. The convergence graph of individual algorithms, representing the averaged minimum temperature error (value of the objective function) reached by the algorithm in dependence to the number of operations, can be seen in Figure 10.

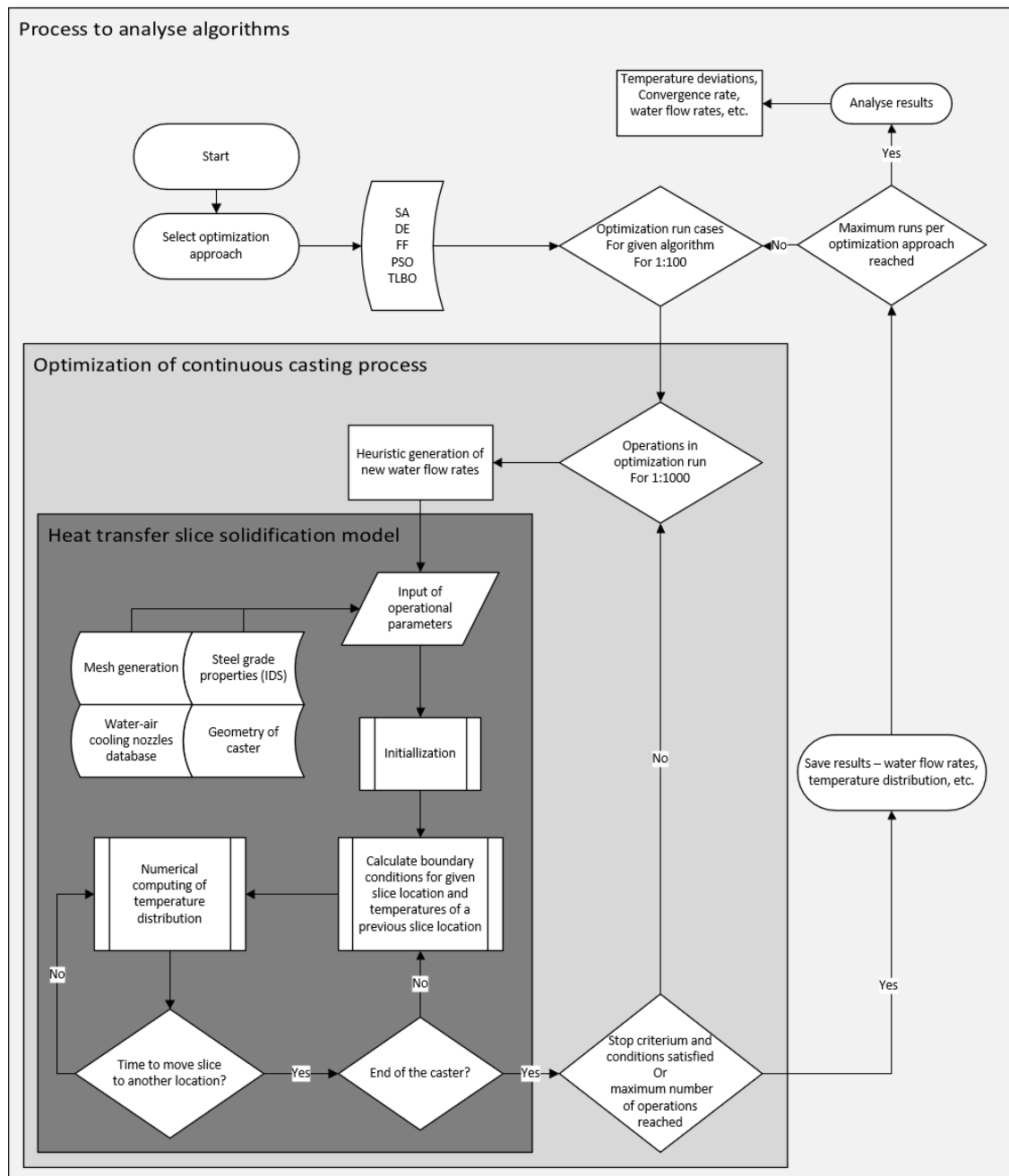
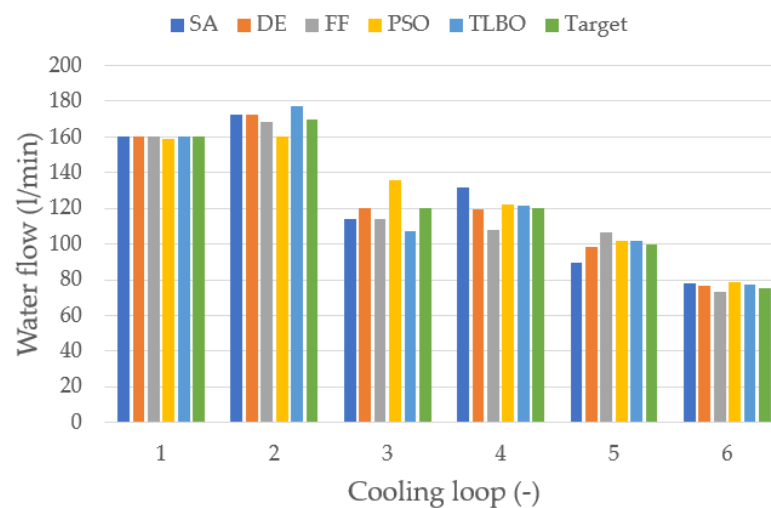


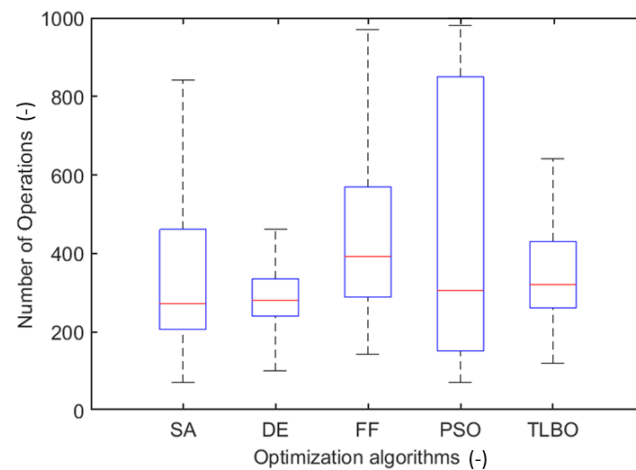
Figure 7. Flow block diagram representing the applied optimization process.

**Table 3.** Mean-value temperature errors and water flow rates and the best temperature error and water flow rates (values in the brackets) for each algorithm for the casting speed of 2.78 m/s.

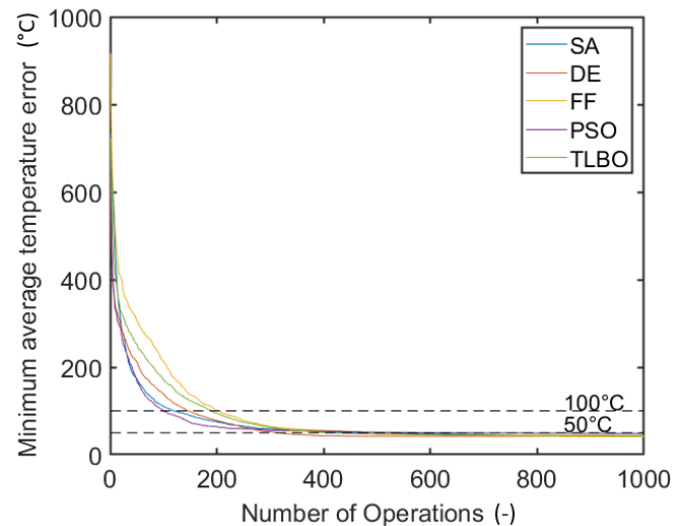
Optimization Algorithm	Temperature Error (°C)	Water Flow Rates						Total (l/min)
		Loop 1 (l/min)	Loop 2 (l/min)	Loop 3 (l/min)	Loop 4 (l/min)	Loop 5 (l/min)	Loop 6 (l/min)	
SA	44.19 (23.35)	160.25 (160.27)	168.06 (172.78)	120.36 (113.7)	118.67 (131.79)	100.86 (89.31)	74.23 (77.75)	742.43 (745.69)
DE	42.11 (11.37)	160.55 (160.53)	167.45 (172.29)	124.61 (119.88)	122.30 (119.66)	100.79 (98.21)	76.32 (76.79)	752.02 (747.36)
FF	41.09 (21.38)	159.67 (160.13)	169.39 (168.41)	121.72 (114.23)	119.05 (107.86)	107.07 (106.71)	74.89 (73.48)	746.66 (730.83)
PSO	48.89 (24.31)	160.04 (159.06)	167.61 (160.54)	125.02 (135.46)	122.10 (121.92)	107.08 (101.71)	74.71 (78.83)	756.56 (757.51)
TLBO	42.96 (23.14)	161.37 (160.39)	165.28 (177.22)	119.84 (107.03)	118.33 (121.17)	104.39 (101.94)	73.45 (77.52)	742.66 (745.28)

**Figure 8.** The water flow rates through the secondary cooling zone of the best solutions of individual algorithms.**Table 4.** Overall results for the considered continuous casting (CC) optimization problem.

-	SA	DE	FF	PSO	TLBO
Median of the number of operations (-)	271	280	392	305	320
Mean of the number of operations (-)	369.18	294.3	433.42	451.7	382.6
Minimum number of operations (-)	70	68	142	73	120
Percentage of cases in which the stop criterium was reached (%)	96	99	100	78	95
Metallurgical length of the best solution (m)	14.175	14.200	14.150	14.175	14.150
Mean temperature error (°C)	44.19	42.11	41.09	48.89	42.96
Best (lowest) temperature error (°C)	23.35	11.37	21.38	24.31	23.14
Worst (highest) temperature error (°C)	154.51	52.27	49.98	194.06	98.03



**Figure 9.** Box plot with the number of operations needed to reach the solution: depicted in box plot with median, 25th percentile and 75th percentile.



**Figure 10.** The averaged minimum temperature error reached by the algorithm to particular operation.

If the stop criterium was set to a lower temperature error, the computational time increased. Based on the obtained results, it can be summarized that overall best behavior was exhibited by the DE algorithm. As for the computer implementation of the algorithms, none of the considered algorithms required more extensive experience but the SA algorithm can be considered as the easiest one from the implementation viewpoint. The worse behavior of the PSO algorithm could be due to inappropriately selected optimization parameters  $\alpha$  and  $\beta$ , which lead to an entrapment in a local minimum, while the algorithm needs a lowest number of operations to reach the limit of the temperature error of 100 °C when compared to other algorithms, as demonstrated in Figure 10. The use of the enhanced PSO—the APSO—would improve the convergence rate of the PSO.

## 5. Conclusions

In the paper, five metaheuristic algorithms from each group of the metaheuristic classification were tested and assessed in the problem of continuous steel casting. A 2.5D slice thermal-solidification numerical model was developed and used for the optimization procedure. The objective of the optimization was to minimize the average temperature errors in each section of the secondary cooling zone within predefined temperature intervals by determination of appropriate water flow rates through cooling nozzles. The target values

of the temperature intervals were specified in certain locations in the secondary cooling zone of the caster according to the literature review focusing on casting of high-quality final products.

- The best median value in terms of the number of operations needed by the algorithms to reach the solution was observed for the simulated annealing (SA) algorithm (with 271 operations per run and with the convergence rate of 96%) and for the differential evolution (DE) algorithm (with 280 operations per run and with the convergence rate of 99%).
- The best convergence rate was achieved in case of the FF algorithm in which all the runs reached the stop criterium, but with approximately 121 more operations per run than the DE algorithm.
- The particle swarm optimization (PSO) was surprisingly the worst algorithm among the considered algorithms, with 22 non-converged runs. A better behavior and performance of the algorithms could further be achieved by tuning of parameters of the individual algorithms.
- The teaching-learning-based optimization (TLBO), which is a method containing no algorithm-specific control parameters, exhibited medium performance among the considered algorithms and its convergence rate was 95%.

In conclusion, the DE algorithm was identified as the best performance algorithm for the considered control problem. Nevertheless, the performance of the SA, the FF and the TLBO algorithms was evaluated as good, which makes them also suitable for the solution of this kind of control problems.

**Author Contributions:** Conceptualization, M.B. and T.M.; Methodology, L.K.; Software, M.B.; Validation, M.B. and T.M.; Formal Analysis, M.B.; Investigation, M.B.; Resources, M.B. and T.M.; Data Curation, T.M.; Writing—Original Draft Preparation, M.B.; Writing—Review and Editing, M.B., T.M. and L.K.; Visualization, M.B.; Supervision, J.S.; Project Administration, J.S.; Funding Acquisition, J.S. All authors have read and agreed to the published version of the manuscript.

**Funding:** This work was supported by the Czech Science Foundation under contract No. 19-20802S “A coupled real-time thermo-mechanical solidification model of steel for crack prediction.” and by the research project funded by Brno University of Technology (FSI-S-20-6295).

**Data Availability Statement:** All necessary data are presented in the article. Other data and computer codes are not publicly available.

**Acknowledgments:** The authors acknowledge the financial support from Czech Science Foundation (project No. 19-20802S) and from Brno University of Technology (project No. FSI-S-20-6295).

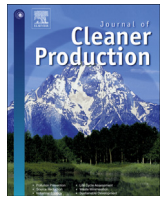
**Conflicts of Interest:** The authors declare no conflict of interest. The funders had no role in the design of the study; in the collection, analyses, or interpretation of data; in the writing of the manuscript and in the decision to publish.

## References

1. Thomas, B.G. Review on Modeling and Simulation of Continuous Casting. *Steel Res. Int.* **2017**, *89*, 21. [[CrossRef](#)]
2. Seetharaman, S. *Treatise on Process Metallurgy*; Elsevier: Oxford, UK, 2014; Volume 3, ISBN 9780080969886.
3. Klimeš, L.; Štětina, J. A rapid GPU-based heat transfer and solidification model for dynamic computer simulations of continuous steel casting. *J. Mater. Process. Technol.* **2015**, *226*, 1–14. [[CrossRef](#)]
4. Brimacombe, J.K. The challenge of quality in continuous casting processes. *Metall. Mater. Trans. A* **1999**, *30*, 1899–1912. [[CrossRef](#)]
5. Santos, C.A.; Spim, J.A.; Garcia, A. Mathematical modeling of heat transfer in the Twin-Roll continuous casting process. *Am. Soc. Mech. Eng. Heat Transf. Div. HTD* **1998**, *357*, 133–138, ISBN: 8415683111.
6. Brimacombe, J.K.; Sorimachi, K. Crack formation in the continuous casting of steel. *Metall. Trans. B* **1977**, *8*, 489–505. [[CrossRef](#)]
7. Xia, G.; Schiefermüller, A. The influence of support rollers of continuous casting machines on heat transfer and on stress-strain of slabs in secondary cooling. *Steel Res. Int.* **2010**, *81*, 652–659. [[CrossRef](#)]
8. Kulkarni, M.S.; Babu, A.S. Managing quality in continuous casting process using product quality model and simulated annealing. *J. Mater. Process. Technol.* **2005**, *166*, 294–306. [[CrossRef](#)]
9. Cheung, N.; Santos, C.A.; Spim, J.A.; Garcia, A. Application of a heuristic search technique for the improvement of spray zones cooling conditions in continuously cast steel billets. *Appl. Math. Model.* **2006**, *30*, 104–115. [[CrossRef](#)]

10. Kong, Y.; Chen, D.; Liu, Q.; Long, M. A prediction model for internal cracks during slab continuous casting. *Metals (Basel)* **2019**, *9*, 18. [[CrossRef](#)]
11. Santos, C.A.; Spim, J.A.; Garcia, A. Mathematical modeling and optimization strategies (genetic algorithm and knowledge base) applied to the continuous casting of steel. *Eng. Appl. Artif. Intell.* **2003**, *16*, 511–527. [[CrossRef](#)]
12. Cheung, N.; Garcia, A. Use of a heuristic search technique for the optimization of quality of steel billets produced by continuous casting. *Eng. Appl. Artif. Intell.* **2001**, *14*, 229–238. [[CrossRef](#)]
13. Kim, K.; Yeo, T.J.; Oh, K.H.; Lee, D.N. Effect of Carbon and Sulfur in Continuously Cast Strand on Longitudinal Surface Cracks. *ISIJ Int.* **1996**, *36*, 284–289. [[CrossRef](#)]
14. Böttger, B.; Apel, M.; Santillana, B.; Eskin, D.G. Relationship between solidification microstructure and hot cracking susceptibility for continuous casting of low-carbon and high-strength low-alloyed steels: A phase-field study. *Metall. Mater. Trans. A Phys. Metall. Mater. Sci.* **2013**, *44*, 3765–3777. [[CrossRef](#)]
15. El-Bealy, M.O. On the Formation of Interdendritic Internal Cracks During Dendritic Solidification of Continuously Cast Steel Slabs. *Metall. Mater. Trans. B* **2012**, *43*, 1488–1516. [[CrossRef](#)]
16. Suzuki, H.G.; Elyon, D. Hot ductility of titanium alloy: A challenge for continuous casting process. *Mater. Sci. Eng. A* **1998**, *243*, 126–133. [[CrossRef](#)]
17. Fic, A.; Nowak, A.J.; Bialecki, R. Heat transfer analysis of the continuous casting process by the front tracking BEM. *Eng. Anal. Bound. Elem.* **2000**, *24*, 215–223. [[CrossRef](#)]
18. Andersson, J.O.; Helander, T.; Höglund, L.; Shi, P.; Sundman, B. Thermo-Calc & DICTRA, computational tools for materials science. *Calphad Comput. Coupling Phase Diagr. Thermochem.* **2002**, *26*, 273–312. [[CrossRef](#)]
19. Miettinen, J.; Louhenkilpi, S.; Kytönen, H.; Laine, J. IDS: Thermodynamic-kinetic-empirical tool for modelling of solidification, microstructure and material properties. *Math. Comput. Simul.* **2010**, *80*, 1536–1550. [[CrossRef](#)]
20. Meng, Y.; Thomas, B.G. Heat-Transfer and Solidification Model of Continuous Slab Casting: CON1D. *Metall. Mater. Trans. B* **2003**, *34B*, 685–705. [[CrossRef](#)]
21. Alizadeh, M.; Edris, H.; Shafyei, A. Mathematical Modeling of Heat Transfer for Steel Continuous Casting. *Int. J. ISSI* **2006**, *3*, 7–16, ISBN: 8415683111.
22. Hardin, R.A.; Liu, K.A.I.; Kapoor, A.; Beckermann, C. A Transient Simulation and Dynamic Spray Cooling Control Model for Continuous Steel Casting. *Metall. Mater. Trans.* **2003**, *34B*, 297–307. [[CrossRef](#)]
23. Tieu, A.K.; Kim, I.S. Simulation of the continuous casting process by a mathematical model. *Int. J. Mech. Sci.* **1997**, *39*, 185–192. [[CrossRef](#)]
24. Tambunan, B. Simulation of Heat Transfer Solidification with Improved Latent Heat Parameter in Continuous Casting. In Proceedings of the Seminar National MIPA 2005; FMIPA: Depok, Indonesia, 25–26 November 2005; p. 7.
25. Ji, Z.; Wang, B.; Xie, Z.; Lai, Z. Ant colony optimization based heat transfer coefficient identification for secondary cooling zone of continuous caster. *IEEE Int. Conf. Integr. Technol.* **2007**, 558–562. [[CrossRef](#)]
26. Zheng, P.; Guo, J.; Hao, X.J. Hybrid strategies for optimizing continuous casting process of steel. In Proceedings of the 2004 IEEE International Conference on Industrial Technology, Hammamet, Tunisia, 8–10 December 2004; Volume 3, pp. 1156–1161. [[CrossRef](#)]
27. Rao, R.V.; Kalyankar, V.D.; Waghmare, G. Parameters optimization of selected casting processes using teaching-learning-based optimization algorithm. *Appl. Math. Model.* **2014**, *38*, 5592–5608. [[CrossRef](#)]
28. Kulkarni, M.S.; Babu, A.S. Optimization of continuous casting using simulation. *Mater. Manuf. Process.* **2005**, *20*, 595–606. [[CrossRef](#)]
29. Bhattacharya, A.K.; Debjani, S.; Roychowdhury, A.; Das, J. Optimization of continuous casting mould oscillation parameters in steel manufacturing process using genetic algorithms. In Proceedings of the IEEE Congress on Evolutionary Computation 2007, Singapore, 25–28 September 2007; pp. 3998–4004. [[CrossRef](#)]
30. Jabri, K.; Dumur, D.; Godoy, D.; Mouchette, A.; Bèle, B. Particle swarm optimization based tuning of a modified smith predictor for mould level control in continuous casting. *J. Process. Control.* **2011**, *21*, 263–270. [[CrossRef](#)]
31. Mauder, T.; Sandera, C.; Stetina, J. Optimal Control Algorithm for Continuous Casting Process by Using Fuzzy Logic. *Steel Res. Int.* **2015**, *86*, 785–798. [[CrossRef](#)]
32. Incropera, F.P.; Bergman, T.L.; Lavine, A.S.; DeWitt, D.S. *Fundamentals of Heat and Mass Transfer*, 7th ed.; John Wiley & Sons: Hoboken, NJ, USA, 2011; ISBN 9780470501979.
33. Zhang, J.; Chen, D.F.; Zhang, C.Q.; Wang, S.G.; Hwang, W.S.; Han, M.R. Effects of an even secondary cooling mode on the temperature and stress fields of round billet continuous casting steel. *J. Mater. Process. Technol.* **2015**, *222*, 315–326. [[CrossRef](#)]
34. Raudenský, M.; Tseng, A.A.; Horský, J.; Komínek, J. Recent developments of water and mist spray cooling in continuous casting of steels. *Metall. Res. Technol.* **2016**, *113*. [[CrossRef](#)]
35. Beyer, H.G.; Sendhoff, B. Robust optimization—A comprehensive survey. *Comput. Methods Appl. Mech. Eng.* **2007**, *196*, 3190–3218. [[CrossRef](#)]
36. Blum, C.; Roli, A. Metaheuristics in Combinatorial Optimization: Overview and Conceptual Comparison. *ACM Comput. Surv.* **2003**, *35*, 268–308. [[CrossRef](#)]
37. Mirjalili, S.; Lewis, A. The Whale Optimization Algorithm. *Adv. Eng. Softw.* **2016**, *95*, 51–67. [[CrossRef](#)]

38. Maier, H.R.; Razavi, S.; Kapelan, Z.; Matott, L.S.; Kasprzyk, J.; Tolson, B.A. Introductory overview: Optimization using evolutionary algorithms and other metaheuristics. *Environ. Model. Softw.* **2019**, *114*, 195–213. [[CrossRef](#)]
39. Das, S.; Suganthan, P.N. Differential evolution: A survey of the state-of-the-art. *IEEE Trans. E Comput.* **2011**, *15*, 4–31. [[CrossRef](#)]
40. Yang, X.S. *Nature-Inspired Optimization Algorithms*; Elsevier Science Publishers, B.V.: Amsterdam, The Netherlands, 2014; ISBN 9780124167452.
41. Mauder, T.; Sandera, C.; Stetina, J.; Seda, M. Optimization of the quality of continuously cast steel slabs using the firefly algorithm. *Mater. Tehnol.* **2011**, *45*, 347–350.
42. Kirkpatrick, S.; Gelatt, C.D.; Vecchi, M.P. Optimization by simulated annealing. *Science* **1983**, *220*, 671–680. [[CrossRef](#)]
43. Storn, R.; Price, K. Differential Evolution—A Simple and Efficient Heuristic for Global Optimization over Continuous Spaces. *J. Global Optim.* **1997**, *11*, 341–359. [[CrossRef](#)]
44. Kennedy, J.; Eberhart, R. Particle swarm optimization. In Proceedings of the ICNN'95—International Conference on Neural Networks, Perth, WA, Australia, 27 November–1 December 1995; pp. 1942–1948. [[CrossRef](#)]
45. Yang, X.S.; Deb, S.; Fong, S. Accelerated particle swarm optimization and support vector machine for business optimization and applications. *Commun. Comput. Inf. Sci.* **2011**, *136*, 53–66. [[CrossRef](#)]
46. Yang, X.S. Firefly algorithm, stochastic test functions and design optimization. *Int. J. Bio-Inspired Comput.* **2010**, *2*, 78–84. [[CrossRef](#)]
47. Rao, R.V.; Savsani, V.J.; Vakharia, D.P. Teaching-learning-based optimization: A novel method for constrained mechanical design optimization problems. *CAD Comput. Aided Des.* **2011**, *43*, 303–315. [[CrossRef](#)]
48. Rao, R.V.; Patel, V. Multi-objective optimization of heat exchangers using a modified teaching-learning-based optimization algorithm. *Appl. Math. Model.* **2013**, *37*, 1147–1162. [[CrossRef](#)]



# Dry cooling as a way toward minimisation of water consumption in the steel industry: A case study for continuous steel casting

Lubomír Klimeš<sup>a,\*</sup>, Michal Březina<sup>b</sup>, Tomáš Mauder<sup>b</sup>, Pavel Charvát<sup>b</sup>,  
Jiří Jaromír Klemeš<sup>a</sup>, Josef Štětina<sup>b</sup>

<sup>a</sup> Sustainable Process Integration Laboratory – SPIL, NETME Centre, FME, Brno University of Technology, Technická 2896/2, 61669, Brno, Czech Republic

<sup>b</sup> Energy Institute, FME, Brno University of Technology, Technická 2896/2, 61669, Brno, Czech Republic

## ARTICLE INFO

### Article history:

Received 25 January 2020

Received in revised form

26 June 2020

Accepted 29 June 2020

Available online 17 July 2020

Handling Editor: Cecilia Maria Villas Bóas de Almeida

### Keywords:

Steel industry

Minimisation of water consumption

Continuous steel casting

Dry cooling

## ABSTRACT

The steel industry represents a chain of technological processes, which consume a vast amount of energy and water, and produce a large quantity of emissions. A number of restrictions and regulations have therefore been recently imposed on the steel industry and involved processes aiming at the improvement of the use of resources, reduction of footprint in the natural environment as well as at the enhancement of overall efficiency of the steel production. In contrast to other research papers, the paper focuses on water use in a particular steelmaking process - continuous steel casting, which is used to cast more than 95% of the worldwide steel production. Approaches allowing the minimisation of water consumption are first identified and analysed. Spray cooling using once-through water and its substitution with dry cooling coupled with internally-cooled rollers by means of closed-loop water is computationally investigated. A 3D heat transfer and solidification model for continuous steel casting, which was validated with data from an actual steel plant, was used for this purpose. The results indicate that partial substitution of water spray cooling with dry cooling can provide a 48% lower once-through water use, which represents approximately a 1.5 m<sup>3</sup>/min reduction in water consumption. The annual potential for water savings at a steel plant operating three casters at 24/7 is about 2.4 Mm<sup>3</sup>.

© 2020 Elsevier Ltd. All rights reserved.

## 1. Introduction

In recent years, there is a considerable effort of the society toward reduction of energy and water consumption, minimisation of emissions and greenhouse gases production (especially CO<sub>2</sub>, SO<sub>2</sub>, NO<sub>x</sub>, and CH<sub>4</sub>), and the use of renewable energy resources. Water and its sustainable development are particularly of very high importance since water, and its resources have key importance for the society, as emphasised in the sixth goal of the Sustainable Development Goals (SDG 6) (Sustainable Development Goal 6, 2019). Due to these reasons, economic restrictions and environmental regulations and penalties such as a carbon tax (He et al., 2018) have been applied to various engineering processes and industrial technologies, which have adverse effects on the above-mentioned objectives. Retrofitting and other improvements of such technologies represent a possible solution for how to

accomplish the imposed requirements (Gharaie et al., 2015).

### 1.1. Production, emissions, energy and other resources in steelmaking

Starting at the iron age and lasting up to these days, steel is a crucial material with beneficial properties, which has a wide range and multidisciplinary use, ranging from the building constructions to transportation and to machinery. Considering the 1960s as the reference state for the assessment of the situation today, the energy efficiency of steelmaking was improved significantly and the energy consumption per 1 t of steel was reduced by 61% (World Steel in Figures, 2019). Due to the responsible management of natural resources, more than 96% of raw materials were converted into steel products in 2017, meaning the production of very little waste. However, despite the recent technological development, steelmaking and steel industry still represent a significant source of emissions as well as solid particles, particulate matter and dust, which are emitted to the atmosphere and natural environment (Zhou and Yang, 2016). World Steel Association reported that in

\* Corresponding author.

E-mail address: [klimes@fme.vutbr.cz](mailto:klimes@fme.vutbr.cz) (L. Klimeš).

2017, about 1.83 t of CO<sub>2</sub>/t of steel was produced (World Steel in Figures, 2019), which means about 4% reduction with respect to the previous year 2016 (World Steel in Figures, 2018). World Steel Association also reported that about 13% and 6% in 2016 and 2017 of the annual revenue of the steel industry were invested in research, innovation and improvement of steelmaking technologies and used in capital investment projects. An et al. (2018) assessed possibilities for the minimisation of energy consumption and production of CO<sub>2</sub> emissions in the steel industry in China, which is becoming a very dominant producer of steel. The authors claimed that there is a great potential for reducing the production of CO<sub>2</sub> emissions of about 800 Mt CO<sub>2</sub> in the period 2015–2030.

The actual trend of the world steel production and steelmaking from the long-term view is constantly increasing: by 3.6%/y on average for the period 2015–2019 (World Steel in Figures, 2020). In the view of the ten-year period 2009–2019, the world crude steel production increased from about 1.239 Gt/y in 2009 to about 1.869 Gt/y in 2019, which makes a 50.8% increase per decade. As for the geographical distribution of steelmaking in the same period 2009–2019, Fig. 1 indicates that China is the dominant producer of steel, which increased its share on the production of finished steel products from almost 48% in 2009 to more than 51% in 2019, causing water resource problems (Tong et al., 2019). A lower increase was experienced in India (0.7%), CIS (0.1%), and NAFTA (0.3%). On the other hand, the production of finished steel products in Japan experienced a decrease of 1% and the EU of 1.5%.

The technological chain of processes involved in steelmaking is very demanding in terms of both energy and water. According to the World Steel Association, the energy consumption related to steel production was about 20 GJ/t in 2017 (World Steel in Figures, 2019). The most demanding processes of steelmaking in terms of energy involve the blast furnace operation (10–13 GJ/t of crude steel), sintering (2–3 GJ/t of crude steel), steel rolling (1.5–3 GJ/t of crude steel), and coke making (0.75–2 GJ/t of crude steel) (He and Wang, 2017). As for the water consumption, (Gao et al., 2016), who introduced the concept of the water carrier and water value considering various levels of the water quality, reported that the amount of water consumed in the steelmaking process determined by means of the water value analysis is about 129 m<sup>3</sup>/t of final steel products. The most water-demanding processes in the chain of steelmaking processes are rolling (about 44 m<sup>3</sup>/t), coking (32 m<sup>3</sup>/t), ironmaking (20 m<sup>3</sup>/t), and casting (13 m<sup>3</sup>/t).

As for steel casting, more than 95% of the total world steel production is cast by means of the continuous steel casting method (Thomas, 2018). In this method demonstrated in Fig. 2, the melted steel from a furnace is transformed into solid semi-finished products, so-called steel strands, by means of gradual cooling in the caster. The cooling process of the strand and its solidification are carried out in a controlled way, as mechanical and material

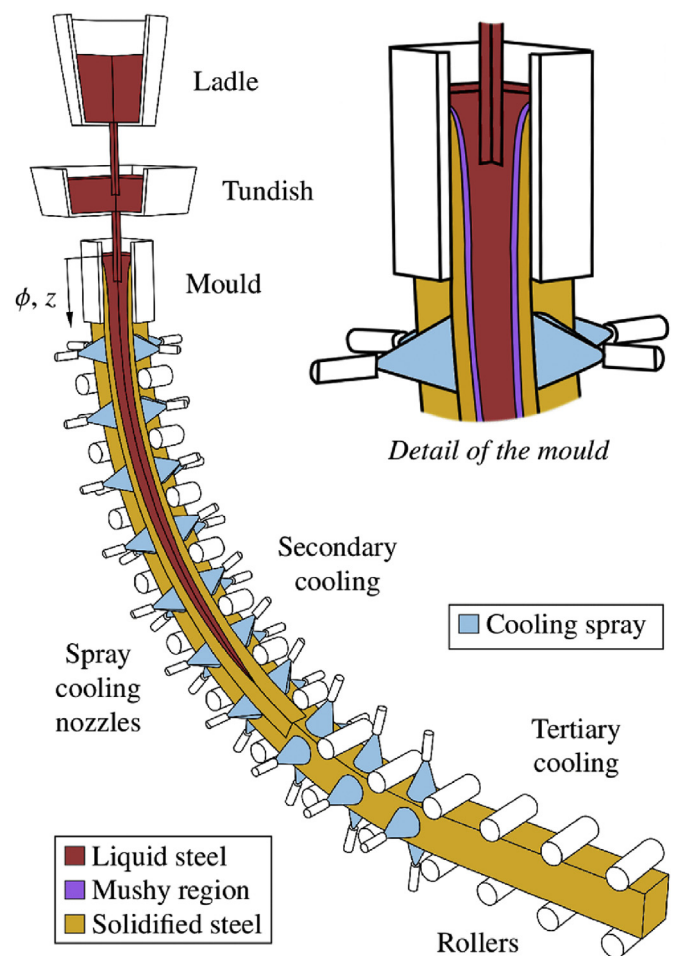


Fig. 2. Schematic of continuous steel casting. Adopted from (Klimeš; Štětina, 2015).

properties, the occurrence of defects, and the overall quality of final steel products are substantially dependent on the cooling pattern applied to the strand. The cooling of the strand is accomplished by four main mechanisms shown in Fig. 2:

- The heat withdrawal in the water-cooled mould where the solidification is initialised and the solid shell on the strand surface is created.
- Spray cooling by means of water or air-mist spray nozzles in the secondary cooling section.

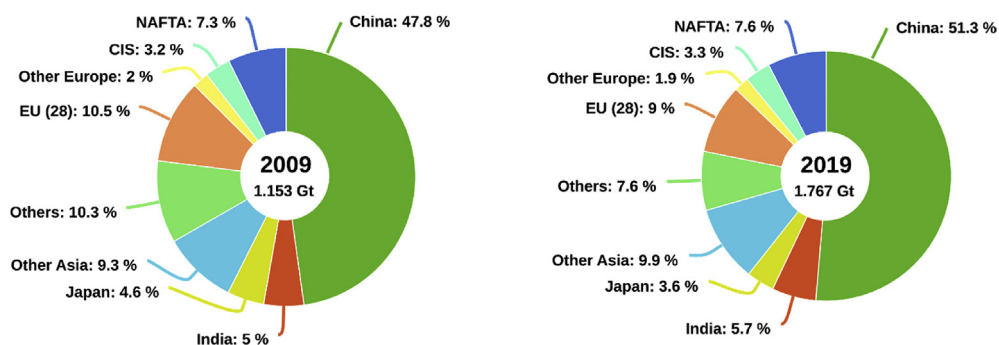


Fig. 1. Geographical distribution of the finished steel products in 2009 and 2019. Data adopted from (World Steel in Figures, 2020).



- (iii) Thermal radiation from the surface of the strand to the ambient environment.
- (iv) Heat withdrawal from the strand due to the contact of the strand with rollers.

As for water consumption, water as a cooling medium is used in the mould and in water spray cooling. In contrast to the mould operating with water in the closed-loop, nozzles operate with water in the open-loop and generate water spray impinging the surface of the strand. When water droplets of the spray hit the surface having a high temperature, their temperature quickly raises, and they eventually evaporate; thereby causing the heat withdrawal from the strand. An important implication of this process is that water used in spray cooling is mostly neither conserved nor recovered for its re-use. That is the reason why steelmaking plants are often located near a natural water source, such as rivers or lakes.

The energy and water consumption of spray cooling in continuous steel casting can be quantified as follows. For simplicity, the production of steel from the scrap can be considered as an example. First, the scrap is melted, typically in an electric furnace, from the room temperature to a temperature, which is slightly higher than the melting temperature. A typical steel grade is completely melted at about 1550 °C, and heated to about 1600 °C for casting. For this process, about 1.25 GJ/t of heat is required, assuming the enthalpy difference of 1250 kJ/kg between the room temperature and the temperature of 1600 °C. This makes approximately 365 kWh/t (1.3 GJ/t) of electricity converted to heat with the conversion efficiency of 95%. The melted steel is, after necessary metallurgical treatment, cast by means of continuous casting. The produced semi-finished steel products, so-called slabs, billets, or blooms having specific dimensions and cross-section, leave the caster at the temperature of about 800–900 °C (Guan et al., 2019). This means that the solidification of steel and its cooling from 1600 °C to 800 °C require the heat withdrawal of about 750 MJ/t. About 60% of this amount of heat is withdrawn by means of spray cooling using once-through water, while the remaining portion of heat is transferred from the mould operating with water in the closed-loop, and due to free convection and thermal radiation to the ambient environment. This consideration makes about 450 MJ/t of heat, which need to be withdrawn from the steel strand by means of spray cooling. Since about 2.6 MJ/kg of heat is needed to raise the water temperature from 10 °C to its boiling point and evaporate it at the barometric pressure, at least approximately 175 L/t of water is consumed for spray cooling in continuous steel casting. Considering about 1.8 Gt of steel produced by continuous casting in 2019, almost 315 Mm<sup>3</sup> of water were used in the steel industry, just for secondary cooling in continuous steel casting. When water demands in the entire steel industry are taken into account, the requirements for water use are even much higher (Gao et al., 2016).

### 1.2. Research gap and the aim of the paper

The above-presented estimation of the water consumption indicates that any improvement of cooling technology leading to the reduction of water consumption has a potential to spare a tremendous amount of water from the natural environment and to minimise the water footprint. The analysis of the state-of-the-art and published research works, which is in detail presented and discussed in the following section, indicates that many papers have recently focused on the assessment of the water and energy treatment and conservation in industrial processes, including steelmaking and ironmaking. However, many of them identify issues and discuss the potential for savings and improvement from a “zoom-out” level of the whole system of processes (steelmaking),

rather than providing a “zoom-in” insight into a particular process (e.g. casting or rolling) and investigation of technical solutions for achieving those aims. The aim and novelty of the present paper can be seen in filling such a knowledge gap. First, a brief literature review is carried out to provide an overall assessment of water consumption in the steel industry and to identify approaches, which could be used for the minimisation of water consumption in a particular process involved - continuous steel casting. In this respect, a previous study of the authors (Klimeš et al., 2019) is used as a basis, and it is further extended to quantify the potential for water savings. Second, a simulation case study employing a dry cooling approach, initially studied by the authors in Brežina et al. (2018), is presented, analysed, and compared to the conventional spray cooling from the water management and consumption viewpoint. The results and comparison indicate that dry cooling integrated into continuous steel casting is a perspective and viable approach in terms of the reduction of water consumption in the steel industry.

### 1.3. Applied method and procedure

The case study presented in the paper focuses on the computational investigation and assessment of dry cooling as an alternative to water spray cooling used for heat withdrawal in continuous steel casting. The idea of dry cooling is based on the use of internally water-cooled rollers, which can operate with a closed-loop water system meaning that water is conserved and re-used. On the contrary, water spray cooling nozzles, which represent a conventional and currently dominant way of heat rejection from the secondary cooling zone in continuous steel casting, use the once-through water. The once-through water in this context means that the water is not re-used as it is atomised in the nozzle into small droplets, which heat up and evaporate when hit the hot surface of the steel strand. The applicability and feasibility of dry cooling, when compared to spray cooling, is assessed in the presented case study by means of an original computer model for continuous steel casting. The model was previously developed and validated by the authors of the present paper, and it has been applied in casting control and optimisation at steelworks.

## 2. A brief overview of the assessment of water consumption in the steel industry

Many research works focusing on an overall analysis of processes involved in the complete chain of steel industry have been recently published. The studies aimed at the identification, assessment and optimisation of processes, in which water is used. Wang et al. (2017) reported a study into the water-energy-emission nexus (WEEN) in the steel industry in China. Flow analysis of material and energy was adopted for the identification of water, energy, and emission flows within the main processes of the steel industry. The authors analysed data for 2015 by means of the industrial-level WEEN model of a Chinese steel plant, and they claimed that approximately 6 m<sup>3</sup>/t of water and 300 kWh/t of electricity were consumed in terms of the WEEN for the production of crude steel. From the overall point of view, these figures account for 66% and 7% of the water and electricity consumption in the steel industry. It has been further reported that approximately 71% of the water consumption was for cooling, while the remaining portion was mainly utilised for the removal of pollutants. Tong et al. (2019) utilised a flow analysis of the material, energy, and water for the evaluation of the water use and discharge. A case study of life cycle water for a steel plant in China was presented, and the authors concluded that the total life cycle water withdrawal, water consumption, and the water discharge were 14.9 m<sup>3</sup>/t, 5.9 m<sup>3</sup>/t, and

9.2 m<sup>3</sup>/t. The steelmaking process and cold rolling were identified as having the largest and smallest share on the above figures.

Gao et al. (2011) analysed the water consumption in the steel industry and the water quantity, as well as the water quality, were considered in their analyses. A model of water-consuming processes was created, and flow analysis was applied. A case study for a steel plant in China was used to demonstrate differences between the actual state and its optimised parameters. The authors claimed that the optimised state could enable an 11% and 95% reduction of the freshwater consumption and the wastewater discharge. In another work by Gao et al. (2016), the water quality index was applied for the evaluation of the consumption of water having different quality, and for the equivalent conversion of consumed water in terms of the freshwater. A case study for a steel plant in China was carried out, and the authors reported that the consumption of the freshwater equivalent was approximately 195 m<sup>3</sup>/t when only the water quantity was considered, while it was about 130 m<sup>3</sup>/t when the water quality was taken into account. The results obtained with the water value analysis demonstrated that about 17 m<sup>3</sup> of water of various levels are utilised for casting. Gao et al. (2020) recently developed a prediction model for the analysis of the energy and water savings in the steel industry in China. Five scenarios and thirty technologies were analysed, from which 21 were focused on the reduction of energy consumption, while 9 accounted for water-related savings. The authors reported that in 2025 the energy and water consumption could decrease to 15–15.6 GJ/t and 54.1–58.8 m<sup>3</sup>/t.

Gu et al. (2016) reviewed and analysed relations between water and energy consumption and conservation in the Chinese industry. They underlined that even though water and energy are strongly related to each other, water policies and regulations are often established without taking into account the energy consumption. A methodology based on the energy-water evaluation utilising an input-output model was introduced. The authors proposed relationship indexes, which were used for the description of energy-water nexus and for the identification of water savings. Wang et al. (2017) carried out an assessment of water-energy nexus in the steel industry in China. A hybrid model was created with the aim to estimate the overall water impacts of energy conservation, and a case study for the steel and iron industry in China was solved. Considerable potential for water conservation was identified in the retrofitting and replacement of blast oxygen furnaces with modern electric furnaces. The authors claimed that such replacement could enable a 10–16% reduction in water consumption.

A life cycle water footprint analysis (Jia et al., 2019), taking into consideration grey and blue water was presented by Ma et al. (2018) as a case study for China. The analysis indicated that the grey water footprint is considerably higher than that of blue water. The authors claimed that an important way of allowing for the reduction of water consumption is the optimisation of indirect processes. Zhang et al. (2018) investigated the optimisation of the multi-scale water network in the steel industry. They created a mixed-integer nonlinear optimisation model adopting an inter- and intra-plant integration. The model was used in a study, in which three different scales were considered, including the unit-scale, plant-scale, and the park-scale. The authors presented an industrial example demonstrating the practicability and efficiency of their approach. The results indicated that the freshwater consumption and the total cost of the water network could be both reduced by 21–22% when the indirect integration strategy is considered.

Conejo et al. (2019) presented a review of current environmental challenges in the steel industry and its value chain. The progress in the minimisation of energy and water consumption and in the production of CO<sub>2</sub> emissions was reviewed. As for the

continuous steel casting, the authors emphasised that the use of the near-net-shape casting of thin semi-finished products can mitigate the energy consumption by about 80% when compared to conventional continuous steel casting as many downstream processes, including reheating and hot rolling, are no longer needed. Moreover, it was reported that about 82% of the water consumption in the steelmaking processes is used only for once-through cooling (Suvio et al., 2012). Colla et al. (2016) reported on the water re-use and water management at steel plants by means of the salt elimination. Two different systems employing water were studied: cooling of hot steel strips and cleaning of blast furnace gases. The authors emphasised that in both cases high concentrations of salts in water, including chlorides, carbonates, and fluorides, can cause serious problems such as the degradation of the steel quality and corrosion of facilities at the steel plant. In this respect, the use of reverse osmosis and ultrafiltration for the water desalination was investigated. The results demonstrated that most salts can be removed by the reverse osmosis, allowing the reduction of freshwater consumption. In the follow-up study of the authors, Colla et al. (2017), the simulation and modelling approach was utilised for the investigation of a process integration solution, aiming at the improvement of the water efficiency. The results demonstrated that in some cases the wastewater produced in a process can be utilised in another process without additional treatment, while in other cases the salt elimination is needed. Sun et al. (2019) reported an analysis of the environmental impacts of the wastewater discharged from steel plants. The authors proposed a total environmental impact score (TEIS), which was used as a measure for the assessment of the wastewater discharge in terms of both water quality and quantity. The authors reported that the steelmaking process contributed 76% to the overall value of the TEIS for the considered plant. As for pollutants, total nitrogen was identified as the most-significantly contributing pollutant to the TEIS.

### 2.1. Implications from the overview

The presented overview of research works indicates that there exist opportunities for the minimisation of energy and water consumption in the steel industry. However, rather than investigating a specific process, most studies analyse the chain of processes involved in the steel industry at a steel plant level and from a system viewpoint. This makes it possible to assess the overall water and energy utilisation and to identify the most demanding processes. In many cases, however, this provides no sufficient detail for a particular improvement or modification of such processes, which would allow the reduction of water and energy consumption. Three particular approaches for the minimisation of water consumption in continuous steel casting have been identified, and their applicability assessed.

## 3. Techniques for the reduction of water consumption in continuous steel casting

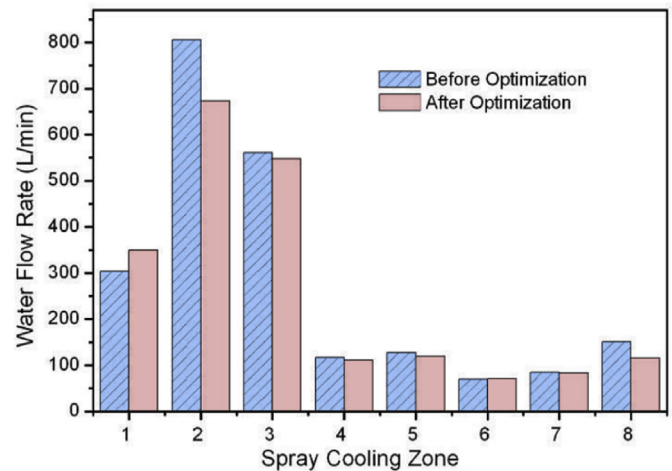
As mentioned in Section 1, water in continuous steel casting is used for cooling and heat withdrawal of the steel strand, which is transformed from the melted steel into solid semi-finished products. Since the mould (see Fig. 2) operates with the water-closed loop, the re-use of water is preserved. On the other hand, the secondary cooling zone utilising water spray cooling nozzles with the once-through water represents a much more interesting opportunity in terms of the minimisation and efficient use of water. It is worth recalling from the introduction that in the secondary cooling zone, about 60% of heat is withdrawn by means of water spray cooling. This share of the heat withdrawal corresponds to the water consumption of about 175 L/t of steel, representing a baseline for

identification and assessment of methods applicable for the minimisation of the water consumption. In the rest of this section, such three promising techniques are discussed and analysed.

### 3.1. Optimisation of water spray cooling system

The optimisation of continuous steel casting represents a wide range of topics, which have been investigated by many researchers. [Rahal et al. \(2020\)](#) studied the use of robust adaptive optimisation for proactive and reactive scheduling of continuous steel casting. The developed model was applied to scheduling under uncertainty, and the authors reported that the results possessed better robustness when compared to a conventional deterministic approach. [Yu et al. \(2019\)](#) utilised dynamic optimisation coupled with a three-dimensional heat transfer model for optimisation of the water quantity used for cooling in continuous steel casting. The authors emphasised that improper cooling during dynamic changes, e.g. due to the fluctuating casting speed, can lead to quality issues of the cast steel. The main objective of optimisation was to determine the flow rates through the cooling nozzles, which minimised the differences between the actual and set-point surface temperatures of the cast steel strand. The results demonstrated the applicability of the proposed control approach, which provided a stable temperature distribution. [Wang et al. \(2019\)](#) presented a model predictive control system for spray cooling in continuous steel casting. A heat transfer model was developed and coupled with particle swarm optimisation, and similarly, as in [Yu et al. \(2019\)](#) the water flow rates through cooling nozzles were optimised in order to minimise the surface temperature fluctuations (deviations) from the set-point values. The results showed good control capability and applicability of the adopted approach for industrial use. [Feng et al. \(2014\)](#) adopted structural optimisation based on heat loss rate for the optimisation of solidification in continuous steel casting. A complex objective function for optimisation was considered, including the surface temperature gradients, shell thickness, and the length of the liquid core. The authors reported that for a specified total water flow rate, the model allowed the determination of optimal water distribution in the secondary cooling zone. They also emphasised that the total water flow rate needs to be reasonably balanced between heat withdrawal and steel quality. [Wang et al. \(2013\)](#) created a coupled optimisation and heat transfer model for continuous steel casting. The model was used to determine water flow rates in the secondary cooling zone, which minimised the water consumption and kept the surface temperature distribution within the specified range of temperature set-points. The results shown in [Fig. 3](#) indicated that the optimised setup of spray cooling allowed for approximately 10% reduction of water consumption.

It can be concluded that the above-mentioned research works were mainly aimed at the optimisation of the water use and its distribution in the secondary cooling zone in terms of steel quality rather than water consumption and its minimisation. In case the water consumption is taken into account, the dependence of the cooling intensity on the water flow rate through the cooling nozzles has to be considered. The cooling performance of the nozzle is particularly characterised by the heat transfer coefficient, which quantifies the intensity of heat transfer according to Newton's law of cooling. [Wendelstorf et al. \(2008\)](#) analysed heat transfer characteristics in water spray cooling of surfaces having high temperatures. The behaviour of the heat transfer coefficient in the wide range of the surface temperatures as well as the water flow rates was experimentally investigated. A full-cone water nozzle was used in the experiments. If the surface temperature is high enough, the Leidenfrost effect occurs, a vapour layer develops on the surface, preventing water droplets from hitting (getting in contact with) the



**Fig. 3.** Optimisation of the water consumption in the secondary cooling zone: the comparison of water flow rates before and after optimisation. Adapted from [Wang et al. \(2013\)](#).

cooled surface. In such a steady film boiling regime, the heat transfer performance of the nozzle is mainly dependent on the water flow density. Once the surface temperature drops to (or below) the Leidenfrost temperature, the surface temperature becomes a parameter significantly influencing the increasing value of the heat transfer coefficient. The authors carried out a set of experiments, which were processed into a correlation between the heat transfer coefficient, surface temperature, and the water flow density of the spray. The proposed empirical formula was compared with results collected from other research works, and good agreement was observed, as shown in [Fig. 4](#). The evaluated correlation in [Fig. 4](#) demonstrates the dependence of the heat transfer coefficient on the water flow density for the temperature difference of 700 °C between the surface and the water temperatures, meaning the stable film boiling regime.

Besides the quantification of spray cooling heat transfer, [Fig. 4](#) also gives the information on the relationship between the cooling performance and water use efficiency, and thus a potential for the reduction of the water consumption. As can be seen from the correlation shown in [Fig. 4](#) (solid line), the heat transfer coefficient increases with the increasing water flow density. However, the gradient of the increase is not constant. First, the slope is increasing when the flow rate is low. At the water flow density of about 9 kg/m<sup>2</sup>s (inflexion point of the curve), it reaches its maximum and then it starts to decline. In the range of the water flux density between about 5 kg/m<sup>2</sup>s and 12 kg/m<sup>2</sup>s (denoted in [Fig. 4](#) with the green and blue point), the slope of the curve is virtually constant and equal to the maximum value reached at the inflexion point. However, for the water flow density higher than 12 kg/m<sup>2</sup>s, the slope of the curve decreases. Similar conclusions were reported in other research works, e.g. in [Pyszko et al. \(2013\)](#). This means that the increase of the water flow density over 12 kg/m<sup>2</sup>s becomes less efficient in terms of the ratio between the enhancement of the heat transfer coefficient and water consumption. Considering equivalent heat withdrawal, it would be more efficient to replace a single nozzle spraying the surface area  $S$  and operating with the heat transfer coefficient of 3000 W/m<sup>2</sup>K at a high water flux density of about 27 kg/m<sup>2</sup>s (indicated by the orange square in [Fig. 4](#)) by two nozzles spraying the surface area  $2S$  and operating with the 50% value of the heat transfer coefficient at a moderate water flux density of about 11 kg/m<sup>2</sup>s (indicated by the cyan square in [Fig. 4](#)). In such an arrangement, the two nozzles would use 22 kg/m<sup>2</sup>s, which is

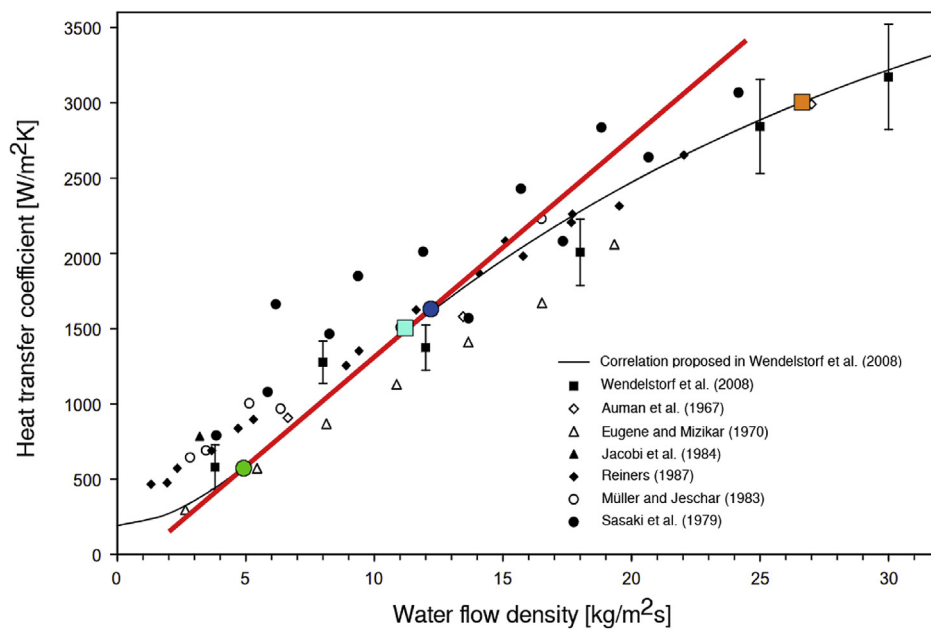


Fig. 4. Characterisation of the cooling intensity of water spray: the dependence of the heat transfer coefficient on the water flow density. The plot shows the case with the temperature difference of 700 °C between the surface and water temperatures. Adapted from Wendelstorf et al., (2008); see this reference for sources listed in the legend.

almost a 19% reduction of water consumption when compared to the single nozzle using 27 kg/m<sup>2</sup>s. It is also worth to emphasise that the ratio between the heat transfer coefficient and the water flux density represents the amount of heat, which can be withdrawn per 1 kg of water and the temperature difference of 1 K. Obviously, the higher the ratio, the higher the efficiency of the heat withdrawal. In particular, this ratio is approximately 111 J/kg·K for a nozzle operating at 3000 W/m<sup>2</sup>K and 27 kg/m<sup>2</sup>s, while it is about 136 J/kg·K for a nozzle operating at 1500 W/m<sup>2</sup>K and 11 kg/m<sup>2</sup>s.

### 3.2. Intensification of water spray cooling by nano additives

Another approach applicable to the enhancement of spray cooling and the increase of the heat transfer coefficient is the use of additives mixed with the coolant. Recently, this approach was extensively studied in relation to nano additives. Suitable nanoparticles are mixed with water before entering the cooling nozzle, and the mixture is referred to as nanofluid. Chakraborty et al. (2018) reported a study into the application of the Cu–Al nanofluid for spray cooling of hot steel plates. The authors prepared several nanofluids with various molar ratios of Cu and Al, and the effect of the Cu–Al ratio of the heat transfer performance was investigated for spray cooling of a steel plate having the thickness of 6 mm and the temperature 600–900 °C. The authors reported that the highest cooling rate was achieved for the Cu–Al ratio of 4:1 and the concentration of 160 ppm, which was 26% higher when compared to conventional water spray cooling. The average heat flux and average heat transfer coefficient in the temperature range 600–900 °C were about 17% and 15% higher when compared to spray cooling with pure water. Later, Chakraborty et al. (2019) studied the effect of surfactants on the cooling performance of Cu–Zn–Al nanofluid. The highest cooling rate was observed for the Cu–Zn–Al nanofluid with a concentration of 600 ppm, which was about 31% higher than in case of pure water.

Al<sub>2</sub>O<sub>3</sub> and TiO<sub>2</sub> nanofluids in the concentration range between 0.01% and 0.07% for cooling of the hot steel plate were investigated by Nayak et al. (2016). It was reported that the addition of nanoparticles increased the heat transfer coefficient reaching its

maximum for a certain concentration. The authors claimed that the Al<sub>2</sub>O<sub>3</sub> nanofluid outperformed the TiO<sub>2</sub> nanofluid in terms of the heat withdrawal performance. The use of the Al<sub>2</sub>O<sub>3</sub> nanofluid caused, under specific configuration, almost double the value of the heat transfer coefficient when compared with pure water. Ravikumar et al. (2015) studied the influence of surfactants in the Al<sub>2</sub>O<sub>3</sub> nanofluid, and they reported that in the case of the Al<sub>2</sub>O<sub>3</sub>-water-Tween 20 mixture, the cooling rate increased by about 33% when compared with pure water. Paul et al. (2020) investigated the Leidenfrost effect for the TiO<sub>2</sub> nanofluid. The authors reported that under specific conditions the Leidenfrost temperature significantly increased for adequately loaded droplets of the nanofluid, and such a rise of the Leidenfrost temperature was explained by the formation of a porous nano-based layer formed from nanofluid, which significantly reduced the lifetime of the droplets. Hsieh et al. (2016) analysed the influence of seven different nanofluids on the enhancement of heat withdrawal. They reported that nanofluids could significantly increase the heat transfer coefficient up to 70% in nucleate boiling, and the Al<sub>2</sub>O<sub>3</sub> nanofluid with a concentration of 0.1% outperformed other considered nanofluids. Ganvir et al. (2017) thoroughly reviewed the heat transfer characteristics of nanofluids and their applications. It was concluded from the overview that nanoparticles allow for the considerable increase in the thermal conductivity when compared with pure water. Up to a 40% and almost 70% enhancement was reported for the Al<sub>2</sub>O<sub>3</sub> and Ag nanofluids.

It seems from the above-mentioned achievements of nanofluids applied in spray cooling that their use is a promising way toward the minimisation of the water consumption in continuous steel casting and steel industry. However, there are also other viewpoints, besides the heat transfer performance, which need to be considered. One of them is the economic assessment and viability. The price of nanoparticles for end-customers has a relatively wide range, depending on the chemical characterisation, purity, size of particles, and other parameters. For example, according to Nanopowders (2020), the price of the single-element oxide Al<sub>2</sub>O<sub>3</sub> nanofluid is 150–500 USD/kg. Considering the nanofluid with a 0.01% concentration of nanoparticles, this makes 15–50 USD/m<sup>3</sup> of

cooling water. Even though the wholesale price of nanofluids could be lower, the additional cost related to the use of nanofluid would be still not negligible. Another open issue is the influence of nanoparticles on the steel surface quality, structure, and mechanical properties. A separate, but an important, issue of the application of nanoparticles for steel cooling is the potential health risk associated with nanoparticles (Warheit et al., 2008).

### 3.3. Dry and fog cooling

Another approach for the reduction of the water consumption in continuous steel casting is the replacement of cooling systems utilising once-through water for spray cooling with a technology employing water in closed-loops, such as in dry and fog cooling. The schematic of dry cooling is shown in Fig. 5. Dry cooling utilises internally-cooled rollers, which provide heat withdrawal due to the direct contact between the rollers and the cooled surface. Besides the dominant heat conduction, heat is also transferred from the surface to the ambient environment by means of thermal radiation and natural convection. Heat transferred to the rollers is mostly rejected to water flowing through the rollers and providing their internal cooling, but some heat is also rejected from the rollers to the ambient environment by means of natural convection and thermal radiation. Since water used for internal cooling of the rollers can circulate in a closed-loop system coupled with a storage tank, this cooling technology is particularly promising in terms of the sustainable water utilisation. In conventional continuous steel casting, about 60% of heat transfer from the steel strand is achieved by the water spray cooling. In dry cooling, there is no spray cooling, which can lead to the high thermal load of the caster and its components. In some cases of dry cooling, a mild spray cooling with low water use is applied to protect the casting facility. Since a low water spray rate is applied, water rapidly evaporates and provides so-called fog cooling.

Javurek et al. (2015) presented various heat transfer models for the prediction of the roller and strand temperatures in dry cooling. The models involved phenomena related to the direct contact between the roller and the surface, heat transfer between the roller and internally-flowing water as well as thermal radiation between the roller and the surface. The models had various dimensionality (OD to 3D) and complexity and were implemented in various software tools, including Abaqus and Matlab. The authors emphasised that a suitable model for real-time use in control systems of steel plants has to be accurate but also simple and computationally effective. Moreover, an appropriate balance between the thermal load of the rollers and their internal cooling

needs to be carefully addressed as these parameters directly influence the quality of cast steel as well as the lifetime of the rollers. Liu et al. (2019) computationally investigated heat transfer between the roller and the steel surface in dry cooling of continuous casting of thick slabs. A 3D model was developed in ANSYS Fluent including a specific structure of water channels inside the roller, and the model was validated with data from a steel plant. The results demonstrated that the conductive heat transfer due to direct contact between the roller and the steel surface is higher than the thermal radiation heat transfer. The authors reported that the maximum surface temperature of the roller was achieved at the place right out of the contact with the steel surface, and the descending order of the factors influencing the thermal load of the rollers is the contact angle, the surface temperature, the casting speed, and the inlet velocity of the cooling water to the rollers. In case of the surface strand temperature of 900 °C, casting speed of 0.5 m/min, the contact angle of 10°, and the inlet water velocity of 5.5 m/s, the maximum surface temperature of the roller was about 190 °C. Bolender and Cappel (2004) presented a concept of an internally-cooled roller with a helical channel for dry cooling in continuous steel casting. Influence of various factors including the strand thickness, roller diameter, strand surface temperature and the roller wall thickness was discussed. The authors emphasised that water spray cooling often leads to uneven cooling and high thermal stress, which cause the occurrence of defects and quality issues. In contrast to low carbon steel, micro-alloyed steel is especially prone to crack formation and requires a soft cooling pattern. Three cooling methods applicable for continuous steel casting were compared to each other, including water spray cooling, air-mist (water mixed with compressed air) spray cooling, and dry cooling. The authors concluded that dry cooling allowed for the highest strand surface temperature, which is beneficial in terms of the surface quality.

As the available studies indicate, dry cooling is a promising technology for the improvement of the steel quality as well as for the minimisation of water consumption in the steel industry. Even though there are some studies addressing dry cooling in terms of heat transfer and steel quality, to the best knowledge of the authors there is no study assessing dry cooling from the viewpoint of the reduction of water consumption. For this reason, a comparative simulation study by means of a validated solidification model for continuous steel casting was carried out and is presented in the following Section 4. The study aims at the analysis and comparison of the thermal behaviour as well as the water use of continuous steel casting under two scenarios: conventional water spray cooling and dry cooling.

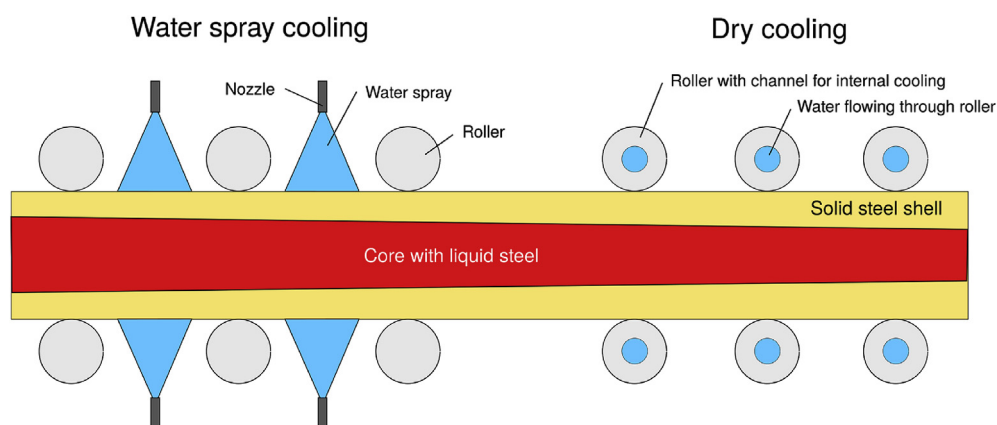


Fig. 5. Schematic of water spray and dry cooling.

#### 4. Simulation case study of continuous steel casting with spray and dry cooling

A heat transfer and solidification model for continuous steel casting (Brno Dynamic Solidification Model - BrDSM® (BrDSM, 2016)), previously developed by some of the authors of the present paper, was utilised to computationally analyse dry cooling and its use for the minimisation of water consumption. The model was validated with experimental data from steelworks, and it has already been used in casting control applications. In the following sections, a brief description of the model is provided. The reader interested in details of the model and its use is referred to previous works of the authors; Mauder et al. (2015) presented the use of the computer model for continuous steel casting for optimal control of the casting process by means of the fuzzy logic, Mauder and Štětina (2018) later reported on the high-quality steel casting for which advanced mathematical methods and models were used.

##### 4.1. Heat transfer and solidification model of continuous steel casting

The computer model determines the transient temperature distribution and the location of the solid-liquid steel interface by means of the numerical solution of the governing heat transfer and solidification equation (Mauder et al., 2015)

$$\frac{\partial H}{\partial t} + v_{\text{casting}} \frac{\partial H}{\partial z} = \nabla \cdot (k_{\text{eff}} \nabla T) \quad (1)$$

where  $H$  is the enthalpy used for phase-change modelling,  $T$  is the temperature distribution,  $t$  is time,  $z$  is the casting direction coordinate,  $v_{\text{casting}}$  is the casting speed, and  $k_{\text{eff}}$  is the effective thermal conductivity taking into consideration convective heat transfer within the liquid steel. The model utilises temperature-dependent thermophysical properties of the steel determined according to its chemical composition with the use of the IDS solidification package (Miettinen et al., 2010). The Eq. (1) is coupled with appropriate initial and boundary conditions, which make the problem mathematically complete. Since the aim of the present paper is the comparison of conventional water spray cooling with dry cooling, only boundary conditions related to these cooling methods are provided here, and the reader is referred to (Mauder et al., 2015) for complete information on initial and boundary conditions.

In case of the secondary cooling zone with water spray cooling, heat flux withdrawn from the slab is determined according to

$$-k \frac{\partial T}{\partial n} = \text{HTC}(T - T_{c,\infty}) + \sigma \varepsilon (T^4 - T_{r,\infty}^4) \quad (2)$$

where  $k$  is the thermal conductivity,  $n$  is the normal vector to the slab surface, HTC is the heat transfer coefficient,  $T_{c,\infty}$  is the counterpart temperature for convective heat transfer,  $\sigma$  is the Stefan-Boltzmann constant,  $\varepsilon$  is the emissivity, and  $T_{r,\infty}$  is the counterpart temperature for radiative heat transfer. At the location on the surface with direct spray cooling, the HTC accounts for forced convection, with the temperatures  $T_{c,\infty}$  and  $T_{r,\infty}$  equal to the water spray temperature. At other locations with no direct spray cooling, the HTC represents natural convection with the temperatures  $T_{c,\infty}$  and  $T_{r,\infty}$  equal to the ambient environment. It is worth emphasising that the value of HTC for spray cooling is 50–1000 higher than that for natural convection to the ambient air, depending on the particular configuration.

As for the roller with internally-cooled channels, with the adoption of some simplifications, the total heat withdrawal can be formulated as the sum of heat rejected to the ambient environment

by natural convection and radiation, and to water flowing through the channels inside the rollers as

$$-k \frac{\partial T}{\partial n} = \frac{f_s \pi D L}{S_{\text{con}}} \left\{ \text{HTC}_{\text{rol}} (T_{\text{rol}} - T_{\text{amb}}) + \sigma \varepsilon (T_{\text{rol}}^4 - T_{\text{amb}}^4) \right\} + \frac{Q_w \rho_w c_w \Delta T_w}{S_{\text{con}}} \quad (3)$$

where  $f_s \in (0, 1)$  is a factor characterising a portion of the roller surface, which is used for rejecting heat from the roller to the ambient (typically,  $f_s = 0.5$  representing the upper half surface of the roller (Mauder et al., 2015)),  $D$  is the diameter of the roller,  $L$  is the length of the roller,  $S_{\text{con}}$  is the contact area between the roller and the slab surface (typically, a part of the roller surface corresponding to the contact angle of 4–12° (Javurek et al., 2015)). The first and second term in the curly bracket on the right-hand side of Eq. (3) represent natural convection and thermal radiation, from the surface of the roller to the ambient environment. The last term on the right-hand side of Eq. (3) accounts for heat rejected from the roller to water flowing through the roller providing its internal cooling where  $Q_w$  is the water flow rate,  $\rho_w$  is the water density,  $c_w$  is the water heat capacity, and  $\Delta T_w$  is the water temperature difference at the inlet and outlet of the roller. In case the roller is not internally-cooled, the water flow rate  $Q_w$  through the roller is set to zero.

##### 4.2. Scenarios for the case study

In the present paper, continuous casting of an austenitic stainless steel grade S30400, often referred to as an 18/8 grade for its content of chromium and nickel of 18% and 8%, is investigated in terms of the water consumption, starting from a previous study of the authors (Brezina et al., 2018) where heat transfer characteristics were discussed. A radial slab caster, which has the casting track with the length of 26 m and casts slabs having the cross-section dimensions of 1500 × 150 mm, is considered. Such the configuration was adopted from an actual casting machine. The model of the slab casting process was created in two configurations (scenarios). The first scenario adopted a conventional water spray cooling in the secondary cooling zone, in which 316 cooling nozzles located in 16 independent cooling loops were used. Such a scenario is referred to as the WSC (Water Spray Cooling) scenario.

Another scenario employed dry cooling. Since the thermal load just below the mould (see Fig. 2) is severe and requires high cooling capacity, water spray cooling was used in the zone below the mould to enhance the heat withdrawal. The spray cooling section with the length of 3.8 m was considered, and it included 136 cooling nozzles located in 4 independent cooling loops. This section has an identical configuration as the corresponding section in the WSC scenario. The number of the cooling loops with spray cooling and their corresponding length was determined as the lowest number of the cooling loops below the mould (in order to minimise the consumption of the once-through water), which can provide sufficiently intensive cooling and smooth temperature profiles with no reheating. Simulations performed for the number of cooling loops lower than 4 indicated uneven cooling and reheating issues, which negatively affect the steel quality, and therefore they need to be avoided. In the remaining part of the caster having the length of 21.3 m, water spray cooling was replaced by means of internally-cooled rollers, which were also used in the section with spray cooling to enhance the heat withdrawal. Overall, 180 nozzles from the WSC scenario were removed and their cooling performance was replaced by 162 internally-cooled rollers of three diameters. The rollers used in the presented case study had the outer

diameters of 180 mm, 230 mm, and 300 mm and their numbers used for dry cooling were 42, 70, and 50. Such a scenario with dry cooling is referred to as the WSDC (Water Spray and Dry Cooling) scenario with semi-dry cooling. The number of the rollers and their location in the dry cooling section of the WSDC scenario were identical to the WSC scenario, but the rollers in the WSDC scenario were internally-cooled ( $Q_w > 0$  in Eq. (3)) while the conventional rollers without internal-cooling were used in the WSC scenario ( $Q_w = 0$  in Eq. (3)).

#### 4.3. Results and comparison of water use and efficiency

The steady-state behaviour of the WSC and WSDC scenarios are shown in Figs. 6–8, which represent the mean surface temperature (of the upper and lower surfaces of the strand) in the centreline of the slab and the location of solidification interfaces (so-called iso-solidus and iso-liquidus interfaces). The thermal behaviour of the WSC scenario was considered as a target and desired state, and process parameters in the WSDC scenario were optimised to provide the thermal behaviour as close as possible to the one corresponding to the WSC scenario. The computational mesh of the model consisted of about 1.2 million spatial nodes, the casting temperature and the casting speed were set to 1500 °C and 2.3 m/min. The temperature increase of the closed-loop water when flowing through the rollers was set to 7 °C, which is consistent with the temperature increase of the water flowing through the moulds in the closed loop systems (typically 6–8 °C).

As can be seen from Figs. 6–8, the WSDC scenario allowed for the temperature distribution and the solidification interfaces, which are similar to the target values reached in the WSC scenario. Even though a slightly higher surface temperature and its more pronounced fluctuations can be observed for the WSDC scenario, the use of a higher number of the internally-cooled rollers (in comparison to the WSC scenario) could increase the total contact area between the slab surface and the rollers providing reduced

surface temperature fluctuations. Table 1 and Table 2 summarise the water flow rates used for cooling in both scenarios. As can be seen from the tables, the total water flow rate of 9166 L/min was used in the WSC scenario, from which 3166 L/min (35%) is once-through water consumed for spray cooling. As for the WSDC scenario employing dry cooling, the total water use increased significantly to 34,417 L/min, which is about 3.75-fold higher value than in the WSC scenario. However, the increased consumption was due to water operating in closed-loop operation (including 26,784 L/min for dry cooling with 5% for internal cooling of roller-related facilities under excessive thermal load), and the once-through water flow rate virtually decreased to 1633 L/min, which is about a 48% reduction when compared to the WSC scenario. This implies that 95% of the total water flow rate in the WSDC scenario was utilised in closed-loop operation, allowing the water re-use, while it was only 65% in the WSC scenario. The ratio for the closed-loop water use between the WSDC and WSC scenario, was about 5.46 while the ratio for the once-through water use was 0.52, indicating the reduction of water consumption. Considering the 24/7 operation of a steel plant with the three slab casters, about 2.4 Mm<sup>3</sup> of cooling water could be annually saved in continuous steel casting when the WSDC scenario is used instead of the conventional WSC scenario.

## 5. Conclusions

The steel industry is responsible for a vast consumption of water and energy, and the current research activities aim at the improvement of the resource use efficiency. Many research studies focus on the analysis of processes involved in the steel industry and on the identification of the most demanding processes in terms of energy, water, and emissions. However, only a limited number of research works provides an insight into particular technologies and engineering solutions, which could improve the use of resources and the overall efficiency of steel production. The present paper

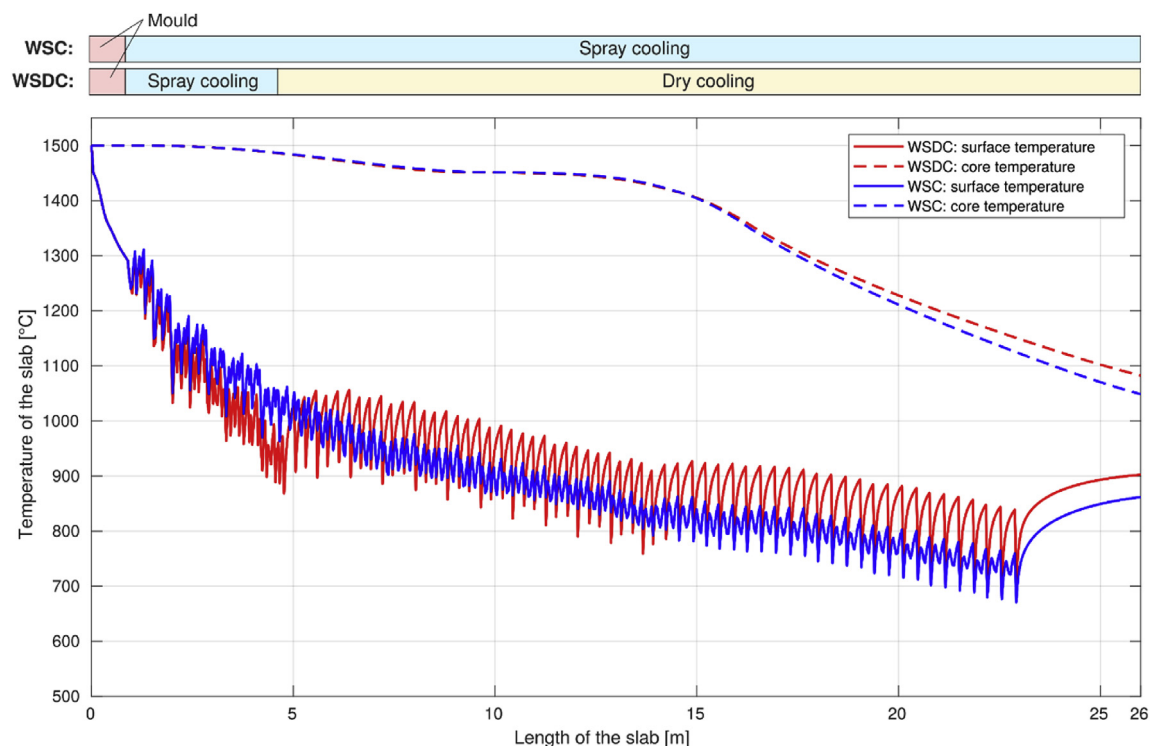


Fig. 6. The mean surface temperature at the centreline of the slab (solid lines) and the temperature distribution at the core of the slab (dashed lines).

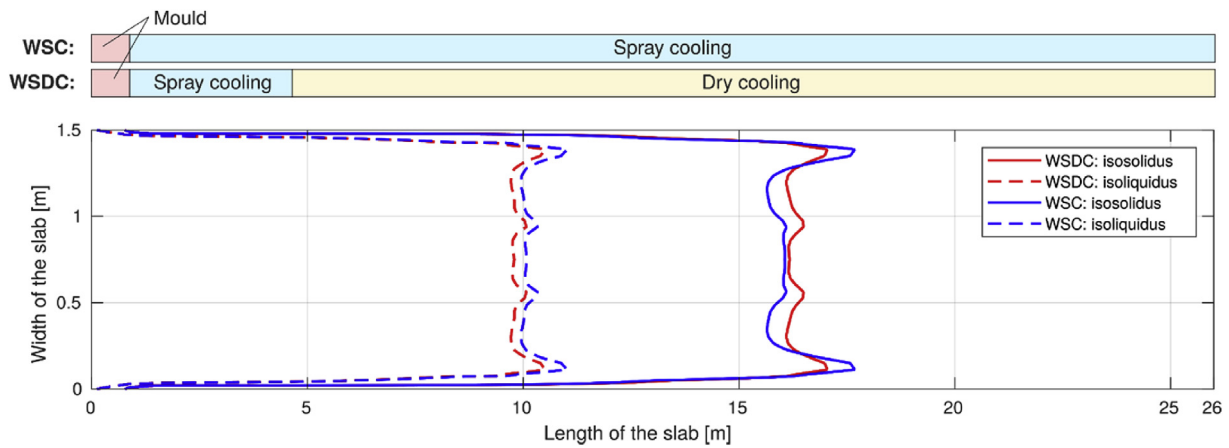


Fig. 7. Location of the solidification interfaces at the horizontal longitudinal cross-section of the slab.

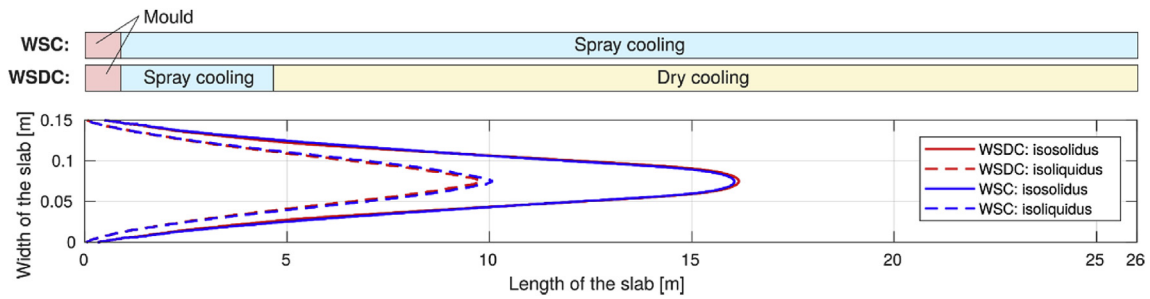


Fig. 8. Location of the solidification interfaces at the vertical longitudinal cross-section of the slab.

**Table 1**  
Comparison of water consumption in cooling systems for the WSC and WSDC scenarios.

Type of water use	Water flow rate for cooling [L/min]		
	Mould	Water spray cooling	Dry cooling
	Closed-loop	Once-through	Closed-loop
WSC scenario	6000	3166	0
WSDC scenario	6000	1633	26,784

**Table 2**  
Comparison of water consumption in terms of water re-use in the WSC and WSDC scenarios.

	Water flow rate for cooling [L/min]		
	Total	Closed-loop	Once-through
WSC scenario	9166	6000/65%	3166/35%
WSDC scenario	34,417	32,784/95%	1633/5%
WSDC-to-WSC ratio	3.75	5.46	0.52

aims at filling these knowledge gaps for one particular process in the steelmaking chain - continuous steel casting, which is currently the prevalent method for steel production. In this respect, the contribution of the present study is particularly a demonstration of the viability, feasibility and the water-saving potential of dry cooling, which allows for the minimisation of the once-through water consumption, improvement of the water conservation and decrease of the water footprint. The present study should be considered as the first step of a comprehensive analysis of water management in the steelmaking industry. In the follow-up studies,

multiple scenarios according to a particular steel-grade casting portfolio, configuration, parameters and requirements of selected steelworks need to be analysed at a higher level of details, which will provide both the particular guidelines for steelworkers as well as a more precise quantification of the water savings. The following conclusions can be drawn from the study:

- Water consumption in excess of 100 m<sup>3</sup> per 1 t of produced steel was mostly reported in the literature.
- Continuous steel casting accounts for more than 95% of the total world steel production, which reached 1.87 Gt in 2019.
- Water conservation in continuous steel casting was investigated through numerical simulations employing a 3D heat transfer and solidification model.
- Water spray cooling (WSC) and the combination of water spray and dry cooling (WSDC) were analysed for water consumption.
- The total water use in case of WSDC was 3.75-fold higher than in case of WSC; however, most of the water used in WSDC was reusable water in the closed water cooling loop.
- In terms of once-through water use, the water consumption of WSDC was 48% lower than that of WSC.
- When compared with optimised spray cooling for which about a 10% reduction of the once-through water consumption was reported, the replacement of WSC with WSDC allowed for about a 50% reduction of the once-through water.
- The annual water saving potential at a steel plant operating three casters at 24/7 is about 2.4 Mm<sup>3</sup> when using WSDC instead of WSC.
- The consumption of the once-through water in spray cooling could also be considerably reduced by nano additives mixed with the cooling water. In terms of the cooling rate, up to about a



70% enhancement was reported in the literature. However, the feasibility of such an approach seems to be economically not viable at the moment. Moreover, the influence of nano additives on the steel quality, structure and properties as well as the potential health risk associated with nano additives remain an open question.

### CRedit authorship contribution statement

**Lubomír Klimeš:** Conceptualization, Investigation, Formal analysis, Writing - original draft, Writing - review & editing. **Michal Brezina:** Software, Investigation, Visualization. **Tomáš Mauder:** Software, Visualization. **Pavel Charvát:** Conceptualization, Formal analysis, Writing - original draft, Writing - review & editing. **Jiří Jaromír Klimeš:** Supervision, Writing - review & editing, Funding acquisition, Project administration. **Josef Štětina:** Conceptualization, Supervision, Funding acquisition, Project administration.

### Declaration of competing interest

The authors declare that they have no known competing financial interests or personal relationships that could have appeared to influence the work reported in this paper.

### Acknowledgement

This paper has been supported by project No. CZ.02.1.01/0.0/0.0/15\_003/0000456 Sustainable Process Integration Laboratory – SPIL, funded by European Research Development Fund, Czech Republic Operational Programme Research, Development and Education, Priority 1: Strengthening capacity for quality research, and by the Czech Science Foundation under project No. 19-20802S A coupled real-time thermo-mechanical solidification model of steel for crack prediction.

### References

- An, R., Yu, B., Li, R., Wei, Y.-M., 2018. Potential of energy savings and CO<sub>2</sub> emission reduction in China's iron and steel industry. *Appl. Energy* 226, 862–880. <https://doi.org/10.1016/j.apenergy.2018.06.044>.
- Bolender, T., Cappel, J., 2004. Continuous casting without secondary spray water cooling. *Steel Grips* 2, 84–89.
- BrDSM, 2016. Brno Dynamic Solidification Model – BrDSM: Software for Modelling, Simulating and Control of Continuous Casting of Steel. Available at: [www.continuouscasting.info](http://www.continuouscasting.info).
- Brezina, M., Mauder, T., Štětina, J., Klimeš, L., 2018. Dry cooling simulation of continuous casting of austenitic steel slabs. In: *Proceedings of 27th International Conference on Metallurgy and Materials (METAL 2018)*, pp. 107–113.
- Chakraborty, S., Sarkar, I., Ashok, A., Sengupta, I., Pal, S.K., Chakraborty, S., 2018. Synthesis of Cu-Al LDH nanofluid and its application in spray cooling heat transfer of a hot steel plate. *Powder Technol.* 335, 285–300. <https://doi.org/10.1016/j.powtec.2018.05.004>.
- Chakraborty, S., Sengupta, I., Sarkar, I., Pal, S.K., Chakraborty, S., 2019. Effect of surfactant on thermo-physical properties and spray cooling heat transfer performance of Cu-Zn-Al LDH nanofluid. *Appl. Clay Sci.* 168, 43–55. <https://doi.org/10.1016/j.clay.2018.10.018>.
- Colla, V., Branca, T.A., Rositto, F., Lucca, C., Vivas, B.P., Delmiro, V.M., 2016. Sustainable Reverse Osmosis application for wastewater treatment in the steel industry. *J. Clean. Prod.* 130, 103–115. <https://doi.org/10.1016/j.jclepro.2015.09.025>.
- Colla, V., Matino, I., Branca, T., Fornai, B., Romaniello, L., Rositto, F., 2017. Efficient use of water resources in the steel industry. *Water* 9, 874. <https://doi.org/10.3390/w9110874>.
- Conejo, A.N., Birat, J.-P., Dutta, A., 2019. A review of the current environmental challenges of the steel industry and its value chain. *J. Environ. Manag.* 109782. <https://doi.org/10.1016/j.jenvman.2019.109782>.
- Feng, H., Chen, L., Xie, Z., Ding, Z., Sun, F., 2014. Generalized constructal optimisation for solidification heat transfer process of slab continuous casting based on heat loss rate. *Energy* 66, 991–998. <https://doi.org/10.1016/j.energy.2013.12.067>.
- Ganvir, R.B., Walke, P.V., Kriplani, V.M., 2017. Heat transfer characteristics in nanofluid—a review. *Renew. Sustain. Energy Rev.* 75, 451–460. <https://doi.org/10.1016/j.rser.2016.11.010>.
- Gao, C.-K., Na, H.-M., Song, K., Tian, F., Strawa, N., Du, T., 2020. Technologies-based potential analysis on saving energy and water of China's iron and steel industry. *Sci. Total Environ.* 699, 134225. <https://doi.org/10.1016/j.scitotenv.2019.134225>.
- Gao, C.-K., Zhang, M.-H., Wei, Y.-X., Na, H.-M., Fang, K.-J., 2016. Construction and analysis of 'water carrier' and 'water value' in the iron and steel production. *J. Clean. Prod.* 139, 540–547. <https://doi.org/10.1016/j.jclepro.2016.08.076>.
- Gao, C., Wang, D., Dong, H., Cai, J., Zhu, W., Du, T., 2011. Optimization and evaluation of steel industry's water-use system. *J. Clean. Prod.* 19, 64–69. <https://doi.org/10.1016/j.jclepro.2010.08.013>.
- Gharaie, M., Panjeshahi, M.H., Kim, J.-K., Jobson, M., Smith, R., 2015. Retrofit strategy for the site-wide mitigation of CO<sub>2</sub> emissions in the process industries. *Chem. Eng. Res. Des.* 94, 213–241. <https://doi.org/10.1016/j.cherd.2014.08.007>.
- Guan, R., Ji, C., Wu, C., Zhu, M., 2019. Numerical modelling of fluid flow and macrosegregation in a continuous casting slab with asymmetrical bulging and mechanical reduction. *Int. J. Heat Mass Tran.* 141, 503–516. <https://doi.org/10.1016/j.ijheatmasstransfer.2019.06.079>.
- Gu, A., Teng, F., Lv, Z., 2016. Exploring the nexus between water saving and energy conservation: insights from industry sector during the 12th Five-Year Plan period in China. *Renew. Sustain. Energy Rev.* 59, 28–38. <https://doi.org/10.1016/j.rser.2015.12.285>.
- He, K., Wang, L., 2017. A review of energy use and energy-efficient technologies for the iron and steel industry. *Renew. Sustain. Energy Rev.* 70, 1022–1039. <https://doi.org/10.1016/j.rser.2016.12.007>.
- He, S., Yin, J., Zhang, B., Wang, Z., 2018. How to upgrade an enterprise's low-carbon technologies under a carbon tax: the trade-off between tax and upgrade fee. *Appl. Energy* 227, 564–573. <https://doi.org/10.1016/j.apenergy.2017.07.015>.
- Hsieh, S.-S., Liu, H.-H., Yeh, Y.-F., 2016. Nanofluids spray heat transfer enhancement. *Int. J. Heat Mass Tran.* 94, 104–118. <https://doi.org/10.1016/j.ijheatmasstransfer.2015.11.061>.
- Javurek, M., Ladner, P., Watzinger, J., Wimmer, P., Shan, G., 2015. Secondary cooling: roll heat transfer during dry cooling. *Proceeding of METEC-ESTAD 2015*.
- Jia, X., Varbanov, P.S., Klimeš, J.J., Wan Alwi, S.R., 2019. Water availability footprint addressing water quality. *J. Sustain. Dev. Energy Water Environ. Syst. - JSDEWES* 7 (1), 72–86.
- Klimeš, L., Charvát, P., Bohunský, T., Klimeš, J.J., Štětina, J., 2019. Possibilities for the reduction of water consumption in steel industry and continuous steel casting: an overview. *Chem. Eng. Trans.* 76, 211–216. <https://doi.org/10.3303/CET1976036>.
- Klimeš, L., Štětina, J., 2015. A rapid GPU-based heat transfer and solidification model for dynamic computer simulations of continuous steel casting. *J. Mater. Process. Technol.* 226, 1–14. <https://doi.org/10.1016/j.jmatprotec.2015.06.016>.
- Liu, S., Ai, S., Long, M., Wu, S., Xu, P., Chen, D., Wang, Q., 2019. Numerical simulation of heat transfer between roll and slab under dry secondary cooling in ultrathick slab continuous casting. *Steel Res. Int.* 1, 1900516. <https://doi.org/10.1002/srin.201900516>.
- Mauder, T., Sandera, C., Štětina, J., 2015. Optimal control algorithm for continuous casting process by using fuzzy logic. *Steel Res. Int.* 86, 785–798. <https://doi.org/10.1002/srin.201400213>.
- Mauder, T., Štětina, J., 2018. High quality steel casting by using advanced mathematical methods. *Metals* 8, 1019. <https://doi.org/10.3390/met8121019>.
- Ma, X., Ye, L., Qi, C., Yang, D., Shen, X., Hong, J., 2018. Life cycle assessment and water footprint evaluation of crude steel production: a case study in China. *J. Environ. Manag.* 224, 10–18. <https://doi.org/10.1016/j.jenvman.2018.07.027>.
- Miettinen, J., Louhenkilpi, S., Kytönen, H., Laine, J.I.D.S., 2010. Thermodynamic–kinetic–empirical tool for modelling of solidification, microstructure and material properties. *Math. Comput. Simulat.* 80, 1536–1550. <https://doi.org/10.1016/j.matcom.2009.11.002>.
- Nanopowders, 2020. US Research Nanomaterials. Inc. <https://www.us-nano.com/nanopowders>. (Accessed 17 January 2020).
- Nayak, S.K., Mishra, P.C., Parashar, S.K.S., 2016. Enhancement of heat transfer by water–Al 2 O 3 and water–TiO 2 nanofluids jet impingement in cooling hot steel surface. *J. Exp. Nanosci.* 11, 1253–1273. <https://doi.org/10.1080/17458080.2016.1209789>.
- Paul, G., Das, P.K., Manna, I., 2020. Nanoparticle deposition from nanofluid droplets during Leidenfrost phenomenon and consequent rise in transition temperature. *Int. J. Heat Mass Tran.* 148, 119110. <https://doi.org/10.1016/j.ijheatmasstransfer.2019.119110>.
- Pyszko, R., Prihoda, M., Burda, J., Fojtik, P., Kubin, T., Vaculik, M., et al., 2013. Cooling nozzles characteristics for numerical models of continuous casting. *Metal* 52, 437–440.
- Rahal, S., Li, Z., Papageorgiou, D.J., 2020. Proactive and reactive scheduling of the steelmaking and continuous casting process through adaptive robust optimisation. *Comput. Chem. Eng.* 133, 106658. <https://doi.org/10.1016/j.compchemeng.2019.106658>.
- Ravikumar, S.V., Haldar, K., Jha, J.M., Chakraborty, S., Sarkar, I., Pal, S.K., et al., 2015. Heat transfer enhancement using air-atomised spray cooling with water–Al<sub>2</sub>O<sub>3</sub> nanofluid. *Int. J. Therm. Sci.* 96, 85–93. <https://doi.org/10.1016/j.ijthermalsci.2015.04.012>.
- Sun, W., Xu, X., Lv, Z., Mao, H., Wu, J., 2019. Environmental impact assessment of wastewater discharge with multi-pollutants from iron and steel industry. *J. Environ. Manag.* 245, 210–215. <https://doi.org/10.1016/j.jenvman.2019.05.081>.
- Sustainable Development Goal 6, 2019. SDGs Knowledge Platform. <https://sustainabledevelopment.un.org/sdg6>. (Accessed 8 January 2020).
- Suvio, P., van Hoorn, A., Szabo, M., Ekdahl, A., 2012. Water management for sustainable steel industry. *Ironmak. Steelmak.* 39, 263–269. <https://doi.org/10.1179/030192311X13135947813898>.

- Thomas, B.G., 2018. Review on modeling and simulation of continuous casting. *Steel Res. Int.* 89, 1700312. <https://doi.org/10.1002/srin.201700312>.
- Tong, Y., Cai, J., Zhang, Q., Gao, C., Wang, L., Li, P., Hu, S., Liu, C., He, Z., Yang, J., 2019. Life cycle water use and wastewater discharge of steel production based on material-energy-water flows: a case study in China. *J. Clean. Prod.* 241, 118410. <https://doi.org/10.1016/j.jclepro.2019.118410>.
- Wang, C., Wang, R., Hertwich, E., Liu, Y., 2017. A technology-based analysis of the water-energy-emission nexus of China's steel industry. *Resour. Conserv. Recycl.* 124, 116–128. <https://doi.org/10.1016/j.resconrec.2017.04.014>.
- Wang, Y., Luo, X., Zhang, F., Wang, S., 2019. GPU-based model predictive control for continuous casting spray cooling control system using particle swarm optimisation. *Contr. Eng. Pract.* 84, 349–364. <https://doi.org/10.1016/j.conengprac.2018.12.006>.
- Wang, Z., Yao, M., Zhang, X., Wang, X., 2013. Optimisation control for solidification process of secondary cooling in continuous casting steel. *Appl. Mech. Mater.* 263–266, 822–827. [10.4028/www.scientific.net/amm.263-266.822](https://doi.org/10.4028/www.scientific.net/amm.263-266.822).
- Warheit, D.B., Sayes, C.M., Reed, K.L., Swain, K.A., 2008. Health effects related to nanoparticle exposures: environmental, health and safety considerations for assessing hazards and risks. *Pharmacol. Ther.* 120, 35–42. <https://doi.org/10.1016/j.pharmthera.2008.07.001>.
- Wendelstorf, J.-H., Spitzer, K., Wendelstorf, R., 2008. Spray water cooling heat transfer at high temperatures and liquid mass fluxes. *Int. J. Heat Mass Tran.* 51, 4902–4910. <https://doi.org/10.1016/j.ijheatmasstransfer.2008.01.032>.
- World Steel in Figures, 2020. World steel association; Brussels, Belgium, 2020. Available at: [www.worldsteel.org](http://www.worldsteel.org).
- World Steel in Figures, 2019. World steel association; Brussels, Belgium, 2019. Available at: [www.worldsteel.org](http://www.worldsteel.org).
- World Steel in Figures, 2018. World steel association; Brussels, Belgium, 2018. Available at: [www.worldsteel.org](http://www.worldsteel.org).
- Yu, Y., Luo, X., Yulin, Zhang, H., Zhang, Q., 2019. Dynamic optimisation method of secondary cooling water quantity in continuous casting based on three-dimensional transient nonlinear convective heat transfer equation. *Appl. Therm. Eng.* 160, 113988. <https://doi.org/10.1016/j.applthermaleng.2019.113988>.
- Zhang, K., Zhao, Y., Cao, H., Wen, H., 2018. Multi-scale water network optimisation considering simultaneous intra- and inter-plant integration in steel industry. *J. Clean. Prod.* 176, 663–675. <https://doi.org/10.1016/j.jclepro.2017.12.158>.
- Zhou, K., Yang, S., 2016. Emission reduction of China's steel industry: progress and challenges. *Renew. Sustain. Energy Rev.* 61, 319–327. <https://doi.org/10.1016/j.rser.2016.04.009>.

## Article

# Reduction of CO<sub>2</sub> Emissions in Steelmaking by Means of Utilization of Steel Plant Waste Heat to Stabilize Seasonal Cooling Water Temperature

Tomas Mauder \* and Michal Brezina 

Faculty of Mechanical Engineering, Brno University of Technology, 616 69 Brno, Czech Republic; Michal.Brezina1@vutbr.cz

\* Correspondence: mauder@fme.vutbr.cz; Tel.: +420-541-143-244

**Abstract:** Production of overall CO<sub>2</sub> emissions has exhibited a significant reduction in almost every industry in the last decades. The steelmaking industry is still one of the most significant producers of CO<sub>2</sub> emissions worldwide. The processes and facilities used at steel plants, such as the blast furnace and the electric arc furnace, generate a large amount of waste heat, which can be recovered and meaningfully used. Another way to reduce CO<sub>2</sub> emissions is to reduce the number of low-quality steel products which, due to poor final quality, need to be scrapped. Steel product quality is strongly dependent on the continuous casting process where the molten steel is converted into solid semifinished products such as slabs, blooms, or billets. It was observed that the crack formation can be affected by the water cooling temperature used for spray cooling which varies during the year. Therefore, a proper determination of the cooling water temperature can prevent the occurrence of steel defects. The main idea is based on the utilization of the waste heat inside the steel plant for preheating the cooling water used for spray cooling in the Continuous Casting (CC) process in terms of water temperature stabilization. This approach can improve the quality of steel and contribute to the reduction of greenhouse gas emissions. The results show that, in the case of billet casting, a reduction in the cooling water consumption can be also reached. The presented tools for achieving these goals are based on laboratory experiments and on advanced numerical simulations of the casting process.

**Keywords:** steelmaking process; quality improvement; waste heat utilization; numerical simulations; optimal control



**Citation:** Mauder, T.; Brezina, M. Reduction of CO<sub>2</sub> Emissions in Steelmaking by Means of Utilization of Steel Plant Waste Heat to Stabilize Seasonal Cooling Water Temperature. *Sustainability* **2021**, *13*, 5957. <https://doi.org/10.3390/su13115957>

Academic Editor: Chunjiang An

Received: 7 April 2021

Accepted: 20 May 2021

Published: 25 May 2021

**Publisher's Note:** MDPI stays neutral with regard to jurisdictional claims in published maps and institutional affiliations.



**Copyright:** © 2021 by the authors. Licensee MDPI, Basel, Switzerland. This article is an open access article distributed under the terms and conditions of the Creative Commons Attribution (CC BY) license (<https://creativecommons.org/licenses/by/4.0/>).

## 1. Introduction

Steel is one of the most essential materials which influences every aspect of our lives, from infrastructure, transport, building structures, to precision tools and instruments. The level of per capita consumption of steel is treated as an important index of the level of socioeconomic development and living standards in a country. On the other hand, the steelmaking industry is one of the most significant producers of CO<sub>2</sub> emissions worldwide. In the last 50 years, the steelmaking industry has reduced its energy consumption by 61% and it is estimated that about 15–20% of that energy consumption can be further reduced [1]. The processes and facilities used at steel plants, such as the blast furnace and the electric arc furnace, generate a large amount of waste heat, which can be recovered and used, for instance in the next steps of steel processing at the plant. Another way to reduce CO<sub>2</sub> emissions is to reduce the number of low-quality steel products that need to be scrapped due to poor final quality. The use of basic oxygen steelmaking and electric arc furnaces transformed the main production processes, making them faster and more energy efficient. In the 1950s, the previous method of ingot casting was replaced by the continuous casting (CC) method, which significantly accelerated and improved steel production [1].

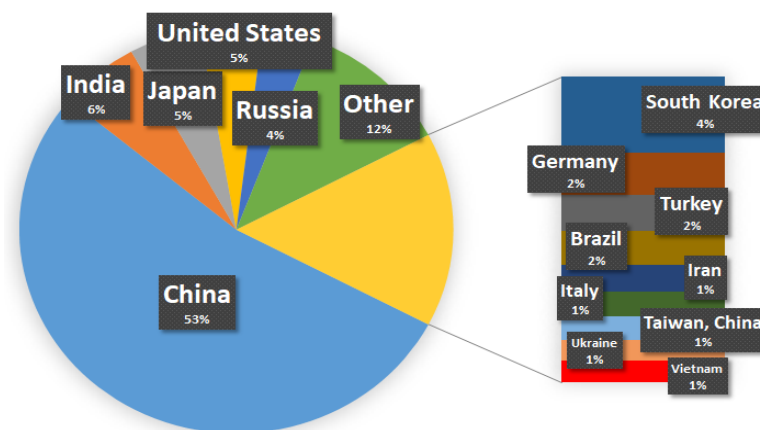
Nowadays, more than 97% of the world's steel is produced by the now well-matured CC technology [2].

### *1.1. Heat Recovery in Steelmaking*

Development in steelmaking has been mainly focused on increasing steel quality, productivity, product variability, and process automatization since the CC method was introduced [3]. There was no significant interest in the reduction of emissions or the waste heat recovery, though the steelmaking industry has a large impact on the overall production of CO<sub>2</sub> emissions, see report [4]. The worldwide community has agreed to hold the increase of the global average temperature below 2 °C with the aim to fit even below 1.5 °C, which requires the reduction of the production of greenhouse gas emissions as soon as possible. This will require a fundamental transformation of energy-intensive industries, including the steel industry. Heat recovery plays an important role in energy saving in the steel production chain [5]. Although industrial waste heat recovery from exhaust and flue gases has increased, the use of radiative heat, which represents a significant share in steelmaking, is still unused. Almost all high temperature facilities, such as the blast furnace, basic oxygen furnace, CC process, hot rolling, etc., involved in the steel industry have a potential for waste thermal energy recovery. Pérez et al. [6] proposed a solution to radiative heat recovery by using a special reflector located directly in the CC machine. Keplinger et al. [7] investigated the use of a heat recovery system which uses the electric arc furnace waste for steam production. Brandt et al. [8] showed an oil-operated heat exchanger within the off-gas of an electric arc furnace. McBrien et al. [9] overviewed a possible heat recovery network for the entire primary steel production supply chain. This paper describes the possibility of direct use of steel plant waste heat for preheating of the cooling water in the CC process [10].

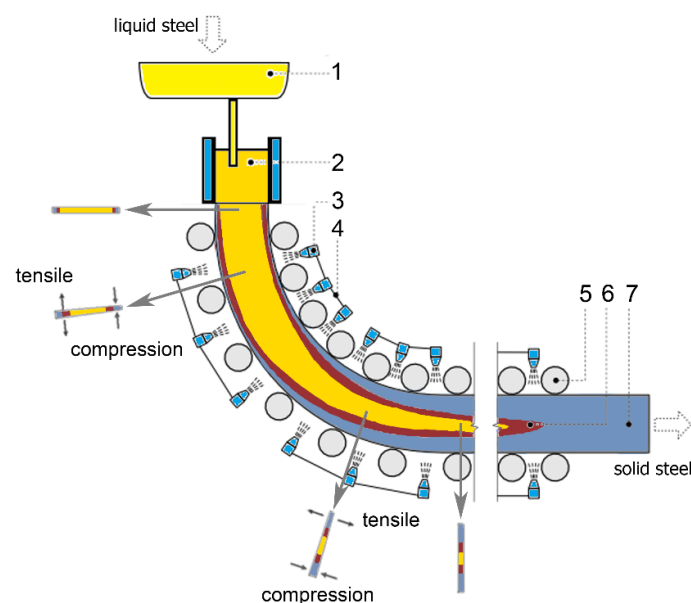
### *1.2. Continuous Casting Process*

The CC process is a predominant way of liquid steel conversion to solid semifinished products in the form of slabs or billets. The CC processes is attributed to more than 97% of the world's steel production [3,10]. The increased local emissions production in the steel industry is most visualized in China. In 1990, China produced only 5% of the world's steel production while, in 2019, China shared more than 53% of world steel production, see Figure 1. The economic crisis in 2008 caused a deep slump of steel production in the EU. Positive economic results have been reached mostly by steel factories which have been focused on special steel production with higher product capabilities [11], such as higher strength grades, steel plates for barrel boilers, steel design for acidic environments, and steel for offshore technologies. However, the production of these special steel grades requires an additional development and research cost. Well-developed countries made large investments in CC installations during the last decade [12]. Penn et al. [3] described the future trends in CC technology. The quality of steel is a frequently discussed topic and some improvements towards quality final products go hand in hand with environmentally friendly approaches, for instance, reducing the cooling water consumption, increasing the speed of casting, optimizing internal logistics, etc. Recently, new concepts appear in the literature, which come from the Industry 4.0, such as Casting 4.0, digital caster, etc. Miśkiewicz and Wolniak [13] showed how the digitization process can be changed based on Industry 4.0 and whether it contributed to an improvement in energy and material efficiency.



**Figure 1.** Ratio of the CC process in the world in 2019 [2].

The description of the technology background of steel casting is as follows: the specially treated molten steel of a given chemical composition is transported in a ladle to the CC machine where the molten steel is subsequently poured into the tundish from which the steel is fed through a submerged nozzle into the primary cooling part of a continuous casting machine referred to as a mold, see Figure 2. The growth of the solid shell starts in an internally water-cooled mold (primary cooling zone) [14]. To avoid the destructive scenario of steel breakout, the steel strand must be solidified to a properly calculated thickness to withstand the ferrostatic pressure from the liquid core. The steel is then transported in the secondary cooling zone by rollers and is cooled down by water cooling nozzles. A group of nozzles divides the secondary cooling zone into several cooling loops. In the tertiary cooling zone, the steel surface is cooled down only by free convection and radiation. The molten steel is continuously cooled down from approximately 1550 °C to 800 °C (in the case of billet casting, even temperatures around 400 °C can be reached). A significant factor which has to be considered in the cooling strategy is the solidification phenomenon in terms of latent heat, where a large amount of heat is released, see [15]. More detailed information about CC technology can be found in [10].



**Figure 2.** Scheme of the CC process and mechanical stresses during bending and straightening. 1–tundish; 2–mold; 3–nozzle; 4–cooling circuit; 5–roller; 6–solidification point; 7–solid steel [16]. Reused from reference [16].

During the process, the solid shell is permanently subjected to thermal and mechanical tensile/compression stresses and can give rise to crack formation, which leads to poor quality of the products [10]. The occurrence of mechanical stress corresponds to the hot ductility of steel, which varies with the steel temperature. This means that the cooling process has a major influence on its quality, see Jansto [17]. To create a required shell thickness, together with the required mechanical properties of a particular steel grade, strong and intensive cooling has to be applied in the first cooling sections. On the other hand, the subsequent sections are generally set to softer cooling to reach a proper temperature in specific locations, for instance, at the unbending point where increased mechanical stress is applied. During the casting, about 60% of the heat is withdrawn by means of water cooling nozzles, see Klimes et al. [18]. The importance of optimal control of cooling intensity is obvious and investigated in many research papers. In an extensive review published by Doctor et al. [19], 25 optimization approaches are discussed. In general, the cooling intensity is the only parameter that is optimized, for instance, as a function of the casting speed, chemical composition of steel, overheating temperature, etc. However, these research works do not consider the water cooling temperature as one of the parameters, which influences the final steel quality. From the statistically evaluated historical data from steelmakers, it was found out that the temperature of cooling water used for spray cooling also has an influence on steel quality. The steel quality difference between winter and summer seasons is statistically attributed to the temperature difference of cooling water, which changes during the year from approximately 5 °C to 40 °C.

### 1.3. Simulation Models

The increase of computer power and cloud computing in recent decades allowed the creation of so-called digital twins as a digital representation of real physical systems [20]. These systems integrate the IoT, artificial intelligence, machine learning, and software analytics that serve as decision making support systems. From the physical point of view, a CC is a complex transient heat and mass transfer problem encompassing the phase change by means of the solidification of steel [21]. Digital twins of the CC process are generally based on the complex numerical heat and mass transfer simulation modes. The pioneer works described 1D heat transfer models, such as Meng and Thomas [22]. Alizadeh et al. [23] proposed a 2D model and observed that the casting speed is the most effective parameter for mold heat removal, which means that it is the most important factor in the control of the solidified shell thickness and strand temperature. One of the first 3D solidification models was introduced by Tieu and Kim [24]. Many of these works were far from use in the real casting process, because of the computer power limitations. Today, fully 3D transient numerical models with real boundary conditions are able to run and control the real casting process [25].

In many cases, the numerical models are supplemented by optimization and/or control algorithms. Previous works dealing with optimal control of CC processes were optimized by mathematical programming or heuristic methods. Santos et al. [26] applied the genetic algorithm; Zhemping et al. [27] verified the usage of the ant colony algorithm; Zheng et al. [28] attempted to use the swarm optimization; Mauder et al. [29] applied the firefly algorithm; etc. Combination of the numerical model and the optimal control algorithm creates digital twins which can directly control the real casting process, store and process the casting data, make decisions, and support the process operators [13].

### 1.4. Aim of the Paper and Applied Methods

This article addresses two basic ideas related to the use of waste heat inside a steel plant for preheating the cooling water used in the CC process. There is an assumption that the temperature of the cooling water affects the final quality of the steel, as is indicated by statistical data from steel mills. The first idea is that the waste heat can be used for so-called cooling water temperature stabilization, which can minimize steel defects and improve the overall quality of steel. The second idea is that the required heat withdrawal in the CC

process can be achieved by different water flows with different cooling water temperatures. Theoretically, it would be possible to minimize the amount of water used for cooling by controlling its temperature and making the casting process more environmentally friendly.

Confirmation of these assumptions by using industrial experiments is too expensive, time-consuming, and, in some particular cases, impossible. This paper uses a combination of the results of experimental laboratory measurements and an advanced numerical solidification model. The numerical model has already been validated by several real casting processes. The experimental measurement was provided by Heat Transfer and Fluid Flow Laboratory at Brno University of Technology. The laboratory is focused on experimental research for academic and industrial projects dealing mainly with spray cooling and heat transfer since 1994 [30].

## 2. Methods

### 2.1. Modelling of Continuous Casting Process

In this study, the original 3D numerical model of the temperature field, the so-called Brno Dynamic Solidification Model<sup>®</sup>, is used [25]. The BrDSM has a long-term history, and its current and previous versions have been successfully applied in several steel plants over the world. During the years of development, this model was gradually improved and refined, based on data from the industry, such as pyrometer measurements, temperature scanner measurements, the radioisotopic method for the measurement of solidification point, etc. The BrDSM can be easily adapted to any geometry of a CC machine, and it can be used for slab, billet, and thin slab casting. The BrDSM also supports massive parallel computing on graphics processing units (GPUs) for high-speed on-line calculations. All outputs are collected and stored in the server database for subsequent statistical evaluation. The advanced optimal control algorithm based on fuzzy logic (FL-BrDSM) has become an integral part of the model. The FL regulator adjusts the input parameters such as the casting speed or cooling intensity in the secondary cooling zone based on actual surface temperatures. The combination of the FL regulator with the GPU model allows the prediction of future temperature behavior of the strand, and it works as a model predictive control system. The detailed description of the BrDSM and FL regulator is described in Mauder et al. [31] and a description of the FL regulator applied to CC can be found in Mauder et al. [16].

The results of the BrDSM strongly depend on the boundary conditions. The boundary conditions include the meniscus temperature, heat flux in the mold and under the rollers, forced convection under the nozzles, and free convection and radiation in the tertiary cooling zone. In the literature, a large number of empirical relationships, to determine boundary conditions through the CC machine, can be found [14,32]. However, these empirical formulas include many constants and parameters and their correct determination for a particular cooling setup is difficult. Proper determination of boundary conditions is crucial in the case of obtaining an accurate result, see Ramirez et al. [33]. The more accurate method is to use the operating temperature measurement. In the mold, the cooling intensity is calculated from the energy balance equation while considering the thickness of the mold walls and the water temperature difference between the entry and exit of the cooling channels. The real data comes directly from the measurement of cooling water temperature and flow rates, which are affected by the casting speed and steel carbon content. In the secondary cooling zone, the strand is mainly cooled by the water or water–air mixture nozzles. The cooling efficiencies of cooling nozzles are affected by parameters such as air and water flow, nozzle position, and impact angles. The domain between two supporting rollers can be divided into four different cooling regions: (1) roller contact area, (2) pre-nozzle and water pool area, (3) spraying area, and (4) post-nozzle area, see Figure 3.

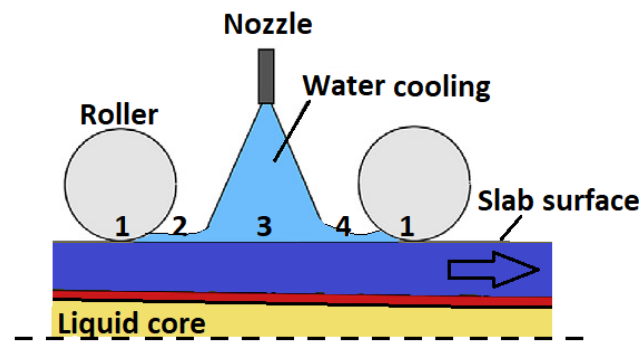


Figure 3. Heat transfer mechanism under the nozzle.

The heat withdrawal in the pre-nozzle (2) and post-nozzle (4) areas involves mainly free convection and radiation. In the spraying area (3), where the spray of water or water-air mixture cools the strand surface, the forced convection plays an important role. Nozzle parameters like air and water flow, nozzle position, air pressure, and impact angle affect the cooling efficiency. The question that needs to be answered is whether the cooling efficiency is also influenced by the cooling water temperature. The boundary condition beneath the spray nozzle can be expressed as:

$$-k \frac{\partial T}{\partial x} \Big|_{x=0} = HTC(T - T_{water}) + \sigma \varepsilon (T^4 - T_{water}^4), \quad (1)$$

where  $T$  is the temperature [K];  $k$  is the thermal conductivity [ $\text{Wm}^{-1}\text{K}^{-1}$ ];  $T_{water}$  is the cooling water temperature [K];  $x$  is the space dimension [m];  $HTC$  is the heat transfer coefficient beneath the nozzle [ $\text{Wm}^{-2}\text{K}^{-1}$ ];  $\sigma$  is the Stefan-Boltzmann constant [ $\text{Wm}^{-2}\text{K}^{-4}$ ];  $\varepsilon$  is the emissivity of the slab surface [-]. The heat flux extracted from the surface can be expressed as a product of the heat transfer coefficient and a difference between the surface temperature and the coolant temperature. The estimation of  $HTC$  values can be made by several empirical formulas such as those in Ha et al. [34]. The main disadvantage of the use of empirical formulas is generally based on many constants and parameters, and their usage is limited to the particular nozzle type and nozzle position. The effect of cooling water temperature is not included in these formulas. The model discussed in this paper uses the  $HTC$  distribution from experimental measurements of the spraying characteristics of all nozzles from a so-called hot plate laboratory instrument.

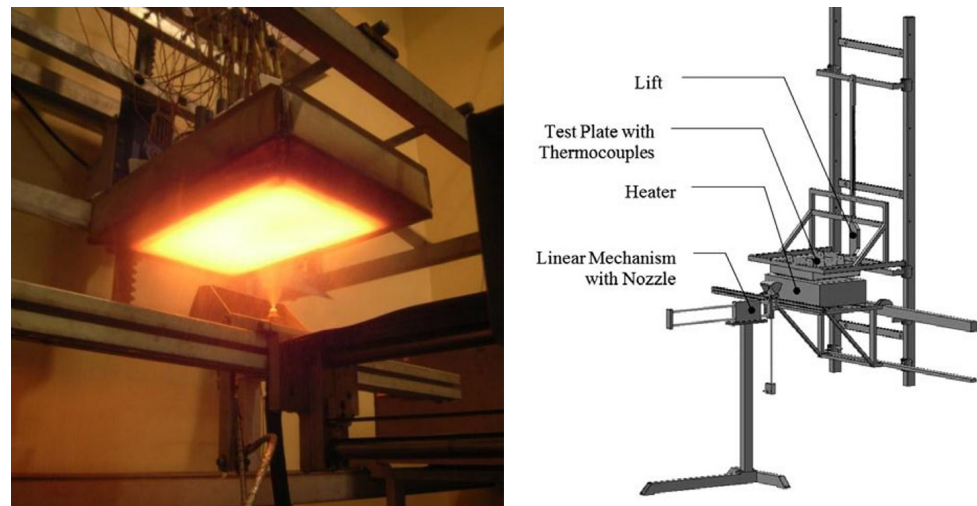
## 2.2. Experimental Setup and HTC Measurement

The cooling water temperature at the steel plants generally changes during the year within a range from 5 °C to 40 °C. This range of cooling water temperature can theoretically influence the cooling characteristics of the nozzles typically used in the CC process and hence influence the final quality of steel. There is an assumption that the  $HTC$  is also a function of cooling water temperature.

The dependence of the  $HTC$  on the surface temperature is well known. The so-called Leidenfrost temperature is the temperature which is the interface between the high intensity and low intensity of cooling [35,36]. Raudensky et al. [37] conducted the  $HTC$  measurements on 7 mm thin carbon plates made of austenitic steel integrating 16 thermocouples. One half of the thermocouples was positioned 1 mm under the surface. The second half was welded directly to the surface. A major part of the laboratory configuration is an electric furnace used for the initial heating of the plate. The test plate was heated to the initial temperature of approximately 1200 °C, and then positioned under a nozzle. The computer control driving linear mechanism moved the spraying nozzle under the plate with a pneumatically driven deflector. The deflector was closed on the way back to its initial position. This simulates the slab movement in the real CC process. For these experiments, small air-mist nozzles, which are usually deployed for the cooling of slab in CC process, were also used. The experiments were conducted with different water

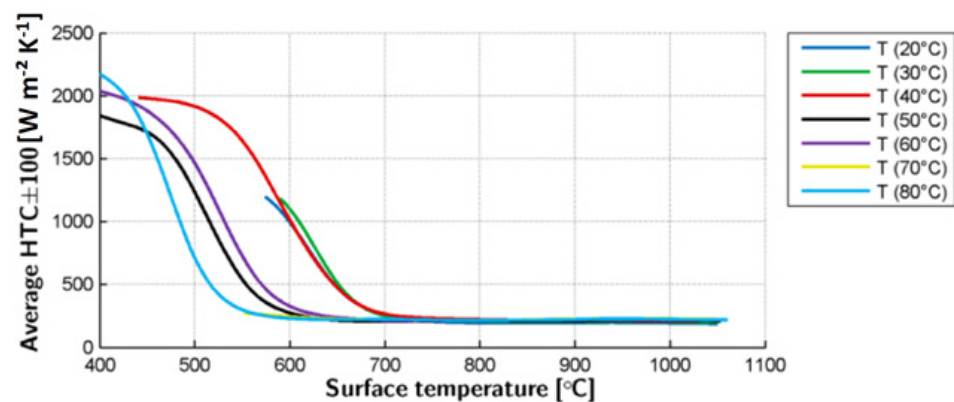


temperatures, which increased by 10 °C from 20 °C to 80 °C. The HTC was then obtained from the measured temperatures by the solution of the inverse heat conduction problem, see Pohanka [38]. The experiment and schematic of the laboratory configuration can be seen in Figure 4.



**Figure 4.** Left—the test plate sprayed by a nozzle, right—basic parts of the experimental laboratory configuration. Reprinted with permission from ref. [38].

The experiment results show a substantial dependence of the spray cooling efficiency on the cooling water temperature, see Hnizdil et al. [39]. The results shown in Figure 5 are the averaged values of the HTC in the impacting area (from  $-150$  mm to  $+150$  mm in the longitudinal and transversal directions). The results demonstrate a significant shift in the Leidenfrost temperature. Changing the water temperature from 20 °C to 80 °C causes a shift in the Leidenfrost temperature by 130 °C to lower temperatures. The HTC values are almost the same for all experiments, but in the high temperature area (Figure 6) it is possible to see that the HTC increased with the increased coolant temperature. The difference of HTC is about  $30 \text{ W m}^{-2} \text{ K}^{-1}$  and provides higher cooling intensity above the Leidenfrost temperature while using warmer water. This result can be explained by the positive effect between the water temperature and the boiling point that allows a faster setting of the boiling regime with high heat transfer rates.



**Figure 5.** The influence of cooling water temperature on HTC [39].

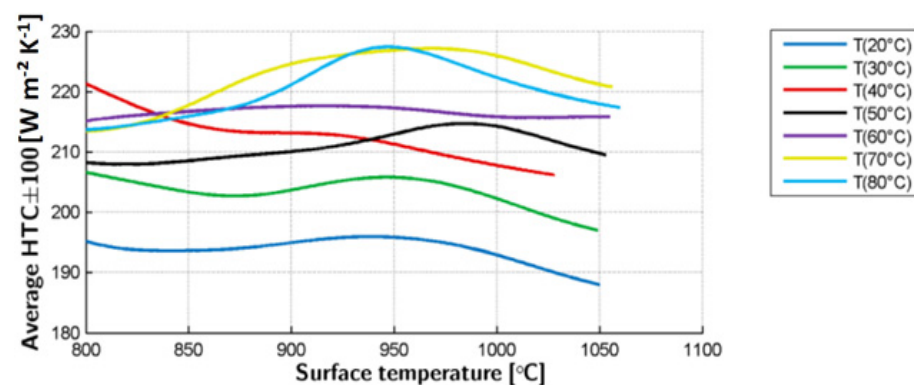


Figure 6. HTC in high temperature area [39].

### 3. Results and Discussion

The average HTCs from the experiments (Figures 5 and 6) were imported to the boundary conditions database in BrDSM. The temperature of cooling water is one of the parameters which can be set at the beginning of the simulation. For comparison, both the billet and the slab casting are investigated. In the first area of billet casting, hard cooling is applied and the surface temperatures of the steel fall below the structural changes of the steel (approximately 500–600 °C). This process has a positive effect on the quality of billets. On the other hand, in slab casting, a smooth decrease in surface temperature leads to a higher quality of the slab [16]. To obtain more general comparison results, the geometries of both casters for slab or billet casting were supposed to have the same dimension in the casting direction. Thus, both casters are 20 m long with the secondary cooling zone divided into six independent regulation loops. This simplification does not affect the principle of the casting process. The cross section of the billet is  $0.12 \times 0.12$  m and the cross section of the slab is  $1.50 \times 0.25$  m.

The numerical results are influenced by the thermophysical properties of the cast steel used in the computation. For the test case, the common stainless steel grade 304 was selected [40]. The thermophysical parameters of the steel used in the presented numerical experiment are listed in Table 1.

Table 1. The thermophysical properties of the steel used in this study [40].

	Specific Heat Capacity	Thermal Conductivity	Density
Liquid steel	780 J/kgK	22 W/mK	6900 kg/m <sup>3</sup>
Solid steel	700 J/kgK	22 W/mK	7200 kg/m <sup>3</sup>
Liquidus temperature	1453 °C		
Solidus temperature	1396 °C		
Latent heat	247 kJ/kgK		

The results of BrDSM are depicted in the form of the temperature curves at specific points (core, top surface, bottom surface, corner, etc.) from the meniscus to the end of the CC machine (in this case 20 m). Four different water cooling temperatures (WCT) were simulated: 20 °C, 40 °C, 60 °C, and 80 °C, to see the difference in the temperature distribution. For comparison, other casting parameters such as the casting speed (1.5 m/min for billet and 0.5 m/min for slab casting), cooling water flow rates, superheat temperature, etc. were kept constant. In Figure 7, the BrDSM results for billet casting where the solidification region between solidus and liquidus temperatures (mushy zone) and cooling zones (mold, secondary and tertiary cooling zone) can be seen. The results of the BrDSM for the slab casting process are visualized in Figure 8.

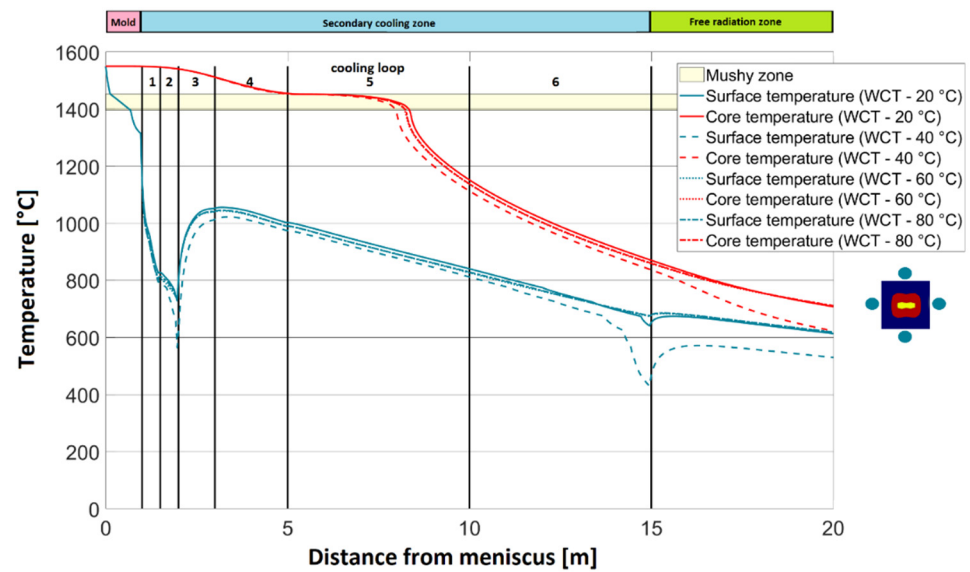


Figure 7. Results of BrDSM simulation for billet caster geometry.

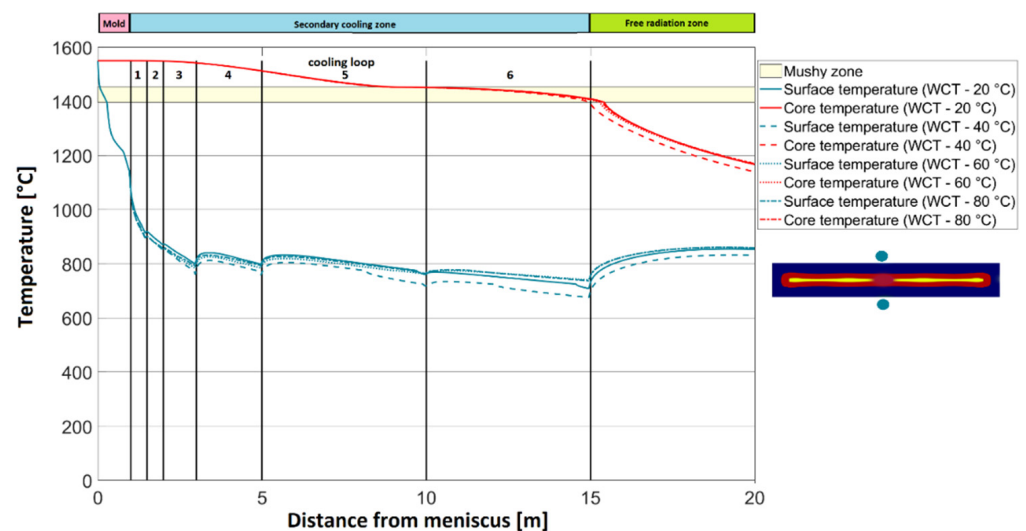


Figure 8. Results of BrDSM simulation for slab caster geometry.

From the results, it can be seen that the steel surface temperatures are influenced by the cooling water temperature. The paper assumption about the temperature distribution difference while using different cooling water temperatures is thus confirmed.

The difference in temperature distribution between the billet and slab casting process is visible. The higher cooling intensity exhibited 40 °C water, which has higher HTC below surface temperature of 840 °C, see Figure 8. The surface temperatures in billet casting are influenced more by different cooling water temperatures than in the case of slab casting. This is caused by the Leidenfrost effect, which is not presented in the slab casting process, because during the slab casting process the surface temperatures did not reach the region under the Leidenfrost temperature approx. 700 °C (Figure 5). On the other hand, in billet casting, the Leidenfrost effect is presented for 40 °C water, see the first cooling loops in Figure 7. The cooling water of 40 °C exhibited similar HTC as 60 °C and 80 °C water in the high surface temperature region and also had an advantage over the 20 °C and 30 °C water where the Leidenfrost temperature was positioned to the higher surface temperatures.

At first sight, temperature profiles in slab casting may look similar, but it must be emphasized that even a small temperature deviation from the optimal surface temperature can cause surface cracks and defects [16]. Therefore, the first idea of water temperature

stabilization during the whole year is a right approach towards a higher quality of continuously cast steel. The use of waste heat recovery towards temperature stabilization which was carried out in this work meets the ecological framework that the metallurgical industry should follow.

The same findings can be applied to the case of billet casting. The simulation of billet casting with the cooling water temperature of 40 °C has significantly larger heat withdrawal due to the Leidenfrost effect. This fact leads to the second idea of this article regarding to the minimization of cooling water consumed during the casting. To achieve the same cooling intensity for a cooling water temperature of 20 °C and a cooling water temperature of 40 °C, it is necessary to reduce the flow of cooling water to a temperature of 40 °C. This calculation has provided in total 6.3% of water savings for billet casting with a 40 °C cooling water temperature. Due to the great amount of water used in billet casting, these savings are not negligible.

To estimate the value of the heat flux which is required to preheat the cooling water, the general heat balance equation can be used:

$$\dot{Q} = (1 - \gamma)^{-1} \cdot \dot{m}_{water} \cdot c_{water} \cdot (T_{required} - T_{water}), \quad (2)$$

where  $\dot{Q}$  is the rate of heat flow [W];  $\gamma$  is the coefficient of energy conversion losses [0,1];  $\dot{m}_{water}$  is the mass flow rate [ $\text{kg s}^{-1}$ ];  $c_{water}$  is the average specific heat of water [ $\text{J kg}^{-1}\text{K}^{-1}$ ] between inlet water temperature and the optimal/required temperature.

For the test case, the required temperature was set to 40 °C and the BrDSM found the optimal mass flow rate of cooling water to be  $16.78 \text{ kg s}^{-1}$ . In the case that the temperature of inlet water is only 10 °C and the estimation of energy loss during the energy conversation is 25%, the rate of heat flow according to Equation (2) is 1406.4 kW. In the case of the special heat capture reflector proposed by Pérez et al. [6], the Tunnel Shaped reflector can capture  $32,700 \text{ Wm}^{-2}$  (assuming the reflector temperature is 500 °C) of radiative heat from the slab. The examined slab dimensions were set to  $1.50 \text{ m} \times 0.25 \text{ m}$ , which means that Tunnel Shaped reflectors must cover the slab in the longitudinal direction at least in 43 m. Due to the size of the steelmaking plant, this distance can be acceptable for most of the CC machines. Moreover, if these reflectors will be placed directly behind the CC machine, then the recovery waste heat does not need any long and loss-making transportation and can directly preheat the cooling water.

#### 4. Conclusions

The heat transfer and solidification model of continuous steel casting (BrDSM) was originally designed and used as a tool to reach optimal casting conditions, which ensure both high-quality steel products as well as increased productivity. Increasing quality of steel products decreases the number of rejected and scrapped slabs/billets and, eventually, the production of CO<sub>2</sub> emissions. It is assumed that 38% of steel defects are related to the incorrect process parameter values, see [41]. This paper shows another possibility of how the final quality of steel products can be increased by using BrDSM and experimental measurements of HTCs. The problem of maintaining high production quality through the year due to different cooling water inlet temperatures can be solved by using steel plant waste heat for preheating cooling water. The proposed approach has two main benefits:

- Cooling water stabilization throughout the seasons, which also stabilizes the surface slab/billet temperatures and can preserve high steel quality (for billet and slab casting).
- By using the BrDSM, the optimal water cooling temperature can be found in the sense of minimizing cooling water consumption (for billet casting).

The experiments supported with computer simulations showed that the temperature of cooling water influences the steel temperature distribution during the casting process and should be taken as one of the parameters which influence the final steel quality. This confirms the assumption that there is an effect of the cooling water temperature on the quality of steel products, which resulted from the statistical evaluation of production data

from the steel plant. In this paper, the pioneer study was presented and the possibility for improvement of CC technology in an ecological way was shown. The future concerns in this field are focused on more HTC experiments and the collection of extensive HTC data for different cooling nozzle types and to run BrDSM simulation for a particular billet/slab casting process with pyrometric verification of the real process.

**Author Contributions:** Conceptualization, T.M. and M.B.; Methodology, T.M.; Software, T.M.; Validation, T.M. and M.B.; Formal Analysis, M.B.; Investigation, T.M.; Resources, T.M. and M.B.; Data Curation, M.B.; Writing–Original Draft Preparation, T.M. and M.B.; Writing–Review & Editing, T.M. and M.B.; Visualization, T.M.; Supervision, T.M.; Project Administration, T.M.; Funding Acquisition, T.M. All authors have read and agreed to the published version of the manuscript.

**Funding:** This work was supported by the Czech Science Foundation under contract No. 19-20802S “A coupled real-time thermo-mechanical solidification model of steel for crack prediction.” and by the research project funded by Brno University of Technology (FSI-S-20-6295).

**Institutional Review Board Statement:** Not applicable.

**Informed Consent Statement:** Not applicable.

**Data Availability Statement:** All necessary data are presented in the article. Other data and computer codes are not publicly available.

**Acknowledgments:** The authors acknowledge the financial support from Czech Science Foundation (project No. 19-20802S) and from Brno University of Technology (project No. FSI-S-20-6295).

**Conflicts of Interest:** The authors declare no conflict of interest. The funders had no role in the design of the study; in the collection, analyses, or interpretation of data; in the writing of the manuscript and in the decision to publish.

## References

- World Steel Association. The White Book of Steel; Pyramidion.be. 2012. Available online: <http://www.voestalpine.com/> (accessed on 11 September 2019).
- World Steel in Figures*; World steel association: Brussels, Belgium, 2020.
- Penn, J.; Pennerstorfer, P.; Jungbauer, A. New Generation of Continuous Casting Plants with Intelligent Manufacturing Strategy. *Berg-und Hüttenmännische Monatshefte* **2018**, *163*, 11–17. [[CrossRef](#)]
- European Environment Agency. Environmental Pressures of Heavy Metal Releases from Europe’s Industry. Available online: <https://www.eea.europa.eu/> (accessed on 24 May 2018).
- Jouhara, H.; Khordehghah, N.; Almahmoud, S.; Delpech, B.; Chauhan, A.; Tassou, S.A. Waste heat recovery technologies and applications. *Therm. Sci. Eng. Prog.* **2018**, *6*, 268–289. [[CrossRef](#)]
- López Pérez, S.; Herrero López, S.; Ubieta Astigarraga, E.; del Hoyo Arce, I.; Gómez de Arteche Botas, M.; Iturralde Iñarga, J. Design of a Radiant Heat Capturing Device for Steel Mills. *J. Sustain. Dev. Energy Water Environ. Syst.* **2019**. [[CrossRef](#)]
- Keplinger, T.; Haider, M.; Steinparzer, T.; Patrejko, A.; Trunner, P.; Haselgrübler, M. Dynamic simulation of an electric arc furnace waste heat recovery system for steam production. *Appl. Therm. Eng.* **2018**, *135*, 188–196. [[CrossRef](#)]
- Brandt, C.H.; Schüler, N.; Gaderer, M.; Kuckelkorn, J.M. Development of a thermal oil operated waste heat exchanger within the off-gas of an electric arc furnace at steel mills. *Appl. Therm. Eng.* **2014**, *66*, 335–345. [[CrossRef](#)]
- McBrien, M.; Serrenho, A.C.; Allwood, J.M. Potential for energy savings by heat recovery in an integrated steel supply chain. *Appl. Therm. Eng.* **2016**, *103*, 592–606. [[CrossRef](#)]
- Birat, J.P.; Chow, C.; Emi, T.; Emling, W.H.; Fastert, H.P.; Fitzel, H. *The Making, Shaping, Treating of Steel: Casting Volume*, 11th ed.; Cramb, A.W., Ed.; The AISE Steel Foundation: Pittsburgh, PA, USA, 2003; p. 1000.
- Sulaiman, H. Steel in automotive industry—the view from the supply chain. In Proceedings of the METEC & 2nd ESTAD 2015, Dusseldorf, Germany, 15–19 June 2015; pp. 1–8.
- Dahmen, B. Economical and flexible tailor-made solutions for the production of new steel grades. In Proceedings of the METEC & 2nd ESTAD 2015, Dusseldorf, Germany, 15–19 June, 2015; pp. 1–8.
- Miśkiewicz, R.; Wolniak, R. Practical Application of the Industry 4.0 Concept in a Steel Company. *Sustainability* **2020**, *12*, 5776. [[CrossRef](#)]
- Gonzalez, M.; Goldschmit, M.B.; Assanelli, A.P.; Dvorkin, E.N.; Berdaguer, E.F. Modeling of the Solidification Process in a Continuous Casting Installation for Steel Slabs. *Metall. Mater. Trans. B* **2003**, *34*, 455–473. [[CrossRef](#)]
- Louhenkilpi, S. *Chapter 1.8—Continuous Casting of Steel, In Treatise on Process Metallurgy*; Seshadri, S., Ed.; Elsevier: Amsterdam, The Netherlands, 2014; pp. 373–434.
- Mauder, T.; Stetina, J. High Quality Steel Casting by Using Advanced Mathematical Methods. *Metals* **2019**, *8*, 1019. [[CrossRef](#)]

17. Jansto, G.S. Steelmaking and Continuous Casting Process Metallurgy Factors Influencing Hot Ductility Behavior of Niobium Bearing Steels. In Proceedings of the METAL 2013, Brno, Czech Republic, 15–17 May 2013; pp. 32–39.
18. Klimes, L.; Charvat, P.; Bohunsky, T.; Klemes, J.J.; Stetina, J. Possibilities for the Reduction of Water Consumption in Steel Industry and Continuous Steel Casting: An Overview. *Chem. Eng. Trans.* **2019**, *76*, 211–216. [[CrossRef](#)]
19. Doctor, Y.N.; Patil, B.T.; Darekar, A.M. Review of Optimization Aspects for Casting Processes. *Int. J. Sci. Res.* **2015**, *4*, 2364–2368.
20. Liu, M.; Fang, S.; Dong, H.; Xu, C. Review of digital twin about concepts, technologies, and industrial applications. *J. Manuf. Syst.* **2020**, 346–361. [[CrossRef](#)]
21. Stefanescu, D.M. *Science and Engineering of Casting Solidification*, 2nd ed; Springer Science: New York, NY, USA, 2009; 402p.
22. Meng, Y.; Thomas, B.G. Heat-Transfer and Solidification Model of Continuous Slab Casting: CON1D. *Metall. Mater. Trans. B* **2003**, *34*, 685–705. [[CrossRef](#)]
23. Alizadeh, M.; Edris, H.; Shafyey, A. Mathematical Modeling of Heat Transfer for Steel Continuous Casting. *Int. J. ISSI* **2006**, *3*, 7–16.
24. Tieu, A.K.; Kim, I.S. Simulation of the continuous casting process by a mathematical model. *Int. J. Mech. Sci.* **1997**, *39*, 185–192. [[CrossRef](#)]
25. BrDSM. Brno Dynamic Solidification Model e BrDSM: Software for Modelling, Simulating and Control of Continuous Casting of Steel. 2016. Available online: [www.continuouscasting.info](http://www.continuouscasting.info) (accessed on 20 May 2021).
26. Santos, C.A.; Spim, J.A.; Garcia, A. Mathematical modelling and optimization strategies (genetic algorithm and knowledge base) applied to the continuous casting of steel. *Eng. Appl. Artif. Intell.* **2003**, *16*, 511–527. [[CrossRef](#)]
27. Ji, Z.; Wang, B.; Xie, Z.; Lai, Z. Ant Colony Optimization Based Heat Transfer Coefficient Identification for Secondary Cooling Zone of Continuous Caster. In Proceedings of the 2007 IEEE International Conference on Integration Technology, Shenzhen, China, 20–24 March 2007; pp. 558–562. [[CrossRef](#)]
28. Zheng, P.; Guo, J.; Hao, X.-J. Hybrid Strategies for Optimizing Continuous Casting Process of Steel. In Proceedings of the 2004 IEEE International Conference on Industrial Technology (ICIT), Hammamet, Tunisia, 8–10 December 2004; pp. 1156–1161. [[CrossRef](#)]
29. Mauder, T.; Sandera, C.; Stetina, J.; Seda, M. Optimization of Quality of Continuously Cast Steel Slabs by Using Firefly Algorithm. *Mater. Tehnol.* **2011**, *45*, 347–350.
30. Heat Transfer and Fluid FLOW Laboratory. Heatlab. Available online: <https://www.heatlab.cz/> (accessed on 20 May 2021).
31. Mauder, T.; Sandera, C.; Stetina, J. Optimal control algorithm for continuous casting process by using fuzzy logic. *Steel Res. Int.* **2015**, *86*, 785–798. [[CrossRef](#)]
32. Totten, G.E.; Bates, C.E.; Clinton, N.A. *Handbook of Quenchants and Quenching Technology*; Haddad, M.T., Ed.; ASM International: Materials Park, OH, USA, 1993; 507p.
33. Ramírez, L.A.; Muñoz, D.F.; Palomar, M.; Romero-Romo, M.A.; Gonzalez, T.J. Heat removal analysis on steel billets and slabs produced by continuous casting using numerical simulation. *Int. J. Adv. Manuf. Technol.* **2017**, *93*, 1545–1565. [[CrossRef](#)]
34. Ha, J.S.; Cho, J.R.; Lee, B.Y.; Ha, M.Y. Numerical Analysis on Secondary Cooling and Bulging in the Continuous Casting of Slabs. *J. Mater. Process. Technol.* **2001**, *113*, 257–261. [[CrossRef](#)]
35. Raudensky, M.; Bohacek, J. Leidenfrost Phenomena at Hot Sprayed Surface. In Proceedings of the 7th ECI Int. Conference on Boiling Heat Transfer, Santa Catarina, Brazil, 3–7 May 2009; Volume 36959, pp. 355–359. [[CrossRef](#)]
36. Bernardin, J.D.; Mudawar, I. The Leidenfrost Point: Experimental Study and Assessment of Existing Models. *ASME J. Heat Transf.* **1999**, *121*, 894–903. [[CrossRef](#)]
37. Raudensky, M.; Hnizdil, M.; Hwang, J.Y.; Lee, S.H.; Kim, S.Y. Influence of the Water Temperature on the Cooling Intensity of Mist Nozzles in Continuous Casting. *Mater. Tehnol.* **2012**, *46*, 311–315.
38. Pohanka, M.; Bellerova, H.; Raudensky, M. Experimental Technique for Heat Transfer Measurements on Fast moving Sprayed Surfaces. *J. ASTM Int.* **2009**, *6*, 1–9. [[CrossRef](#)]
39. Hnizdil, M.; Raudensky, M. Influence of Water Temperature on the Cooling Intensity During Continuous Casting and Hot Rolling. In Proceedings of the METAL 2012, Brno, Czech Republic, 23–25 May 2012; pp. 1–6.
40. Zhou, J.; Tsai, H.L.; Wang, P.C. Transport Phenomena and Keyhole Dynamics during Pulsed Laser Welding. *ASME J. Heat Transf.* **2006**, *128*, 680–690. [[CrossRef](#)]
41. Kulkarni, M.S.; Babu, A.S. Managing quality in continuous casting process using product quality model and simulated annealing. *J. Mater. Process. Technol.* **2005**, *166*, 294–306. [[CrossRef](#)]

# Kapitola 4

## Závěr

Tato práce shrnuje možnosti a výhody využití digitálního dvojčete zařízení pro plynulé odlévání oceli (ZPO). Plynulé lití oceli je komplexním výrobním procesem obsahující zejména přenos tepla a látky za přítomnosti změny fáze kapalina-mushy zóna-pevná fáze. Digitální dvojče ZPO je založeno na matematickém modelu, který numericky řeší tzv. Fourierovu-Kirghoffovu rovnici (parciální diferenciální rovnici 2. řádu), která pracuje s nelineárními parametry a s nelineárními okrajovými podmínkami. Praktické aplikaci předcházela dlouholetá verifikace vytvořeného digitálního dvojčete s reálnými procesy lití přes různé instalace ZPO, různé chemické složení odlévaných ocelí a různé okrajové podmínky. Další evolucí digitálního dvojčete bylo vytvoření optimalizačních/regulačních algoritmů na hledání optimálních licích parametrů za účelem zvýšení produktivity výroby a snížení výrobních vad. Za tímto účelem byl vytvořen původní fuzzy regulátor, který ve svém výkonu překonal nespočet testovaných heuristických optimalizačních přístupů. V postupném vývoji digitální dvojče ZPO dospělo do fáze, kdy je jeho výpočetní jádro masivně paralelizováno na GPU. Paralelizace zvýšila, pro jemné výpočetní síť, výpočetní rychlost až cca. 50-krát a našla řešení výrazně rychleji, než je reálný čas. V kombinaci s fuzzy regulací je pak představen komplexní model prediktivního řízení procesu plynulého lití, který reguluje intenzitu chlazení podle budoucího teplotního vývoje. Kromě využití ve smyslu zvyšování produktivity a kvality odlévané oceli se pro využití digitálního dvojčete hledal další potenciál, který byl nalezen v možnosti úspor vodních zdrojů, které jsou v procesu lití nezbytné k řízenému chlazení. Byla tak představena ekologická optimalizace s využitím digitálního dvojčete ZPO.

Výpočetní jádro digitálního dvojčete bylo odděleno od vstupní uživatelské vrstvy, která pak jednoduše implementuje rozdílné geometrie ZPO a další vstupní parametry pro konkrétní licí stroj. Tím se z původního modelu stal univerzální nástroj pro digitalizaci procesu lití. Pro uživatele bylo vytvořeno grafické rozhraní, které je možné ovládat pomocí dotykového tabletu a tím integrovat původní model do řídicího systému v souladu s filozofií Průmysl 4.0. Integrace digitálního dvojčete do systémů ocelárny rovněž umožňuje spolu s daty měřeními ukládat i velké množství dat ze simulace. Další statistická práce s takto získanými daty pomáhá hledat úzká místa procesu a pomocí shlukové analýzy hledat další spojitosti mezi parametry lití a výstupní kvalitou oceli.

Za dobu vývoje digitálního dvojčete ZPO bylo vytvořeno několik verzí původního modelu, které se postupně více přibližovali realitě. Tím však rostla náročnost na výpočetní kapacitu (složitý model se složitými okrajovými podmínkami vyžaduje velice jemnou výpočetní síť). Navíc testované optimalizační algoritmy vyžadovaly opakované přepočítávání modelu, čímž se kombinace přesného 3D modelu a optimalizačního algoritmu stala ve smyslu nalezení optima v reálném čase nepoužitelná. Tento problém se podařilo překonat překlo-

pením a paralelizací výpočetního jádra na GPU. Časová úspora pro velmi jemné výpočetní sítě předčila všechny původní očekávání. Pro případ, kdy není k dispozici výpočetní stanice s grafickou kartou umožňující paralelní výpočty, byla vytvořena 2,5 D verze modelu (parametricky nastavena tak, aby co nejvíce svými výsledky odpovídala výsledkům 3 D modelu), která je rovněž schopna vypočítat teplotní rozložení předlitku několikanásobně rychleji, než je reálný čas. To znamená, že je možné reagovat s předstihem na dynamické změny v licích parametrech a tím zachovávat kvalitu oceli na požadované úrovni.

Hlavním cílem vývoje digitálního dvojčete ZPO bylo nalezení optimálních parametrů lití (zejména jde o intenzitu chlazení v sekundární chladicí zóně, licí rychlost, licí teplotu apod.), které zajistí vysokou produktivitu procesu lití a zároveň tato produktivita nebude mít negativní vliv na výslednou kvalitu oceli. Popř. pakliže je kvalita oceli nedostatečná, jsou hledány takové parametry chlazení, aby byla zvýšena. Za tímto účelem byla testována řada optimalizačních a regulačních technik. Vzhledem k rychlosti a kvalitě dosažených výsledků byl nalezen a poté modifikován algoritmus založený na fuzzy logice a metodě prediktivního řízení. Tento přístup se zejména osvědčil při sledování dynamických změn v procesu lití, kterými se obecně velká část autorů nevěnuje. Jsou to však velice často právě dynamické změny v procesu, které způsobují větší či menší vady na odlité oceli. Zlepšení procesu lití pomocí digitálního dvojčete ZPO spolu s optimalizačním/regulačním algoritmem pak rovněž vede ke snížení ekologické stopy výroby oceli, což byla dlouho opomíjená oblast. Dnes však s rozvíjející se ekologickou legislativou (např. Zelená dohoda pro Evropu angl. European Green Deal) začíná být toto téma velmi diskutované a aktuální. Výroba oceli je ekologicky náročným procesem, bez ní si však nedokážeme představit moderní život.

V případě aplikace digitálního dvojčete do reálného provozu lze dosáhnout následujících benefitů:

- Zvýšení produktivity lití a tím snížení výrobní doby, což vede nejen ke zvýšení ekonomických parametrů ale rovněž ke snížení emisí skleníkových plynů.
- Hledání licích parametrů, které zachovají v teplotní rovině děj lití konstantní a tím nebude docházet ke snižování kvality oceli ani v případě dynamických změn. Tento faktor je klíčový k udržení konkurenceschopnosti firmy. V případě odlití nekvalitní oceli dochází často k sešrotování, roztavení a nutnosti opakování procesu lití. Předcházení těchto situací opět vede ke snížení emisí skleníkových plynů.
- Snížení množství vody potřebné pro chlazení je dalším krokem ke snížení ekologické stopy procesu. Predikce stavu vodních zdrojů vzhledem k očekávaným dopadům klimatických změn ukazuje scénáře, že voda jako strategická surovina bude nedostatečná a jakékoliv její úspory ve výrobním řetězci budou nezbytné.
- Prototypování v odlévání nových druhů ocelí na základě jejich chemického složení. Ocelárny v EU a USA nemohou konkurovat produkci oceli v Číně. Jediná konkurence je možná v odlévání speciálních druhů ocelí s vysokou přidanou hodnotou. Jejich výroba je ale náročná a hledání vhodného nastavení licích parametrů metodou pokus omyl by vedlo k obrovské zmetkovitosti a s tím spojené neekologičnosti. S digitálním dvojčetem ZPO je možné nalezení optimálního nastavení licího stroje a následná výroba nových značek ocelí potom již probíhá v optimálních licích podmínkách.
- Konstrukční úpravy samotného ZPO, kdy je možné pomocí digitálního dvojčete hledat optimální způsoby chlazení předlitku, např. typ nebo rozložení chladících trysek, využití suchého chlazení apod.



- Získání, ukládání a statistické vyhodnocení dat ze simulace, které mohou doplnit data měřená/provozní. Výsledkem pak může být ucelený obraz procesu lití, který může sloužit pro jeho lepší pochopení a jeho další optimalizaci.

Digitální dvojče ZPO je již finálním produktem a případné modifikace probíhají pouze na přání zákazníka a jeho specifické požadavky. V rámci projektu GAČR (GA 19-20802S) byl v nedávné době teplotní model úspěšně propojen s modelem mechanickým (pro výpočet mechanického a teplotního napětí a namáhání). Ukázala se tak další potenciální cesta k ještě hlubšímu pochopení problematiky plynulého lití a vzniku trhlin a vad. Do řešení toho výzkumného úkolu byl zapojen průmyslový partner Třinecké Železárny a.s., který poskytl data o teplotním průběhu lití velkých válcových profilů a data ze systému hlídání kvality. Jedná se tak zřejmě o další cestu v rozšíření digitálního dvojčete ZPO a alternativu k hledání optimálního licího stavu pomocí statistického vyhodnocení výrobních dat, tak jak bylo prezentováno v kapitole 3.4 [43].

Autor této práce vytvořil výpočetní numerické jádro digitálního dvojčete ZPO. Porovnal dostupné metody numerické diskretizace sítě a dostupné metody pro výpočet změny fáze s pohledu výpočetní efektivity, robustnosti řešení, přesnosti a paralelizovatelnosti. Provedl rozsáhlou verifikaci modelu pomocí reálných výrobních dat, zejména pro bramové lití ve spolupráci s firmou Evraz Vítkovice Steel, a.s., a pro sochorové lití potom s firmou Třinecké železárny, a.s. Vytvořil a porovnal výsledky několika optimalizačních algoritmů pro nalezení optimálního nastavení ZPO. Vytvořil numerické jádro s možností paralelizace na CPU/GPU. Navrhl a vytvořil původní fuzzy regulační přístup na optimální řízení procesu lití. Výsledky simulací digitálního dvojčete ZPO použil v rámci několika projektů základního výzkumu GAČR (GACR 106/09/0940, GAR P107/11/1566, GA15-11977S, GA 19-20802S) a v interních projektech FSI VUT v Brně (FSI-J-10-8, FSI-J-11-7, FSI-J-12-22, FSI-J-13-1977). V rámci kontrahovaného výzkumu vytvořil off-line model digitálního dvojčete ZPO pro lití tenkých bram spolu s grafickým uživatelským rozhraním pro Jihokorejskou firmu Pohang Iron and Steel Company (POSCO) (HS13457086). Navrhl úspěšnou výměnu chladících trysek na bramovém ZPO firmy Evraz Vítkovice Steel, a.s. Po této výměně došlo k lepší regulaci teplot v místě rovnání předlitku což u vybraných značek ocelí statisticky zvýšilo jejich kvalitu. Výsledky pak publikoval v řadě mezinárodních recenzovaných časopisů s impakt faktorem podle WOS a na mnoha celosvětových, evropských a národních konferencích zabývajících se problematikou zpracování oceli, přenosu tepla a optimalizace výrobních procesů.

# Literatura

- [1] ALIZADEH, M.; EDRIS, H.; SHAFYEI, A. Mathematical Modeling of Heat Transfer for Steel Continuous Casting Process. In *International Journal of ISSI*. Isfahan, Iran : ISSI, 2006. s. 7 - 16.
- [2] AUGUSTO, Juan Carlos, ed. Handbook of Smart Cities: 1st ed. 10.07.2021. IOS Press, 2021. ISBN 978-3030696979.
- [3] BAZARAA, M. S.; SHERALI, H. D.; SHETTY, C. M. *NONLINEAR PROGRAMMING - Theory and Algorithms*, Third Edition, New Jersey, Wiley and Sons, 2006, 8553 p. ISBN-13 978-0-471-48600-8.
- [4] BIRAT, Jean-Pierre, et al. *The Making, Shaping and Treating of Steel: Casting Volume : 11th. EDITION*. ALAN W. CRAMB. Pittsburgh, PA, USA : The AISE Steel Foundation, 2003. 1000 s. ISBN 0-930767-04-7.
- [5] BOUHOUCHE, Salah; LAHRECHE, Malek; BAST, Jäürgen. Control of Heat Transfer in Continuous casting Process Using Netural Networks. *ACTA AUTOMATICA SINICA*. 2008, 34, s. 701 - 706. ISSN 0254-4156.
- [6] BÖHM, ZDENĚK, et al. *Plynulé Odlévání Oceli*. Praha : SNTL, 1992. 448 s. ISBN 80-03-00661-9.
- [7] BOWMAN, Horace Dale. *History and Development of the Steel Industry*. ILLINOIS, 1910. Master Thesis. University of Illinois.
- [8] BRDIČKA, Bořivoj. *4. průmyslová revoluce*. Metodický portál: Spomocník [online]. 02. 05. 2016, [cit. 2022-06-06]. Dostupný z WWW: <<https://spomocnik.rvp.cz/clanek/20857/4.-PRUMYSLOVA-REVOLUCE.html>>. ISSN 1802-4785.
- [9] BŘEZINA, M.; MAUDER, T.; KLIMEŠ, L.; ŠTĚTINA, J. Comparison of optimization-regulation algorithms for secondary cooling in continuous steel casting. *Metals*, 2021, vol. 11, no. 2, p. 1-19.
- [10] BÜHLMANN, Peter, Petros DRINEAS, Michael KANE a Mark LAAN, ed. *Handbook of Big Data: Statistical Methods*. 11.11.2019. Chapman and Hall/CRC, 2019. ISBN 9780367330736.
- [11] CAGLAR, Tayfun; Teker, Suat. Industrial Revolitions and its Effects on Quality of Life. In *Global Business Research Congress*, 2019. s. 304-311. DOI: 10.17261/Pressacademia.2019.1109.

- [12] ÇENGEL, Yunus A. *Heat Transfer: A Practical Approach*. New York, USA : McGraw-Hill Companies, 2002. 932 s. ISBN 0-07-245893-3, ISBN-13 978-0072458930.
- [13] CLIFFORD, Jerrold; Steven, CLIFFORD; Adelaide, R. RODRIQUEZ. *The Put the YOU in IoT Handbook: Everone's Guide to the Internet of Things*. 21.03.2020. Independently published, 2020. ISBN 978-1700350206.
- [14] CONSTALES, D.; KAČUR, J.; KEER, R. VAN. On the Optimal Cooling Strategy for Variable-Speed Continuous Casting. *INTERNATIONAL JOURNAL FOR NUMERICAL METHODS IN ENGINEERING*. 2002, 53, s. 539 - 565. ISSN 1097-0207.
- [15] DOBROVSKÁ, Jana. *Chemická Heterogenita Kovových Slitin*. Ostrava : MONTANEX, 2005. 124 s. ISBN 80-7225-182-1.
- [16] DUSINBERRE, G. M. Numerical Methods for Transient Heat Flows. *Trans. ASME*, 1945. Vol. 67, pp. 703–712.
- [17] Ekholm, Nils. On the Variations of the Climate of the Geological and Historical Past and Their Causes. *Quarterly Journal of the Royal Meteorological Society*. 1901. vol. 27. s. 1-61. ISSN:1477-870X.
- [18] European Environment Agency. Environmental Pressures of Heavy Metal Releases from Europe's Industry. Available online: <https://www.eea.europa.eu/> (accessed on 24 May 2018).
- [19] FRANĚK, Zdeněk. *Vliv tepelných procesů na kvalitu plynule litých bram a návrh predikce vad*. Ostrava, Czech Republic, 2011. 149 s. Dizertační práce. Vysoká škola báňská - Technická univerzita Ostrava.
- [20] *Gartner Survey Reveals Digital Twins Are Entering Mainstream Use*. Gartner.com [online]. 2019 [cit. 2022-06-06]. Dostupné z: <https://www.gartner.com/en/newsroom/press-releases/2019-02-20-gartner-survey-reveals-digital-twins-are-entering-mainstream>
- [21] GRIEVES, Michael a John VICKERS. *Digital Twin: Mitigating Unpredictable, Undesirable Emergent Behavior in Complex Systems (Excerpt)* [online]. 2016, s. 1-7 [cit. 2022-06-06]. Dostupné z: doi:10.13140/RG.2.2.26367.61609
- [22] GRIFFIN, Emma Alice. *The 'industrial revolution': interpretations from 1830 to the present*. Norwich: UEA, 2022, s. 1-19.
- [23] GONZALEZ, Marcial, et al. Modeling of the Solidification Process in a Continuous Casting Installation for Steel Slabs. *Metallurgical and Materials Transactions B*. 2003, 34, s. 455-473. ISSN :1073-5615.
- [24] HARDIN, R.; DU, P.; BECKERMANN, C. Three-dimensional Simulation of Heat Transfer and Stresses in a Steel Slab Caster. In *METEC InSteelCon 2011 Proceedings*. Düsseldorf, Germany, TEMA Technologie Marketing AG. 2011. s. 6.
- [25] HEGER, Jaromír. *Numerická Simulace Technologického Procesu Kontinuálního Odlevání Oceli*. Ostrava, 2002. 41 s. Habilitační práce. Vysoká škola báňská, Technická univerzita Ostrava.

- [26] HNÍZDIL, M.; RAUDENSKÝ, M. Influence of Water Temperature on the Cooling Intensity During Continuous Casting and Hot Rolling, *Proceedings of METAL 2012*, 2012, pp. 1–6.
- [27] HOUGHTON, John. *Global Warming: The Complete Briefing*. THIRD EDITION. New York: Cambridge university press, 2004. ISBN 978-0-521-52874-0.
- [28] CHANG, Yun-He, et al. Development and Application of Dynamic Secondary Cooling and Dynamic Soft Reduction Control for Slab Castings. In *METEC InSteelCon 2011 Proceedings*. Düsseldorf, Germany : METEC, 2011. s. 6.
- [29] CHEN, Rong-Hong; HUANG, Yung-Li . Collision of a Liquid Drop on The Edge Region of a Plate Heated Above the Leidenfrost Temperature. *Experiments in Fluids*. 2009, 47, s. 223 – 237. ISSN 0723-4864, EISSN: 1432-1114.
- [30] CHEN, W., et al. Optimization for Secondary Cooling Parameters in Continuous Casting of High Carbon Chromium Bearing Steel. *Advanced Materials Research*. 2009, 83 - 86, s. 465-472. ISSN 1662-8985.
- [31] CHEN, W., et al. Thermo-mechanical Simulation and Parameters Optimization for Beam Blank Continuous Casting. *Materials Science and Engineering A*. 2009, 499, s. 58 - 63. ISSN 0921-5093.
- [32] INCROPERA, Frank P.; DEWITT, David P. *Fundamentals of Heat and Mass Transfer: FORTH EDITION*. New York, USA : John Wiley & Sons, Inc, 1996. 886 s. ISBN 0-471-30460-3.
- [33] *INICIATIVA PRŮMYSL 4.0* [online]. Ministerstvo průmyslu a obchodu ČR, 2014, s. 1-233 [cit. 2022-06-06]. Dostupné z: <https://www.mpo.cz/assets/dokumenty/53723/64358/658713/priloha001.pdf>
- [34] JI, Zhemping, et al. Ant Colony Optimization Based Heat Transfer Coefficient Identification for Secondary Cooling Zone of Continuous Caster. In *Proceedings of the 2007 IEEE International Conference on Integration Technology*. Shenzhen, China : IEEE, 2007. s. 558 - 562. ISBN 1-4244-1092-4.
- [35] JI, Zhemping; XIE, Zhi. Multi-objective Optimization of Continuous Casting Billet Based on Ant Colony system Algorithm. In *Computational Intelligence and Industrial Application, 2008. PACIIA '08. Pacific-Asia Workshop on*. Wuhan, Asia : IEEE, 2008. s. 262 - 266. ISBN 978-0-7695-3490-9.
- [36] KAVIČKA, F. et. all. Matematické a experimentální řešení nestacionárního teplotního pole kontinuálně lité bramy. II. Experimentální výzkum teplotního pole. *Hutnické listy*. 2001, č. 6- 7, s. 54, ISSN: 0018- 8069.
- [37] KLIMEŠ, L.; BŘEZINA, M.; MAUDER, T.; CHARVÁT, P.; KLEMEŠ, J.; ŠTĚTINA, J. Dry cooling as a way toward minimisation of water consumption in the steel industry: A case study for continuous steel casting. *Journal of Cleaner Production*, 2020. Vol. 275, no. 1, p. 123109-1 (123109-12 p.).
- [38] KORŠEC, Petr, et al. Ant Stigmergy on the Grid: Optimizing the Cooling Process in Continuous Steel Casting. In *Parallel and Distributed Processing Symposium, 2006. IPDPS 2006. 20th International* . Greece : IEEE, 2006. s. 8. ISBN 1-4244-0054-6.

- [39] KÜHN, Wolfgang. Handbook of Digital Enterprise Systems: Digital Twins, Simulation and AI: 1st Edition. 29.05.2019. Book Depository US., 2019. ISBN 13: 978-9811200731.
- [40] LUDWIG, Oliver; ALOE, Marco; THEVOZ Philippe. State of the Art in Modelling of Continuous Casting. In *METEC InSteelCon 2011 Proceedings*. Düsseldorf, Germany, TEMA Technologie Marketing AG. 2011. s. 12.
- [41] MAUDER, Tomáš; CHARVÁT, Pavel; ŠTĚTINA, Josef; KLIMEŠ Lubomír. Assessment of Basic Approaches to Numerical Modeling of Phase Change Problems—Accuracy, Efficiency, and Parallel Decomposition. *Journal of Heat Transfer*. 2017, Volume 139, s 5, <https://doi.org/10.1115/1.4036081>.
- [42] MAUDER, T.; ŠANDERA, Č.; ŠTĚTINA, J. Optimal Control Algorithm for Continuous Casting Process by Using Fuzzy Logic. *STEEL RESEARCH INTERNATIONAL*. 2015, vol. 86, no. 7, s. 785-798. ISSN: 1611-3683, <https://doi.org/10.1002/srin.201400213>.
- [43] MAUDER, T.; ŠTĚTINA, J. High Quality Steel Casting by Using Advanced Mathematical Methods. *Metals*, 2018, vol. 8, no. 12, p. 1-13.
- [44] MAUDER, T.; ŠANDERA, Č.; ŠTĚTINA, J.; ŠEDA, M. Optimization of Quality of Continuously Cast Steel Slabs by Using Firefly Algorithm. *Materiali in tehnologije*, 2011. vol. 45, no. 4, p. 347-350.
- [45] MAUDER, T.; BŘEZINA, M. Reduction of CO2 Emissions in Steelmaking by Means of Utilization of Steel Plant Waste Heat to Stabilize Seasonal Cooling Water Temperature. *Sustainability*, 2021. Vol. 13, no. 11, p. 1-12.
- [46] MIETTINEN, Jyrki. *IDS Solidification Analysis Package for Steels : User manual of DOS version 2.0.0*. Helsinki, Finland : Helsinki University of Technology, 1999. 22 s.
- [47] MINKOWYCZ, W. J.; SPARROW, E. M.; MURTHY, J. Y. *Handbook of Numerical Heat Transfer : Second Edition*. New Jersey, USA : John Wiley & Sons, Inc, 2006. 967 s. ISBN 978-0-471-34878-8.
- [48] MITRA, Sanjit Kumar; James F. KAISER. *Handbook for digital signal processing*. New York: John Wiley, 1993. ISBN 978-0471619956.
- [49] MUHIEDDINE, Mohamad; CANOT, Édouard; MARCH, Ramiro. Various Approaches for Solving Problems in Heat Conduction with Phase Change. *IJFV International Journal On Finite Volumes*. 2006, 3, s. 20. ISSN 1634-0655.
- [50] NAQVI, Al a Mark MUNOZ, ed. *Handbook of Artificial Intelligence and Robotic Process Automation: Policy and Government Applications*. 01.11.2020. London: Athem Press, 2020. ISBN 9781785274954.
- [51] Oláh, J.; Aburumman, N.; Popp, J.; Khan, M.A.; Haddad, H.; Kitukutha, N. Impact of Industry 4.0 on Environmental Sustainability. *Sustainability* 2020, 12, 4674. <https://doi.org/10.3390/su12114674>
- [52] PAJDO, P. The world's wealthiest responsible for nearly 50% of carbon emissions. *National Ethnic Press and Media Council of Canada* [online]. 2021, 20.12.2021, 1 [cit. 2022-06-06]. Dostupné z: <https://www.corriere.ca/focus-english-version/the-worlds-wealthiest-responsible-for-nearly-50-of-carbon-emissions/>.

- [53] *PARIS AGREEMENT* [online]. In: . UNITED NATIONS. 2015, s. 1-27 [cit. 2022-06-06]. Dostupné z: [https://unfccc.int/sites/default/files/english\\_paris\\_agreement.pdf](https://unfccc.int/sites/default/files/english_paris_agreement.pdf)
- [54] PATERSON, David. *The Origin Story of the PLC* [online]. In: . Control Automation, 2022 [cit. 2022-06-08]. Dostupné z: <https://control.com/technical-articles/the-origin-story-of-the-plc/>
- [55] PASCON, F.; CESCOTTO, S.; HABRAKEN, A. M. . A 2.5D Finite Element Model for Bending and Straightening in Continuous Casting of Steel Slabs. *INTERNATIONAL JOURNAL FOR NUMERICAL METHODS IN ENGINEERING*. 2006, 68, s. 125 - 149. ISSN 1097-0207.
- [56] PASCUAL, Diego Galar, Pasquale DEPONTE a Uday KUMAR. *Handbook of Industry 4.0 and SMART Systems: 1st Edition*. 24.09.2019. CRC Press, 2019. ISBN 9781138316294.
- [57] PENN, J.; PENNERSTORFER, P; JUNGBAUER, A. New Generation of Continuous Casting 409 Plants with Intelligent Manufacturing Strategy. *Berg Huetttenmaenn Monatsh*. 2018, Volume 163, s. 11–17, <https://doi.org/10.1007/s00501-017-0694-4>.
- [58] PEPLOW, Mark. Can industry decarbonize steelmaking?: Major steelmakers and disruptive start-ups look to hydrogen and renewable electricity to make green steel. *Chemical & Engineering News* [online]. 2021, 13.06.2021, 99(22) [cit. 2022-06-08]. Dostupné z: <https://cen.acs.org/environment/green-chemistry/steel-hydrogen-low-co2-startups/99/i22>
- [59] POHANKA, Michal. *Technical Experiment Based Inverse Tasks in Mechanics*. Brno, Czech Republic, 2006. 142 s. Dizertační práce. Brno University of Technology, Faculty of Mechanical Engineering.
- [60] RAUDENSKY, M.; BOHÁČEK, J. Leidenfrost Phenomena at Hot Sprayed Surface. Proceedings of 7th ECI International Conference on Boiling Heat Transfer. 2009, pp. 3–7, <https://doi.org/10.1115/HT2003-47585>.
- [61] RAO, Singiresu S. *Engineering Optimization : Theory and Practice, Fourth Edition*. New Jersey, USA : John Wiley & Sons, Inc, 2009. 813 s. ISBN 978-0-470-18352-6.
- [62] RISSO, J. M.; HUESPE, A. E.; CARADONA, A. Thermal stress evaluation in the steel continuous casting process. *INTERNATIONAL JOURNAL FOR NUMERICAL METHODS IN ENGINEERING*. 2005, 65, s. 1355-1377. ISSN 0029-5981.
- [63] SANTILLANA, Begoña, et al. Thermal Analysis of Commercial Steel Grades. In *ME-TEC InSteelCon 2011 Proceedings*. Düsseldorf, Germany, TEMA Technologie Marketing AG. 2011. s. 6.
- [64] SANTOS, C. A.; SPIM, J. A.; GARCIA, A. Mathematical Modeling and Optimization Strategies (Genetic Algorithm and Knowledge Base) Applied to the Continuous Casting of Steel. *Engineering Applications of Artificial Intelligence*. 2003, 16, s. 511 - 527. ISSN 0952-1976.
- [65] SEDLÁK, Michal. Miliardy na unikátní technologii. Liberty Ostrava má být ocelářským lídrem. *Deník.cz* [online]. 2020, 1 [cit. 2022-06-06]. Dostupné z:

<https://www.denik.cz/ekonomika/gfg-alliance-chce-do-liberty-ostrava-investovat-19-miliard-korun-20200219.html>.

- [66] SPUY, D. deV. Van Der; CRAIG, I. K.; PISTORIUS, P. C. An Optimization Procedure for the Secondary Cooling Zone of a Continuous Billet Caster. *The Journal of The South African Institute of Mining and Metallurgy*. 1999, 99-01, s. 49 - 56. ISSN 0038-223X.
- [67] STEFANESCU, Doru Michael. *Science and Engineering of Casting Solidification*. New York, USA : Springer Science, 2009. 402 s. ISBN 978-0-387-74609-8.
- [68] SUZUKI, H.G.; ELYON, D. Hot ductility of titanium alloy: A challenge for continuous casting process. *Materials Science and Engineering: A*. 1998, Volume 243, Issues 1–2, s. 126-133, [https://doi.org/10.1016/S0921-5093\(97\)00789-2](https://doi.org/10.1016/S0921-5093(97)00789-2).
- [69] ŠTĚTINA, Josef. *Dynamický Model Teplotního Pole Plynule Odlévané Bramy*. Ostrava, Czech Republic, 2007. 105 s. Dizertační práce. Technická univerzita Ostrava.
- [70] VOLLER, V. An Explicit Numerical Method to Track a Moving Phase Change Front. *International Journal of Heat and Mass Transfer*, 1983. Vol. 26,(1), pp. 147–150.
- [71] WANG, Hongming, et al. Mathematical Heat Transfer Model Research for the Improvement of Continuous Casting Slab Temperature. *ISIJ International*. 2005, 45, s. 1291 - 1296. ISSN 0915-1559, eISSN 1347-5460.
- [72] WORAPRADYA, Kiatkajohn; THANAKIJKASEM, Purit. Optimum Spray Cooling in Continuous Slab Casting Process under Productivity Improvement. In *Industrial Engineering and Engineering Management, 2009*. IEEM 2009. IEEE International Conference on. Hong Kong : IEEE, 2009. s. 120 - 124. ISBN 978-1-4244-4869-2.
- [73] *World Steel in Figures, 2020*. World steel association. Brussels, Belgium, 2020.
- [74] World Steel Association. The White Book of Steel; Pyramidion.be. 2012. Available online: <http://www.voestalpine.com/> (accessed on 11 September 2019).
- [75] WU, Guo-Hua; WU, RONG-Yang. Identification of Convection Heat Transfer Coefficient Parameters Based on Hybrid Particle Swarm Algorithm in the Secondary Cooling Zone for Steel Continuous Casting Process. In *Computational Intelligence Methods and Applications, 2005 ICSC Congress on*. Istanbul, Turkey : IEEE, 2005. s. 6. ISBN 1-4244-0020-1.
- [76] YANG, Won Y., et al. *Applied Numerical Methods Using Matlab®*. New Jersey, USA : John Wiley & Sons, Inc, 2005. 509 s. ISBN 0-471-69833-4.
- [77] YANG, Xin-She. *Nature-Inspired Metaheuristic Algorithms*. Second Edition. United Kingdom : Luniver Press, 2010. 150 s. ISBN 978-1-905986-28-6.
- [78] ZADEH, L. A. Fuzzy sets. *Information and Control* 8 (3). 1965. pp. 338–353. DOI:10.1016/S0019-9958(65)90241-X. ISSN 0019-9958.
- [79] ZHANG, J.; CHEN, D.F.; ZHANG, C.Q.; WANG, S.G.; HWANG, W.S.; HAN, M.R. Effects of an even secondary cooling mode on the temperature and stress fields of round billet continuous casting steel. *Journal of Materials Processing Technology*. 2015, Volume 222, s 315-326, <https://doi.org/10.1016/j.jmatprotec.2015.03.022>

- [80] ZHENG, Peng; GUO, Juan; HAO, Xiao-Jing. Hybrid Strategies for Optimizing Continuous Casting Process of Steel. In *2004 IEEE International Conference on Industrial Technology (ICIT)*. Hammamet, Tunisia : IEEE, 2004. s. 1156 - 1161. ISBN 0-7803-8662.